Macroscopic quantum phenomena in strongly interacting fermionic systems

Jérôme Rech

C.E.A. / D.S.M.

SERVICE DE PHYSIQUE THÉORIQUE

THÈSE DE DOCTORAT DE L'UNIVERSITÉ PARIS XI

Spécialité : PHYSIQUE THÉORIQUE

présentée par :

Jérôme RECH

pour obtenir le grade de DOCTEUR DE L'UNIVERSITÉ PARIS XI

Sujet de la thèse :

Phénomènes quantiques macroscopiques dans les systèmes d'électrons fortement corrélés

soutenue le 19 Juin 2006 devant le jury composé de :

Mme LHUILLIER Claire	Présidente
Melle PEPIN Catherine	Co-Directrice
M. COLEMAN Piers	Co-Directeur
M. JOLICOEUR Thierry	Rapporteur
M. PUJOL Pierre	Rapporteur
M. KOTLIAR Gabriel	Examinateur
M. GLASHAUSSER Charles	Invité

MACROSCOPIC QUANTUM PHENOMENA IN STRONGLY INTERACTING FERMIONIC SYSTEMS

BY JÉRÔME RECH

A dissertation submitted to the

Graduate School – New Brunswick

Rutgers, The State University of New Jersey

in partial fulfillment of the requirements

for the degree of

Doctor of Philosophy

Graduate Program in Physics and Astronomy

Written under the direction of

Doctor Catherine Pépin and

Professor Piers Coleman

and approved by

Prof. Piers Coleman

Prof. Charles Glashausser

Prof. Gabriel Kotliar

Dr. Catherine Pépin

New Brunswick, New Jersey

June, 2006

À ma famille. . .

Remerciements

"-How did you find America?
-Turned left at Greenland"
John Lennon, répondant à un journaliste.

Cette thèse a été le résultat d'une expérience - à ma connaissance une des premières en la matière - puisqu'elle a été effectuée au sein de deux structures séparées de plus de 6000 km, tout en étant reconnues par les "autorités locales" des deux pays.

Je tiens tout d'abord à remercier le Service de Physique théorique du CEA et le département de physique de l'université de Rutgers ainsi que leurs directeurs respectifs Henri Orland et Charles Glashausser pour m'avoir accueilli dans leurs départements.

Je remercie ensuite chaleureusement Catherine Pépin et Piers Coleman d'avoir accepté chacun d'encadrer un demi-étudiant avec les problèmes d'indisponibilité temporaire que cela impliquait. Bien sûr, j'ai beaucoup appris de nos nombreuses discussions, de leur vaste culture scientifique et de leur encadrement si différent et pourtant complémentaire. Ils ont toujours été très patients et disponibles pour mes questions, avec le dynamisme qui les caractérise tous deux. Mais au delà de l'aspect purement scientifique, ce fut aussi une expérience humaine des plus agréables. Merci donc à Catherine pour son inébranlable sourire, ses théories sur la dernière performance de l'équipe de France et ses nombreux problèmes informatiques qu'il m'a fallu résoudre. Merci à Piers pour son humour so british, son rire tonitruant, son enthousiasme sans faille et les petites histoires de physique et de physiciens qu'il se plait à conter réguli'erement.

Je souhaite aussi remercier Olivier Parcollet qui au fil de nos collaborations a fini, un peu malgré lui, par jouer le rôle de "troisième directeur de thèse". En plus de me convertir au numérique en m'initiant au C++ et au Python, Olivier a toujours été disponible, offrant une oreille attentive à mes questions numériques, physiques et mathématiques. J'ai enormément appris à son contact.

Je me sens tout aussi redevable envers mes autres collaborateurs. Tout d'abord Andrey Chubukov pour m'avoir, entre autres choses, initié à l'art du calcul de diagrammes. Puis Indranil Paul, qui a été un ami avant d'être un collaborateur. Enfin

Contents

Introduction

From the crystallization of water into snowflakes, the alignment of electron spins in a ferromagnet, the emergence of superconductivity in a cooled metal, to the very formation of the large scale structure of the universe, all involve phase transitions. These phase transitions can be either dramatic - first order - or smooth - second order.

Understanding the so-called "critical behavior" occuring at a second order phase transition, has been a great challenge and more than a century has gone by from the first discoveries until a consistent picture emerged. The theoretical tools and concepts developed in the meantime now belong to the central paradigms of modern physics.

When the temperature at which a phase transition occurs is suppressed to near absolute zero, quantum effects become important and the new puzzling behavior that develops around this "quantum critical point" is still very far from being completely resolved.

1   From critical opalescence to quantum criticality

A typical material consist of many elementary particles or degrees of freedom. The fundamental microscopic laws that capture the physics of such systems are known: we have to solve a Schrödinger equation for an ensemble of about 10^{23} atoms. This, however, is like trying to understand the layout of a city by examining it one brick at a time.

Instead, new ways of thinking are required, ones that can describe the behavior of complex collections of atoms. Statistical physics, by arguing that although the individual motions are complex the collective properties acquire qualitatively new forms of simplicity, does exactly that. Collective behavior is also important at the unstable interface between two stable states: the critical point.

The notion of a critical phenomenon traces back to 1869, when Andrews [1] discovered a very special point in the phase diagram of carbon dioxide: at 31°C and under 73 atm, the properties of the liquid and the vapor become indistinguishable. Andrews called this point a "critical point", and the associated strong scattering of light displayed by the system close to this point, the critical opalescence. At the critical point, the system undergoes a transition from one state to another – a phase

transition – in a quest to minimize its free energy. Close to this critical point, the material is in maximum confusion, fluctuating between the two competing phases.

Seventy years later, pioneering work by Lev Landau [2] proposed that the development of phases in a material can be described by the emergence of an "order parameter", a quantity which describes the state of order as it develops at each point in the material. In this picture, the critical state of the system, close to a second order phase transition, corresponds to the development of thermal fluctuations (responsible for the "confusion" of the system at criticality) over successively larger regions: the associated length scale ξ diverges at the critical point. In the meantime, the typical time scale τ that determines the relaxation of the order parameter also diverges at criticality, verifying:

$$\tau \sim \xi^z \tag{1}$$

where z is the dynamical exponent.
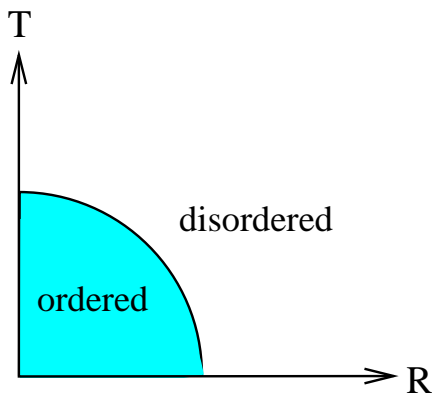
Ordered state	Disordered state	Order parameter
Gas	Liquid	Density difference
Ferromagnet	Paramagnet	Magnetization
Ferroelectric	Paraelectric	Polarization
Nematic liquid crystal	Isotropic liquid	Director

a)   b)

Figure 1: a) Typical phase diagram of a classical continuous phase transition. The line separating the ordered and disordered states is a line of critical points. b) A few examples of order parameters and their associated phase transition.

Later on, it was realized that in the vicinity of the critical point, the physical properties of the system could be described by a handful of numbers: the critical exponents. The critical exponent z defined above is one of them.

It turns out that the same set of these exponents allows to describe phase transitions with totally different microscopic origins. This feature led to the concept of universality: the details of the microscopic laws governing the behavior of atoms in the material are no longer important in specifying its physical properties.

In the mid-seventies, when the study of phase transitions was undergoing a renaissance triggered by the development of Wilson's renormalization group, John Hertz [3] asked the following question: what happens to a metal undergoing a phase transition whose critical temperature is tuned down to absolute zero?

16

2 Stirring up a quantum cocktail

What is so special about a zero-temperature phase transition? First of all, if the temperature is fixed at absolute zero, one needs another control parameter to drive the system through the critical point: the change of state now results from modifying pressure, magnetic field, or even chemical composition.

Moreover, at zero temperature, the thermal fluctuations that drive the transition no longer exist. In this situation, the phase transition is triggered by quantum fluctuations: due to the uncertainty principle, a particle cannot be at rest at zero temperature (since then both its position and velocity would be fixed), so that all particles are in the state of quantum agitation. This "zero point motion" plays the same role as the random thermal motion of the classical phase transitions: when it becomes too wild, it can melt the long-range order.

Hertz showed in his original work that the key new feature of the quantum phase transition is an effective increase of the number of dimensions, associated to quantum mechanics. While a statistical description of a classical system is based on an average over all possible spatial configurations of the particles, weighted by the Boltzmann factor[1] $e^{-E/(k_B T)}$, a probabilistic description of a quantum system relies on averaging all the ways in which a particle moves in time weighted by a Schrödinger factor $e^{-iHt/\hbar}$. Due to the close resemblance of these two weighting factors, a single combined description of a quantum statistical system is possible. Therefore a quantum phase transition looks like a classical one, except that the configurations now vary in "imaginary time" in addition to varying in space. The imaginary time now appears as an extra dimension, or more accurately as z extra dimensions, where z is the dynamical critical exponent defined in Eq. (1). The effective dimensionality d_{eff} of the model increases compared to the spatial dimension d according to:

$$d_{\text{eff}} = d + z \tag{2}$$

One might legitimately wonder why the appearance of such new dimensions do not invalidate previous classical thermodynamic results. It turns out that at finite temperature, there always exist a region close to the critical point, where the thermal fluctuations are much more important than the quantum ones. It follows that, in the vicinity of a finite temperature critical point, the phase transition can be described within the framework of classical statistical mechanics. This naturally does not mean that quantum mechanics plays no role in this case as it might determine the very existence of the order parameter. This only points out that the behavior of this order parameter, close to the finite temperature critical point, is controlled by classical thermal fluctuations.

Hertz's idea of a quantum critical point may seem like a rather esoteric theoretical observation. After all, the zero temperature is impossible to access experimentally,

---

[1]where E is the energy of the configuration

so that quantum critical points look more like mathematical oddities rather than observable physical phenomena.

It took several years after Hertz's work to realize that the quantum critical point governs the physics of a whole region of the phase diagram: the quantum critical regime. Moving away from the quantum critical point by increasing the temperature, one enters a region of the phase diagram where there is no scale to the excitations other than temperature itself (which restricts the extent of the "imaginary time" dimension): the system "looks" critical, as the quantum fluctuations are still very strong. As a consequence, the properties of the system in this region of the phase diagram are qualitatively transformed in a fashion that is closely related to the physics behind the quantum phase transition.
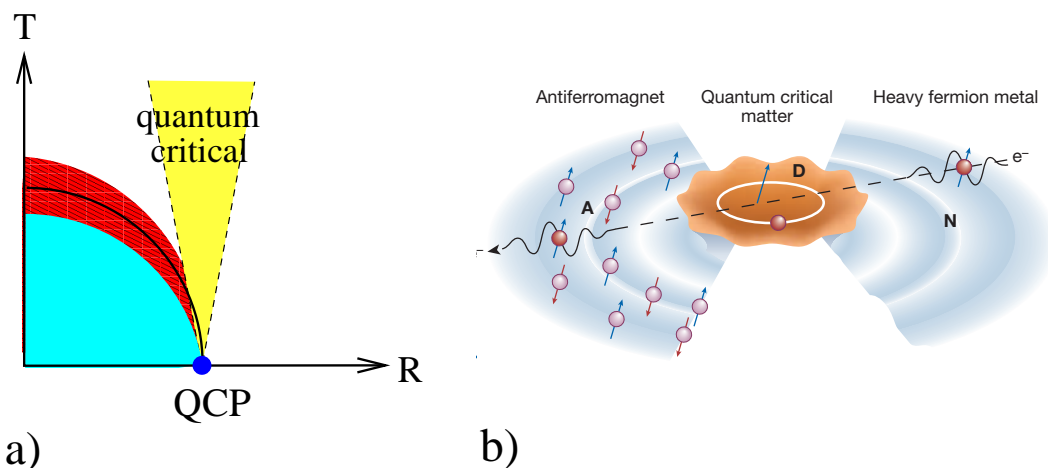
Figure 2: a) Typical phase diagram of a phase transition whose critical temperature has been tuned to zero, leading to a quantum critical point, and the corresponding quantum critical region. b) Picturesque view of droplets of nascent order developing at quantum criticality. Inside the droplet, the intense fluctuations radically modify the motion of the electrons (from [4]).

3 Quantum criticality observed

Indeed, the quantum critical region, through its unusual properties, has been extensively observed experimentally. The best studied examples involve magnetism in metals. Gold-doped $CeCu_6$ was among the first ones [5].

When pressure is applied to this compound, the transition towards an antiferromagnetic ordering (associated to the cerium atoms acting as local magnetic moments) is tuned to occur at zero temperature. In the quantum critical region, experimentalists found an almost linear resistivity (unseen in both phases surrounding the quantum critical region) extending way above the quantum critical point,

on almost a decade in temperature. Since then, more than fifty other compounds, built on the same recipe of localized moments buried inside a non-magnetic bulk, have been discovered. We even have an apparent case of a line of quantum criticality instead of a single point.

But the observation of quantum criticality is not limited to these magnetic materials. Quantum critical behavior has been reported, e.g., in organic material where the change of pressure or chemical doping leads to quantum critical fluctuations of the electric charge. Quantum criticality has even been observed in a surprisingly simple metal: chromium.

Hertz's original idea of a zero-temperature phase transition was once regarded as an intellectual curiosity. It has now become a rapidly growing field of condensed-matter physics.
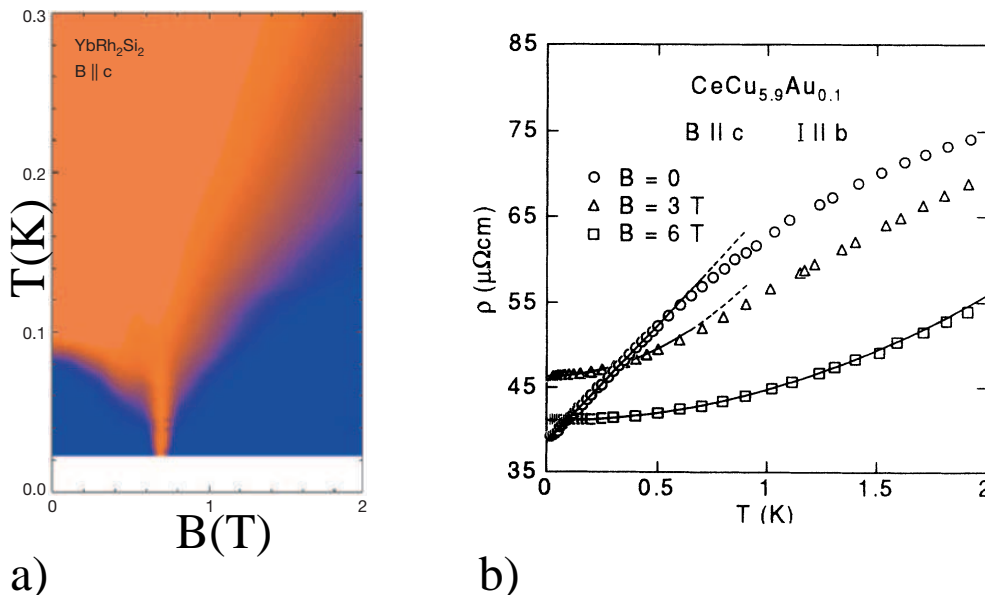
Figure 3: a) Temperature-magnetic field phase diagram of YbRh$_2$Si$_2$. Blue regions indicate normal metallic behavior. Orange regions correspond to the quantum critical regime (from [6]). b) Resistivity as a function of temperature for the compound CeCu$_{5.9}$Au$_{0.1}$. Solid lines indicate a linear ($B = 0$) and a quadratic fit ($B \neq 0$) (from [5]).

4   Unsolved puzzles

Some of the strange properties reported experimentally in the quantum critical region echo the predictions of Hertz (and subsequent extensions of his original theory). But this conventional wisdom is flouted in several aspects, and Hertz thirty-year-old theory cannot account for present experiments. The discrepancy ranges from an

incorrect order of the transition (like itinerant ferromagnetic systems that turn out to order magnetically through a first-order transition where a continuous one was predicted) to a profound inadequacy in the physical properties of the quantum critical regime (like the antiferromagnetic transition of Ce and Yb-based compounds, the so-called "heavy fermion" materials).

A series of compounds, which a priori do not seem so different from the ones matching perfectly Hertz predictions, created the controversy. Some physicists believe that Hertz theory can be saved, and that provided one can derive a new extension that could take proper account of the complexity of the material, new experiments can be explained based on Hertz framework of quantum critical phenomena. However, none of these attempts have been convincing enough, and the "ultimate extension" of Hertz theory remains to be found.

Others argue that the discrepancy between the canonical theory and the recent experimental results comes from a failure of Hertz's original approximations. This failure can be attributed to an incomplete account of the realities of the materials (like, say, disorder), or to an unjustified assumption in the mathematical derivation. This is the point of view we develop in the first part of the present text, where we show that independently of its failures to explain experimental results, Hertz theory is bound to break down in the special case of a ferromagnetic quantum critical point.

Finally, a third possibility considers that a new starting point is needed for a proper examination of the fluctuations: a new framework for quantum phase transitions is required. If it were the case, such a new development would be quite remarkable, as the current conventional picture relies on two cornerstones of modern physics, namely the theory of classical critical phenomena and the quantum mechanics. In the second part of this work, we develop a new approach towards the understanding of the quantum critical behavior of heavy fermion materials. Motivated by the failures of Hertz theory to account for the recent experimental results for these compounds, we seek new insights from an unexplored route towards criticality. Such new elements may help in devising a new mean field theory for the quantum critical point in these systems.

5   Outline

The present dissertation is divided up into two parts.

In the first part, we study the stability of the ferromagnetic critical point in close relation with Hertz theory.

Chapter 1 is an introduction to the ideas and assumptions behind Hertz canonical theory of quantum critical phenomena. After reviewing some of the experimental successes of the latter, we focus on the main failures and the possible explanations advanced to account for them.

Chapter 2 presents the phenomenological model used as a starting point of our analysis. After a short treatment based on a perturbative expansion, we show

what the crucial elements are for deriving a controllable scheme that could describe the quantum critical behavior of itinerant ferromagnets. We then move on to this derivation, and later verify that the various approximations made in the beginning are indeed justified.

Chapter 3 contains our main results. It presents the computation of the static spin susceptibility and shows that a non-analytic contribution arises, leading to a breakdown of the continuous transition towards ferromagnetism below a given energy scale. This same result is recast within the framework of Hertz theory. We further argue that the breakdown is a peculiarity of the ferromagnetic case and does not seem to appear in closely related models.

Chapter 4 recalls the main conclusions of this first part and presents the future work towards a better understanding of the ferromagnetic quantum critical point.

Some of the results of this first part have been published in a short letter (Publication 1) but most of the present work is unpublished at the moment and will give rise to a longer publication, still in preparation (Publication 2). For this reason, we choose to present all technical details either in the main text or in the appendices.

In the second part, we study a large-N approach of quantum impurity models based on a bosonic representation of the localized spin.

Chapter 5 is an introduction to the Kondo and Anderson models, and to their modern applications to the physics of quantum dots and heavy fermion materials.

Chapter 6 recalls the main results of the bosonic large-N approach to the description of the overscreened and underscreened Kondo impurity. We then prove that contrarily to the common wisdom, the same method can be used to describe the exactly screened case as well.

Chapter 7 presents an extension of the previous bosonic large-N approach to the case of two coupled impurities. Our results suggest that the approach is not only capable of handling magnetic correlations but also to describe the physics of the quantum critical point. They are in line with previous results for this system. The results of Chapters 6 and 7 have been grouped in Publication 4.

Chapter 8 seeks a generalized procedure that could cure some of the failures of the original large-N method. We show that although this promising new approach do lead to a better description of the exactly screened single impurity, it does not account for the full physics of the Fermi liquid state. These results led to Publication 5.

Chapter 9 concerns an extension of the large-N bosonic approach to the Kondo lattice model. Some of these results, along with technical derivations of an extended Luttinger-Ward description of this model, are presented in Publication 3.

Introduction
Quantum criticality

Part I: Instability of a ferro-QCP

Chapter 1

Ferro-QCP:
Hertz-Millis-
Moriya theory

Chapter 2

Spin-fermion
and Eliashberg
theory

Chapter 3

Instability of
a ferro-QCP

Chapter 4

Conclusions

Chapter 5

Kondo effect:
from the impurity
to the lattice

Chapter 6

One-impurity
multichannel
Kondo model

Chapter 8

Conserving
approx. for a
single impurity

Chapter 7

Two-impurity
multichannel
Kondo model

Chapter 9

Kondo lattice:
first results

Part II: Bosonic approach for Kondo

Conclusion

Figure 4: Layout of the thesis

Part I

Instability of a Ferromagnetic Quantum Critical Point

CHAPTER 1

Introduction and motivations

Contents

In this chapter, we review the canonical quantum critical theory for the itinerant electronic systems, the so-called Hertz-Millis-Moriya theory (HMM). We then present some of the experimental puzzles related to the ferromagnetic quantum critical point in these systems as well as some recent analytical studies questioning the validity of the HMM theory.

1.1 Quantum critical theory of itinerant ferromagnets

The simplest model of a metal is the non-interacting Fermi gas. In such a system, however, there is an equal number of electrons occupying either spin states in the

conducting band and there are no interesting magnetic effects to be found. Introducing an interaction between the electrons leads to strong correlations, ultimately giving rise to instabilities into new ordered electronic phases, including magnetic ones.

To be more concrete, we consider a lattice model with repulsion between the electrons, such as the Hubbard model [7], whose Hamiltonian writes:

$$H = \sum_{\mathbf{k}} \sum_{\sigma=\uparrow,\downarrow} (\epsilon_{\mathbf{k}} - \mu)c^{\dagger}_{\mathbf{k}\sigma}c_{\mathbf{k}\sigma} + U \sum_{i} n_{i\uparrow}n_{i\downarrow} \tag{1.1}$$

where we consider the system at low density (to stay far away from the Mott transition at half-filling). This model Hamiltonian is characterized by a competition between the kinetic term and the Coulomb interaction U, and as such is a good candidate for displaying a quantum phase transition between a Fermi liquid (where the kinetic term dominates) and a magnetically ordered state (where the repulsion is dominant).

The Coulomb repulsion term can be written in terms of the charge and spin density variables:

$$U \sum_{i} n_{i\uparrow}n_{i\downarrow} = \frac{U}{4} \sum_{i} (n_{i\uparrow} + n_{i\downarrow})^2 - \frac{U}{4} \sum_{i} (n_{i\uparrow} - n_{i\downarrow})^2 \tag{1.2}$$

where $(n_{i\uparrow} - n_{i\downarrow})/2 = \phi_i^z$ is the magnetization, and $N_i = n_{i\uparrow} + n_{i\downarrow}$ the total number of electrons at site i.

1.1.1 Mean-field theory and Stoner criterion

Let's assume that there exists a net magnetization $M_z = \langle \phi_i^z \rangle$ and ask under what condition this is energetically favorable compared to the unmagnetized state.

Treating this model in a mean-field way, each electron sees an effective magnetic field $B_{\text{eff}} = 2UM_z$ due to the magnetization of its fellow electrons, as well as a renormalization of the chemical potential:

$$-U\left(\phi_i^z\right)^2 \quad \xrightarrow[MF]{} \quad U(-2M_z\phi_i^z + M_z^2) \tag{1.3a}$$

$$\frac{U}{4}N_i^2 \quad \xrightarrow[MF]{} \quad \frac{U}{4}\left(2\langle N \rangle N_i - \langle N \rangle^2\right) \tag{1.3b}$$

The variational energy of the ground-state then writes:

$$\begin{aligned} E_{\text{var}}(M_z) &= \langle H_{\text{eff}} \rangle \\ &= E_{\text{kin}}(M_z) - M_z B_{\text{eff}} + UM_z^2 \end{aligned} \tag{1.4}$$

where $E_{\text{kin}}(M_z) = \sum_{\mathbf{k},\sigma}(\epsilon_k - \tilde{\mu})\langle c^{\dagger}_{\mathbf{k}\sigma}c_{\mathbf{k}\sigma} \rangle$, and $\tilde{\mu}$ is the renormalized chemical potential.

As we are interested in the onset of ferromagnetism, the spontaneous magnetization M_z can be assumed to be small, so that one can treat the electron gas in the linear response regime. Introducing the Pauli susceptibility χ_0 of the non-interacting Fermi gas in zero magnetic field, one has:

$$E_{\text{kin}}(M_z) = E_{\text{kin}}(0) + \frac{M_z^2}{2\chi_0} \tag{1.5}$$

It follows that an instability towards the development of a spontaneous magnetization occurs when:

$$2U\chi_0 = 1 \tag{1.6}$$

which is known as the Stoner criterion [8] for the onset of ferromagnetism in metals.

1.1.2 Hertz-Millis-Moriya effective theory (HMM)

Now that we know from this simple mean-field approach that a quantum critical point is expected as a function of the Coulomb interaction U, we turn to a more careful analysis of the behavior of the system as one approaches this QCP from the paramagnetic side.

□ Derivation

The derivation of the effective theory was first carried out by Béal-Monod and Hertz [9, 10, 3]. Starting from the Hubbard model, Eq. (1.2), and performing a Hubbard-Stratonovich decomposition on the interacting term in the spin channel, the partition function reads:

$$Z = Z_0 \int \mathcal{D}[c, \phi] exp \left[-\int_0^\beta d\tau \left(\phi_i^z(\tau)\phi_i^z(\tau) - \sqrt{U}\phi_i^z(\tau)c_{i\alpha}^\dagger(\tau)\sigma_{\alpha\beta}^z c_{i\beta}(\tau) \right) \right] \tag{1.7}$$

where we chiefly focused on the spin fluctuations and disregarded the charge ones, assuming they are unimportant close to the ferromagnetic QCP.

Integrating the fermionic degrees of freedom out of the partition function, one obtains a purely bosonic effective theory in terms of the order-parameter field $\phi(x, \tau)$, given by the Landau-Ginzburg-Wilson (LGW) free energy functional:

$$
\begin{aligned}
\Phi[\phi] &= \int_0^\beta d\tau \int_0^\beta d\tau' \left[\phi_i(\tau)\phi_i(\tau)\delta(\tau - \tau') - \text{Tr}\left(1 - \sqrt{U}\phi_i G_0^{ij}(\tau - \tau') \right) \right] \\
&= \sum_{\omega_n, q} \left(1 - U\chi_0(q, i\omega_n) \right) \phi(q, i\omega_n)\phi(-q, -i\omega_n) \\
&\qquad + T\sum_{\omega_i, q_i} u(1, 2, 3, 4)\phi(q_1, i\omega_1)\phi(q_2, i\omega_2)\phi(q_3, i\omega_3)\phi(q_4, i\omega_4) \\
&\qquad\qquad \times \delta(q_1 + q_2 + q_3 + q_4)\delta(\omega_1 + \omega_2 + \omega_3 + \omega_4) + \dots
\end{aligned} \tag{1.8}
$$

27

where we expanded in the last expression up to fourth power in ϕ, and used the notation G_0 for the conduction electron Green's functions at $U = 0$.

The bare dynamical susceptibility $\chi_0(q, i\omega_n)$ is given by a Lindhard expansion around $q = \omega = 0$ close to the ferromagnetic phase transition:

$$\chi_0(q, \omega_n) = \chi_0 - b\frac{q^2}{k_F^2} + a\frac{|\omega_n|}{v_F q} \tag{1.9}$$

The same kind of derivation can be extended to a vector order parameter, so that the spin rotation invariance is preserved. This only affects the numerical prefactors so that the effective bosonic theory we refer to in the rest of this chapter ultimately writes:

$$
\begin{aligned}
\Phi[\mathbf{S}] \;=\; & \sum_n \int \frac{d^d q}{(2\pi)^d} \left(\delta + q^2 + \frac{|\omega_n|}{q} \right) \mathbf{S}(\mathbf{q}, \omega_n) \cdot \mathbf{S}(-\mathbf{q}, -\omega_n) \\
& + uT \sum_{n_1, n_2, n_3, n_4} \int \frac{d^d q_1}{(2\pi)^d} \cdots \frac{d^d q_4}{(2\pi)^d} \, \delta(\mathbf{q_1} + \mathbf{q_2} + \mathbf{q_3} + \mathbf{q_4}) \, \delta_{n_1 + n_2 + n_3 + n_4} \\
& \times \left[\mathbf{S}(\mathbf{q_1}, \omega_{n_1}) \cdot \mathbf{S}(\mathbf{q_2}, \omega_{n_2}) \right] \left[\mathbf{S}(\mathbf{q_3}, \omega_{n_3}) \cdot \mathbf{S}(\mathbf{q_4}, \omega_{n_4}) \right] \tag{1.10}
\end{aligned}
$$

where δ is the distance to the QCP and, following Hertz, we assumed that the quartic term u can be approximated by a constant.

☐ A few comments

▷ *Landau damping*

The dependence on $|\omega_n|$ of the quadratic term arises because the spin modes $\mathbf{S}$ lie inside the particle-hole continuum of the Fermi liquid (see Fig. 1.1) and are therefore overdamped: the decay mechanism is Landau damping [11]. In the ferromagnetic case, the conservation of the order parameter fluctuations enforces the damping rate, which appears in the denominator, to vanish as $q \to 0$. The overdamping leads, in the quantum critical regime, to a dynamical exponent $z > 1$.

▷ *Stoner criterion*

Note that the constant appearing in the quadratic term in ϕ vanishes when the Stoner criterion is satisfied, i.e. at the transition. This term thus measures the distance to the magnetic instability.

▷ *Assumptions*

In order to derive the effective bosonic action (1.10), one has to make a few assumptions:

- all other excitations are neglected with respect to the spin fluctuations. Indeed, in the derivation, we assumed the interaction in the charge channel was

unimportant, and disregarded any possible pairing instability. Making this assumption, we only exclude the case of bi-critical points, considering that close enough to the ferromagnetic QCP, all other excitations are gapped, and can be safely neglected. In practice, this is true for charge fluctuations. However, the spin fluctuations can lead to an effective attractive interaction between the electrons, and eventually to a $p-$wave superconducting instability.

- the bosonic modes are "slower" than the fermionic ones. This is a necessary condition to perform the integration over the fermionic degrees of freedom. In the Hertz derivation, this cannot be justified a priori. However, assuming this is true, the final result of Eq. (1.10) suggests that the typical bosonic momentum and frequency are related by $\omega \sim q^3$. Comparing this to the low-energy fermions, for which $\omega \sim |k - k_F|$, we see that there is no contradiction with the original assumption, which can be seen as an a posteriori justification.[1]

- the coefficient of the ϕ^4 term can be approximated by a constant. This is again unjustified a priori, and is related to the difficulty of treating this coefficient exactly. Hertz argued however from a Renormalization Group treatment (see the next paragraph for the main results) that this ϕ^4 term is irrelevant in dimensions 2 and higher.

We argue later in the text (Section 3.1) that these last two approximations are actually questionable at criticality, and their violation leads, all at once, to the breakdown of both the HMM theory and the ferromagnetic QCP.
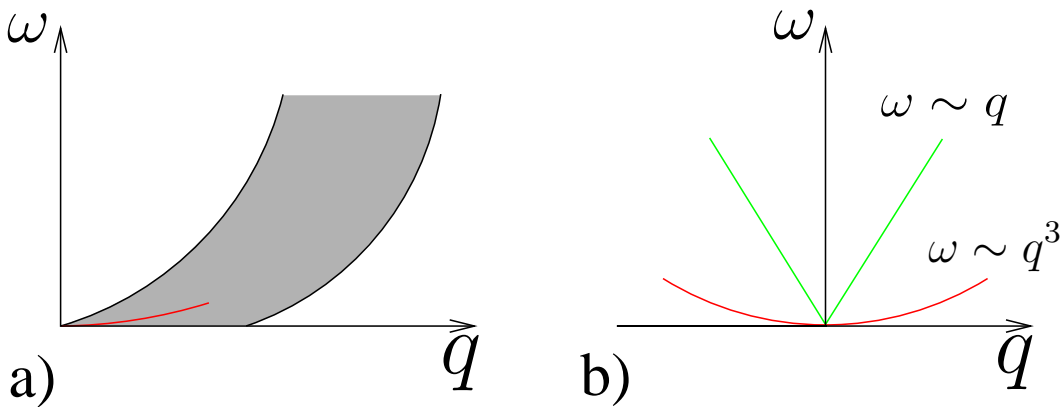
Figure 1.1: a) Particle-hole continuum (shaded region) and ferromagnetic modes (red line), b) Schematic view of the bosonic (red) and fermionic (green) dispersion.

---

[1]Further in the text, we refer to these regions of the $(d+1)$-dimensional space of frequency and momentum, as the fermionic and bosonic mass-shells.

□ Millis and Moriya additions

In order to obtain a quantitative description, Moriya and Kawabata developed a more sophisticated theory, the so-called self-consistent theory of spin fluctuations [12]. This theory is very successful in describing magnetic materials with strong spin fluctuations outside the quantum critical region. As for the quantum critical regime of itinerant ferromagnets, this leads to identical results to those of Hertz theory [13].

Later, Millis [14] revisited the theory developed by Hertz. He considered an additional scaling equation for the temperature, which allowed him to correct some of Hertz' results concerning the crossover behavior at finite temperature.

For these reasons, the quantum critical theory, associated to the effective action (1.10), is known as the Hertz-Millis-Moriya theory.

□ Results

We now present the main results of the HMM theory for the ferromagnetic QCP.

From the effective action (1.10), Hertz applied a Renormalization Group (RG) treatment. Eliminating the outer-shell defined as:

$$
\begin{cases}
e^{-l} & < q < 1 \\
e^{-zl} & < \omega < 1
\end{cases}
\tag{1.11}
$$

where z is the dynamical exponent and l an infinitesimal scaling factor, one can leave the quadratic and the quartic terms of the effective action unchanged by rescaling q, ω and $\mathbf{S}$, and imposing scaling conditions on the parameters δ and u. The rescaling of frequency and momentum requires that $z = 3$ in order for the q^2 term to scale like the Landau damping.

Incorporating the contribution of the outer-shell beyond the simple rescaling, this leads to the following:

$$
\frac{d\delta}{dl} = 2\delta + 2u f(T, \delta) \tag{1.12a}
$$

$$
\frac{du}{dl} = \left(4 - (d + z)\right) u - 4u^2 g(T, \delta) \tag{1.12b}
$$

$$
\frac{dT}{dl} = zT \tag{1.12c}
$$

where f and g are complicated integrals depending on T and δ. The last equation, missed by Hertz, was proved by Millis to be important for the finite temperature crossover regime.

The set of equations (1.12) already suggests the existence of an unstable Gaussian fixed point at $T = u = \delta = 0$. Moreover, close to this critical point, the interaction u is irrelevant if $d + z > 4$ (i.e. if $d > d_c^+ = 1$) , and one then expects the exponents to be those of the Gaussian model.

Solving the set of RG equations, one can extract the behavior in temperature of several physical properties in the quantum critical regime for a 3-dimensional system:

$$\text{Specific heat:} \quad C_v \sim T \log\left(\frac{T_0}{T}\right) \tag{1.13a}$$

$$\text{Resistivity:} \quad \rho(T) \sim T^{5/3} \tag{1.13b}$$

$$\text{Susceptibility:} \quad \chi(T) \sim \chi_0 - \chi_1 T^{4/3} \tag{1.13c}$$

$$\text{Critical temperature:} \quad T_c(\delta) \sim |\delta - \delta_c|^{3/4} \tag{1.13d}$$

1.2 Experiments

Magnetic quantum phase transitions are among the most studied ones experimentally. In this section, we present some experimental results concerning the quantum critical regime of some itinerant ferromagnetic compounds.

1.2.1 Successes

The behavior of many physical properties in the quantum critical regime of itinerant ferromagnets, as predicted by the Hertz-Millis-Moriya theory, was observed in several compounds.

□ $\mathbf{Ni}_x\mathbf{Pd}_{1-x}$

Pd is a strongly enhanced Pauli paramagnet, close to ferromagnetic order. It has long been known [15] that roughly 2.5% of nickel ions doped into palladium induce such a ferromagnetic order. Below 10% of doping, the induced structural and magnetic disorder is rather small and is believed to play only a minor role.

Nicklas and collaborators [16] studied samples of Ni_xPd_{1-x} for doping concentrations $0 \leq x \leq 1$. They observed the following:

- close to $x = 0.1$, a clear change of slope appears in the $\log T_c$ vs. $\log(x - x_c)$ plot, revealing a $(x - x_c)^{3/4}$ behavior at low doping (see Fig. 1.2). They could extract from these data that the critical concentration $x_c = 0.026 \pm 0.002$,

- at $x = 0.026$, the resistivity follows a $T^{5/3}$ dependence for more than two decades in temperature (see Fig. 1.2). The exponent changes quickly as one departs form x_c either way, signaling that the quantum critical behavior is limited to a narrow region around the critical doping,

- the heat capacity linear coefficient C_v/T increases logarithmically towards low temperature for a range of doping $0.022 \leq x \leq 0.028$ (see Fig. 1.3),

All these results match the predictions of the HMM theory for the quantum critical regime.
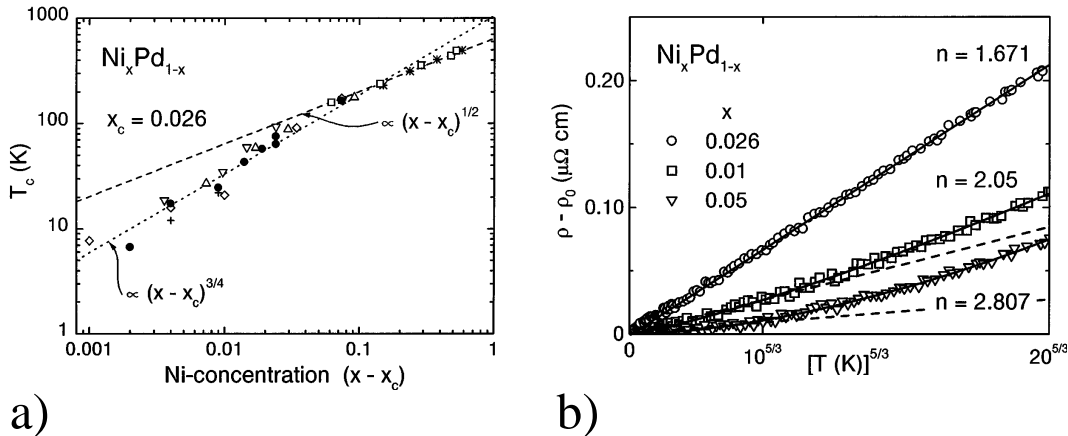
Figure 1.2: Ni_xPd_{1-x}, data from [16]: a) Curie temperature T_c as a function of $x-x_c$. The dashed line indicates $(x-x_c)^{1/2}$ and the doted line $(x-x_c)^{3/4}$; b) Resistivity as a function of temperature for three concentrations: in the paramagnet $x = 0.01$, in the ferromagnet $x = 0.05$, and at the critical doping $x_c = 0.026$. The solid lines stand for $\rho = \rho_0 + AT^n$.

□ $\mathbf{Zr_{1-x}Nb_xZn_2}$

Although it is made of non-magnetic constituents, $ZrZn_2$ is a ferromagnetic compound at low temperature. The Curie temperature at which the ferromagnetic ordering develops can be reduced towards zero by applying pressure (see next paragraph) or doping with niobium.

Sokolov and collaborators [17] studied the phase diagram of Nb-doped $ZrZn_2$, for concentrations $0 \leq x \leq 0.14$. They observed that upon doping, the critical temperature of the ferromagnetic transition continuously drops like a power-law: $T_c(x) \sim (x-x_c)^{3/4}$ (see Fig. 1.3). The critical concentration where the extrapolated critical temperature terminates is estimated to be $x_c = 0.083 \pm 0.002$.

They could also measure the susceptibility close to this critical doping, in the paramagnetic region. The temperature dependent part of the susceptibility behaves as $1/\chi^* = (\chi^{-1} - \chi_0^{-1}) = aT^{4/3}$ (see Fig. 1.3) close to the QCP. The temperature $T^*(x)$ below which this power-law behavior develops is maximum for $x = x_c$ and drops as one departs from it, ultimately vanishing at $x = 0.15$.

The quantum critical behavior documented by Sokolov et al. is in excellent agreement with the theoretical predictions of the HMM theory.

1.2.2 Departures from HMM results

Nevertheless, experimental studies have revealed notable differences from the standard second order behavior predicted by Hertz, Millis and Moriya.
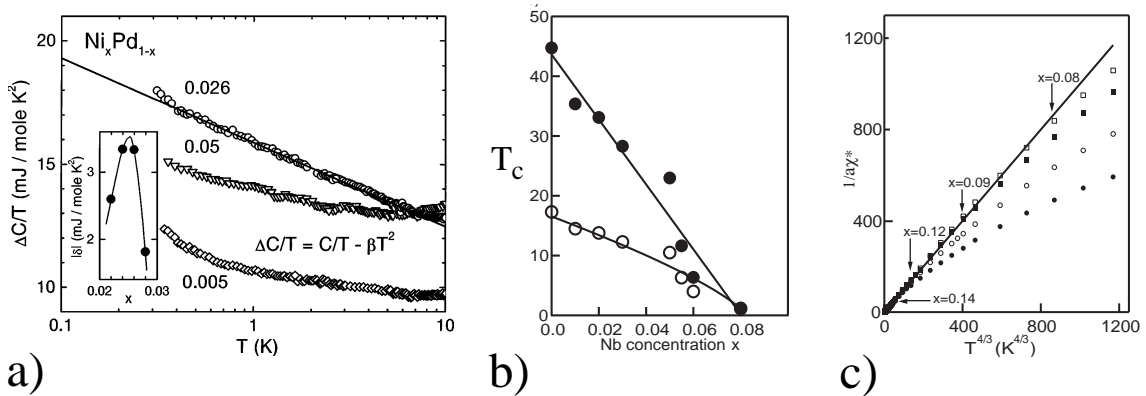
Figure 1.3: Ni_xPd_{1-x}, data from [16]: a) Specific heat vs. $\log T$ for three concentrations. The quadratic temperature dependence has been subtracted from these data, and the prefactor δ of the logarithmic term is shown in the inset. $Zr_{1-x}Nb_xZn_2$, data from [17]: b) Variation of the Curie temperature T_c (white dots) and $T_c^{4/3}$ (black dots) as a function of the Nb concentration. The solid lines are fits to $T_c \propto (x - x_c)$ and $T_c^{4/3} \propto (x - x_c)$; c) The inverse susceptibility $1/\chi^* = (\chi^{-1} - \chi_0^{-1})$ for $x \geq x_c$ is proportional to $T^{4/3}$ (solid line) for $T \leq T^*$.

□ **Superconductivity**

The first departure from the HMM results concerns the development of a superconducting instability. This is actually expected as in order to derive the effective bosonic action, we made the assumption that all excitations but the spin fluctuations could be neglected. As a result, it would be quite surprising that the HMM theory predicts the existence of a superconducting phase without including a possible instability towards that state from the very beginning.

A superconducting instability has been reported at very low temperature in several compounds, among which $ZrZn_2$ [18], UGe_2 [19] and URhGe [20] (see Fig. 1.4).

The existence of such a superconducting state generated a lot of interest as it seems to develop only inside the ferromagnetically ordered phase, and might have ties with the magnetic quantum critical point. We choose not to detail here the various aspects of the controversy these results initiated, since we will not discuss in this work the properties of the ordered state.

□ **First order transition**

The second and most interesting departure from the standard results of the HMM theory stands in the order of the transition towards the ferromagnetic state. Hertz, Millis and Moriya predicted a second order transition all the way down to the quantum critical point. However, a first order transition at low temperature has been

observed in almost all the itinerant materials investigated to date[2].

UGe$_2$, for example, shows in addition to a low temperature superconducting phase, a first order transition between the ferro- and the para-magnetic states close to the QCP (see Fig. 1.4). This first order transition was not predicted by the HMM theory, but this compound has a complicating factor: it is a strongly uniaxial (Ising) system.

ZrZn$_2$, however, is a straightforward itinerant ferromagnet, and the neutron diffraction is consistent with all the hallmarks of a three-dimensional itinerant ferromagnet. Although the ferromagnetic transition at ambient pressure is continuous, the ferromagnetism disappears in a first order fashion as pressure is increased beyond $p_c = 16.5$ kbar. The experimental magnetization data suggest that a tricritical point separates a line of first order transitions from second order behavior at high pressure (see Fig. 1.4).

One last example of a first order transition close to the QCP is MnSi.
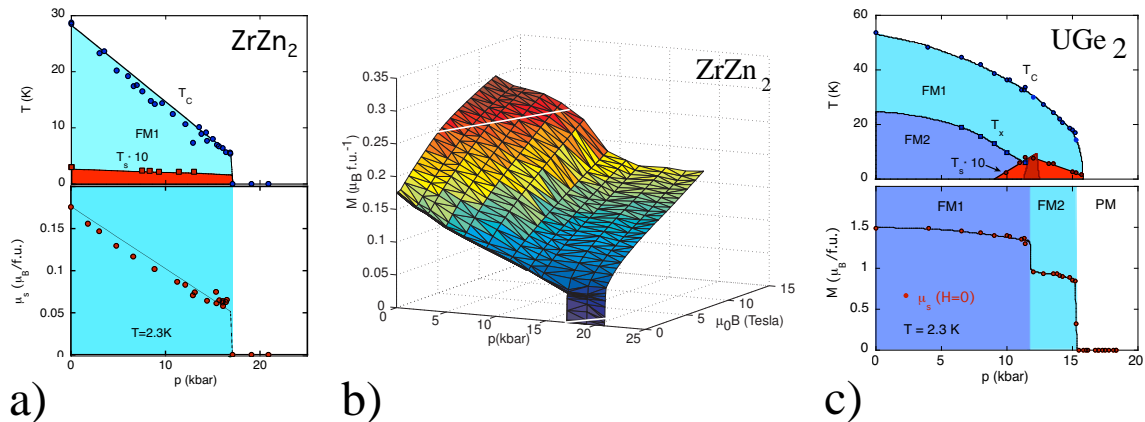
Figure 1.4: ZrZn$_2$, data from [18, 21]: a) (T, p) phase diagram, the ferromagnetic region appears in blue, and the superconducting phase in red; Magnetization as a function of pressure for $T = 2.3K$, the sudden drop at $p = 16.5$ kbar is characteristic of a first order transition towards the paramagnet; b) Magnetization as a function of pressure and magnetic field. UGe$_2$, data from [19, 22]: c) (T, p) phase diagram, the ferromagnetic regions appear in blue, and the superconducting phase in red; Magnetization as a function of pressure for $T = 2.3K$, the sudden drop at $p = 12.2$ kbar and $p = 15.8$ kbar are characteristic of a first order transition.

---

[2]Some argue that even the compounds which seem to perfectly match the HMM predictions do present a first order transition, but only at a temperature below the lowest temperature investigated experimentally.

1.2.3   The puzzling case of MnSi

For completeness, we present here some of the results associated to MnSi, which was one of the first itinerant magnet where a first order transition was discovered [23]. It turns out that the behavior of this compound deviates from the HMM picture in several aspects beyond the simple order of the transition [24, 25].

MnSi is a very well-known system, perhaps the most extensively studied itinerant electron magnet apart from iron, cobalt, nickel and chromium. At ambient pressure, the ground-state below the magnetic ordering temperature $T_c = 29.5K$ is a three-dimensional weakly spin-polarized Fermi-liquid state. As the pressure in increased, the critical temperature continuously approaches zero. The order of the transition, however, changes from second order at ambient pressure to first order below $p^* = 12$ kbar.

The ordered state of MnSi is not a simple ferromagnet: the crystalline structure lacks an inversion symmetry, and weak spin-orbit interactions (of a Dzyaloshinsky-Moriya form) destabilizes the uniform ferromagnetic order and introduces a helical modulation. Further spin-orbit interactions lock the direction of the spiral in the direction $\mathbf{Q} = \langle 111 \rangle$.

The most surprising features of MnSi come from the region of the phase diagram above the critical pressure p_c where the transition temperature vanishes. This region of the phase diagram seems to be the cleanest example of an extended non-Fermi liquid (NFL) state in a three-dimensional metal: the bulk properties of MnSi suggest that sizable quasi-static magnetic moments survive far into the NFL phase. These moments are organized in an unusual pattern with partial long-range order. The resistivity displays a power-law behavior $\rho \sim T^{1.5}$, characteristic of the NFL state, up to the highest pressure achieved experimentally, i.e. extending at low temperature far away from the QCP (see Fig. 1.5).

MnSi seems to question not only the results of the HMM theory, but the whole quantum criticality paradigm, and remains an understood puzzle to date.

1.3   Non-analytic static spin susceptibility

1.3.1   Long-range correlations

It is well known that in fluids, that is in interacting many-body systems, there are long-range correlations between the particles. For example, in classical fluids in thermal equilibrium, there are dynamical long-range correlations in time that manifest themselves as long-time tails. However long-range spatial correlations in classical systems in equilibrium are impossible due to the fluctuation-dissipation theorem.

In quantum statistical mechanics, though, statics and dynamics are coupled and need to be considered together, allowing long-range spatial correlations to develop.
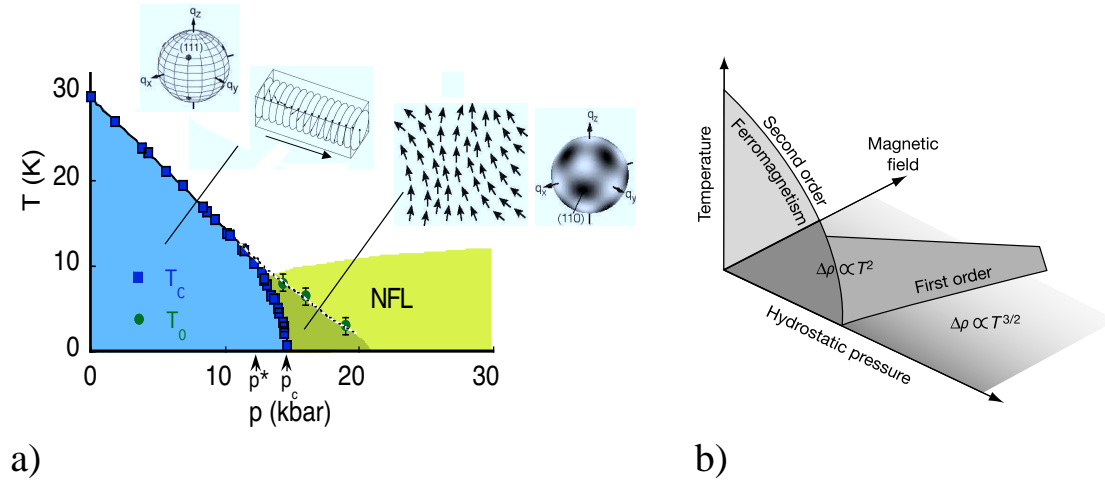
Figure 1.5: a) Temperature vs. pressure phase diagram of MnSi. The insets qualitatively show the location and key features of elastic magnetic scattering intensity in reciprocal space. At high pressure, the neutron scattering signal disappears above a temperature T_0 represented by a dotted line. b) Schematic phase diagram with applied magnetic field in the third direction. The non-Fermi liquid behavior seems to extend to the region of finite magnetic field.

In return, this leads to non-analyticities in the limit of small momentum.

Following this idea, Belitz, Kirkpatrick and Vojta (BKV) [26] studied the long-wavelength properties of the spin-density correlation function (i.e. the spin susceptibility) of a Fermi liquid using a perturbative expansion in the interaction.

The existence of non-analytic corrections to the Fermi liquid theory has a long-standing history and it has been predicted that such non-analyticities occur in the specific heat coefficient [27] but was thought not to affect the spin and charge susceptibilities.

BKV proved that in a three-dimensional Fermi liquid, away from criticality, the leading long-wavelength dependence of the static susceptibility reads, up to second-order in perturbation theory:

$$\frac{\chi^{3D}(\mathbf{q})}{\chi^{3D}(\mathbf{0})} = 1 + c_3 \frac{|\mathbf{q}|^2}{k_F^2} \log\left(\frac{|\mathbf{q}|}{2k_F}\right) + O(|\mathbf{q}|^2) \tag{1.14}$$

where c_3 is a negative prefactor.

Later on, Chubukov and Maslov confirmed that a non-analytic dependence of the static spin susceptibility survives below $d = 3$ [28, 29], becoming:

$$\frac{\chi^{2D}(\mathbf{q})}{\chi^{2D}(\mathbf{0})} = 1 + c_2 \frac{|\mathbf{q}|}{k_F} + O(|\mathbf{q}|^2) \tag{1.15}$$

in two dimensions, where c_2 is again a negative prefactor.

Both groups of authors argued that these non-analytic corrections to the Fermi-liquid theory originate from the singularities in the dynamic particle-hole response function.

Following these results, Belitz and collaborators argued that the LGW functional, derived in the HMM approach, was formally ill-defined as the spin susceptibility enters the quadratic term in ϕ. The non-analyticities in the static susceptibility would then prevent a continuous quantum phase transition towards the ferromagnetic order. The authors argued that such a mechanism could explain the failures of the HMM approach, and the appearance of a first order ferromagnetic transition close to the QCP.

1.3.2 Effect on the quantum critical regime

It is a priori unclear, however, whether the results of Belitz et al. can be extended to the quantum critical regime. We emphasize that these results have been derived in a generic Fermi liquid, away from criticality.

Approaching the quantum critical point, one expects the effective four-fermion interaction to be strongly renormalized (which is consistent with a divergence of the effective mass at criticality). This would lead to a breakdown of the simple perturbative expansion performed by Belitz et al. Moreover, experimentally, the Fermi liquid behavior does not seem to survive as one approaches the QCP [30, 31] which may invalidate the results derived perturbatively for a Fermi liquid.

The first main motivation of our work is to clarify this issue and check whether the non-analytic behavior predicted in the Fermi liquid phase survives as one approaches the QCP (perhaps under a somewhat different form) or is washed out in the quantum critical regime.

In the next chapters, we re-analyze the problem of the quantum critical regime of itinerant ferromagnets. We build a controllable expansion close to the QCP, without integrating out the low-energy fermions, and analyze in details the stability of the ferromagnetic quantum critical point.

As one can see from (1.14) and (1.15), the effect of long-range correlations is more dramatic as the dimensionality is lowered. For that reason, we focus in all this work on the case of a two-dimensional system, close to criticality.

CHAPTER 2

Eliashberg theory of the spin-fermion model

Contents

In this chapter, we describe the starting model for our study of the ferromagnetic quantum critical point. After a direct perturbative treatment which justifies the need to include the curvature, we carry out a self-consistent approximate treatment (also known as "Eliahberg theory") and check a posteriori that the assumptions made for these computations are indeed justified.

2.1 Spin-fermion model

We argued in the previous chapter that integrating the fermions out of the partition function was a questionable way of studying the quantum critical regime, because of the possible non-analyticities that are missed in such a procedure.

Therefore, our starting point for the study of the ferromagnetic quantum critical point is a model describing low-energy fermions interacting with Landau over-damped collective bosonic excitations. These excitations are spin-fluctuations and become gapless at the quantum critical point.

2.1.1 Low-energy model

The general strategy to derive such a low-energy model is to start with a model describing the fermion-fermion interaction, and assume that there is only one low-energy collective degree of freedom near the QCP. This assumption is basically the same as one of the HMM assumptions: the idea is to exclude all excitations but the ferromagnetic spin fluctuations we are interested in. One then has to decouple the four-fermion interaction term using the critical bosonic field as an Hubbard-Stratonovich field, and integrate out of the partition function all high-energy degrees of freedom, with energies between the fermionic bandwidth W and some cutoff Λ [32].

If this procedure was performed completely we would obtain a full Renormalization Group treatment of the problem. Unfortunately, there is no controllable scheme to perform this procedure. It is widely believed, though that although the propagators of the remaining low-energy modes possess some memory of the physics at high energies, the integration of high-energy fermions does not give rise to anomalous dimensions for the bare fermionic and bosonic propagators in the low-energy model.

In practical terms, this assumption implies that the bare propagator of the relevant collective mode is an analytic function of momentum and frequency, and the fermionic propagator has the Fermi liquid form:

$$G(k, \omega) = \frac{Z_0}{i\omega - \epsilon_k}, \tag{2.1}$$

where $Z_0 < 1$ is a constant, and ϵ_k is the renormalized band dispersion.

Near the Fermi surface,

$$\epsilon_k = v_F k_\perp + \frac{k_\parallel^2}{2m_B}. \tag{2.2}$$

Here $\mathbf{k}$ is the momentum deviation from $\mathbf{k_F}$, the parallel and perpendicular components are with respect to the direction along the Fermi surface at $\mathbf{k_F}$, m_B is the band mass, the Fermi velocity $v_F = k_F/m$, and for a circular Fermi surface one has $m = m_B$.

Following this scheme, the original model of fermions interacting with themselves can be recast into an effective low-energy fermion-boson model. In the context of the magnetic QCP, this model is known as the "spin-fermion model" and was first suggested by Chubukov and collaborators [32].

Close to the ferromagnetic quantum critical point, the low-energy degrees of freedom are:

- fermions, whose propagator is given by Eq. (2.1);

- long-wavelength collective spin excitations whose propagator (in this case, the spin susceptibility) is analytic near $q = \Omega = 0$, and is given by:

$$\chi_{s,0}(q, \Omega) = \frac{\chi_0}{\xi^{-2} + q^2 + A\Omega^2 + O(q^4, \Omega^4)}. \tag{2.3}$$

In this last expression, A is a constant, and ξ is the correlation length of the magnetic spin fluctuations, which diverges at the QCP. We prove, further in this chapter, that the quadratic term in frequency does not play any role in our analysis. Indeed, one can argue that the interaction of these collective bosonic modes with fermions close to the Fermi surface generates a Landau damping of the spin fluctuations, as we demonstrate in the next section. As a consequence, we neglect from now on the Ω^2 term in the spin susceptibility, and approximate the above bare propagator by the static one $\chi_{s,0}(q)$.

The model can then be described by the following Hamiltonian:

$$H_{sf} = \sum_{k,\alpha} \epsilon_k c_{k,\alpha}^\dagger c_{k,\alpha} + \sum_q \chi_{s,0}^{-1}(q) \mathbf{S}_q \mathbf{S}_{-q} + g \sum_{k,q,\alpha,\beta} c_{k,\alpha}^\dagger \boldsymbol{\sigma}_{\alpha\beta} c_{k+q,\beta} \cdot \mathbf{S}_q. \tag{2.4}$$

where $\mathbf{S}_q$ are vector bosonic variables, and g is the effective fermion-boson interaction. For convenience, we incorporated the fermionic residue Z_0 into g.

We emphasize that the above spin-fermion model cannot be derived in a true RG-like procedure, and has to be considered as a phenomenological model which captures the essential physics of the problem.

2.1.2 Forward scattering model

To illustrate how this effective Hamiltonian can, in principle, be derived from the microscopic model of interacting conduction electrons, we consider a model in which

the electrons interact with a short range four-fermion interaction $U(q)$ and assume that only the forward scattering is relevant $(U(0) = U)$:

$$H = \sum_{k,\alpha} \epsilon_k c^\dagger_{k,\alpha} c_{k,\alpha} + \frac{1}{2} \sum_q U \sum_{k,k',\alpha,\beta} c^\dagger_{k,\alpha} c_{k+q,\alpha} c^\dagger_{k'\beta} c_{k'-q,\beta}, \qquad (2.5)$$

In this situation, the interaction is renormalized independently in the spin and in the charge channels [33]. Using the identity for the Pauli matrices:

$$\sigma_{\alpha\beta} \cdot \sigma_{\gamma\delta} = -\delta_{\alpha\beta}\delta_{\gamma\delta} + 2\delta_{\alpha\delta}\delta_{\beta\gamma} \qquad (2.6)$$

one can demonstrate [33] that in each of the channels, the Random Phase Approximation (RPA) summation is exact, and the fully renormalized four-fermion interaction $U^{full}_{\alpha\beta,\gamma\varepsilon}(q)$ is given by:

$$U^{full}_{\alpha\beta,\gamma\varepsilon}(q) = U \left[\delta_{\alpha\gamma}\delta_{\beta\varepsilon} \left(\frac{1}{2} + \mathcal{G}_\rho \right) + \sigma_{\alpha\gamma}\sigma_{\beta\varepsilon} \left(\frac{1}{2} + \mathcal{G}_\sigma \right) \right], \qquad (2.7)$$

where $\sigma_{\alpha\beta}$ are Pauli matrices, and

$$\mathcal{G}_\rho \equiv \frac{1}{2}\frac{1}{1 - U\Pi(q)}; \qquad \mathcal{G}_\sigma \equiv -\frac{1}{2}\frac{1}{1 + U\Pi(q)}, \qquad (2.8)$$

with $\Pi(q) = -\frac{m}{2\pi}(1 - a^2(q/k_F)^2)$ is the fermionic bubble made out of high-energy fermions, and $a > 0$.

For positive values of U satisfying $mU/2\pi \approx 1$, the interaction in the spin channel is much larger than the one in the charge channel. Neglecting then the interaction in the charge channel, we can simplify the Hamiltonian (2.5):

$$H = \sum_{k,\alpha} \epsilon_k c^\dagger_{k,\alpha} c_{k,\alpha} + \frac{1}{2} \sum_q U_{eff}(q) \sum_{k,k',\alpha,\beta,\gamma,\delta} c^\dagger_{k,\alpha}\sigma_{\alpha\beta}c_{k+q,\beta} \cdot c^\dagger_{k'\gamma}\sigma_{\gamma\delta}c_{k'-q,\delta}. \qquad (2.9)$$

where $U_{eff}(q) = (1/2)U^2\Pi(q)/(1 + U\Pi(q))$. Performing a Hubbard-Stratonovich decomposition in the three fields $\mathbf{S}_q$, one recasts (2.9) into Eq. (2.4) with:

$$\begin{cases} g &= U\frac{a}{2} \\ \chi_0 &= 2\frac{k_F^2}{Ua^2} \\ \bar{g} &= g^2\chi_0 = (U/2)k_F^2 \\ \xi^{-2} &= \frac{k_F^2}{a^2}\left(\frac{2\pi}{mU} - 1\right) \end{cases} \qquad (2.10)$$

The QCP is reached when $mU/2\pi = 1$, i.e., $\xi^{-2} = 0$. This coincides with the Stoner criterion for a ferromagnetic instability [8].

We emphasize that the bosonic propagator in Eq. (2.3) does not contain the Landau damping term. This is because we only integrated out the high-energy
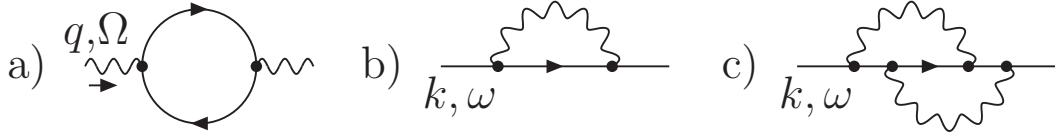
Figure 2.1: a) Polarization bubble b) One-loop fermionic self-energy c) Two-loop fermionic self-energy. The fermions are represented by straight lines and the bosons by wavy lines.

fermions, whereas the Landau damping of a collective mode of energy Ω comes from fermions of energy $\omega < \Omega$, and can only be generated within the low-energy theory. The dynamics of both the bosonic fields $\mathbf{S}_q$ and the fermionic c and $c^\dagger$ is determined self-consistently by treating both fluctuations on equal footing.

To put under control the computations carried out later in the text, it is necessary to extend the model by introducing N identical fermion species, while keeping the $SU(2)$ spin symmetry. The Hamiltonian (2.4) can then be rewritten as:

$$
\begin{aligned}
H_{sf} &= H_f + H_b + H_{int} \quad \text{where} \\
H_f &= \sum_{k,j,\alpha} \epsilon_k c^\dagger_{k,j,\alpha} c_{k,j,\alpha} \\
H_b &= \sum_q \chi^{-1}_{s,0}(q) \mathbf{S}_q \cdot \mathbf{S}_{-q} \\
H_{int} &= g \sum_{k,q,j,\alpha,\beta} c^\dagger_{k,j,\alpha} \boldsymbol{\sigma}_{\alpha\beta} c_{k+q,j,\beta} \cdot \mathbf{S}_q,
\end{aligned}
\tag{2.11}
$$

where the index $j = 1 \ldots N$ labels the fermionic species.

2.2 Direct perturbative results

In this section we compute the fermionic and bosonic self-energies for the model presented in Eq. (2.4) using a perturbative expansion around non-interacting fermions. Our goal here is three-fold: to relate the Landau damping coefficient to the fermion-boson coupling constant g, to evaluate the significance of the momentum-dependent part of the fermionic self-energy and to demonstrate the importance of the curvature of the Fermi surface.

We emphasize that this perturbative expansion is only used as a motivation for a further, more sophisticated approach detailed in the next sections, and for illustrative purposes. It is *not* a self-consistent computation, and most probably breaks down as one approaches the QCP.

2.2.1 Bosonic polarization

The full bosonic propagator depends on the self-energy $\Pi(q, \Omega)$ according to:

$$\chi_s(q, \Omega) = \frac{\chi_0}{\xi^{-2} + q^2 + \Pi(q, \Omega)}. \tag{2.12}$$

At the lowest order in the spin-fermion interaction, the bosonic self-energy is given by the first diagram in Fig. 2.1, and reads:

$$\Pi(\mathbf{q}, \Omega) = 2N\bar{g} \int \frac{d^2k \; d\omega}{(2\pi)^3} \; G(\mathbf{k}, \omega) \; G(\mathbf{k} + \mathbf{q}, \omega + \Omega). \tag{2.13}$$

The curvature of the fermionic dispersion does not affect much the result of this computation as it only leads to small corrections in $q/m_B v_F$. Neglecting the quadratic term in the fermionic propagators, we introduce the angle θ defined as $\epsilon_{\mathbf{k+q}} = \epsilon_{\mathbf{k}} + v_F q \cos\theta$ and perform the integration over $\epsilon_{\mathbf{k}}$, which gives us:

$$
\begin{aligned}
\Pi(\mathbf{q}, \Omega) &= i\frac{N\bar{g}m}{2\pi^2} \int_{-\infty}^{+\infty} d\omega \; (\theta(\omega + \Omega) - \theta(\omega)) \int_0^{2\pi} d\theta \; \frac{1}{i\Omega - v_F q \cos\theta} \\
&= \frac{Nm\bar{g}}{\pi} \frac{|\Omega|}{\sqrt{(v_F q)^2 + \Omega^2}}.
\end{aligned} \tag{2.14}
$$

At the QCP, the bosonic mass-shell corresponds to the region of momentum and frequency space for which the terms in the inverse propagator are of the same order, i.e. near a mass shell q and Ω satisfies $\Pi(q, \Omega) \sim q^2$. It follows that, at the QCP, near the bosonic mass shell, $v_F q/\Omega \sim v_F(m\bar{g}v_F^2/\Omega^2)^{1/3} \gg 1$ at small enough frequency, so that $v_F q$ is the largest term in the denominator of $\Pi(q, \Omega)$. The expression of the bosonic self-energy then reduces to:

$$\Pi(\mathbf{q}, \Omega) = \gamma \frac{|\Omega|}{q}, \tag{2.15}$$

where $\gamma = \dfrac{Nm\bar{g}}{\pi v_F}$.

We see that the lowest order bosonic self-energy recovers the form of the Landau damping presented in Chapter 1, with a prefactor depending on the fermion-boson coupling constant.

As explained earlier, this term is larger than a regular $O(\Omega^2)$ term, and fully determines the dynamics of the collective bosonic mode.

2.2.2 One-loop fermionic self-energy

We now turn to the fermionic self-energy, right at the QCP, where $\xi^{-1} = 0$. To the lowest order in the interaction, the fermionic self-energy contains one bosonic line,

as represented in Fig.2.1.b, and its analytic form writes:

$$\Sigma_1^{\text{free}}(\mathbf{k}, \omega) = 3ig^2 \int \frac{d^2q \, d\Omega}{(2\pi)^3} G_0(\mathbf{k} + \mathbf{q}, \omega + \Omega) \chi(\mathbf{q}, \Omega). \tag{2.16}$$

The superscript "free" implies that we use the free fermionic $G_0(k, \omega)$ in the integral for the self-energy.

In a direct perturbation theory in g, one would have to use the bare form of the bosonic propagator, Eq. (2.3), which leads to $\Sigma(\omega) \propto \log \omega$. However, this result is useless, as we already know that the Landau damping term completely overshadows a regular frequency dependence in (2.3). It makes more sense then to estimate the perturbative self-energy using the full bosonic propagator Eq. (2.12). This is *not* a fully self-consistent procedure, but we use it here to estimate the functional form of the self-energy at various orders in perturbation around free fermions.

It is instructive to distinguish between $\Sigma(\mathbf{k_F}, \omega) = \Sigma(\omega)$ and $\Sigma(\mathbf{k}, 0) = \Sigma(\mathbf{k})$. Indeed, there is an asymmetry in the behavior of the fermionic self-energy depending on whether one computes it at zero frequency or at zero momentum departure from the Fermi surface. This feature is one of the key elements of the self-consistent treatment presented in the next section.

☐ **Frequency dependence**

Substituting the renormalized bosonic propagator with the Landau damping term into (2.16), the frequency-dependent self-energy reads:

$$\Sigma_1^{\text{free}}(\omega) = \frac{3i\bar{g}}{(2\pi)^3} \int d\Omega \, qdq \, d\theta \, \frac{1}{q^2 + \gamma \frac{|\Omega|}{q}} \frac{1}{i(\omega + \Omega) - v_F q \cos \theta}. \tag{2.17}$$

Here θ is the angle between $\mathbf{k_F}$ and $\mathbf{q}$, and we linearized the fermionic dispersion. Evaluating the integral over the angle, and using that the typical internal bosonic momentum $q \sim \Omega^{1/3}$ is much larger than $\Omega \sim \omega$, we obtain:

$$\begin{aligned}
\Sigma_1^{\text{free}}(\omega) &= \frac{3\bar{g}}{2\pi^2 v_F} \int_0^\omega d\Omega \int \frac{dq \, q}{q^3 + \gamma |\Omega|} \\
&= \omega_0^{1/3} \omega^{2/3},
\end{aligned} \tag{2.18}$$

where

$$\omega_0 = \frac{3\sqrt{3}\bar{g}^3}{8\pi^3 v_F^3 \gamma} = \frac{3\sqrt{3}\bar{g}^2}{8\pi^2 N m v_F^2}. \tag{2.19}$$

This result has been first obtained in Ref. [34, 35] when treating the interaction of low-energy fermions with singular gauge fields. It suggests that in $D = 2$, the interaction between bare fermions and critical bosons leads to a breakdown of the Fermi-liquid behavior: at low energies, the $\omega^{2/3}$ term in (2.18) is larger than the bare ω in the fermionic propagator. This obviously makes one wonder if higher order insertions lead to even more singular contributions.

□ Momentum dependence

Before looking at higher-order self-energy corrections, we compute the one-loop momentum-dependent self-energy $\Sigma(\mathbf{k})$, given by:

$$
\begin{aligned}
\Sigma_1^{\text{free}}(\mathbf{k}) &= \frac{3i\bar{g}}{(2\pi)^3} \int d\Omega \; qdq \; d\theta \; \frac{1}{q^2 + \gamma\frac{|\Omega|}{q}} \frac{1}{i\Omega - \epsilon_k - v_F q \cos\theta} \\
&= \frac{3\bar{g}}{(2\pi)^2}\epsilon_{\mathbf{k}} \int \frac{d\Omega \; dq}{q^2 + \gamma\frac{|\Omega|}{q}} \frac{q|\Omega|}{(\Omega^2 + (v_F q)^2)^{3/2}}.
\end{aligned}
\tag{2.20}
$$

One can make sure that the integral is infrared-convergent, i.e. $\Sigma^{\text{free}}(\epsilon_{\mathbf{k}}) \propto \epsilon_{\mathbf{k}}$, with an interaction dependent prefactor, which also depends on the upper cutoff of the theory, Λ.

This suggests that the momentum dependent part of the fermionic self-energy, unlike the frequency-dependent part derived earlier, is regular at the QCP and only leads to a finite mass renormalization.

2.2.3   Two-loop fermionic self-energy

As the one-loop frequency-dependent self-energy seems to dominate over the bare ω term of the fermionic propagator, one could wonder whether higher-order insertions lead to even more singular contributions.

To investigate this issue, we next calculate the contribution to the fermionic self-energy $\Sigma(\omega)$ from diagrams at the two-loop level, and focus, for illustrative purposes, on the diagram presented in Fig. 2.1.c, which writes:

$$
\Sigma_2^{\text{free}}(\omega) \sim \bar{g}^2 \int d\omega_1 d^2 q_1 \int d\omega_2 d^2 q_2 \; G(\mathbf{k_F} + \mathbf{q_1}, \omega + \omega_1) \; G(\mathbf{k_F} + \mathbf{q_2}, \omega + \omega_2)
$$

$$
\times \; G(\mathbf{k_F} + \mathbf{q_1} + \mathbf{q_2}, \omega + \omega_1 + \omega_2) \; \chi_s(\mathbf{q_1}, \omega_1) \; \chi_s(\mathbf{q_2}, \omega_2),
\tag{2.21}
$$

where we use the full bosonic propagator, the free fermionic one, and we restrict ourselves to the frequency dependence of this contribution to the self-energy.

We first compute this integral expanding the dispersion of the internal fermions to linear order, since the quadratic term was not significant in the computation of the one-loop bosonic and fermionic self-energy. Choosing the x axis along the external $\mathbf{k} = \mathbf{k_F}$ and integrating over q_1^x and q_2^x, we are left with:

$$
\begin{aligned}
\Sigma_2^{\text{free}}(\omega) &\sim \frac{\bar{g}^2}{v_F^2 \omega} \int_0^\omega \frac{d\omega_1 dq_{1y}}{q_{1y}^2 + \frac{\gamma|\omega_1|}{q_{1y}}} \int_{\omega-\omega_1}^\omega \frac{d\omega_2 dq_{2y}}{q_{2y}^2 + \frac{\gamma|\omega_2|}{q_{2y}}} \\
&\sim \omega_0^{2/3} \omega^{1/3}.
\end{aligned}
\tag{2.22}
$$

where ω_0 is defined in (2.19).

At low-energy, this two-loop self-energy diverges faster than the one-loop self-energy obtained in (2.18). Estimating higher-order diagrams, we find that they form a series in powers of $(\omega_0/\omega)^{1/3}$, such that the perturbative expansion around free fermions breaks down at $\omega \sim \omega_0$.

This result is in line with the one obtained by Lawler et al. [36], in the context of a QCP in the charge channel using a two-dimensional bosonization scheme. The scale ω_0 is related by $\omega_0 = v_F/x_0$ to the spatial scale at which the equal time fermionic Green's function $G(x)$, obtained from bosonization, begins decaying exponentially $(G(x) \propto e^{-(x/x_0)^{1/3}})$.

However, the divergence of the perturbation theory can be cured once the curvature of the fermionic dispersion is included, as we now show. We re-evaluate the two-loop self-energy (2.21), using now the full fermionic dispersion, Eq. (2.2), without neglecting the quadratic term. After integrating over the momentum component q_1^x and q_2^x, one has:

$$
\begin{aligned}
\Sigma_2^{\text{free}}(\omega) &\sim \frac{\bar{g}^2}{v_F^2} \int_0^\omega \frac{d\omega_1 dq_{1y}}{q_{1y}^2 + \frac{\gamma|\omega_1|}{q_{1y}}} \int_{\omega-\omega_1}^\omega \frac{d\omega_2 dq_{2y}}{q_{2y}^2 + \frac{\gamma|\omega_2|}{q_{2y}}} \frac{1}{i\omega - \frac{q_{1y}q_{2y}}{m_B}} \\
&\sim \frac{m_B^2 \bar{g}^2}{\gamma^2 v_F^2} \, \omega \log^2 \omega.
\end{aligned}
\tag{2.23}
$$

When the curvature of the fermionic dispersion is included, we see that the two-loop self-energy turns out to be small compared to its one-loop counterpart, at low energy. In a separate study [37], Chubukov and Khveshchenko reconsidered the bosonization procedure in the presence of the curvature and obtained the same results as in (2.23).

2.2.4 Conclusion

As a conclusion, this first crude approach suggests that both the fermionic and the bosonic self-energies are important at the QCP. The bosonic self-energy sets the dynamics of the bosons, while the fermionic self-energy is non-analytic and parametrically larger than the bare ω term at low energy, which implies a breakdown of the Fermi-liquid behavior at criticality.

We argued that only the frequency-dependent part of the self-energy matters, the momentum-dependent one only leads to a regular renormalization of the effective mass.

We also found that the curvature of the Fermi surface actually plays a very important role in regularizing the perturbative expansion, which was missed by previous studies in comparable low-energy models.

However, the full account of these effects cannot be obtained from this simple analysis. For example, we did not account here for the mutual effects of the self-energies onto each other. One has to develop a controllable way to treat the bosonic and fermionic self-energies on equal footing, in a self-consistent fashion.

Since we found that only the frequency-dependent $\Sigma(\omega)$ is relevant, a way to proceed is to verify whether an Eliashberg-like theory, similar to the one developed in the context of phonon superconductivity[38], may be such a controllable approximation.

2.3 Eliashberg theory

The Eliashberg procedure allows to compute the fermionic self-energy $\Sigma(\omega)$ and the bosonic polarization $\Pi(q, \Omega)$, by solving the self-consistent set of coupled Dyson's equations, neglecting all contributions coming from the vertex corrections and the momentum-dependent fermionic self-energy.

2.3.1 Self-consistent solution

Specifically the Eliashberg theory follows three steps:

- neglect both the vertex corrections and the momentum dependent part of the fermionic self-energy, i.e. approximate:

$$\Sigma(\mathbf{k}, \omega_n) = \Sigma(\omega_n)$$
$$g_{\text{Tot}} = g + \Delta g = g \quad (2.24)$$

- construct the set of self-consistent Dyson's equations:

$$G^{-1}(k, \omega_n) = i\omega_n - v_F(k - k_F) + i\Sigma(\omega_n)$$
$$\chi_s(q, \Omega_m) = \frac{\chi_0}{\xi^{-2} + q^2 + \Pi(q, \Omega_m)}, \quad (2.25)$$

with the following fermionic and bosonic self-energies:

$$i\Sigma(\omega_n) \quad = \quad \underset{k,\,\omega_n}{\overset{}{\rule{0pt}{0pt}}} $$
$$\chi_0^{-1}\Pi(q, \Omega_m) \quad = \quad \overset{q,\nu_m}{\rule{0pt}{0pt}} \quad (2.26)$$

The fermionic Green's functions in (2.26) are full (they are represented diagrammatically by a straight line) and $\chi_s(q, \Omega_m)$ is the full bosonic propagator (represented by a wavy line).

- check a posteriori that the neglected terms Δg and $\Sigma(\mathbf{k})$, are all parametrically small.

The evaluation of the momentum integral for the fermionic self-energy in the Eliashberg theory requires care. Since fermions are faster than bosons, the leading contribution to $\Sigma(\omega)$ is obtained if one integrates over the momentum component transverse to the Fermi surface only in the fermionic propagator and sets this component to zero in the bosonic propagator (this implies that the momentum integral is factorized).

One can show that the corrections that arise from keeping the transverse component of momentum in the bosonic propagator are small to the same parameter as $\Delta g/g$ and should therefore be neglected, as keeping them would be beyond the accuracy of the theory.

The evaluation of the bosonic and fermionic self-energies within the Eliashberg theory is presented in Appendices A and B. We list here the main results.

□ **Away from the QCP**

At large but finite correlation length ξ and for a bosonic momentum and frequency satisfying $v_F q \gg \Sigma(\Omega)$ we obtain:

$$
\begin{cases}
\Pi(q, \Omega) = \gamma \dfrac{|\Omega|}{q} \;\text{, and} \\[3mm]
\Sigma(\omega) = \lambda \omega F\left(\gamma \omega \xi^3\right),
\end{cases}
\tag{2.27}
$$

where $F(x \ll 1) = 1 + O(x)$, and $F(x \gg 1) = \frac{2}{\sqrt{3}} x^{-1/3}$. The parameter γ is the same as for free fermions,

$$
\gamma = \frac{N m \bar{g}}{\pi v_F},
\tag{2.28}
$$

and λ is the dimensionless coupling

$$
\lambda = \frac{3\bar{g}}{4\pi v_F \xi^{-1}} \qquad \bar{g} = g^2 \chi_0
\tag{2.29}
$$

At finite ξ^{-1} and vanishing ω, the self-energy has a Fermi liquid form:

$$
\Sigma(\omega) = \lambda \omega.
\tag{2.30}
$$

The Fermi liquid theory is stable in this case, and the low-energy quasiparticles have a finite effective mass:

$$
m^* = m(1 + \lambda).
\tag{2.31}
$$

The effective mass diverges proportionally to ξ in the vicinity of the QCP.

□ At criticality

At $\omega \gg (\gamma\xi^3)^{-1}$, however, the system is in the quantum-critical regime. Here the Fermi liquid theory breaks down in the sense that the quasiparticles damping becomes comparable to its energy. We have:

$$\Sigma(\omega) = \omega_0^{1/3}|\omega|^{2/3}\text{sign}(\omega), \tag{2.32}$$

where $\omega_0 = 3\sqrt{3}\bar{g}^2/(8\pi^2 N m v_F^2)$ is the same as in (2.19).

At the QCP, $\xi^{-1} = 0$, the region of Fermi-liquid behavior collapses in frequency space, and the $\omega^{2/3}$ dependence of the self-energy extends down to the lowest frequencies. The expression for $\Sigma(\omega)$ is valid for all frequencies below the cutoff Λ.

However, only frequencies $\omega \leq \omega_0$ are actually relevant for the quantum critical regime, as at higher frequencies the system behaves as a nearly ideal Fermi gas.

2.3.2   A few comments

□ General remarks

One has to make a few remarks concerning the Eliashberg solution obtained at the QCP:

▷ Curvature

  Note that the curvature of the fermionic dispersion is unimportant here for both self-energies, and only accounts for small corrections containing higher powers of frequencies.

▷ Direct perturbative expansion

  Comparing (2.27) and (2.32) with (2.15) and (2.18), we see that the self-energies in the Eliashberg theory coincide with the one-loop perturbative results around free fermions that we carried out in the previous section. This arises from the fact that the full fermionic propagator appears in both self-energies only via the fermionic density of states (DOS):

$$N(\omega) = \frac{i}{\pi} \int d\epsilon_k \frac{1}{\omega + \Sigma(\omega) - \epsilon_k}. \tag{2.33}$$

  This DOS reduces to $N(\omega) = \text{Sign}(\omega)$, independently on the self-energy: it remains the same as for free fermions.

▷ Bosonic momentum and frequency

  Note that Eq. (2.27) for the bosonic self-energy is only valid as long as the interplay between the external momentum and frequency is such that $v_F q \gg \Sigma(\Omega)$. When this is verified, the Landau damping term no longer depends on

the fermionic self-energy, which explains why we recover the same expression for the self-consistent treatment and the direct perturbative expansion. In the opposite limit, the vertex corrections cannot be neglected as we argue in the next section.

□ Mass-shells

A lot of the computations we carry out in the further sections are estimated based on the typical bosonic and fermionic momenta and frequencies. Indeed, from inspecting the propagators, one can isolate a region of the three-dimensional momentum-frequency space where they are maximum. It follows that the quantities we compute are dominated by these regions of the phase space.

We thus distinguish two "mass shells", defined respectively as:

- the fermionic one is given by $G(\mathbf{k}, \omega)^{-1} \simeq 0$, i.e. at the fermionic mass-shell, one has:

$$|\mathbf{k} - \mathbf{k_F}| \sim \frac{\omega + \Sigma(\omega)}{v_F} \tag{2.34}$$

- the bosonic mass-shell, on the other hand, is given by:

$$|\mathbf{q}| \sim (\gamma |\Omega|)^{1/3} \tag{2.35}$$

In the computations carried out in the next sections, we argue that the result strongly depends on the typical internal bosonic momentum and frequency. Depending whether one, two, or none of the components of this internal bosonic momentum vibrate on the bosonic mass-shell, we end up with very different results.

□ Factors of N

We argue in the next section that the extension of the model to N fermionic flavors is essential for the validity of the current approach. However, it can be readily seen from (2.27) and (2.32) that both self-energies contain factors of N through their prefactors.

In a "conventional" large-N approach, one would have to rescale the effective interaction $\bar{g}$ prior to taking the infinite N limit. In this situation, the bosonic polarization is of order $O(1)$ but the fermionic one vanishes like $1/N$ so that the large-N limit describes free fermions and overdamped bosons. However, we saw that the frequency dependence of the fermionic self-energy suggests that it might dominate over the bare propagator for N finite. It is thus reasonable to analyze the effects of this frequency-dependent self-energy.

Following this reasoning, we argue that our approach is *not* an infinite N limit, but rather an asymptotic expansion, where we keep N finite but consider it is large enough to allow us to neglect higher-powers of N.

For further analysis of the corrections to the Eliashberg theory, it is then convenient to rescale N out of the formulas for $\Sigma(\omega)$ and for $\Pi(q, \Omega)$. This can be done by rescaling m, m_B and k_F leaving v_F intact:

$$m \rightarrow m/N \qquad m_B \rightarrow m_B/N \qquad k_F \rightarrow k_F/N. \qquad (2.36)$$

We emphasize that the fermionic self-energy $\Sigma \propto \omega^{2/3}$ and the Landau damping term in the bosonic propagator do not contain N after rescaling. They are included into the new "zero-order" theory about which we then expand using $1/N$ as a small parameter. This theory includes:

$$\begin{cases} \chi(q, \Omega) &= \dfrac{\chi_0}{\xi^{-2} + q^2 + \gamma|\Omega|/q} \\ G(k, \omega) &= \dfrac{1}{i(\omega + \Sigma(\omega)) - \epsilon_k}. \end{cases} \qquad (2.37)$$

We can reformulate the Eliashberg theory by introducing the following effective Lagrangian describing the fermion-boson interaction:

$$L = L_F + L_B + L_{int} \text{ , with}$$

$$\begin{aligned} L_B &= T \sum_{q,n} \mathbf{S}_{q,n} \chi^{-1}(q, \Omega_n) \mathbf{S}_{-q,-n}, \\ L_F &= T \sum_{k,n,\alpha,j} c^\dagger_{k,j,n,\alpha} G^{-1}(k, \omega_n) c_{k,j,n,\alpha}, \\ L_{int} &= g T^2 \sum_{n,m,k,q} \mathbf{S}_{q,m} c^\dagger_{k,j,n\alpha} \sigma_{\alpha\beta} c_{k-q,j,n-m,\beta}, \end{aligned} \qquad (2.38)$$

where n, m number Matsubara frequencies, α, β are spin indices, j is a flavor index, and G and χ are given by (2.37). The upper limit of the frequency summation is the cutoff Λ.

We emphasize that there is no double counting in the bosonic propagator (2.37a). The integration of high-energy fermions, above the cutoff Λ leads to the momentum dependence of the static bosonic propagator, whereas the interaction at frequencies below Λ gives rise to the Landau damping, without affecting the static part.

To summarize, the Eliashberg-type theory at the QCP contains a non-analytic fermionic self-energy which scales as $\omega^{2/3}$ and breaks down the Fermi liquid description of fermions. At the same time, the bosonic propagator is regular – the only effect of the interaction with low-energy fermions is the appearance of a Landau damping.

We emphasize that the fully renormalized *bosonic* susceptibility does not necessarily coincide with the one in (2.37) and may, in particular, acquire an anomalous dimension [39]. However, this can only be due to infra-red divergent corrections to the Eliashberg theory, which are fully captured by the effective low-energy model of Eq. (2.38). An anomalous dimension was proved to emerge at the antiferromagnetic QCP in $d = 2$ [32, 39], but not in our case.

Expression	Definition	Eq.
v_F	Fermi velocity	(2.2)
m	bare quasiparticle mass, $m = k_F/v_F$	(2.2)
m^*	effective (renormalized) quasiparticle mass	(2.31)
m_B	band mass, determines the curvature of the Fermi surface	(2.2)
g	spin-fermion coupling constant	(2.4)
ξ	ferromagnetic correlation length	(2.3)
$\chi_0 \xi^2$	value of the spin susceptibility at $q = 0$	(2.3)
N	number of fermionic flavors	
$\bar{g} = g^2 \chi_0$	effective four-fermion interaction	(2.29)
$\gamma = \frac{N m \bar{g}}{\pi v_F}$	Landau damping coefficient	(2.28)
$\lambda = \frac{3 \bar{g} \xi}{4 \pi v_F}$	dimensionless coupling constant, it measures the mass enhancement: $\lambda = \frac{m^*}{m} - 1$	(2.29)
$\omega_0 = \frac{3\sqrt{3}\bar{g}^3}{8\pi^3 \gamma v_F^3} \sim \frac{\bar{g}^2}{E_F}$	frequency up to which $\Sigma(\omega)$ dominates over ω in the fermionic propagator	(2.32)
$\omega_{\text{Max}} = \sqrt{\gamma v_F^3} \sim \sqrt{\bar{g} E_F}$	frequency up to which the fermionic and the bosonic mass-shells are well separated	(2.42)
$\alpha = \frac{\bar{g}^2}{\gamma v_F^3} \sim \frac{\bar{g}}{E_F}$	small parameter measuring the slowness of the bosonic modes compared to the fermionic ones; the same small parameter justifies the low-energy description	(2.39)
$\beta = \frac{m_B}{mN}$	small parameter related to the curvature of the fermionic dispersion	(2.53)

Table 2.1: List of the various parameters used in the text, their expression before the rescaling in N, and the reference equation where it is defined in the text.

2.4 Validity of the approach

The essential part of the Eliashberg procedure is an a posteriori verification that the neglected terms in the self-energies are small. Quite generally, the validity of this procedure is based on the idea that the fermions are fast excitations compared to the bosons, and hence the fermionic and bosonic mass shells are well separated in energy.

When scattering off physical mass-shell bosons, the fermions are forced to vibrate on the bosonic mass shell, which is far away from their own. The electronic spectral function near the bosonic mass-shell is then small and this reduces the self-energy that arises from true fermion-boson scattering. In the case of the electron-phonon interaction, this is known as the Migdal theorem, and ensures that the corrections to the electron-phonon vertex are small.

The computation of the fermionic self-energy $\Sigma(\omega)$ gives us an idea of what the typical intermediate momenta and frequencies are in the problem. One can make sure that at criticality the typical fermionic momenta $k - k_F$ are of order $\Sigma(\omega)/v_F = \omega_0^{1/3}\omega^{2/3}/v_F$. On the other hand, the typical bosonic momenta $q_\perp$ along the direction of $\mathbf{k}_F$ (i.e. transverse to the Fermi surface) are of the same order as the typical fermionic momenta, while the momenta $q_\parallel$ transverse to $\mathbf{k}_F$ (i.e. along the Fermi surface) are of order $(\gamma\omega)^{1/3} \gg \omega_0^{1/3}\omega^{2/3}/v_F$. We see that for a given frequency ω, the typical $|q| = \sqrt{q_\perp^2 + q_\parallel^2}$ are much larger than $k - k_F$, i.e. the effective boson velocity is much smaller than v_F. One then expects that the extension of Migdal theorem to our model holds.

The ratio of the typical fermionic $k - k_F$ and bosonic $|q|$ at the same frequency ω is $(\omega_0\omega/\gamma v_F^2)^{1/3}$. At $\omega \sim \omega_0$, this ratio then becomes, after rescaling in N:

$$\alpha = \left(\frac{\omega_0^2}{\gamma v_F^3}\right)^{1/3} \sim \frac{\bar{g}}{E_F}, \tag{2.39}$$

and the slowness of the bosonic mode is then ensured in the quantum critical regime provided that $\alpha \ll 1$. This condition coincides, in our case, with the condition that the interaction should be smaller than the bandwidth. This is a necessary condition for the effective low-energy model to be valid, for if it is not satisfied, one cannot distinguish between contributions coming from low and from high energies.

However, the smallness of α is not sufficient. In the integral for the fermionic self-energy, only one component of the bosonic momentum, $q_\parallel$, is much larger than $k - k_F$, the other one is comparable: $q_\perp \sim k - k_F$. One needs to check whether the corrections to the Eliashberg theory scale as the ratio of $k - k_F$ to the modulus of $|\mathbf{q}|$ or one of its components.

To address these issues, we explicitly compute the vertex corrections and the fermionic self-energy at the two-loop level.

2.4.1 Vertex corrections

We consider the vertex corrections due to the insertion of one bosonic propagator (three-leg vertex) and two bosonic propagators (four-leg vertex). The behavior of these vertex corrections strongly depends on the interplay between the internal and external momenta and frequencies. We present the results below and discuss technical details of the calculations in Appendix C.

In the case of the three-leg vertex, the result strongly depends on the interplay between external as well as internal momentum and frequency. We thus distinguish between three cases.

□ Three-leg vertex with zero external momentum and frequency

We begin with the simplest 3-leg vertex, with strictly zero incoming frequency Ω and momentum q. The one-loop vertex renormalization diagram contains one bosonic line and is presented in Fig. 2.2a. In analytic form, it writes:

$$
\begin{aligned}
\left.\frac{\Delta g}{g}\right|_{q=\Omega=0} \quad &\sim \quad g^2 \int d\omega d^2p \; G(\mathbf{k_F},\omega)^2 \; \chi(\mathbf{p},\omega) \\
&\sim \quad \bar{g}\int \frac{d\omega d^2p}{\frac{\gamma|\omega|}{p} + p^2} \frac{1}{\left(i\tilde{\Sigma}(\omega) - v_F p_x - \frac{p_y^2}{2m_B}\right)^2},
\end{aligned}
\tag{2.40}
$$

where we defined $\tilde{\Sigma}(\omega) = \omega + \Sigma(\omega)$ and we have chosen $\mathbf{k}_F$ along the x axis, so that $p_x = p_\perp$ and $p_y = p_\parallel$.

Since the poles coming from the fermionic Green's functions are in the same half plane, the integral over q_x is only non-zero because of the branch cut in the bosonic propagator. At the branch cut $p_x \sim p_y$, so that we can safely drop the quadratic term in the fermionic propagators. Introducing polar coordinates, and integrating successively over the angle between $\mathbf{k_F}$ and $\mathbf{p}$, then over the modulus p, we obtain:

$$
\left.\frac{\Delta g}{g}\right|_{q=\Omega=0} \quad \sim \quad \frac{\bar{g}}{\gamma v_F^3}\int_0^{\omega_{\mathrm{Max}}} d\omega \frac{\tilde{\Sigma}(\omega)}{\omega},
\tag{2.41}
$$

where ω_{Max} is the frequency up to which bosons are slow modes compared to fermions, i.e. up to which $\tilde{\Sigma}(\omega)/v_F \ll (\gamma\omega)^{1/3}$. This frequency exceeds ω_0, so to find it we have to use $\tilde{\Sigma}(\omega) \approx \omega$. We then obtain:

$$
\omega_{\mathrm{Max}} \sim \sqrt{\gamma v_F^3}.
\tag{2.42}
$$

which reduces to $\omega_{\mathrm{Max}} \sim \sqrt{\bar{g}E_F}$ after the rescaling in N. Note that for small values of α, $\omega_{\mathrm{Max}} \gg \omega_0$, and the maximum frequency up to which the bosons can be treated as slow modes well exceeds the upper limit of the quantum-critical behavior.

Substituting $\tilde{\Sigma}$ and ω_{Max} into (2.41), we obtain

$$\left. \frac{\Delta g}{g} \right|_{q=\Omega=0} \sim \sqrt{\alpha} \tag{2.43}$$

This correction to the vertex can then be neglected provided that α is small.

□ Three-leg vertex with finite external momentum

We now turn to the three-leg vertex with zero external frequency but a finite bosonic momentum $\mathbf{q}$. The one-loop renormalization is given in Fig.2.2, and its analytic form writes:

$$\begin{aligned}
\left. \frac{\Delta g}{g} \right|_{q,\Omega=0} \sim \; & g^2 \int d\omega d^2p \; G(\mathbf{k_F} + \mathbf{p} + \mathbf{q}, \omega) G(\mathbf{k_F} + \mathbf{p}, \omega) \chi(\mathbf{p}, \omega) \\
\sim \; & \bar{g} \int \frac{d\omega d^2p}{\frac{\gamma|\omega|}{p} + p^2} \frac{1}{i\tilde{\Sigma}(\omega) - v_F p_x - \frac{p_y^2}{2m_B}} \\
& \times \frac{1}{i\tilde{\Sigma}(\omega) - v_F q_x - v_F p_x - \frac{p_y^2}{2m_B} - \frac{q_y p_y}{m_B}},
\end{aligned} \tag{2.44}$$

where p_x is the projection of $\mathbf{p}$ along $\mathbf{k_F}$.

As before, the integral over p_x can be reduced to the contribution from only the branch cut in the bosonic propagator. At the branch cut, $p_x \sim p_y$, hence we can neglect the quadratic term in the fermionic Green's function, which then allows us to integrate over p_y. Expanding in q_x, and subtracting the constant term at zero momentum calculated in (2.41), we obtain:

$$\begin{aligned}
\left. \frac{\Delta g}{g} \right|_{q,\Omega=0} - \left. \frac{\Delta g}{g} \right|_{q=\Omega=0} \sim \; & i \frac{q_x}{k_F} \int_{|v_F q_x|} \frac{d\omega}{|\omega|} \log[i\tilde{\Sigma}(\omega)] \\
\sim \; & \frac{q_x}{k_F} \log|q_x|,
\end{aligned} \tag{2.45}$$

When not only the bosonic momentum q is finite but also the external fermionic momentum is away from k_F, the $q \log q$ dependence of the static vertex correction survives, but the argument of the logarithm is the maximum of the bosonic q and fermionic $k - k_F$ (we directed both along x).

In general, the typical value of q_x is much smaller than k_F, hence the momentum dependent part of this vertex correction is small. However, we argue in the next chapter that because of the logarithmic term in (2.45), the insertion of this vertex correction into the static susceptibility gives rise to a non-analytic term.

We also emphasize that although the calculations of $\left. \frac{\Delta g}{g} \right|_{q=\Omega=0}$ and $\left. \frac{\Delta g}{g} \right|_{q,\Omega=0}$ look similar, the characteristic bosonic momenta are different for the two cases. At

$q = \Omega = 0$, the typical bosonic momenta in (2.40) are of order $(\gamma\omega)^{1/3}$, i.e. near the bosonic mass shell. On the other hand, the typical bosonic momenta in (2.44) are of order $\tilde{\Sigma}(\omega)/v_F$, i.e. near the fermionic mass shell. This is why only one of these two vertex corrections is small in α, as this parameter measures the slowness of the bosonic modes compared to the fermionic ones.

□ Generic three-leg vertex

We next consider the same vertex with small but finite external momentum q and frequency Ω. This diagram, presented in Fig. 2.2b, reads:

$$
\begin{aligned}
\left.\frac{\Delta g}{g}\right|_{q,\Omega} &\sim g^2 \int d\omega d^2 p \; G(\mathbf{k_F} + \mathbf{p} + \mathbf{q}, \omega + \Omega) G(\mathbf{k_F} + \mathbf{p}, \omega) \; \chi(\mathbf{p}, \omega) \\
&\sim \bar{g} \int \frac{d\omega d^2 p}{\frac{\gamma|\omega|}{p} + p^2} \frac{1}{i\tilde{\Sigma}(\omega) - v_F p_x - \frac{p_y^2}{2m_B}} \\
&\qquad \times \frac{1}{i\tilde{\Sigma}(\omega + \Omega) - v_F q_x - v_F p_x - \frac{p_y^2}{2m_B} - \frac{q_y p_y}{m_B}},
\end{aligned}
\tag{2.46}
$$

where we have chosen $\mathbf{k}_F$ along the x axis, so that $q_x = q_\perp$ and $q_y = q_\parallel$.

Integrating over p_x first, one obtains two contributions: one arising from the poles in the fermionic Green's functions (which now can be in different half-planes since Ω is finite), and the other from the branch cut in the bosonic propagator. The latter leads to the same result as (2.41), up to small corrections due to the finiteness of the external q and Ω.

Focusing on the other contribution, one has:

$$
\left.\frac{\Delta g}{g}\right|_{q,\Omega} \sim i\frac{\bar{g}}{v_F} \int_0^\Omega d\omega \int dp_y \frac{|p_y|}{\gamma|\omega| + |p_y|^3} \frac{1}{i\tilde{\Sigma}(\Omega - \omega) + i\tilde{\Sigma}(\omega) - v_F q_x - \frac{q_y p_y}{m_B}},
\tag{2.47}
$$

where the simplification of the frequency integral comes from the pole structure in p_x.

This generic correction to the vertex strongly depends on the interplay between the external q_x, q_y, and Ω.

When q and Ω are both finite,

$$
\left.\frac{\Delta g}{g}\right|_{q,\Omega} \sim \mathcal{F}\left(\frac{v_F q}{\Sigma(\Omega)}\right),
\tag{2.48}
$$

where

$$
\mathcal{F}(x) = \int_0^1 \frac{dz}{z^{1/3}} \frac{1}{(1-z)^{2/3} + z^{2/3} + ix}
\tag{2.49}
$$

has the following asymptotic behavior:

$$
\begin{cases}
\mathcal{F}(x \ll 1) &= O(1) \\
\mathcal{F}(x \gg 1) &= O\left(\frac{1}{x}\right)
\end{cases}
\tag{2.50}
$$

If the typical external momentum q is on the bosonic mass shell, then $q \sim (\gamma\Omega)^{1/3}$, and one has:

$$\left.\frac{\Delta g}{g}\right|_{q,\Omega} \sim \frac{\Sigma(\Omega)}{v_F q_x} \sim \sqrt{\alpha} \left(\frac{\Omega}{\omega_{\text{Max}}}\right)^{1/3}. \tag{2.51}$$

This is obviously small in α.

It turns out that the behavior of the vertex correction is more complex and the result for $\Delta g/g$ strongly depends on the direction of q compared to the direction of $\mathbf{k}_F$.

This directional dependence is important for our purposes as we saw in previous computations that in the fermionic self-energy, only the y component of the internal bosonic momentum is near the bosonic mass shell and scales as $(\gamma\Omega)^{1/3}$, while the x component of the bosonic momentum is much smaller and is actually of the order of $\tilde{\Sigma}(\omega)/v_F$, i.e. is near the fermionic mass shell.

Let's take a more careful look at this vertex correction, depending on the direction of q.

For the case where $q_x \sim \tilde{\Sigma}(\Omega)/v_F$ and $q_y \sim (\gamma\Omega)^{1/3}$, one would argue from (2.51) that the vertex correction now becomes of order $O(1)$ and is no longer parametrically small. However, the computation that lead to (2.51) cannot be extended to the strongly anisotropic case as for external $q_x \sim \tilde{\Sigma}(\Omega)/v_F$ and $q_y \sim (\gamma\Omega)^{1/3}$, the curvature of the fermionic dispersion becomes relevant and changes the result.

The full dependence on q_x and q_y is rather complex and we restrict ourselves to the case when the importance of the curvature ensures that $\frac{1}{N}\frac{m_B}{m} \ll 1$. In this situation, $q_y^2/m_B \sim (v_F q_x)/\beta \gg v_F q_x$, so that the quadratic term in the fermionic propagator dominates.

Performing the integration, we then find that:

$$\left.\frac{\Delta g}{g}\right|_{q,\Omega} \sim \beta^2 \left(\frac{\gamma\Omega}{q_y^3}\right)^{2/3} \log^2\left[\beta\frac{(\gamma\Omega)^{1/3}}{q_y}\right]$$
$$\sim \beta^2 \log^2 \beta, \tag{2.52}$$

where

$$\beta = \frac{1}{N}\frac{m_B}{m} \ll 1. \tag{2.53}$$

It follows that even when only one component of the bosonic momentum is near the bosonic mass shell, the vertex correction is small if β is small. This is the second condition for the Eliashberg theory to be controllable at criticality.

The smallness of β can be ensured by either extending the theory to large values of N, or by considering a very strong curvature of the Fermi surface which implies that $m_B \ll m$. Even though the latter can hardly be satisfied for realistic Fermi surfaces, we emphasize that the curvature of the dispersion plays a crucial role in the theory, for even in the case of $N \gg 1$, the vertex correction is of order $O(1)$ without this very curvature.
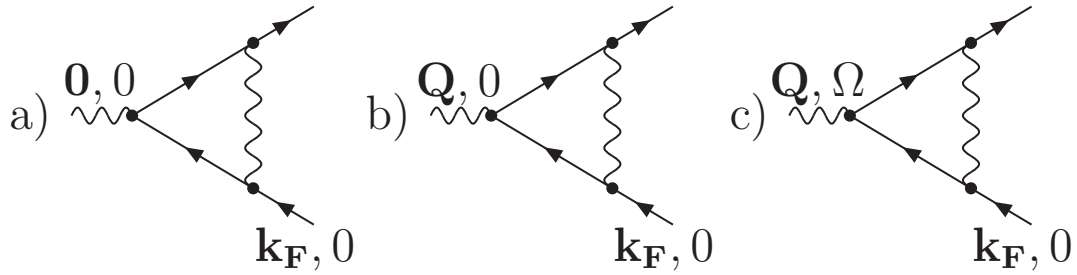
Figure 2.2: Three-leg vertices: a) zero external momentum and frequency b) finite momentum c) generic vertex.

☐ **Pairing vertex**

By contrast to the previous vertices we studied, the pairing vertex in the Cooper channel is not sensitive to the curvature of the Fermi surface. This leads to a vertex of order $O(1)$ even in the large-N limit and the pairing problem then has to be carried out exactly within the Eliashberg theory.

This vertex renormalization is presented in Fig. 2.3 and its analytic form is given by:

$$
\frac{\Delta g}{g}\bigg|_{\text{Cooper}} \sim g^2 \int d\omega d^2q \ \chi(\mathbf{q},\omega) \ G(\mathbf{k_F}+\mathbf{q},\omega)G(-\mathbf{k_F}-\mathbf{q},-\omega-\Omega)
$$

$$
\sim \bar{g} \int \frac{d\omega d^2q}{\frac{\gamma|\omega|}{q}+q^2} \frac{1}{i\tilde{\Sigma}(\omega)-v_Fq_x-\frac{q_y^2}{2m_B}} \frac{1}{-i\tilde{\Sigma}(\omega+\Omega)-v_Fq_x-\frac{q_y^2}{2m_B}}.
$$

Integrating over q_x, restricting ourselves to the contribution from the fermionic poles (the one from the branch cut can be proved to be smaller), we find that the quadratic terms cancel out, leaving us with:

$$
\frac{\Delta g}{g}\bigg|_{\text{Cooper}} \sim \frac{\bar{g}}{v_F} \int_{|\Omega|}^D \frac{d\omega}{\tilde{\Sigma}(\omega+\Omega)+\tilde{\Sigma}(\omega)} \int_0^\infty \frac{dq_y \ q_y}{\gamma\omega+q_y^3}. \tag{2.54}
$$

Performing the remaining integral, the prefactor simplifies and we obtain:

$$
\frac{\Delta g}{g}\bigg|_{\text{Cooper}} \sim \frac{\bar{g}}{\gamma^{1/3}\omega_0^{1/3}v_F} \log\left|\frac{\Omega}{D}\right|
$$

$$
\sim \log\left|\frac{\Omega}{D}\right|, \tag{2.55}
$$

where we assumed that we were in the quantum critical regime, i.e. $|\Omega| < \omega_0$.

We emphasize that the prefactor of the log in (2.55) is $O(1)$, even when one takes into account the curvature of the fermionic dispersion. The result of Eq. (2.55) confirms previous studies [40] advocating that the system at a ferromagnetic QCP can lead to a superconducting instability.

□ Four-leg vertex

We consider now higher-order corrections to the vertex through the example of a four-leg vertex correction with two crossed bosonic lines, also called a Cooperon insertion. Analytically, the expression for this renormalized vertex, presented diagrammatically in Fig. 2.3, writes:

$$
\Gamma_2(q, \Omega) \sim \bar{g}^2 \int d\omega d^2p \, \chi_s \left(\frac{\Omega + \omega}{2}, \frac{\mathbf{p} + \mathbf{q}}{2} \right) \chi_s \left(\frac{\Omega - \omega}{2}, \frac{\mathbf{q} - \mathbf{p}}{2} \right)
$$
$$
\times G \left(\frac{\Omega + \omega}{2}, \mathbf{k_F} + \frac{\mathbf{p} + \mathbf{q}}{2} \right) G \left(\frac{\Omega - \omega}{2}, \mathbf{k_F} + \frac{\mathbf{q} - \mathbf{p}}{2} \right) \quad (2.56)
$$

After integrating over p_x (projection of $\mathbf{p}$ along $\mathbf{k_F}$), and ω, we are left with:

$$
\Gamma_2(q, \Omega) \sim \frac{\bar{g}^2}{v_F} \frac{\Omega}{|q_y|^3} \int dz \frac{\sqrt{\left(z^2 + \frac{q^2}{q_y^2} \right)^2 - 4z^2}}{2i\Sigma\left(\frac{\Omega}{2} \right) - v_F q_x - \frac{q_y^2}{4m}(1 + z^2)}
$$
$$
\times \frac{1}{\left(z^2 + 2z + \frac{q^2}{q_y^2} \right)^{3/2} + \frac{\gamma|\Omega|}{|q_y|^3}} \frac{1}{\left(z^2 - 2z + \frac{q^2}{q_y^2} \right)^{3/2} - \frac{\gamma|\Omega|}{|q_y|^3}}, \quad (2.57)
$$

where we have changed p_y into $z = p_y/|q_y|$.

This renormalized 4-leg vertex $\Gamma_2(q, \Omega)$ has to be compared with the bare four-leg vertex, whose analytic form is given by the bosonic propagator multiplied by g^2:

$$
\Gamma_1(q, \Omega) \sim \frac{\bar{g}}{q^2 + \frac{\gamma|\Omega|}{q}}. \quad (2.58)
$$

In the case of a typical external momentum $q_x \sim q_y \sim (\gamma\Omega)^{1/3}$, the ratio Γ_2/Γ_1 is of order α. For a typical $q_x \sim \tilde{\Sigma}(\omega)/v_F$ and $q_y \sim (\gamma\omega)^{1/3}$, we obtain, to logarithmic accuracy:

$$
\frac{\Gamma_2}{\Gamma_1} \sim \beta \ll 1. \quad (2.59)
$$

This last result again critically depends on the curvature of the Fermi surface: neglecting the quadratic terms in the fermionic propagators, one would obtain $\Gamma_2/\Gamma_1 = O(1)$. We see that likewise to the three-loop vertices, the smallness of the crossed vertex $\Gamma_2(q, \Omega)$ requires both α and β to be small.

2.4.2 Self-energy corrections

The second element one has to check in order to validate the Eliashberg procedure concerns the momentum-dependent self-energy. After verifying on the practical example of the two-loop self-energy, that the vertex correction analyzed above are indeed small, we turn to the computation of the momentum-dependent self-energy and the density of states.
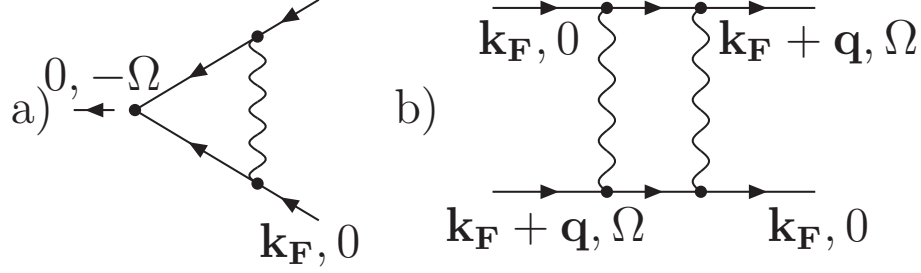
Figure 2.3: a) Cooper pairing vertex b) Four-leg vertex

□ Corrections to the self-energy at the two-loop level

We found in our analysis of the vertex corrections that the result depends on the interplay between the typical momentum and frequency. In our estimates, we considered two regions of external q and Ω, namely $q_x \sim q_y \sim (\gamma\Omega)^{1/3}$ and $q_x \sim \tilde{\Sigma}(\omega)/v_F$, $q_y \sim (\gamma\Omega)^{1/3}$. In both cases, we found that the vertex corrections are small.

We verify here that the two-loop self-energy, obtained by inserting vertex corrections into the one-loop self-energy diagram, is also small.

The two-loop self-energy diagram is presented in Fig. 2.1. We have:

$$\Sigma_2(\omega) \sim \bar{g}^2 \int d\omega_1 d^2q_1 \int d\omega_2 d^2q_2 \; \chi(\mathbf{q_1}, \omega_1) \; \chi(\mathbf{q_2}, \omega_2) \; G(\mathbf{k_F} + \mathbf{q_1}, \omega + \omega_1)$$
$$\times G(\mathbf{k_F} + \mathbf{q_2}, \omega + \omega_2) \; G(\mathbf{k_F} + \mathbf{q_1} + \mathbf{q_2}, \omega + \omega_1 + \omega_2)$$
$$\sim \bar{g}^2 \int d\omega_1 d^2q_1 \int d\omega_2 d^2q_2 \frac{q_1}{\gamma|\omega_1| + q_1^3} \frac{q_2}{\gamma|\omega_2| + q_2^3}$$
$$\times \frac{1}{i\tilde{\Sigma}(\omega + \omega_1) - v_F q_{1x}} \frac{1}{i\tilde{\Sigma}(\omega + \omega_2) - v_F q_{2x} - \frac{q_{2y}^2}{2m_B}}$$
$$\times \frac{1}{i\tilde{\Sigma}(\omega + \omega_1 + \omega_2) - v_F q_{1x} - v_F q_{2x} - \frac{q_{1y}^2}{2m} - \frac{q_{2y}^2}{2m_B}}, \qquad (2.60)$$

where we recall $\tilde{\Sigma}(\omega) = \omega + \Sigma(\omega)$.

Integrating successively over q_{1x} and q_{2x}, and rescaling the remaining momentum components by introducing $x = q_{1y}/(\gamma|\omega_1|)^{1/3}$ and $y = q_{2y}/(\gamma|\omega_2|)^{1/3}$, we obtain:

$$\Sigma_2(\omega) \sim \frac{m_B \bar{g}^2}{v_F^2} \int_0^\omega d\omega_2 \int_{\omega - \omega_2}^\omega d\omega_1 \frac{1}{(\gamma^2 \omega_1 \omega_2)^{2/3}} \int_{-\infty}^\infty \frac{dx dy}{xy + i\zeta} \frac{|xy|}{(1 + |x|^3)(1 + |y|^3)} \qquad (2.61)$$

where $\zeta = m_B \frac{\tilde{\Sigma}(\omega + \omega_1) + \tilde{\Sigma}(\omega + \omega_2) - \tilde{\Sigma}(\omega + \omega_1 + \omega_2)}{(\gamma^2 \omega_1 \omega_2)^{1/3}}$.

As the typical frequencies ω_1 and ω_2 are of order ω, the typical value of ζ is of order $\beta \ll 1$. Expanding then in (2.61) to first order in ζ and performing the

remaining integrals, we obtain in the quantum-critical regime:

$$\Sigma_2(\omega) \sim \frac{m\bar{g}^2}{v_F^2} \int_0^\omega d\omega_2 \int_{\omega-\omega_2}^\omega d\omega_1 \frac{\zeta \log^2 \zeta}{(\gamma^2 \omega_1 \omega_2)^{2/3}}$$
$$\sim \Sigma(\omega) \, \beta^2 \log^2 \beta, \tag{2.62}$$

where $\Sigma(\omega) = \Sigma_1(\omega) = \omega_0^{1/3} \omega^{2/3}$ is the self-energy in the Eliashberg theory.

This result agrees with the one obtained in [30], and shows that $\Sigma_2(\omega) \sim \Sigma_1(\omega) \times \frac{\Delta g}{g}\Big|_{q,\Omega}$ where $\frac{\Delta g}{g}\Big|_{q,\Omega}$ is given by (2.52). This last result implies that the typical internal q and Ω for the Eliashberg self-energy and for $\Sigma_2(\omega)$ are the same.

It is also instructive to compare these two-loop results, obtained as an expansion around the Eliashberg solution, to the perturbative expansion around free fermions. In the latter, we found in Eq. (2.23) that $\Sigma_2(\omega) \sim \omega \log^2 \omega$ whereas in the former we have $\Sigma_2(\omega) \propto \beta(\omega_0^{1/3}\omega^{2/3}) \log^2 \beta$, Eq. (2.62). The free-fermion result can be reproduced if we neglect the self-energy in (2.61). We see that the expansion around free fermions does not reproduce the correct frequency dependence of $\Sigma_2(\omega)$. This obviously implies that if one expands around free fermions, there exist higher-order terms associated with insertions of the self-energy $\Sigma(\omega)$ into the internal fermionic lines, which may overshadow the two-loop result around free fermions. Accordingly, near the QCP, the expansion around free fermions does not converge, even if the curvature of the fermionic dispersion is included. On the other hand, the expansion around the Eliashberg solution is regular and holds in powers of the small parameters α and β.

□ Momentum dependence of the self-energy and the density of states

Along with the vertex corrections, we also neglected the momentum dependence of the fermionic self-energy in order to proceed with the Eliashberg scheme. We now verify whether the momentum dependent part of the self-energy $\Sigma(\mathbf{k}, \omega = 0) = \Sigma(\mathbf{k})$ remains small when evaluated with the full fermionic propagator. The k dependent self-energy is given by:

$$\Sigma(\mathbf{k}, 0) = 3ig^2 \int \frac{d^2q \, d\Omega}{(2\pi)^3} G(\mathbf{k} + \mathbf{q}, \Omega) \chi(\mathbf{q}, \Omega)$$
$$= \frac{3i\bar{g}}{(2\pi)^3} \int \frac{d\Omega d^2q}{i\tilde{\Sigma}(\Omega) - \epsilon_{k+q}} \frac{q}{\gamma|\Omega| + q^3}. \tag{2.63}$$

Defining the angular variable θ as $\epsilon_{k+q} = \epsilon_k + v_F q \cos\theta$, integrating over it, and expanding to linear order in $\epsilon_\mathbf{k}$ we obtain:

$$\Sigma(\mathbf{k}, 0) = -3i\epsilon_k \times \frac{\bar{g}}{2\pi^2} \int_0^\infty d\Omega \, \tilde{\Sigma}(\Omega) \int \frac{q^2 dq}{\left(q^3 + (\gamma|\Omega|)\right) \left((v_F q)^2 + \tilde{\Sigma}(\Omega)^2\right)^{3/2}}. \tag{2.64}$$

A simple experimentation with the integrals shows that the integration over momentum is confined to $q \sim \tilde{\Sigma}(\Omega)/v_F$, while the frequency integral is confined to $\Omega < \omega_{\text{Max}}$, where ω_{Max}, defined in (2.42), is the scale where $(\gamma\Omega)^{1/3} = \tilde{\Sigma}(\Omega)/v_F$. The computation of $\Sigma(\mathbf{k})$ is given in the Appendix B, and the result is

$$\Sigma(\mathbf{k}, 0) = -i\epsilon_k \times \frac{3 \times 1.3308}{2\sqrt{2}\pi^{3/2}}\sqrt{\alpha} = -i\epsilon_k \ 0.253\sqrt{\alpha} \tag{2.65}$$

Plugging this back into the fermionic propagator, we then obtain that $\Sigma(\mathbf{k}, 0)$ gives rise to a small, regular correction to the quasiparticle mass $\epsilon_k - i\Sigma(\mathbf{k}, 0) = \epsilon_k^* = v_F^*(k - k_F)$, where

$$v_F^* = v_F \ \left(1 - 0.253\sqrt{\alpha}\right). \tag{2.66}$$

Like the vertex correction at zero external bosonic momentum and frequency, this small correction is of order $O(\sqrt{\alpha})$ and comes from frequencies of order ω_{Max}.

The momentum dependent self-energy, unlike the frequency dependent part, generally gives rise to corrections to the fermionic density of states (DOS)

$$N(\omega) \sim -\int \frac{d\epsilon_k}{\pi} \text{Im} G(\epsilon_k, \omega). \tag{2.67}$$

Assuming that $\Sigma(\mathbf{k})$ is small and expanding in it in the fermionic propagator, we obtain, in real frequencies

$$\frac{N(\omega)}{N_0} \sim 1 - \text{Im} \left(\left. \frac{\Sigma(\mathbf{k})}{\epsilon_k} \right|_{\epsilon_k = i\tilde{\Sigma}(-i\omega)} \right), \tag{2.68}$$

where N_0 is the density of states of free fermions.

Substituting (2.65) into (2.68), we find that the density of states just shifts by a constant. It follows that in order to extract the frequency dependence of the density of states, one has to evaluate the momentum-dependent self-energy to the next order in ϵ_k and on the mass shell, where $\epsilon_k = i\tilde{\Sigma}(\omega)$.

The evaluation of the self-energy near a mass shell generally requires extra caution as the self-energy may possess mass-shell singularities [33]. We, however, have checked in Appendix F that in our case the self-energy does not possess any mass-shell singularity, and the self-energy remains finite on the mass shell.

The calculation of the self-energy to order ϵ_k^2 is displayed in the Appendix B, and the result is

$$\Sigma(\mathbf{k}, \omega) = i\epsilon_k \times \frac{0.45}{8\pi}\alpha|\Sigma(\omega)| \log \frac{\omega_1}{|\omega|} \tag{2.69}$$

on the mass-shell.

Substituting this self-energy into the expression for the DOS and converting to real frequencies, we find at small ω

$$N(\omega) \sim N_0 \left(1 - \left(\frac{\omega}{\omega_1}\right)^{2/3} \log^2 \frac{\omega_{\text{Max}}}{\omega}\right), \tag{2.70}$$

where we explicitly defined

$$\omega_1 = \frac{128\pi^{5/2}}{0.45^{3/2}\ 3^{3/4}}\frac{\bar{g}}{\alpha^2}. \tag{2.71}$$

2.4.3 Summary

We have shown in this section that there are two conditions for the validity of the Eliashberg theory that one can recast as the smallness of two parameters:

$$\alpha \sim \frac{\bar{g}^2}{\gamma v_F^3} \sim \frac{\bar{g}}{E_F} \ll 1 \qquad \beta \sim \frac{m\bar{g}}{\gamma v_F} \sim \frac{m_B}{Nm} \ll 1. \tag{2.72}$$

The first condition is quite generic for a low-energy theory since it requires that the fermion-fermion interaction mediated by the exchange of a boson should be smaller than the Fermi energy. Otherwise, the physics is not restricted to the vicinity of the Fermi surface anymore. The parameter α plays the same role as the Migdal parameter for the electron-phonon interaction: it sets the condition that fermions are fast excitations compared to bosons. In the scattering processes that are small in α, fermions are forced by the interaction to vibrate at frequencies near the bosonic mass shell. They are then far from their own resonance and thus have a small spectral weight.

However, the condition $\alpha \ll 1$ is not sufficient to construct a fully controllable perturbative expansion around the non-Fermi liquid state at the QCP. In spatially isotropic systems there exist vertex corrections for which the external momentum has a component on the fermionic mass-shell. These corrections don't contain α. However, these corrections are sensitive to the curvature of the Fermi surface, and are small if β is small which can be achieved either by imposing $m_B \ll m$ or by extending the theory to a large number N of fermionic flavors.

In evaluating the renormalization of the static vertex, we silently assumed that $\sqrt{\alpha} \ll \beta$, i.e., $\bar{g}/E_F < (m_B/m)^2/N$. At very large N, this is no longer valid, but in this situation our estimates show that the static vertex is even smaller than $\sqrt{\alpha}$.

Finally, the pairing vertex in the Cooper channel stays of order $O(1)$, signaling the possibility of a pairing instability close to the quantum critical point. Nevertheless, we assume, based on explicit calculations worked out in [40], that the quantum critical behavior extends in the parameter space to a region where the superconductivity is not present.

CHAPTER 3

Static spin susceptibility

Contents

In this chapter, we revisit the Hertz-Millis-Moriya ϕ^4 theory using the solution of our Eliashberg scheme at criticality. We then turn to the computation of the static spin susceptibility, following the remarks of Belitz and collaborators: now that we
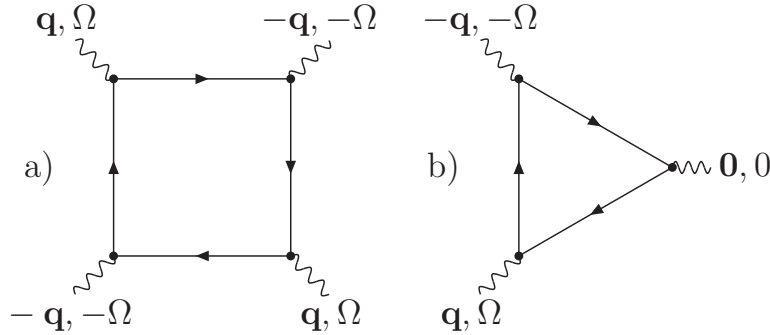
Figure 3.1: "ϕ^4" and "ϕ^3" type diagram

have derived a controllable way of describing the quantum critical regime, we can estimate whether the non-analytic corrections associated to the Fermi liquid regime survives at criticality. We indeed prove that this non-analytic term does not survive at criticality but another one, weaker, is still present. Finally, we study whether this analysis is limited to the ferromagnetic QCP or can be extended to other physical models.

3.1   Revisiting the Hertz-Millis-Moriya theory

As we argued in the first chapter, it is widely believed that an itinerant fermionic system near a ferromagnetic QCP is adequately described by a phenomenological $2 + 1$D ϕ^4 bosonic theory (in our case, the role of ϕ is played by the vector field **S**) with the dynamic exponent $z = 3$ and a constant prefactor for the ϕ^4 term [3, 14, 13]. In dimensions $d \geq 4 - z = 1$, the model lies above its upper critical dimension and the ϕ^4 term is simply irrelevant.

   In this section, we derive the effective ϕ^4 theory from the spin-fermion model Hamiltonian, and show that it contains two new elements absent from the phenomenological HMM approach. First, the prefactor of the ϕ^4 term strongly depends on the ratio between the external momenta and frequencies, and contains a non-analytic term in addition to the constant one. Second, there also exists a cubic ϕ^3 term whose prefactor, although vanishing in the static limit, also strongly depends on the interplay between the external momenta and frequencies.

3.1.1 ϕ^4 **term**

In order to derive a quantum critical ϕ^4 model, one has to integrate the fermions out of the partition function, noticing that the Lagrangian of the spin-fermion model is quadratic in the fermions.

   Expanding then in the number of bosonic fields **S**, the quartic term in the effective

66

action reads:

$$\int \frac{d^2q d^2p d^2p' \, d\Omega d\nu d\nu'}{(2\pi)^9} \, A(\mathbf{p}, \mathbf{p}', \mathbf{q}, \nu, \nu', \Omega) \left[\mathbf{S}_{p+q/2} \cdot \mathbf{S}_{q/2-p} \, \mathbf{S}_{p'-q/2} \cdot \mathbf{S}_{-p'-q/2} \right.$$

$$\left. + \, \mathbf{S}_{p+q/2} \cdot \mathbf{S}_{-p'-q/2} \, \mathbf{S}_{q/2-p} \cdot \mathbf{S}_{p'-q/2} \, - \, \mathbf{S}_{p+q/2} \cdot \mathbf{S}_{p'-q/2} \, \mathbf{S}_{-q/2-p'} \cdot \mathbf{S}_{q/2-p} \right] \tag{3.1}$$

where p, p', q are bosonic momenta, and ν, ν', Ω are bosonic frequencies.

Our goal here is to prove that the prefactor A is not a regular function of momenta and frequencies. To simplify the presentation, we choose to study only the dependence of A on $\mathbf{q}$ and Ω and set $\mathbf{p}, \mathbf{p}', \nu, \nu'$ to zero (see Fig 3.1).

The analytic form of this prefactor then writes:

$$A(q, \Omega) \sim N g^4 \int d\omega \, \int d^2k \, G(\mathbf{k}, \omega)^2 \, G(\mathbf{k} + \mathbf{q}, \omega + \Omega)^2. \tag{3.2}$$

Defining θ as the angle between $\mathbf{k}$ and $\mathbf{q}$, and performing the integration over ϵ_k, and the angular variable, we find:

$$A(q, \Omega) \sim \frac{m g^4}{\omega_0 \Omega} \int_0^1 dy \frac{\left[\left(\frac{v_F q}{\Sigma(\Omega)} \right)^2 - 2 \left(y^{2/3} + (1-y)^{2/3} \right)^2 \right]}{\left[\left(\frac{v_F q}{\Sigma(\Omega)} \right)^2 + \left(y^{2/3} + (1-y)^{2/3} \right)^2 \right]^{5/2}}, \tag{3.3}$$

where we performed the rescaling in N, defined $y = \omega/\Omega$, and neglected at this stage a regular part that comes from large values of ϵ_k and for which the curvature is relevant.

We see that $A(q, \Omega)$ depends on the interplay between the momentum and frequency. We can identify two regimes

- If $|q| \sim (\gamma|\Omega|)^{1/3}$, i.e. if the bosonic momenta are near the bosonic mass shell, the self-energy in the denominator can be neglected. The frequency factors in the numerator and the denominator then cancel out, and we obtain:

$$A(\Omega) \sim \frac{m g^4}{\gamma v_F^3} \sim \frac{m}{\chi_0^2} \, \alpha \,, \tag{3.4}$$

We see that A can be safely replaced by a constant $O(\alpha)$. This is consistent with the previous works of Hertz, Millis and Moriya. The agreement is not surprising as the relation $q \sim (\gamma|\Omega|)^{1/3}$ is assumed in the power counting based on the fact that the dynamic exponent $z = 3$. Note that the condition $|q| \sim (\gamma|\Omega|)^{1/3}$ only specifies the magnitude of q, one of its components (e.g., q_x) can be much smaller.

- If $q \sim \tilde{\Sigma}(\omega) \sim \omega_0^{1/3} \Omega^{2/3} v_F$ (at $\omega < \omega_0$), i.e. when a boson resonates near a fermionic mass shell, the scaling arguments of the $z = 3$ theory are no longer applicable. We have in this regime:

$$A(q, \Omega) \sim \frac{mg^4}{\omega_0 \Omega} \sim \frac{m}{\chi_0^2} \frac{E_F}{\Omega}. \tag{3.5}$$

  In this case, $A(\Omega)$ is a singular function of frequency, and cannot be replaced by a constant.

We see therefore that the prefactor of the ϕ^4 term is actually singular outside the scaling regime of a $z = 3$ theory.

3.1.2 ϕ^3 term

In the similar spirit, one can construct a cubic term in the bosonic fields.

$$\int \frac{d^2q d^2p d\Omega d\nu}{(2\pi)^9} \, B(\mathbf{p}, \mathbf{q}, \nu, \Omega) \, \mathbf{S}_p \cdot (\mathbf{S}_{q-p/2} \times \mathbf{S}_{-q-p/2}), \tag{3.6}$$

where the prefactor B is a convolution of three fermionic Green's functions as presented in Fig.3.1, and is given by:

$$B(\mathbf{q}, \mathbf{p}, \Omega, \nu) \sim Ng^3 \int d\omega \, d^2k \, G(\mathbf{k} - \mathbf{p}, \omega - \nu) G\left(\mathbf{k} - \frac{\mathbf{p}}{2} - \mathbf{q}, \omega - \frac{\nu}{2} - \Omega\right) \, G(\mathbf{k}, \omega)$$

Proceeding as for the quartic term, we set for simplicity $\mathbf{p} = \mathbf{0}$, $\nu = 0$, and integrate over ϵ_k and the angular variable, leading to:

$$B(q, \Omega) \sim \frac{mg^3}{\omega_0^{2/3} \Omega^{1/3}} \int_0^1 dy \frac{\left(y^{2/3} + (1 - y)^{2/3}\right)}{\left[\left(\frac{v_F q}{\Sigma(\Omega)}\right)^2 + \left(y^{2/3} + (1 - y)^{2/3}\right)^2\right]^{3/2}}, \tag{3.7}$$

where we again introduced the rescaled frequency $y = \omega/\Omega$, and performed the rescaling in N.

We can again identify two regimes.

- In the $z = 3$ regime where $q \sim (\gamma\Omega)^{1/3}$, one can expand for large $\frac{v_F q}{\Sigma(\Omega)}$, which leads to:

$$B(q, \Omega) \sim \frac{mg}{\chi_0} \alpha \left(\frac{\Omega}{\omega_{\text{Max}}}\right)^{2/3}, \tag{3.8}$$

  where ω_{Max} is given by (2.42). This term is small in the quantum critical regime where $\Omega < \omega_0 \sim \omega_{\text{Max}} \alpha^{3/2}$, and can be safely neglected.

- For $q \sim \Sigma(\Omega)$, the remaining integral is of order $O(1)$ and the result writes:

$$B(q,\Omega) \sim \frac{mg}{\chi_0} \frac{1}{\sqrt{\alpha}} \left(\frac{\omega_{\text{Max}}}{\Omega}\right)^{1/3}, \tag{3.9}$$

which is large and cannot be neglected.

We demonstrate in the next section how the singular behavior of the ϕ^3 and ϕ^4 terms lead to a non-analytic contribution to the static spin susceptibility.

3.2 Static spin susceptibility

We found that the Eliashberg theory for fermions interacting with gapless long-wavelength bosons is stable and controlled by two small parameters. We verified this by calculating the fermionic self-energy in a two-loop expansion around the Eliashberg solution

One may wonder whether the same conclusions hold for the bosonic self-energy as well. In particular, what are the corrections to the static susceptibility $\chi_s(q,0)$?

For a ferromagnetic $SU(2)$ QCP, for which the massless bosons are spin fluctuations, we show in this section that the corrections to the static spin susceptibility are non-analytic: they scale like $q^{3/2}$, and *do not* contain any prefactor except for a proper power of k_F. Such terms obviously overshadow the regular q^2 of the bare susceptibility at small enough momenta.

The physics behind the $q^{3/2}$ term in $\chi(q,0)$ at a ferromagnetic QCP is, by itself, not directly related to criticality: far away from the QCP, the spin susceptibility also contains negative, non-analytic $|q|$ term as we argued in the first chapter. This term gradually evolves as the correlation length ξ increases, and transforms into the $q^{3/2}$ term at the QCP. Both these non-analyticities, at and away from the QCP, emerge because the boson-mediated interaction between fermions contain a long-range dynamic component, generated from the Landau damping.

We now estimate the effect of these singularities on physical quantities. Both the ϕ^3 and ϕ^4 terms in the effective action give rise to corrections to the ϕ^2 term, i.e. to the spin susceptibility. These corrections are obtained diagrammatically by contracting the external legs of the ϕ^3 and ϕ^4 terms, as shown in Fig. 3.2.

The contributions from the ϕ^4 terms have been considered in Publication 1. The contributions from cubic terms were missed, and were first considered in [41] in the analysis of the spin susceptibility in the paramagnetic phase, away from a QCP.

Using the bosonic Dyson's equation:

$$\chi(q,0) = \frac{\chi_0}{\xi^{-2} + q^2 + \Pi(q,0)} \tag{3.10}$$

we define the static polarization bubble at this order by $\Pi = \Pi_1(q,0) + \Pi_2(q,0) + \Pi_3(q,0) + \Pi_4(q,0)$, where the individual contributions are presented in Fig. 3.2, and

write:

$$
\Pi_1(q,0) = \frac{\Gamma_1^S N \bar{g}^2}{(2\pi)^6 \chi_0} \int d^2k d\omega d^2l d\Omega \; \chi_s(l,\Omega) \; G(\omega,k) \; G(\omega+\Omega,k+l)
$$
$$
\times G(\omega+\Omega,k+q+l) \; G(\omega,k+q) \tag{3.11a}
$$

$$
\Pi_2(q,0) = \frac{\Gamma_2^S N \bar{g}^2}{(2\pi)^6 \chi_0} \int d^2k d\omega d^2l d\Omega \; \chi_s(l,\Omega) \; G(\omega,k)^2 \; G(\omega+\Omega,k+l)
$$
$$
\times G(\omega,k+q) \tag{3.11b}
$$

$$
\Pi_3(q,0) = \frac{\Gamma_3^S N^2 \bar{g}^3}{(2\pi)^9 \chi_0^2} \int d^2k d\omega d^2k' d\omega' dl d\Omega \; \chi_s(l,\Omega) \; \chi_s(q+l,\Omega) \; G(\omega,k)
$$
$$
\times G(\omega+\Omega,k+l+q) \; G(\omega',k') \; G(\omega'+\Omega,k'+l+q)
$$
$$
\times G(\omega,k+q) \; G(\omega',k'+q) \tag{3.11c}
$$

$$
\Pi_4(q,0) = \frac{\Gamma_4^S N^2 \bar{g}^3}{(2\pi)^9 \chi_0^2} \int d^2k d\omega d^2k' d\omega' dl d\Omega \; \chi_s(l,\Omega) \; \chi_s(l,\Omega) \; G(\omega,k)
$$
$$
\times G(\omega,k+q) \; G(\omega+\Omega,k+l+q) \; G(\omega',k')
$$
$$
\times G(\omega'+\Omega,k'+l) \; G(\omega'+\Omega,k'+l+q) \tag{3.11d}
$$

The factors of N come from the fermionic loops and the numerical prefactors from the following spin summations:

$$
\Gamma_1^S = \sum_{\alpha,\beta,\gamma,\delta} \sigma_{\alpha\beta}^Z \boldsymbol{\sigma}_{\beta\gamma} \sigma_{\gamma\delta}^Z \boldsymbol{\sigma}_{\delta\alpha} = -2 \tag{3.12a}
$$

$$
\Gamma_2^S = \sum_{\alpha,\beta,\gamma,\delta} \sigma_{\alpha\beta}^Z \boldsymbol{\sigma}_{\beta\gamma} \cdot \boldsymbol{\sigma}_{\gamma\delta} \sigma_{\delta\alpha}^Z = 6 \tag{3.12b}
$$

$$
\Gamma_3^S = \sum_{\alpha,\beta,\gamma,\delta,\epsilon,\zeta} \sigma_{\alpha\beta}^Z \left(\boldsymbol{\sigma}_{\beta\gamma} \cdot \boldsymbol{\sigma}_{\delta\epsilon} \right) \left(\boldsymbol{\sigma}_{\gamma\alpha} \cdot \boldsymbol{\sigma}_{\zeta\delta} \right) \sigma_{\epsilon\zeta}^Z = 8 \tag{3.12c}
$$

$$
\Gamma_4^S = \sum_{\alpha,\beta,\gamma,\delta,\epsilon,\zeta} \sigma_{\alpha\beta}^Z \left(\boldsymbol{\sigma}_{\beta\gamma} \cdot \boldsymbol{\sigma}_{\epsilon\delta} \right) \left(\boldsymbol{\sigma}_{\gamma\alpha} \cdot \boldsymbol{\sigma}_{\delta\zeta} \right) \sigma_{\zeta\epsilon}^Z = -8 \tag{3.12d}
$$

These four diagrams are related by pairs. To verify this, it is useful to expand the products of Green's functions according to:

$$
G(\omega_1,k_1)G(\omega_2,k_2) = \frac{G(\omega_1,k_1) - G(\omega_2,k_2)}{G^{-1}(\omega_2,k_2) - G^{-1}(\omega_1,k_1)}. \tag{3.13}
$$

Applying this to $\Pi_2(q,0)$, we find that it splits into two parts. In one part, the poles in ϵ_k are located in the same half-plane, leading to a vanishing contribution. The remaining term in $\Pi_2(q,0)$ is related to $\Pi_1(q,0)$ in such a way that:

$$
\Pi_1(q,0) = -\frac{2\Gamma_1}{\Gamma_2}\Pi_2(q,0). \tag{3.14}
$$

(see Appendix D for details).

70
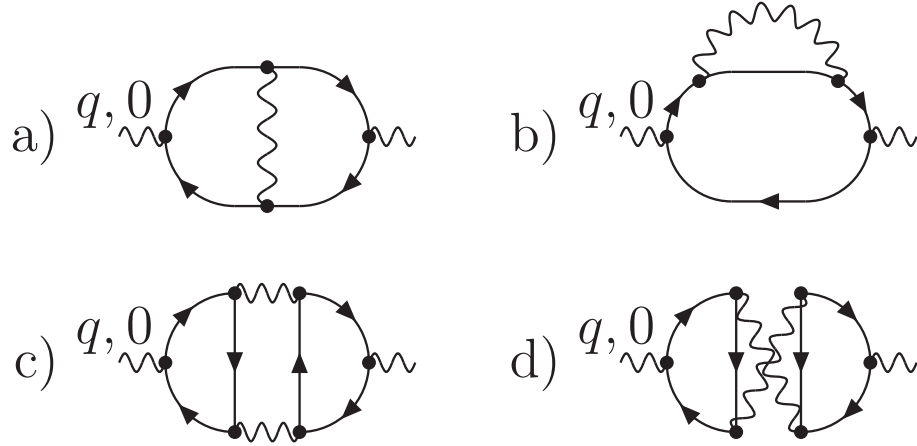
Figure 3.2: Corrections to the polarization bubble from diagrams with one and two extra bosonic lines

Similarly, $\Pi_3(q,0)$ and $\Pi_4(q,0)$ are related as

$$\Pi_3(q,0) = -\frac{\Gamma_3}{\Gamma_4}\Pi_4(q,0). \tag{3.15}$$

Collecting all four contributions and using the relations between prefactors, we obtain:

$$
\begin{aligned}
\Pi(q,0) &= \Pi_A(q,0) + \Pi_B(q,0) \;, &(3.16)\\
\Pi_A(q,0) &= \Pi_1(q,0) + 2\Pi_2(q,0)\\
&= 16\frac{N\bar{g}^2}{(2\pi)^6}\int d^2K d\omega d^2l d\Omega \; \chi_s(l,\Omega)G(\omega,k)^2 G(\omega+\Omega,k+l)G(\omega,k+q)\\
\Pi_B(q,0) &= \Pi_3(q,0) + \Pi_4(q,0)\\
&= 16\frac{N^2\bar{g}^3}{(2\pi)^9\chi_0^2}\int d^2k d\omega d^2k' d\omega' dl d\Omega \; \chi_s(l,\Omega) \; \chi_s(q+l,\Omega) \; G(\omega,k)\\
&\quad \times G(\omega,k+q) \; G(\omega+\Omega,k+l+q) \; G(\omega',k'+q)\\
&\quad \times G(\omega',k') \; G(\omega'+\Omega,k'+l+q) &(3.17)
\end{aligned}
$$

3.2.1 Away from the QCP

Away from criticality, the correlation length ξ is finite, and at low frequency, the system is in the Fermi-liquid regime. The fermionic self-energy is given by $\Sigma(\omega) = \lambda\omega$, Eq. (2.30).

The spin susceptibility in this regime has been analyzed in [42, 43, 29, 44, 45, 46, 41]. It was shown there that to the lowest order in the interaction, $\Pi_B(q,0) = \Pi_A(q,0)$, i.e., $\Pi(q,0) = 2\Pi_A(q,0)$. Beyond leading order, $\Pi_B(q,0)$ and $\Pi_A(q,0)$ are not equivalent but are of the same sign and of comparable magnitude. For

simplicity, we assume that the relation $\Pi_B(q, 0) = \Pi_A(q, 0)$ holds in the whole Fermi liquid regime. We will see below that even at the QCP, $\Pi_B(q, 0)$ and $\Pi_A(q, 0)$ are quite similar (at criticality $\Pi_B(q, 0) \simeq 1.3 \Pi_A(q, 0)$).

Introducing $\cos\theta = \frac{\mathbf{k}\cdot\mathbf{l}}{|\mathbf{k}||\mathbf{l}|}$ and $\cos\theta' = \frac{\mathbf{k}\cdot\mathbf{q}}{|\mathbf{k}||\mathbf{q}|}$, and successively integrating over $|\mathbf{k}|$, ω and θ', (3.16) can be rewritten as:

$$
\begin{aligned}
\Pi(q, 0) &= \frac{8\bar{g}|q|}{\pi^3(1+\lambda)v_F} \int_0^\infty dz \int_0^{\frac{\pi}{2}} d\phi \int_0^\pi d\theta \frac{1}{\frac{1}{\tilde{\gamma}\xi^2} + \tan\phi} \\
&\quad \times \frac{\cos\phi\sin\phi}{(i\sin\phi - \cos\theta\cos\phi)^2} \frac{z}{\sqrt{1 + z^2(\sin\phi + i\cos\phi\cos\theta)^2}} \quad (3.18)
\end{aligned}
$$

where we defined $\tilde{\gamma} = \frac{\gamma v_F}{1+\lambda}$, and introduced the new variables z and ϕ, which satisfy $z\cos\phi = \frac{l}{q}$ and $z\sin\phi = \frac{(1+\lambda)\Omega}{v_F q}$.

The universal part of $\Pi(q, 0)$ can be isolated by subtracting from it the constant part $\Pi(0, 0)$. The integral over z then becomes convergent. Integrating successively over z, ϕ and θ, we obtain:

$$
\delta\Pi(q, 0) = \Pi(q, 0) - \Pi(0, 0) = -\frac{4}{\pi^2}\frac{\bar{g}}{v_F(1+\lambda)}|q|\,\mathcal{H}\left(\frac{1+\lambda}{\tilde{\gamma}\xi^2}\right), \quad (3.19)
$$

where $\mathcal{H}(0) = \frac{1}{3}$, and $\mathcal{H}(x \gg 1) \simeq 2/(3x^2)$. We do recover the non-analytic $|q|$ correction to the static spin susceptibility in $D = 2$, as obtained in earlier studies [26, 29, 42, 43, 44].

Note that Eq. (3.21) does not contradict the Fermi liquid relation:

$$
\chi_s(q \to 0, \omega = 0) \propto \frac{(1 + F_{1,s})}{(1 + F_{0,a})} \quad (3.20)
$$

where $F_{1,s}$ and $F_{0,a}$ are Landau parameters. The Fermi liquid theory only implies that the static spin susceptibility saturates to a constant value as $q \to 0$, but does not impose any formal constraint on the $q-$dependence of $\chi_s(q, \omega)$.

As one gets closer to the QCP, $\lambda = 3\bar{g}/(4\pi v_S \xi^{-1})$ diverges and the prefactor of the $|q|$ term vanishes as:

$$
\delta\Pi(q, 0) = -\frac{16}{9\pi}\xi^{-1}|q|. \quad (3.21)
$$

This is not surprising since the Fermi liquid regime extends on a region of the phase diagram that shrinks and ultimately vanishes as one approaches the QCP.

Now, two different scenarios are possible:

- the divergence of ξ at the QCP completely eliminates the non-analyticity and the expansion of $\Pi(q, 0)$ begins as q^2, like the bare spin susceptibility,

- the self-energy $\Sigma(\omega) \propto \omega^{2/3}$ at the QCP still leads to a non-analytic term $\Pi(q, 0) \propto |q|^\delta$, with $1 < \delta < 2$, which dominates over the bare q^2 term.

We show in the next subsection that the second scenario is realized, and at the QCP, one has $\Pi(q, 0) \propto |q|^{3/2}$.

3.2.2 At criticality

At the QCP, we have to take into account two new elements: the bosonic propagator is massless ($\xi^{-1} = 0$) and the fermionic self-energy is no longer Fermi-liquid-like, it is given by (2.32).

The full calculation of $\Pi_A(q,0)$ and $\Pi_B(q,0)$ is presented in Appendix D. We just outline here the main steps of the computation and show where the $q^{3/2}$ term comes from.

Consider first $\Pi_A(q,0)$. Using (3.16) as a starting point, and substituting the full form of the spin susceptibility[1], Eq. (A.8), we then expand $\epsilon_{\mathbf{k+l}}$ and $\epsilon_{\mathbf{k+q}}$, and integrate successively over l_y (projection of $\mathbf{l}$ perpendicular to $\mathbf{k_F}$) and ϵ_k, leading to:

$$
\Pi_A(q,0) = i\frac{16m\bar{g}^2}{(2\pi)^5} \int_0^{2\pi} d\theta \int_{-\infty}^{+\infty} dl_x \int_{-\infty}^{+\infty} d\Omega \int_{-\Omega}^0 d\omega \frac{(\gamma|\Omega|)^{-1/3}}{(i\Sigma(\omega+\Omega) - i\Sigma(\omega) - v_F l_x)^2}
$$
$$
h\left(\frac{\sqrt{l_x^2 + c^2\Sigma^2(\Omega)}}{(\gamma|\Omega|)^{1/3}}\right) \frac{1}{i\Sigma(\omega+\Omega) - i\Sigma(\omega) - v_F l_x + v_F q \cos\theta}, \quad (3.22)
$$

where $c \simeq 1.19878$ (see A.6), and $h(x)$ is the bosonic propagator integrated over the momentum component l_y. The asymptotic behavior of $h(x)$ is given by:

$$
\begin{cases}
h(x \gg 1) = \frac{\pi}{x} \\
h(x \ll 1) = \frac{4\pi}{3\sqrt{3}} + (\log 2 - 1)x^2 - \frac{x^2 \log x^2}{2}
\end{cases}
\quad (3.23)
$$

Since the integrand in (3.22) has poles in l_x located in the same half-plane, the only non-vanishing contributions to Π comes from the non-analyticities in $h(x)$.

There are two non-analyticities in $h(x)$. The first one comes from the $1/x$ behavior at large x, which extends to $x \sim 1$. This is a conventional non-analyticity associated with bosons vibrating near their own mass shell, since at $x \sim 1$, $l_x \sim l_y \sim (\gamma|\Omega|)^{1/3}$.

Subtracting the non-universal $\Pi_A^{(a)}(0,0)$, expanding in q in (3.22) and substituting $l_x \sim (\gamma|\Omega|)^{1/3}$, we find for this contribution to Π:

$$
\begin{aligned}
\delta\Pi_A^{(a)} &\propto q^2 \frac{m\bar{g}^2}{v_F^3 \gamma^{5/3}} \int_0^{\Omega_{\mathrm{Max}}} \frac{d\Omega}{\Omega^{2/3}} \\
&\propto \sqrt{\alpha} q^2,
\end{aligned}
\quad (3.24)
$$

where $\Omega_{\mathrm{Max}} \sim \sqrt{\gamma v_F^3}$.

We see that the integration over the momentum range relevant to the $z = 3$ scaling regime yields a regular q^2 contribution to the static susceptibility. Not only

---

[1]To account for a possible contribution from bosonic momentum near the fermionic mass-shell, we have computed in Appendix A, the one-loop bosonic polarization in the regime where $v_F q \sim \tilde{\Sigma}(\omega)$. This is the expression we use here.

this contribution is regular in q, but it is also small in α. This result is similar to the one we obtained in (2.41) for the static vertex at a vanishing momentum.

However, Eq. (3.23) shows that $h(x)$ has a non-analytic $x^2 \log x$ term already at small x, i.e. far from the bosonic mass shell: the branch cut associated with the logarithmic term emerges at $v_F l_x \sim \Sigma(\omega)$. The typical value of l_y in the integral that leads to this $x^2 \log x$ term is also of the same order, although larger in the logarithmic sense. This implies that this second non-analyticity comes from a process in which the bosons are vibrating near a fermionic mass shell and far from their own.

Furthermore, this logarithmic term in (3.23) comes exclusively from the Landau damping term in the bosonic propagator – the q^2 term in $\chi(l, \Omega)$ can be safely omitted. Indeed, one has:

$$\int_{-\Lambda}^{\Lambda} dl_y \frac{1}{\frac{\gamma|\Omega|}{\sqrt{l_x^2 + l_y^2}}} = f(\Lambda) - \frac{l_x^2 \log l_x^2}{2\gamma\Omega}. \tag{3.25}$$
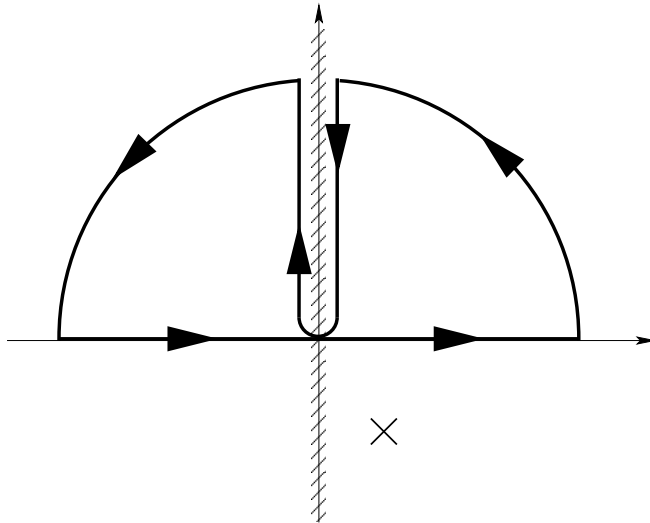
Figure 3.3: Integration contour: the hatched region stands for a branch cut, and the cross for a pole.

Substituting the logarithmic term from (3.23) into (3.22), we subtract the non-universal constant term $\Pi_A^{(b)}(0,0)$, which makes the integral over l_x convergent. Introducing $z = l_x/(c\Sigma(\Omega))$, one can perform the integral over z over the contour of

Fig. 3.3, which leads to the following contribution to Π:

$$
\begin{aligned}
\Pi_A^{(b)}(q,0) - \Pi_A^{(b)}(0,0) &= \frac{4Nm\bar{g}^2}{c^2\pi^4\gamma v_F}q^2 \int_0^{\pi/2} d\theta \int_1^{+\infty} dy \int_0^{+\infty} \frac{d\omega}{\Sigma(\Omega)^2} \\
&\quad \int_0^1 dw \frac{\cos^2\theta}{\left[c^{-1}\left((1-w)^{2/3}+w^{2/3}\right)+y\right]^3} \\
&\quad \frac{1-y^2}{\left[y+c^{-1}\left((1-w)^{2/3}+w^{2/3}\right)\right]^2 + \left(\frac{v_F q \cos\theta}{c\Sigma(\Omega)}\right)^2}, \quad (3.26)
\end{aligned}
$$

where we defined $w = \omega/\Omega$. Introducing the new variables $t = \left(\frac{c\Sigma(\Omega)}{v_F q \cos\theta}\right)^{3/2}$ and $v = t\left[y + c^{-1}\left((1-w)^{2/3}+w^{2/3}\right)\right]$, it becomes possible to separate the integrals, leading to the following final result:

$$
\begin{aligned}
\Pi_A^{(b)}(q,0) - \Pi_A^{(b)}(0,0) &= -0.8377 q^{3/2} \frac{Nm\bar{g}^2}{\pi^4 \gamma v_F^{3/2} \omega_0^{1/2}} \\
&= -0.1053\,\sqrt{k_F}\,q^{3/2}. \quad (3.27)
\end{aligned}
$$

We emphasize that this dependence comes from bosonic modes vibrating at the fermionic mass-shell. This explains why the result of (3.27) is not small in α, as this small parameter measures the softness of the mass-shell bosons compared to the mass-shell fermions.

The integrals for $\Pi_B(q,0)$ cannot be exactly evaluated analytically, but an approximate calculation, detailed in Appendix D, yields:

$$
\Pi_B^{(b)}(q,0) - \Pi_B^{(b)}(0,0) = -0.14 q^{3/2}\sqrt{p_F}, \quad (3.28)
$$

such that the total contribution of all four diagrams reads:

$$
\Pi(q,0) - \Pi(0,0) = -0.25\ q^{3/2}\sqrt{k_F}. \quad (3.29)
$$

We see that $\Pi(q,0)$ is still non-analytic in q and the prefactor is negative. At small q, the negative $q^{3/2}$ term well exceeds the regular q^2 term in the static spin susceptibility, which reads at criticality:

$$
\chi_s(q,0) = \frac{\chi_0}{q^2 - 0.25\ q^{3/2}\sqrt{k_F}} \quad (3.30)
$$

This implies that *the static spin susceptibility is negative at small momenta, i.e. a ferromagnetic QCP is unstable.* We discuss the consequences of this instability in the concluding chapter. The momentum q_{min} below which χ_s is negative is determined by:

$$
\chi_s^{-1}(q_{min}) \propto q_{min}^2 - 0.25 q_{min}^{3/2}\sqrt{k_F} = 0, \quad (3.31)
$$

which gives $q_{min} = 0.06k_F$.

Parametrically, q_{min} is of order k_F, which is the largest momentum scale in our problem. Strictly speaking, this suggests that the whole quantum-critical theory for the ferromagnetic case is not valid, since the quantum critical behavior extends up to energies of order ω_0, i.e. up to momenta of order $q \leq \omega_0/v_F \sim \alpha^2 k_F \ll k_F$. Numerically, however, q_{min} is much smaller than k_F. This implies that for reasonable values of α, there exists an intermediate momentum and energy range $q_{min} < q < \omega_0/v_F$ where the system is in the quantum-critical regime, but the static spin susceptibility is still positive.

The $q^{3/2}$ non-analyticity can also be viewed as emerging from the momentum dependence of the static vertex analyzed in the previous chapter. Using Eq. (2.45), one can rewrite:

$$\Pi(q,0) \sim N\bar{g} \int d^2k d\omega \frac{1}{i\Sigma(\omega) - \epsilon_k} \frac{\left.\frac{\Delta g}{g}\right|_{q,\Omega=0}}{i\Sigma(\omega) - \epsilon_{k+q}} \tag{3.32}$$

Performing the contour integration over ϵ_k, and changing variables into $y = \epsilon_k/\Sigma\omega$ and $t = \sqrt{\omega_0}\omega/(v_F q)^{3/2}$, we obtain:

$$\Pi(q,0) \sim \sqrt{k_F}q^{3/2} \tag{3.33}$$

We note in this regard that the non-analytic momentum dependence of the fermion-boson static vertex also comes from bosons vibrating near the fermionic mass shell, i.e. it emerges due to the same physics as we outlined above.

3.3   Related results

3.3.1   Finite temperature result

We can also prove that the non-analyticity appears in the temperature-dependent uniform static susceptibility $\chi_s(T)$. We show below that $\chi_s^{-1}(T) \propto T|\log T|$, again with a negative prefactor.

In this section, we show that the static uniform susceptibility is negative at finite temperature above a ferromagnetic QCP. To demonstrate this, we compute the static uniform $\Pi_A(q = 0, \omega = 0, T) = \Pi_A(T)$, assuming that $\xi^{-1} = 0$. The contribution from $\Pi_B(T)$ is of the same sign and comparable in magnitude. We have

$$\Pi_A(0,T) = 16iN\frac{m\bar{g}^2}{(2\pi)^3}T\sum_{p\neq 0}\Omega_p\int d^2q \frac{1}{q^2 + \frac{\gamma|\Omega_p|}{q}}\frac{1}{\left(i\Sigma(\Omega_p) - v_F q_x - \frac{q_y^2}{2m}\right)^3}. \tag{3.34}$$

Since the poles in q_x from the fermionic Green's functions are all in the same half-plane, one expects that $q_x^{\text{Typ}} \sim (\gamma\Omega)^{1/3}$ and thus dominates over the q_y^2 term,

which in turn can be neglected in the fermionic Green's functions. It then becomes possible to perform the integral over q_y, which gives

$$\Pi_A(0,T) = 2iN \frac{m\bar{g}^2}{\pi^3 \gamma v_F^3} T \sum_{p\neq 0} \frac{\Omega_p}{|\Omega_p|} \int_0^{(\gamma\Omega_p)^{1/3}} dq_x \frac{q_x^2 \log |q_x|}{(i\tilde{\Sigma}(\Omega_p) - v_F q_x)^3} \qquad (3.35)$$

Integrating over the half-space where there is no triple pole, we find that the integral is determined by the branch cut in $\log |q_x|$. Evaluating the integral we obtain

$$\int \frac{dq_x q_x^2 \log |q_x|}{(i\tilde{\Sigma}(\Omega_p) - v_F q_x)^3} = \text{Sign}(\Omega_p) \frac{i\pi}{v_F^3} \log \left(\frac{E_F}{|\tilde{\Sigma}(\Omega_p)|} \right) . \qquad (3.36)$$

Thus

$$\Pi_A(0,T) = \frac{2N}{3} \frac{m\bar{g}^2}{\pi^2 \gamma v_F^3} T \sum_{p\neq 0} \log \frac{E_F}{|\Omega_p|} \qquad (3.37)$$

To perform the summation over p, we notice that when the summand does not depend on p

$$T \sum_{-\Lambda/T}^{\Lambda/T} A = 2A\Lambda , \qquad (3.38)$$

is independent on T. Then the same sum but without the term at $p = 0$ will be $2A\Lambda - AT$. Using this, we obtain with logarithmic accuracy

$$T \sum_{p\neq 0} \log \frac{E_F}{|\Omega_p|} = -T \log \frac{E_F}{T} + ... \qquad (3.39)$$

where dots stand for $O(T)$ terms. Substituting this into (3.37), we obtain the final result:

$$\Pi_A(0,T) = -\frac{2k_F^2}{3\pi^2} \alpha \frac{T}{E_F} \log \left(\frac{E_F}{T} \right) . \qquad (3.40)$$

Although small, because of the prefactor in α, this term dominates at low temperature over any regular T^2 term. The sign of this $T \log E_F/T$ term is opposite to the sign of a conventional correction to the HMM theory, which comes from a constant part of the prefactor of the ϕ^4 term. In the HMM theory the temperature dependence of the spin susceptibility is $bT^{\frac{d+z-2}{z}}$, where $b > 0$, which in $d = 2$ leads to a linear in T contribution with positive prefactor. The negative sign of the non-analytic temperature correction in (3.40) implies that the static spin susceptibility is negative right above the QCP. This is another indication that the ferromagnetic QCP is unstable.

77
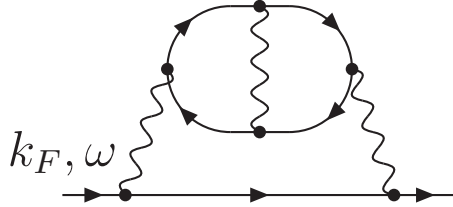
Figure 3.4: Three-loop contribution to the fermionic self-energy

3.3.2 Three-loop fermionic self-energy

Finally, we show how one can detect the instability of a ferromagnetic QCP from an analysis of higher order self-energy diagrams. This analysis is complimentary to the calculations that we have already done in the previous subsections. We show that upon inserting the contributions from the diagrams presented in Fig. 3.2 into the fermionic self-energy, we obtain series of singular corrections in powers of ω_{min}/ω, where $(\gamma\omega_{min})^{1/3} = q_{min}$, and q_{min} is the scale at which the static susceptibility $\chi_s(q)$ becomes negative, Eq. (3.31).

To illustrate this, we consider one of the three-loop diagrams, represented in Fig. 3.4. In the case of a spin interaction, we obtained a finite result after collecting the various diagrams, so we restrict ourselves here with just one of these contributions. The analytic form of the diagram in Fig. 3.4 writes:

$$\Sigma_3(\omega) \sim \bar{g} \int d\omega_1 d^2 q_1 \frac{C(q_1, \omega_1)}{i\Sigma(\omega - \omega_1) - v_F q_{1x} - \frac{q_{1y}^2}{2m}} \left(\frac{1}{q_1^2 + \frac{\gamma|\omega_1|}{q_1}} \right)^2, \tag{3.41}$$

where $C(q_1, \omega_1)$ is the dynamic fermionic bubble given by:

$$C(q_1, \omega_1) \sim N\bar{g}^2 \int d^2 k d\Omega \int d^2 q_2 d\omega_2 \frac{1}{q_2^2 + \frac{\gamma|\omega_2|}{q_2}} \frac{1}{i\Sigma(\Omega) - \epsilon_k} \frac{1}{i\Sigma(\Omega - \omega_1) - \epsilon_{k+q_1}}$$

$$\times \frac{1}{i\Sigma(\Omega + \omega_1 + \omega_2) - \epsilon_{k+q_1+q_2}} \frac{1}{i\Sigma(\Omega + \omega_2) - \epsilon_{k+q_2}}. \tag{3.42}$$

Approximating $C(q_1, \omega_1)$ by its singular static part $q_1^{3/2}\sqrt{k_F}$ and substituting into (3.4) we obtain:

$$\Sigma_3(\omega) \sim \bar{g}\sqrt{k_F} \int d\omega_1 d^2 q_1 \left(\frac{q_1}{q_1^3 + \gamma|\omega_1|} \right)^2 \frac{q_1^{3/2}}{i\Sigma(\omega - \omega_1) - v_F q_{1x} - \frac{q_{1y}^2}{2m}}. \tag{3.43}$$

A simple analysis of this expression shows that the dominant contribution to $\Sigma_3(\omega)$ comes from $q_{1x} \sim q_{1y} \sim (\gamma\omega_2)^{1/3}$ since the integral over q_{1x} is determined by the branch cut in the bosonic propagator. One can then safely drop the quadratic

term in the fermionic propagator and integrate over the angle θ between $\mathbf{k_F}$ and $\mathbf{q_1}$. This leads to:

$$
\begin{aligned}
\Sigma_3(\omega) \quad &\sim \quad \bar{g}\sqrt{k_F} \int_0^\omega d\omega_1 \int dq_1 \, \frac{q_1^{9/2}}{(q_1^3 + \gamma\omega_1)} \frac{1}{\sqrt{(v_F q_1)^2 + \Sigma(\omega)^2}} \\
&\sim \quad \frac{\bar{g}\sqrt{k_F}}{v_F\sqrt{\gamma}} \int_0^\omega \frac{d\omega_1}{\sqrt{\omega_1}}.
\end{aligned}
\tag{3.44}
$$

Collecting the prefactors, we find:

$$
\Sigma_3(\omega) \sim (\bar{g}\omega)^{1/2} .
\tag{3.45}
$$

We see that the non-analyticity in the static spin susceptibility feeds back into the fermionic self-energy leading to a contribution from the three loop self-energy whose frequency dependence is more singular than the $\omega^{2/3}$ dependence that we obtained assuming that the static susceptibility is regular. Comparing these two contributions, we see that they become comparable at a frequency:

$$
\omega_0^{1/3}\omega_{min}^{2/3} \sim \sqrt{\bar{g}\omega_{min}} \implies \omega_{min} \sim \frac{q_{min}^3}{\gamma} \sim \frac{E_F^2}{\bar{g}}.
\tag{3.46}
$$

where q_{min} is given by (3.31). Parametrically, q_{min} is not small since $q_{min} \sim k_F$, and $\omega_{min} \sim E_F/\alpha$ is larger than E_F. However, $q_{min} \sim 0.06 k_F$ is small numerically so that ω_{min} is four orders of magnitude smaller than E_F/α.

3.3.3 Conclusion

To summarize, we found that the Eliashberg theory for an $SU(2)$ symmetric ferromagnetic QCP has to be extended to include extra singular terms into both the spin susceptibility and the fermionic self-energy. These terms originate from the "anti-Migdal" processes in which slow bosons are vibrating near the fermionic mass shell. Physically, these extra processes originate from the dynamic long-range interaction between fermions, which is still present at the QCP despite the fact that fermions are no longer good quasiparticles.

We demonstrated that these extra non-analytic terms can be understood in the framework of HMM ϕ^4 theory of quantum criticality. We showed that the prefactor for the ϕ^4 term is non-analytic and depends on the interplay between momentum and frequency. The non-analytic bosonic self-energy is the feedback from the non-analytic ϕ^4 term to the quadratic ϕ^2 term.

We found that these extra terms in the Eliashberg theory make a ferromagnetic QCP unstable below a certain momentum/energy scale. We detected the instability by analyzing the momentum and temperature dependence of the spin susceptibility, and also the fermionic self-energy at the three-loop order.

3.4   Non-$SU(2)$ symmetric case

3.4.1   Discussion

The low-energy model used to describe the ferromagnetic quantum critical point is actually quite similar to other models. The problem of fermions interacting with bosonic collective modes with a propagator similar to the one we considered, is quite general, and one can wonder to what extent our analysis for a ferromagnetic case can be extended to these systems.

Indeed, even though it arises from very different underlying microscopic models, one can use an effective Hamiltonian comparable to the spin-fermion one in other problems, namely:

- fermions interacting with singular gauge fields (as studied in [34, 35, 30]);

- a quantum critical point in the charge channel;

- a quantum critical point towards a nematic-type ordering [47, 36, 48, 49, 50];

- a ferromagnetic QCP with Ising symmetry;

The essential difference between these cases and the ferromagnetic one lies in the symmetry of the order parameter. In an SU(2) spin-symmetric ferromagnetic case, the order parameter (magnetization) is a three-dimensional vector, while in the other cases, it is a scalar.

The Eliashberg theory, and the analysis of its validity at the two-loop level can be carried out equally for systems with vector and with scalar order parameter: the only unessential difference is in the numerical prefactors. On the other hand, the evaluation of the corrections to the static susceptibility leads to different results for scalar and vector order parameters, as we now demonstrate.

3.4.2   Ising case

Consider first the situation of a magnetically-mediated interaction, where we change the spin symmetry of the bosons from SU(2) to Ising. The Ising case was argued to be relevant for metamagnetic quantum critical points [51].

The use of Ising spins doesn't change the expression for the Green's functions but replaces the Pauli matrix $\boldsymbol{\sigma}$ at the fermion-boson vertex by σ^z. As a consequence, the computations performed for the SU(2) case still hold, but the interplay between different diagrams changes because of a change in the numerical prefactors. In particular, instead of Eq. (3.12) we now have:

$$
\begin{aligned}
\Gamma_1^{\text{Ising}} &= \Gamma_2^{\text{Ising}} = 2, \\
\Gamma_3^{\text{Ising}} &= \Gamma_4^{\text{Ising}} = 0.
\end{aligned}
\tag{3.47}
$$

Under these circumstances, the non-analytic contributions from the diagrams in Fig. 3.2 cancel each other out. As a result, the static spin susceptibility remains analytic and scales as $\chi^{-1}(q) \propto q^2$ with a positive prefactor at the QCP.

This result can be extended to the case of a nematic instability, following the same arguments.

3.4.3 Charge channel

For a charge vertex, one has to replace the Pauli matrices present at the vertex by Kronecker symbols $\delta_{\alpha\beta}$. We then have:

$$
\begin{aligned}
\Gamma_1^{\text{Charge}} &= \Gamma_2^{\text{Charge}} = \sum_{\alpha,\beta,\gamma,\delta} \delta_{\alpha\beta}\delta_{\beta\gamma}\delta_{\gamma\delta}\delta_{\delta\alpha} = 2, \\
\Gamma_3^{\text{Charge}} &= \Gamma_4^{\text{Charge}} = \sum_{\alpha,\beta,\gamma,\delta,\epsilon,\zeta} \delta_{\alpha\beta}\delta_{\beta\gamma}\delta_{\delta\epsilon}\delta_{\gamma\alpha}\delta_{\zeta\delta}\delta_{\epsilon\zeta} = 4.
\end{aligned}
$$

Substituting these Γ^{Charge} into the expressions for Π, we find that the diagrams Π_1 and Π_2, as well as Π_3 and Π_4 cancel each other out. This leaves only a regular q^2 term in the static charge susceptibility.

3.4.4 Physical arguments

The cancellation of the non-analytic terms in the charge susceptibility is not a direct consequence of the conservation laws. These laws impose constraints on the behavior of the susceptibilities in the opposite limit $q = 0$, $\omega \neq 0$ ($\chi_c(q = 0, \omega)$ vanishes as a uniform perturbation cannot affect a time independent, conserved quantity).

Instead, the absence of the non-analytic terms in the charge channel is related to the fact that this susceptibility measures the response of the system to a change in the chemical potential. We showed that the origin of the singular behavior of the static spin susceptibility lies in the Landau damping term in the bosonic propagator (see (3.25), (3.29)). The Landau damping does not depend in a singular way on k_F (i.e. on the density of electrons), and therefore there is no singular response of the system to a change in the chemical potential.

Conversely, the effect of a magnetic field on the Landau damping is singular. For a fermionic bubble with opposite spin projections of the two fermions, one has, in the presence of a small magnetic field H:

$$
\Pi_{\pm} \sim \frac{|\Omega|}{\sqrt{(\Omega + 2i\mu_B H)^2 + (v_F l)^2}} \tag{3.48}
$$

instead of the usual $\Pi_{\pm} \sim |\Omega|/\sqrt{\Omega^2 + (v_F l)^2}$.

As a consequence, taking the second derivative of $\Pi_\pm$ over H and setting $H = 0$ later, one obtains, for $v_F l \gg \Omega$, the following non-analytic term:

$$\frac{d^2 \Pi_\pm}{dH^2} \sim \frac{\mu_B}{v_F^3} \frac{\Omega}{l^3}. \tag{3.49}$$

This non-analyticity ultimately gives rise to the $q^{3/2}$ term in the static spin susceptibility [46, 41]. For an Ising ferromagnet, this effect does not exist as there are no bubbles with opposite spin projections in the theory.

The above reasoning shows that the non-analyticity appears in the spin response but not in the charge one. To further verify this argument, we computed the subleading, three-loop diagrams for the charge susceptibility and found that the non-analytic contributions from individual diagrams all cancel out. We present the calculations in Appendix E.

The same argument holds for the self-energy at the three-loop and higher orders. The singular $\omega^{1/2}$ term obtained in Eq. (3.45) appears in individual diagrams, but in the case of a QCP in the charge channel (or an Ising QCP in the spin channel) the total singular contribution cancel out.

CHAPTER 4

Conclusions and perspectives

We have constructed a fully controllable quantum critical theory describing the interaction of fermions with gapless long-wavelength collective bosonic modes. Our approach, similar but not identical to the Eliashberg theory for the electron-phonon interaction, allows us to perform detailed calculations of the fermionic self-energy and the vertex corrections at the QCP.

We constructed a controllable expansion at the QCP as follows: we first created a new, non Fermi-liquid "zero-order" theory by solving a set of coupled equations for the fermionic and the bosonic propagators, neglecting the vertex corrections as well as the momentum dependence of the fermionic self-energy, and then analyzed the residual interaction effects in a perturbative expansion around this new zero-order theory.

We have proved that this approach is justified under two conditions:

(i) the interaction $\bar{g}$ should be smaller than the fermionic bandwidth (which we assumed for simplicity to be of the same order as E_F),

(ii) either the band mass m_B should be smaller than $m = p_F/v_F$, or the number of fermionic flavors N should be large. When $N = O(1)$ and $m_B \sim m$, the corrections are of order $O(1)$.

We found that the corrections that are small in $\bar{g}/E_F$ come from bosons near their resonance, as in the Eliashberg theory for the electron-phonon interaction. The corrections small in $m_B/(Nm)$ come from bosons for which one of the momentum component (the larger one) is near the bosonic resonance, while the other component is close to the fermionic mass-shell.

Conclusions and perspectives

For an SU(2)-symmetric quantum critical point towards ferromagnetic ordering, we found that there exists an extra set of singular renormalizations which come from bosons with both momentum components vibrating near the fermionic mass-shell. These processes can be understood as a consequence of an effective long-range dynamic interaction between quasiparticles, generated by the Landau damping term. They give rise to a negative non-analytic $q^{3/2}$ correction to the static spin susceptibility, signaling that the ferromagnetic QCP is unstable.

We also demonstrated that the non-analytic $q^{3/2}$ term can be understood in the framework of Hertz-Millis-Moriya ϕ^4 theory of quantum criticality. We showed how the effective long-range dynamic interaction between fermions affects the structure of the ϕ^4 theory, once fermions are integrated out: we found that the prefactors of the ϕ^3 and ϕ^4 terms appearing in the effective action are non-analytic and depend on the interplay between the typical external momentum and frequency.

We showed that the non-analytic corrections to the bosonic propagator are specific to the SU(2)-symmetric case when the order parameter is a vector. For systems with a scalar order parameter, like a QCP in the charge channel, a nematic QCP, or a ferromagnetic QCP with Ising symmetry, the $q^{3/2}$ contributions from individual diagrams cancel out in the full expression of the susceptibility.

The consequences of the instability of the ferromagnetic QCP still needs to be fully understood. There are two possible scenarios for the behavior of the system: either the ferromagnetic transition becomes first order [52, 53], or the instability occurs at a finite q, leading to a second order transition towards an incommensurate state [54, 55]. The full analysis of these two scenarios is clearly called on.

Note however that in all the experimental examples presented in Chapter 1 where a first order transition has been observed, the latter usually appear at very low temperature, well below the typical energy scale where the quantum critical behavior is observed. Such features do strongly suggest that a first order transition is the most likely to occur in our case.

PUBLICATION 1

Instability of the Quantum Critical Point of itinerant ferromagnets

Instability of the Quantum-Critical Point of Itinerant Ferromagnets

Andrey V. Chubukov,[1] Catherine Pépin,[2] and Jerome Rech[2,3]

[1]*Department of Physics, University of Wisconsin–Madison, 1150 University Avenue, Madison, Wisconsin 53706-1390, USA*
[2]*SPhT, CEA-Saclay, L'Orme des Merisiers, 91191 Gif-sur-Yvette, France*
[3]*Center for Materials Theory, Rutgers University, Piscataway, New Jersey 08855, USA*
(Received 18 November 2003; published 9 April 2004)

We study the stability of the quantum-critical point for itinerant ferromagnets commonly described by the Hertz-Millis-Moriya (HMM) theory. We argue that in $D \leq 3$ long-range spatial correlations associated with the Landau damping of the order parameter field generate a universal *negative*, nonanalytic $|q|^{(D+1)/2}$ contribution to the static magnetic susceptibility $\chi_s(q, 0)$, which makes HMM theory unstable. We argue that the actual transition is either towards incommensurate ordering, or first order. We also show that singular corrections are specific to the spin problem, while charge susceptibility remains analytic at criticality.

The critical behavior of itinerant paramagnets at the onset of ferromagnetic ordering is the subject of intensive experimental [1] and theoretical [2,3] studies. Of particular interest is the existence of a ferromagnetic second-order transition at low temperatures, and the emergence of superconductivity near the phase boundary. The critical theory of itinerant ferromagnets was developed by Hertz, Millis, and Moriya [4] (HMM) and is based on the action of the form

$$S = \int d^d q \, d\omega_m \left[\xi^{-2} + q^2 + \frac{|\omega_m|}{|q|} \right] \phi_{q,\omega}^2 + b_4 \phi^4 + b_6 \phi^6 + \cdots, \tag{1}$$

where ϕ is a bosonic field associated with the order parameter, and ξ is the correlation length, which diverges at the phase transition. The two assumptions behind Eq. (1) are that the $b_{2n,n\geq 2}$ terms are nonsingular and can be approximated by constants, and that the static spin susceptibility has a regular q^2 momentum dependence. The HMM theory has been successfully applied to explain quantum-critical behavior in a number of materials [1]; however, its key assumptions have been questioned in recent studies [5,6]. The analyticity of the b_{2n} terms was analyzed in detail for an antiferromagnetic transition where it was demonstrated that, for $D \leq 3$, all b_{2n} prefactors do have nonanalytic pieces which depend on the ratio between momenta and frequencies of the ϕ fields [5]. For a 2D antiferromagnetic quantum-critical theory (2D fermions and 2D spin fluctuations) these nonanalytic terms give rise to singular vertex corrections [5]. For a 2D ferromagnetic case, nonanalytic terms in b_{2n} are still present; however, we found that they do not give rise to an anomalous exponent in the spin susceptibility for $D > 1$ and therefore are not dangerous.

In this Letter, we question another key assumption of the HMM theory, namely, that the momentum dependence of the static spin propagator is analytic at small q. This assumption is based on the belief that in itinerant

ferromagnets the q dependence of the ϕ^2 term comes solely from fermions with high energies, of order of E_F, in which case the expansion in powers of $(q/p_F)^2$ should generally hold for $q \ll p_F$. This reasoning was disputed in Refs. [6,7]. These authors considered a static spin susceptibility $\chi_s(q)$ in a weakly interacting Fermi liquid, i.e., well away from a quantum ferromagnetic transition, and argued that for $D \leq 3$ and arbitrary small interaction, the small q expansion of $\chi_s(q)$ begins with a nonanalytic $|q|^{D-1}$ term. This nonanalyticity originates from a $2p_F$ singularity in the particle-hole polarization bubble [6–8] and comes from *low-energy* fermions with energies of the order of $v_F q \ll E_F$. In Ref. [6], it was further argued that within the RPA, the nonanalyticity in $\chi_s(q)$ gives rise to the emergence of a nonanalytic $|q|^{D-1}\phi_{q,\omega}^2$ term in Eq. (1). Furthermore, the prefactor of this term turns out to be negative, which signals the breakdown of the continuous transition to ferromagnetism.

The weak point of this reasoning is that within the RPA one assumes that fermionic excitations remain coherent at the quantum-critical point (QCP). Meanwhile, it is known [9] that, upon approaching the QCP, the fermionic effective mass m^* diverges as $\log\xi$ in $D = 3$ and as ξ^{3-D} in smaller dimensions. We checked that m/m^* appears as a prefactor of the $|q|^{D-1}$ term; this term *vanishes* at the QCP. Does this imply that Eq. (1) is valid at the transition? Not necessarily, since one has to verify explicitly whether or not the divergence of m^* completely eliminates a nonanalyticity in $\chi_s(q)$ or just makes the nonanalytic term weaker than away from QCP. If the latter is true, the nonanalytic term can still be much larger than q^2 at small q at criticality.

In this Letter, we report explicit calculations which show that the nonanalytic term is still present at the QCP and accounts for the breakdown of the HMM theory. We first consider the problem in the Eliashberg approximation and argue that this approximation leads to a non-Fermi liquid behavior at the QCP, but the magnetic susceptibility $\chi_s(q)$ remains analytic in q. We then

demonstrate that the corrections to the Eliashberg theory are singular and give rise to a universal contribution to $\chi_s^{-1}(q)$ in the form q^β, with $\beta \le 2$ for $D \le 3$ and a *negative* prefactor. We show that this universal contribution makes the ferromagnetic QCP unstable and gives rise to either a continuous transition into a spiral state or a first-order transition into a ferromagnet.

The model.—The starting point for our theory is a low-energy effective spin-fermion Hamiltonian obtained by integrating the fermions with energies between fermionic bandwidth W and $\Lambda \ll W$ out of the partition function [3,9]:

$$\mathbf{H} = \sum_{p,\alpha} v_F(p - p_F)c_{p,\alpha}^\dagger c_{p,\alpha} + \sum_q \chi_{s,0}^{-1}(q)\mathbf{S}_q\mathbf{S}_{-q}$$
$$+ g\sum_{p,q} c_{p+q,\alpha}^\dagger \boldsymbol{\sigma}_{\alpha,\beta} c_{p,\beta}\mathbf{S}_q. \quad (2)$$

Here $\mathbf{S}_q$ describe collective bosonic degrees of freedom in the spin channel, and g is the residual spin-fermion coupling. The upper cutoff Λ is roughly the scale up to which fermionic dispersion can be linearized near the Fermi surface. The bare spin susceptibility $\chi_{s,0}(q)$ is assumed to be analytic at $q \ll p_F$ and have an Ornstein-Zernike form $\chi_{s,0} = \chi_0/(\xi^{-2} + q^2)$. The coupling and χ_0 appear in the theory only in the combination $\bar{g} = g^2\chi_0$.

The perturbation theory for Eq. (2) is an expansion into two parameters [3]:

$$\alpha = \frac{3^{3/4}}{4\pi}\frac{\bar{g}}{E_F} \quad \text{and} \quad \lambda = \frac{3}{4\pi}\frac{\bar{g}}{v_F\xi^{-1}} \sim \alpha(\xi p_F), \quad (3)$$

where E_F is the electron's Fermi energy and the prefactor in α is chosen for future convenience. We assume that $\bar{g}$ is small compared to E_F; i.e., α is a small parameter [3,10]. That $g \ll E_F$ is in line with the very idea of a separation between high-energy and low-energy physics. At the same time, near a ferromagnetic QCP, ξ diverges, and the dimensionless coupling $\lambda \propto \xi$ is large. Fortunately, one can solve explicitly the strong coupling problem in λ while keeping the zeroth order in α [3,9]. This amounts to neglecting the vertex correction $\delta g/g$ and the momentum-dependent piece in the self-energy $\Sigma(p)$, which are of next order in α. The analogous theory for electron-phonon interaction is known as Eliashberg theory [11].

Eliashberg theory.—The Eliashberg theory for a ferromagnetic quantum-critical point has been described in detail in the literature [3,9]. The results are presented here for $D = 2$, but their validity holds for general $D \le 3$. The elements of the theory are coupled fermionic and bosonic self-energies $\Sigma(\omega_m)$ and $\Pi(q, \omega_m) = \Phi(\omega_m)/|q|$, respectively [3] $\{G^{-1}(p, \omega_m) = i[\omega_m + \Sigma(\omega_m)] - v_F(p - p_F);$ $\chi_s(q, \omega_m) = \chi_0/[q^2 + \xi^{-2} + \Pi(q, \omega_m)]\}$. The self-consistent solution yields $\Phi(\omega_m) = \gamma|\omega_m|$, where $\gamma = \bar{g}p_F/(\pi v_F^2)$, and

$$\Sigma(\omega_m) = \lambda\omega_m f\left(\frac{(p_F\xi)^3\omega_m\bar{g}}{E_F^2}\right), \quad (4)$$

where $f(0) = 1$, $f(x \gg 1) = (32\pi/3\sqrt{3}x)^{1/3}$, and $E_F = p_Fv_F/2$. At the QCP, $\xi = \infty$ and $\Sigma(\omega_m) = \omega_m^{2/3}\omega_0^{1/3}$, where $\omega_0 = \alpha^2E_F$ is the typical bosonic frequency of our problem. Note that $\omega_0 \ll E_F$. The $\omega^{2/3}$ dependence of Σ implies that at the QCP, the Fermi-liquid description is broken down to the lowest energies. At the same time, Eliashberg theory reproduces the form of the spin propagator from Eq. (1), $\chi_s(q, \omega_m) \propto (\xi^{-2} + q^2 + \gamma|\omega_m|/q)^{-1}$. Alternatively speaking, in the Eliashberg approximation, the Fermi liquid is destroyed at QCP, but the magnetic transition remains continuous, and $\chi_s(q)$ is analytic.

Beyond Eliashberg theory.—The validity of the Eliashberg theory is generally based on Migdal's theorem that states that vertex correction $\delta g/g$ and $\Sigma(p)$ are small when the bosonic velocity v_B is much smaller than v_F. In our case, *a posteriori* analysis of typical bosonic and fermionic momenta which contribute to $\Phi(\omega)$ and $\Sigma(\omega)$ within the Eliashberg theory shows that for the same $\omega \sim \omega_0$, typical $q_B \sim (\gamma\omega_0)^{1/3} \sim \alpha p_F$, while typical fermionic momenta $|p - p_F| \sim \omega_0/v_F \sim \alpha^2 p_F$ are much smaller. This implies that for $\alpha \ll 1$, the effective bosonic velocity $v_B \sim \alpha v_F$ is much smaller than v_F; i.e., Migdal's theorem is valid. To verify this, we computed the corrections to $\partial\Sigma(p)/\partial p$ and to the static vertex in the limit of zero bosonic momentum and for external fermions at the Fermi surface and at zero frequency and indeed found $\alpha^{1/2}$ smallness.

Still, this does not immediately imply that $\chi_s(q)$ remains analytic beyond Eliashberg theory. To verify this, we have to go beyond the limit of zero momentum, evaluate the correction to the static susceptibility at a finite q, and check whether it remains analytic in q. Let us do this. Consider, e.g., the diagram in Fig. 1(a) with the insertion of $\Sigma(p)$ into the particle-hole bubble. Expanding this diagram to order q^2 we find that it scales as q^2I, where

$$I \propto \alpha^2\frac{E_F^3}{\gamma^{1/3}}\int\frac{dl_x d\Omega|\Omega|^{2/3}}{(v_Fl_x - i|\Omega + \Sigma(\Omega)|)^5}S\left(\frac{l_x^2}{(|\Omega|\gamma)^{2/3}}\right). \quad (5)$$

Here $l^2 = l_x^2 + l_y^2$, and $S(\cdots) \sim (|\Omega|\gamma)^{1/3}\int dl_y/(l^2 + |\Omega|\gamma/|l|)$ is, up to a prefactor, the boson propagator integrated along the Fermi surface. In the two limits, $S(0) = O(1)$ and $S(x \gg 1) \propto x^{-1/2}$. The integrand for I has a highly degenerate pole in the upper half-plane of l_x, at $v_Fl_x \propto |\Omega + \Sigma(\Omega)|$. This degenerate pole can be avoided by closing the integration contour in the lower
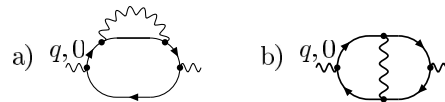

FIG. 1.   The two lowest-order diagrams for the corrections to the static spin susceptibility. The self-energy insertion is $\Sigma(p)$; the frequency dependent piece $\Sigma(\omega_m)$ is already incorporated into "zero-order" Eliashberg theory.

half-plane of l_x, in which case the nonvanishing part in I comes from the nonanalyticity in $S(x)$. This physically implies that fermions undergo forced vibrations at typical bosonic frequencies. The issue then is what is the typical bosonic x for the nonanalyticity in $S(x)$. By analogy with the electron-phonon problem, one could expect that corrections to the Eliashberg theory come from the processes in which typical bosonic frequencies are near bosonic mass shell. Then typical l_x are of order $(\Omega\gamma)^{1/3}$ as in the Eliashberg theory; i.e., typical x in $S(x)$ are of order 1. Substituting this typical x into (5), we obtain $I \sim \alpha^{1/2}$, i.e., a small and an analytic correction to the static susceptibility $\delta\chi_s(q) \propto q^2 \alpha^{1/2}$. However, a careful examination of the scaling function $S(x)$ reveals that it is *nonanalytic* already at the smallest x, such that there is another contribution to I from bosons vibrating at typical l_x comparable to those near the *fermionic* mass shell. Indeed, expanding $S(x)$ in powers of x at $x \ll 1$ we obtain, to logarithmical accuracy,

$$S(x) = 1 - \frac{3\sqrt{3}}{8\pi} \frac{l_x^2}{(\gamma|\Omega|)^{2/3}} \log[l_x^2]. \qquad (6)$$

The $\log l_x^2$ term is the most important here—its presence implies that $S(x)$ possesses a branch cut along the imaginary axis of l_x down to the smallest l_x. One can easily make sure that this logarithmic singularity is the consequence of the $\Omega/|l|$ nonanalyticity of the Landau damping piece in the bosonic propagator, i.e., of the existence of the long-range spatial component of the dynamical susceptibility. Substituting the small x form of $S(x)$ into (5) and evaluating integrals, we find a much larger, divergent contribution to I which behaves as $|q|^{-1/2}$. This implies that the low-q expansion of $\delta\chi_s$ is actually nonanalytic in q and begins as $q^{3/2}$. Performing an explicit calculation without expanding in q, and combining the results from the two diagrams for $\chi(q)$ in Fig. 1 we obtain for the static spin susceptibility

$$\chi_s(q) = \frac{\chi_0}{q^2 - 0.17|q|^{3/2} p_F^{1/2}}. \qquad (7)$$

Observe that the $q^{3/2}$ term in (7) is not small in α. This is not surprising, since the only excitations involved are those near the fermion mass shell, while α measures how soft the mass shell bosons are compared to the mass shell fermions. Note in passing that the self-energy insertion in the diagram of Fig. 1(a) is not a double counting, since the correction to static susceptibility comes only from the momentum-dependent piece in the self-energy. The frequency-dependent $\Sigma(\omega)$ is already incorporated at the zero-order level, and it does not affect $\chi_s(q)$.

The nonanalyticity of the correction to the susceptibility and the disappearance of α could be also detected by analyzing vertex corrections away from the limit of $q = 0$ and zero fermion frequency ω. Indeed, evaluating $\delta g(q, \omega)/g$ at finite q and ω, we obtain

$$\delta g(q, \omega) \propto g\alpha^{1/2}\psi\left(\frac{m\bar{g}}{q^2}, \frac{\omega}{E_F}\right), \qquad (8)$$

where $\psi(x \ll 1, y \ll 1) \propto \sqrt{x} \ll 1$, and $\psi(x \gg 1, y \ll 1) = 1 + A(\log y)/\sqrt{x}$, $A = O(1)$. We see that, although $\psi(x, y) \lesssim 1$ (i.e., vertex correction is small in $\alpha^{1/2}$), the small q expansion of $\delta g(q)/g$ begins as $\alpha^{1/2}|q||\log\omega|/\sqrt{m\bar{g}} \sim |q||\log\omega|/p_F$; i.e., it is nonanalytic in q and in ω, and the $|q\log\omega|$ term does not contain $\alpha^{1/2}$. This singular term again comes from fermions near their own resonance and can be traced back to the nonanalyticity of the Landau damping term. Substituting this $\delta g(q, \omega)$ into the susceptibility diagram and performing computations we find $\log\omega$ dependence makes $\delta\chi_s(q)$ nonzero in the static limit (without it, the correction would be proportional to $\Phi(\omega)$ and vanish at $\omega = 0$), and the overall power of q is $|q|$ from the vertex correction times the ratio of typical ω and $v_F l_x$. As typical $v_F l_x \sim \Sigma(\omega) \propto \omega^{2/3}$, this ratio yields $\omega^{1/3} \propto (l_x)^{1/2} \sim q^{1/2}$; hence the overall power in $\delta\chi_s(q)$ is $q^{3/2}$, as above.

What happens with higher-order terms? We analyzed higher-order particle-hole insertions into the susceptibility bubble and found that they add only small, $O(\alpha^{1/2})$, corrections to the $q^{3/2}$ term in (7) since at least one internal momentum is near the boson mass shell. Higher-order particle-particle insertions give rise to $O(1)$ corrections to the $q^{3/2}$ term and, in principle, should be included. However, the nonsmallness of particle-particle insertions is not specific to our problem and is, in fact, customary in Eliashberg-type theories [2,5,3,11,12,10]. Particle-particle vertex corrections are known to give rise to a pairing instability close to the ferromagnetic QCP at $T_c = O(\omega_0)$, which implies that there exists a dome around the QCP where the normal state analysis is invalid. However, a ferromagnetic T_c has an order of magnitude of roughly $T_c \lesssim 0.015\omega_0$ [3]. Hence the typical bosonic momenta for the pairing are of order $0.01\alpha p_F$, much smaller than typical q in Eq. (7). Because of this separation of energy scales, we do not expect particle-particle insertions to be relevant.

Equation (7) is the central result of our Letter. It shows that the static susceptibility becomes negative around a ferromagnetic QCP at $q < q_1 = 0.029 p_F$. Although the prefactor is small, q_1 is parametrically larger than the typical fermion and boson momenta that contribute to the fermion self-energy in the quantum-critical regime ($|k - k_F| \sim \alpha^2 p_F$ and $q_B \sim \alpha p_F$, respectively). This implies that the whole quantum-critical region is, in fact, *unstable*. Alternatively speaking, $Z = 3$ quantum-critical behavior at a ferromagnetic transition is internally destroyed by infrared singularities associated with the nonanalytic momentum dependence of the Landau damping.

A negative static susceptibility up to a finite q implies either that the instability occurs when ξ^{-1} is still finite, into an incommensurate state with a finite $|q| \sim q_1$ [13], or the ordering is commensurate, but the magnetic transition is of the first order. Which of the two scenarios

holds remains to be studied. We also verified that away from the QCP, when ξ is finite, the $q^{3/2}$ term transforms into $|q|\xi^{-1}$ at the smallest q. The interpolation formula between the $q^{3/2}$ and $|q|$ forms is rather involved and we do not present it here.

For arbitrary $D < 3$, our calculations yield the "correction" to χ_s^{-1} in the form $|q|^{(D+1)/2}$, again with a negative prefactor. In 3D it scales as $q^2 \log|q|$. Hence, HMM theory is destroyed for all $D \leq 3$. For $D > 3$, the correction term is smaller than q^2, and HMM theory survives.

Charge susceptibility and gauge theory. — We repeated the same calculations for the charge susceptibility and found in $D = 2$ that the singular $|q|^{3/2}$ terms from the two diagrams in Fig. 1 cancel each other, and the q^2 behavior survives. The same holds for the propagator of the gauge field — singular $|q|^{3/2}$ terms from self-energy and vertex correction insertions into the particle-hole bubble again cancel each other. We verified the cancellation of nonanalytic terms for the second-order diagrams as well. Furthermore, we verified in two orders of perturbation that the momentum dependence of $\chi_c(q, 0)$ comes in powers of $(q/p_F)^2$; i.e., it is entirely due to the existence of a curvature of the dispersion. Physically, the distinction between spin and charge susceptibilities is in that the $\Omega/|q|$ singularity in the dynamical particle-hole response function (which generates the $q^{3/2}$ nonanalyticity) is sensitive to a magnetic field but is insensitive to the change of the chemical potential. Hence, the singularity shows up in the total spin response but does not appear in the total charge response [14]. Mathematically, this distinction is due to the presence, in the spin case, of the Pauli matrices in the vertices of the diagrams in Fig. 1, such that the self-energy and vertex correction diagrams do not cancel each other. Note that the cancellation or noncancellation of the singularities is not directly related to the conservation laws for charge and spin susceptibilities, since conservation laws require only that $\chi_c(q = 0, \omega)$ and $\chi_s(q = 0, \omega)$ vanish but impose no constraints on the forms of the susceptibilities in the other limit of finite q and zero frequency. More specifically, Fermi-liquid relations between $\chi_{s,c}(q \to 0, \omega = 0)$ and $\chi_{s,c}(q = 0, \omega \to 0)$ imply [15] that $\chi_{s,c}(q \to 0, \omega = 0) \to Cst$ but impose no formal constraints on the form of the actual q dependence in $\chi_{s,c}(q, \omega = 0)$ at finite q.

To summarize, we studied the stability of the quantum-critical point for itinerant ferromagnets, in the limit when the spin-fermion coupling is much smaller than the bandwidth, and one would naively expect Eliashberg theory to be valid. Within Eliashberg theory, the Fermi-liquid is destroyed at criticality, but the magnetic transition is still continuous and is described by bosonic Hertz-Millis-Moriya action. We demonstrated, however, that in $D \leq 3$, long-range spatial correlations associated with the Landau damping of the bosonic order parameter field break the Eliashberg theory and give rise to a universal, *negative*, nonanalytic $|q|^{(D+1)/2}$ contribu-

tion to the static magnetic susceptibility $\chi_s(q, 0)$. This term makes the continuous critical theory unstable. We argued that the actual transition is either towards incommensurate ordering or first-order into a commensurate state. We also demonstrated that singular corrections are specific to the spin problem, while charge susceptibility remains analytic at criticality.

[1] See, e.g., G. R. Stewart, Rev. Mod. Phys. **73**, 797 (2001), and references therein.

[2] R. Roussev and A. J. Millis, Phys. Rev. B **63**, 140504 (2001); Z. Wang, W. Mao, and K. Bedell, Phys. Rev. Lett. **87**, 257001 (2001); for related developments, see also P. Coleman, C. Pepin, Q. Si, and R. Ramazashvili, J. Phys. Condens. Matter **13**, 723 (2001).

[3] A. Chubukov, A. Finkelstein, R. Haslinger, and D. Morr, Phys. Rev. Lett. **90**, 077002 (2003).

[4] J. A. Hertz, Phys. Rev. B **14**, 1165 (1976); A. Millis, Phys. Rev. B **48**, 7183 (1993); T. Moriya, *Spin Fluctuations in Itinerant Electron Magnetism* (Springer-Verlag, Berlin, New York, 1985).

[5] A. Abanov, A. V. Chubukov, and J. Schmalian, Adv. Phys. **52**, 119 (2003); Ar. Abanov, A. V. Chubukov, and A. M. Finkel'stein, Europhys. Lett. **54**, 488 (1999).

[6] D. Belitz, T. R. Kirkpatrick, and T. Vojta, Phys. Rev. B **55**, 9452 (1997).

[7] A. V. Chubukov and D. L. Maslov, Phys. Rev. B **68**, 155113 (2003); see also A. Houghton, H-J. Kwon, and B. Marston, Adv. Phys. **49**, 141 (2000); S. Das Sarma and E. H. Hwang, Phys. Rev. Lett. **83**, 164 (1999).

[8] G. Y. Chitov and A. J. Millis, Phys. Rev. Lett. **86**, 5337 (2001); Phys. Rev. B **64**, 054414 (2001).

[9] B. Altshuler, L. B. Ioffe, and A. J. Millis, Phys. Rev. B **52**, 5563 (1995).

[10] M. Dzero and L. P. Gorkov, Phys. Rev. B **69**, 092501 (2004)].

[11] G. M. Eliashberg, Sov. Phys. JETP **16**, 780 (1963); D. J. Scalapino, in *Superconductivity*, edited by R. D. Parks (Dekker Inc., New York, 1969), Vol. 1, p. 449; F. Marsiglio and J. P. Carbotte, in *The Physics of Conventional and Unconventional Superconductors*, edited by K. H. Bennemann and J. B. Ketterson (Springer-Verlag, Berlin, 2002).

[12] A. V. Chubukov, D. Pines, and J. Schmalian, in *The Physics of Superconductors*, edited by K. H. Bennemann and J. B. Ketterson (Springer, New York, 2003), Vol. 1, p. 495.

[13] S. A. Brazovskii, Sov. Phys. JETP **41**, 85 (1975).

[14] D. Belitz and T. R. Kirkpatrick, Phys. Rev. B **67**, 024419 (2003); (unpublished).

[15] E. M. Lifshitz and L. P. Pitaevskii, *Statistical Physics* (Pergamon Press, Oxford, 1980).

PUBLICATION 2

Quantum critical behavior of itinerant ferromagnets

cond-mat/0605306*

Appendices

APPENDIX A

Bosonic self-energy

In this section, we compute the bosonic self-energy at the one-loop level, in the case of both free and fully renormalized fermions. We prove that for an external bosonic momentum on the bosonic mass-shell, this self-energy becomes independent on the actual form of the fermionic self-energy, and reduces to the usual Landau damping term, whereas an extra term has to be included if this same external momentum is on the fermionic mass shell.

After performing the sum over spin matrices, we are left with the following expression:

$$\Pi(\mathbf{q}, \Omega) = 2N\bar{g} \int \frac{d^2k \; d\omega}{(2\pi)^3} \; G(\mathbf{k}, \omega) \; G(\mathbf{k} + \mathbf{q}, \omega + \Omega). \tag{A.1}$$

Introducing the angle θ defined by $\epsilon_{k+q} = \epsilon_k + v_F q \cos\theta$, this writes:

$$\Pi(\mathbf{q}, \Omega) = N\frac{\bar{g}m}{4\pi^3} \int d\omega \; d\epsilon_k \; d\theta \; \frac{1}{i(\omega + \Sigma(\omega)) - \epsilon_k}$$
$$\times \frac{1}{i(\omega + \Omega + \Sigma(\omega + \Omega)) - \epsilon_k - v_F q \cos\theta}. \tag{A.2}$$

Proceeding with a contour integration over ϵ_k, and noticing that ω and $\Sigma(\omega)$ have the same sign, we get:

$$\Pi(\mathbf{q}, \Omega) = iN\frac{\bar{g}m}{2\pi^2} \int_{-\infty}^{+\infty} d\omega \int_0^{2\pi} d\theta \left(\theta(\omega + \Omega) - \theta(\omega)\right)$$
$$\times \frac{1}{i(\Omega + \Sigma(\Omega + \omega) - \Sigma(\omega)) - v_F q \cos\theta}. \tag{A.3}$$

Performing the integration over θ, and rearranging a little bit the integration over Ω, we are left with:

$$\Pi(\mathbf{q}, \Omega) = N \frac{m\bar{g}}{\pi v_F} \int_0^\Omega d\omega \; \frac{\mathrm{Sign}(\Omega)}{\sqrt{(v_F q)^2 + (\Omega + \Sigma(\Omega - \omega) + \Sigma(\omega))^2}}. \qquad (A.4)$$

We know from direct perturbative calculation that the fermionic self-energy goes like $\Sigma(\omega) = \omega_0^{1/3} \omega^{2/3}$, where $\omega_0 \sim \alpha\bar{g}$. It follows that if the external bosonic momentum is on the bosonic mass-shell, i.e. if $q \sim \Omega^{1/3}$, it dominates over the frequency-dependent term in the integral, so that:

$$\begin{aligned}
\Pi(\mathbf{q}, \Omega) &= N \frac{m\bar{g}}{\pi} \int_0^\Omega d\omega \; \frac{\mathrm{Sign}(\Omega)}{v_F q} \\
&= N \frac{m\bar{g}}{\pi v_F} \frac{|\Omega|}{q}.
\end{aligned} \qquad (A.5)$$

We recover here the expression of the Landau damping term with a prefactor depending on the details of the interaction considered in our model. This result is independent on the fermionic self-energy provided that $v_F q \gg (\Omega + \Sigma(\Omega))$.

However, if the external bosonic momentum is on the fermionic mass shell, i.e. if $v_F q \sim \Sigma(\Omega)$, the frequency-dependent term can no longer be neglected. Defining $z = \frac{\omega}{\Omega}$, one then has:

$$\Pi(\mathbf{q}, \Omega) = N \frac{m\bar{g}}{\pi} \left| \frac{\Omega}{\Sigma(\Omega)} \right| \int_0^1 dz \; \frac{1}{\sqrt{\left(\frac{v_F q}{\Sigma(\Omega)} \right)^2 + \left(z^{2/3} + (1-z)^{2/3} \right)^2}}. \qquad (A.6)$$

For the calculations of the static spin susceptibility, we not only need the leading $O(1/q)$ but also the subleading $O(1/q^3)$ terms in $\Pi(q, \Omega)$. Expanding (A.6) in $1/q$ to first two orders, we find for $\Omega < \omega_0$:

$$\Pi(q, \Omega) = \gamma \frac{|\Omega|}{q} \left(1 - \frac{c^2 \Sigma^2(\Omega)}{v^2 q^2} \right) \qquad (A.7)$$

where $c \sim 1.19878$.

To simplify the notation, we use the expression for the polarization operator with the frequency dependence appearing in the denominator, which amounts to plugging the Σ^2 term back into the denominator:

$$\Pi(\mathbf{q}, \Omega) = N \frac{m\bar{g}}{\pi} \; \frac{|\Omega|}{\sqrt{(v_F q)^2 + c^2 \Sigma(\Omega)^2}}. \qquad (A.8)$$

APPENDIX B

Fermionic self-energy

In this section, we compute the fermionic self-energy at the one, two and three loop levels, for an external momentum taken to be on the Fermi surface. We also analyze the momentum dependence of the one-loop fermionic self-energy.

B.1 One-loop

B.1.1 At the Fermi level

After summing over the spin matrices, the fermionic self-energy at the one-loop level is given by:

$$
\begin{aligned}
\Sigma(\omega) &= 3ig^2 \int \frac{d^2q\, d\Omega}{(2\pi)^3} G(\mathbf{k_F} + \mathbf{q}, \omega + \Omega)\chi(\mathbf{q}, \Omega) \\
&= \frac{3i\bar{g}}{(2\pi)^3} \int d\theta\, \frac{d\Omega\, dq}{\xi^{-2} + q^2 + \gamma\frac{|\Omega|}{q}} \frac{q}{i(\omega + \Omega + \Sigma(\omega + \Omega)) - v_F q \cos\theta}, \quad \text{(B.1)}
\end{aligned}
$$

where we defined θ as the angle between $\mathbf{k}$ and $\mathbf{q}$, and considered an external fermionic momentum $k \simeq k_F$. The i prefactor comes from the convention $G^{-1} = G_0^{-1} + i\Sigma$.

Since the pole in q from the fermionic propagator is in a definite half-plane, the integral in q is dominated by poles coming from the bosonic Green's function, so that one can perform the integral over the angular variable and simplify the result

as follows:

$$
\begin{aligned}
\Sigma(\omega) &= -\frac{3g^2}{(2\pi)^2} \int d\Omega \, dq \, \frac{\chi_0}{q^3 + \gamma|\Omega| + q\xi^{-2}} \frac{q^2 \text{Sign}(\omega + \Omega)}{\sqrt{(v_F q)^2 + (\omega + \Omega + \Sigma(\omega + \Omega))^2}} \\
&= -\frac{3\bar{g}}{(2\pi)^2} \int_{-\infty}^{+\infty} d\Omega \int_0^{+\infty} dq \, \frac{q^2 \text{Sign}(\omega + \Omega)}{v_F q} \frac{1}{q^3 + \gamma|\Omega| + q\xi^{-2}}.
\end{aligned} \quad \text{(B.2)}
$$

Defining the new variables $z = \frac{\Omega}{\omega}$ and $u = \frac{v_F q}{\omega}$, this leads to:

$$
\Sigma(\omega) = \frac{3\bar{g}}{2\pi^2} \frac{\omega^2}{\gamma v_F^3} \int_0^1 dz \int_0^{+\infty} du \, \frac{u}{z + au + bu^3}, \quad \text{(B.3)}
$$

where we have used $a = \dfrac{1}{\gamma v_F \xi^2}$ and $b = \dfrac{\omega^2}{\gamma v_F^3}$

Let's denote by I the last double integral, and define the new variables $y = \sqrt{\frac{b}{a^3}} z = (\omega\gamma\xi^3) z$ and $t = \sqrt{\frac{b}{a}} u = \frac{\xi\omega}{v_F} u$. Now I reduces to:

$$
\begin{aligned}
I &= \left(\frac{v_F}{\xi\omega}\right)^2 \int_0^{\gamma\omega\xi^3} dy \int_0^{+\infty} dt \, \frac{t}{t^3 + t + y} \\
&= \left(\frac{v_F}{\xi\omega}\right)^2 h(\gamma\omega\xi^3). \quad \text{(B.4)}
\end{aligned}
$$

Substituting this back into our expression for the self-energy:

$$
\Sigma(\omega) = \frac{3}{2\pi m \xi^2} h(\gamma\omega\xi^3), \quad \text{(B.5)}
$$

with the following asymptotic behavior: $h(x \to 0) = \frac{\pi x}{2}$ and $h(x \to \infty) = \frac{\pi x^{2/3}}{\sqrt{3}}$.

In the two regimes we are interested in, this last result can be rewritten as:

$$
\Sigma(\omega) = \begin{cases} \lambda\omega & \text{for } \xi^{-1} \gg 1, \\ \omega_0^{1/3}\omega^{2/3} & \text{for } \xi^{-1} \to 0, \end{cases} \quad \text{(B.6)}
$$

where the constant prefactors are defined as:

$$
\begin{cases} \lambda &= \dfrac{3}{4\pi} \dfrac{\bar{g}\xi}{v_F}, \\ \omega_0 &= \dfrac{3\sqrt{3}}{8\pi^3} \dfrac{\bar{g}^3}{\gamma v_F^3}. \end{cases} \quad \text{(B.7)}
$$

B.1.2 Momentum dependence

For definiteness, we set $\xi^{-1} = 0$. We first compute the momentum-dependent part of the one-loop fermionic self-energy at zero external frequency:

$$
\begin{aligned}
\Sigma(\mathbf{k}, \omega = 0) &= 3ig^2 \int \frac{d^2q \, d\Omega}{(2\pi)^3} G(\mathbf{k} + \mathbf{q}, \Omega) \chi(\mathbf{q}, \Omega) \\
&= \frac{3i\bar{g}}{(2\pi)^3} \int \frac{d\Omega d^2q}{i\tilde{\Sigma}(\Omega) - \epsilon_{k+q}} \frac{q}{\gamma|\Omega| + q^3} \ .
\end{aligned}
\tag{B.8}
$$

Expanding $\epsilon_{k+q} = \epsilon_k + v_F q \cos\theta$ and integrating over θ, we obtain

$$
\Sigma(\mathbf{k}, 0) = \frac{3\bar{g}}{4\pi^2} \int d\Omega \, \text{Sign}(\Omega) \int \frac{q^2 dq}{q^3 + \gamma|\Omega|} \frac{1}{\left((v_F q)^2 + (\tilde{\Sigma}(\Omega) + i\epsilon_k)^2\right)^{1/2}}.
\tag{B.9}
$$

At $\epsilon_k = 0$, the integral vanishes by parity. Expanding to linear order in ϵ_k we obtain:

$$
\Sigma(\mathbf{k}, 0) = -3i\epsilon_k \times \frac{\bar{g}}{2\pi^2} \int_0^\infty d\Omega \, \tilde{\Sigma}(\Omega) \int \frac{q^2 dq}{(q^3 + (\gamma|\Omega|)) \left((v_F q)^2 + \tilde{\Sigma}(\Omega)^2\right)^{3/2}}.
\tag{B.10}
$$

Simple estimates show that the result depends on the interplay between $(\gamma\Omega)^{1/3}$ and $\tilde{\Sigma}(\Omega)/v_F$. Introducing the scale ω_{Max}, defined as the frequency for which $(\gamma\Omega)^{1/3} = \tilde{\Sigma}(\Omega)/v_F$ (see (2.42)), and rescaling variables as $q = (\gamma\omega_{\text{Max}})^{1/3}y$, $\Omega = \omega_{\text{Max}}x$, we re-write (B.10) as

$$
\Sigma(\mathbf{k}, 0) = -3i\epsilon_k \times \frac{\bar{g}\omega_{\text{Max}}}{2\pi^2 v_F^3 \gamma} I
\tag{B.11}
$$

where

$$
I = \int_0^\infty dx \int_0^\infty dy \frac{xy^2}{(x^2 + y^2)^{3/2}(x + y^3)} \simeq 1.3308
\tag{B.12}
$$

Substituting $\omega_{\text{Max}} = (\gamma v_F^3)^{1/2}$, we obtain (2.65).

To obtain the frequency dependence of the fermionic density of states at small ω, we have to evaluate the second order term in ϵ_k at the mass shell, where $\epsilon_k = i\tilde{\Sigma}(\omega)$ and convert the result to real frequencies. We therefore will keep both ω and ϵ_k finite, and use

$$
\Sigma(\mathbf{k}, \omega) = \frac{3i\bar{g}}{(2\pi)^3} \int d\Omega d^2q \frac{q}{\gamma|\Omega| + q^3} \frac{1}{i\tilde{\Sigma}(\omega + \Omega) - \epsilon_{k+q}}.
\tag{B.13}
$$

Writing, as before, $\epsilon_{k+q} = \epsilon_k + v_F q \cos\theta$ and integrating over θ, we obtain

$$
\Sigma(\mathbf{k}, \omega) = \frac{3\bar{g}}{4\pi^2} \int \frac{d\Omega q^2 dq}{\gamma|\Omega| + q^3} \frac{\text{sign}(\omega + \Omega)}{\sqrt{(\tilde{\Sigma}(\omega + \Omega) + i\epsilon_k)^2 + (v_F q)^2}}.
\tag{B.14}
$$

We assume and then verify that the internal $v_F q$ are still larger than $\tilde{\Sigma}(\omega + \Omega)$ and ϵ_k, which allows us to expand

$$\Sigma(\mathbf{k}, \omega) = -\frac{3\bar{g}}{8\pi^2 v_F^3} \int d\Omega \, \text{Sign}(\omega + \Omega) \int \frac{dq}{q(\gamma|\Omega| + q^3)} \left(\tilde{\Sigma}(\omega + \Omega) + i\epsilon_k \right)^2 \quad (B.15)$$

The lower limit of the momentum integral is $(\tilde{\Sigma}(\omega + \Omega) + i\epsilon)k)/v_F$. At the mass shell, $i\epsilon_k = \tilde{\Sigma}(\omega)$. Substituting, we find

$$\Sigma(\mathbf{k}, \omega) = -\frac{3\bar{g}}{8\pi^2 v_F^3} \int d\Omega \, \text{Sign}(\omega + \Omega) \int \frac{dq}{q(\gamma|\Omega| + q^3)} \left(\tilde{\Sigma}(\omega + \Omega) - \tilde{\Sigma}(\omega) \right)^2 \quad (B.16)$$

We will need the contribution which is confined to $\Omega \sim \omega$. The contributions from $|\Omega| \gg |\omega|$ diverge in our expansion procedure, and account for the regular $O(\epsilon_k)$ term in the self-energy, and also for regular $O(\omega)$ term. The last term is even smaller in α than the regular (ϵ_k) term and is totally irrelevant. As $\Omega \sim \omega$ is small, $\tilde{\Sigma}(\Omega) \approx \Sigma(\Omega) = \Omega^{2/3} \omega_0^{1/3}$.

Because of the sign factor in the numerator of (B.14), there are two distinct contributions from $\Omega \sim \omega$. For both of them, the momentum integral is logarithmic (this justifies the expansion) and yields $(1/3) \log(\omega_1/\omega)$, where $\omega_1 \sim N^2 E_F^2/\bar{g}$. The first contribution comes from $|\Omega| \leq |\omega|$ and to logarithmic accuracy is

$$\Sigma(\mathbf{k}, \omega)_A = -\frac{\bar{g}}{8\pi^2 v_F^3 \gamma} \text{sign}(\omega) \int_{-\omega}^{|\omega|} \frac{d\Omega}{|\Omega|} \left(\Sigma(|\omega| + \Omega) - \Sigma(|\omega|) \right)^2 \, \log \frac{\omega_1}{|\omega|} \quad (B.17)$$

Rescaling the frequency, we obtain from (B.17)

$$\Sigma(\mathbf{k}, \omega)_A = -\frac{\bar{g} I_1}{4\pi^2 v_F^3 \gamma} \Sigma(\omega)|\Sigma(\omega)| \log \frac{\omega_1}{\omega}. \quad (B.18)$$

where

$$I_1 = \frac{1/2}{\int} \int_{-1}^{1} \frac{dx}{|x|} \left((1 + x)^{3/2} - 1 \right)^2 = 0.254 \quad (B.19)$$

Another comes from $|\Omega| > |\omega|$, and is

$$\Sigma(\mathbf{k}, \omega)_B = \frac{\bar{g}\Sigma(\omega)}{4\pi^2 v_F^3 \gamma} \, \log \frac{\omega_1}{|\omega|} \int_{|\omega|}^{\infty} \frac{d\Omega}{\Omega} \left(\Sigma(|\omega| + \Omega) + \Sigma(\Omega - |\omega| - 2\Sigma(\Omega)) \right) \quad (B.20)$$

Rescaling, we obtain

$$\Sigma(\mathbf{k}, \omega)_B = \frac{\bar{g} I_2}{4\pi^2 v_F^3 \gamma} \Sigma(\omega)|\Sigma(\omega)| \log \frac{\omega_1}{\omega}. \quad (B.21)$$

where

$$I_2 = \int_1^{\infty} \frac{dx}{|x|} \left((1 + x)^{2/3} + (x - 1)^{2/3} - 2x^{2/3} \right) = -0.195 \quad (B.22)$$

100

Combining $\Sigma(\mathbf{k}, \omega)_A$ and $\Sigma(\mathbf{k}, \omega)_B$, we obtain

$$\Sigma(\mathbf{k}, \omega)_= -\frac{0.45\bar{g}}{4\pi^2 v_F^3 \gamma} \Sigma(\omega)|\Sigma(\omega)| \log \frac{\omega_1}{\omega}. \tag{B.23}$$

on the mass-shell.

B.2 Two-loop

We here compute one of the contributions to the two-loop self-energy, as given by Fig. 2.1, which originates from the insertion of the vertex correction into the Eliashberg self-energy.

We have:

$$\Sigma_2(\omega) \sim \bar{g}^2 \int d\omega_1 d^2q_1 \int d\omega_2 d^2q_2 \ \chi(\mathbf{q_1}, \omega_1) \ \chi(\mathbf{q_2}, \omega_2) \ G(\mathbf{k_F} + \mathbf{q_1}, \omega + \omega_1)$$

$$\times G(\mathbf{k_F} + \mathbf{q_2}, \omega + \omega_2) \ G(\mathbf{k_F} + \mathbf{q_1} + \mathbf{q_2}, \omega + \omega_1 + \omega_2), \tag{B.24}$$

which gives, once we replace each propagator by its full expression:

$$\begin{aligned}
\Sigma_2(\omega) \ \sim \ &\bar{g}^2 \int d\omega_1 d^2q_1 \int d\omega_2 d^2q_2 \frac{q_1}{\gamma|\omega_1| + q_1^3} \frac{q_2}{\gamma|\omega_2| + q_2^3} \\
&\times \frac{1}{i\tilde{\Sigma}(\omega + \omega_1) - v_F q_{1x}} \frac{1}{i\tilde{\Sigma}(\omega + \omega_2) - v_F q_{2x} - \frac{q_{2y}^2}{2m_B}} \\
&\times \frac{1}{i\tilde{\Sigma}(\omega + \omega_1 + \omega_2) - v_F q_{1x} - v_F q_{2x} - \frac{q_{1y}^2}{2m_B} - \frac{q_{2y}^2}{2m_B}}, \tag{B.25}
\end{aligned}$$

where we use the shorter notation $\tilde{\Sigma}(\omega) = \omega + \Sigma(\omega)$.

Integrating successively over q_{1x} and q_{2x}, closing each contour on the upper half-plane, one has:

$$\begin{aligned}
\Sigma_2(\omega) \ \sim \ &\frac{m_B \bar{g}^2}{v_F^2} \int d\omega_1 \int d\omega_2 \ \Theta(\omega, \omega_1, \omega_2) \int dq_{1y} \frac{|q_{1y}|}{|q_{1y}|^3 + \gamma|\omega_1|} \\
&\times \int dq_{2y} \frac{|q_{2y}|}{|q_{2y}|^3 + \gamma|\omega_2|} \frac{1}{(\gamma^2 \omega_1 \omega_2)^{1/3}} \frac{1}{\frac{q_{1y} q_{2y}}{(\gamma^2 \omega_1 \omega_2)^{1/3}} + i\zeta} \tag{B.26}
\end{aligned}$$

where $\zeta = m_B \dfrac{\tilde{\Sigma}(\omega + \omega_1) + \tilde{\Sigma}(\omega + \omega_2) - \tilde{\Sigma}(\omega + \omega_1 + \omega_2)}{(\gamma^2 \omega_1 \omega_2)^{1/3}}$ and $\Theta(\omega, \omega_1, \omega_2)$ comes from the choice of a contour for the integration and is given in our case by:

$$\begin{aligned}
\Theta(\omega, \omega_1, \omega_2) = \ &(\theta(\omega + \omega_1) - \theta(\omega + \omega_1 + \omega_2)) \\
&\times \left(\theta(\omega + \omega_2) - \theta(\tilde{\Sigma}(\omega + \omega_1 + \omega_2) - \tilde{\Sigma}(\omega + \omega_1)) \right). \tag{B.27}
\end{aligned}$$

101

It is convenient at this stage to rescale the perpendicular components of the bosonic momenta. Introducing $x = q_{1y}/(\gamma|\omega_1|)^{1/3}$ and $y = q_{2y}/(\gamma|\omega_2|)^{1/3}$, we obtain:

$$\Sigma_2(\omega) \sim \frac{m\bar{g}^2}{v_F^2} \int d\omega_2 \int d\omega_1 \int_0^\infty dxdy \, \frac{\Theta(\omega, \omega_1, \omega_2)}{(\gamma^2\omega_1\omega_2)^{2/3}}$$

$$\times \frac{i\zeta}{x^2y^2 + \zeta^2} \frac{xy}{(1+x^3)(1+y^3)}, \tag{B.28}$$

where we rearranged the double integral over x and y to make it real.

Since all internal frequencies typically go like ω, the typical value of ζ is given by the small parameter β given in (2.53). Expanding the double integral for small values of ζ, the leading contribution from the integral over x and y reads:

$$\int_0^\infty dxdy \, \frac{1}{x^2y^2 + \zeta^2} \frac{xy}{(1+x^3)(1+y^3)} \sim \log^2 \zeta. \tag{B.29}$$

If one considers now free fermions, it becomes possible to reduce the expression of the two-loop self-energy to:

$$\begin{aligned}
\Sigma_2^{\text{free}}(\omega) &\sim \frac{m_B^2\bar{g}^2}{v_F^2} \int_0^\omega d\omega_2 \int_{\omega-\omega_2}^\omega d\omega_1 \frac{\log^2\left(\frac{m_B\omega}{(\gamma^2\omega_1\omega_2)^{2/3}}\right)}{\gamma^2\omega_1\omega_2} \\
&\sim \frac{m_B^2\bar{g}^2}{\gamma v_F^2}\omega \int_0^1 dz_2 \int_{1-z_2}^1 dz_1 \frac{\log^2\left(\frac{m_B^3\omega}{\gamma z_1 z_2}\right)}{z_1 z_2} \\
&\sim \beta^2\omega\log^2\omega, \tag{B.30}
\end{aligned}$$

where we only kept the leading contribution in the last expression, and $\beta = m_B/mN$ is one of the small parameters defined in the text.

Now, in the case of dressed fermions, we need to take $\tilde{\Sigma}(\omega) = \omega_0^{1/3}\omega^{2/3}$. The procedure is identical to the free fermion case, but the final expression is a bit more complicated:

$$\begin{aligned}
\Sigma_2^{\text{Dressed}}(\omega) &\sim \frac{m^2\bar{g}^2}{\gamma^2 v_F^2}\omega_0^{1/3}\omega^{2/3} \int_0^1 dz_2 \int_{1-z_2}^1 dz_1 \frac{1}{z_1 z_2} \\
&\times \left[(1-z_1)^{2/3} + (1-z_2)^{2/3} + (z_1+z_2-1)^{2/3}\right] \\
&\times \log^2\left(\frac{(1-z_1)^{2/3} + (1-z_2)^{2/3} + (z_1+z_2-1)^{2/3}}{\frac{\gamma^{2/3}}{m\omega_0^{1/3}}z_1^{1/3}z_2^{1/3}}\right). \tag{B.31}
\end{aligned}$$

Expanding the $\log^2$, one is left with a double integral that only contributes as a numerical prefactor, and the dominant term is then given by:

$$\Sigma_2(\omega) \sim \Sigma_1(\omega) \, \beta^2 \log^2 \beta, \tag{B.32}$$

where $\Sigma_1(\omega) = \omega_0^{1/3}\omega^{2/3}$ is the self-energy in the Eliashberg theory.

B.3   Three loop

We now turn to the computation of the three-loop self energy. We are only interested here in one diagram, given in Fig. 3.4, where we try to analyze the feedback of the non-analytic susceptibility into the the higher-order diagrams for the fermionic self-energy. For spin interaction, there is no cancellation between different diagrams for the static susceptibility, which justifies that we restrict ourselves to just one contribution.

The analytic expression for this diagram is:

$$\Sigma_3(\omega) \sim \bar{g} \int d\omega_1 d^2 q_1 \frac{A(q_1, \omega_1)}{i\Sigma(\omega - \omega_1) - v_F q_{1x} - \frac{q_{1y}^2}{2m_B}} \left(\frac{1}{q_1^2 + \frac{\gamma|\omega_1|}{q_1}} \right)^2, \tag{B.33}$$

where $A(q_1, \omega_1)$ is the factor from the fermionic bubble:

$$\begin{aligned} A(q_1, \omega_1) &\sim N\bar{g}^2 \int d^2 k d\Omega \int \frac{d^2 q_2 d\omega_2}{q_2^2 + \frac{\gamma|\omega_2|}{q_2}} \frac{1}{i\Sigma(\Omega + \omega_1 + \omega_2) - \epsilon_{k+q_1+q_2}} \\ &\times \frac{1}{i\Sigma(\Omega) - \epsilon_k} \frac{1}{i\Sigma(\Omega - \omega_1) - \epsilon_{k+q_1}} \frac{1}{i\Sigma(\Omega + \omega_2) - \epsilon_{k+q_2}}. \end{aligned} \tag{B.34}$$

Approximating $A(q_1, \omega_1)$ by its singular static part $q_1^{3/2} \sqrt{k_F}$ and substituting into the expression of Σ_3 we obtain:

$$\Sigma_3(\omega) \sim \bar{g} \sqrt{k_F} \int d\omega_1 d^2 q_1 \left(\frac{q_1}{q_1^3 + \gamma|\omega_1|} \right)^2 \frac{q_1^{3/2}}{i\Sigma(\omega - \omega_1) - v_F q_{1x} - \frac{q_{1y}^2}{2m_B}}. \tag{B.35}$$

The integral over q_{1x} is determined by the branch-cut in the bosonic propagator and one then expects that this very integral is dominated by $q_{1x} \sim (\gamma\omega_1)^{1/3}$. It follows that the term in q_{1x} dominates inside the fermionic propagator allowing us to neglect the curvature term. Defining the angle θ between $\mathbf{k_F}$ and $\mathbf{q_1}$, and integrating over it, this leads to:

$$\Sigma_3(\omega) \sim \frac{\bar{g}\sqrt{k_F}}{v_F} \int \frac{d\omega_1 dq_1 \, \text{sign}(\omega - \omega_1)}{\sqrt{q_1^2 + \frac{\Sigma(\omega - \omega_1)^2}{v_F^2}}} \frac{q_1^{9/2}}{(q_1^3 + \gamma|\omega_1|)^2}. \tag{B.36}$$

Since the dominant contribution comes from $q_1 \sim (\gamma\omega_1)^{1/3}$, one can neglect the fermionic self-energy in the denominator. This in turn allows to simplify the frequency integral, which then writes:

$$\begin{aligned} \Sigma_3(\omega) &\sim \frac{\bar{g}\sqrt{k_F}}{v_F} \int_0^\omega d\omega_1 \int dq_1 \frac{q_1^{7/2}}{(q_1^3 + \gamma\omega_1)^2} \\ &\sim \frac{\bar{g}\sqrt{k_F}}{\sqrt{\gamma}v_F} \int_0^\omega \frac{d\omega_1}{\sqrt{\omega_1}}, \end{aligned} \tag{B.37}$$

103

where we introduced $z = q_1/(\gamma\omega_1)^{1/3}$, so that the integral over z just contribute to the numerical prefactor.

Collecting prefactors, one finally has:

$$\Sigma_3(\omega) \sim \sqrt{\bar{g}\omega}. \tag{B.38}$$

APPENDIX C

Vertex corrections

In this section, we compute the various vertex corrections analyzed in the text.

C.1 $q = \Omega = 0$

Consider first the simplest 3-leg vertex, with strictly zero incoming frequency Ω and momenta q, as presented in Fig. 2.2a. Its analytic expression writes:

$$
\left.\frac{\Delta g}{g}\right|_{q=\Omega=0} \quad \sim \quad g^2 \int d\omega d^2p \; G(\mathbf{k_F}, \omega)^2 \; \chi(\mathbf{p}, \omega)
$$

$$
\sim \quad \bar{g} \int \frac{d\omega d^2p}{\frac{\gamma|\omega|}{p} + p^2} \; \frac{1}{\left(i\tilde{\Sigma}(\omega) - v_F p_x - \frac{p_y^2}{2m_B}\right)^2},
$$

where we defined $\tilde{\Sigma}(\omega) = \omega + \Sigma(\omega)$ and we have chosen $\mathbf{k}_F$ along the x axis.

Since both poles coming from the fermionic Green's functions are in the same half plane, the integral over q_x is finite only because of the branch cut in the bosonic propagator. Since at the branch cut p_x and p_y are of the same order, we can drop the curvature term in the fermionic propagators and introduce polar coordinates for the internal bosonic momentum. Defining θ as the angle between $\mathbf{k_F}$ and $\mathbf{p}$, and integrating over it, one has:

$$
\left.\frac{\Delta g}{g}\right|_{q=\Omega=0} \sim \bar{g} \int \frac{d\omega dp}{p^3 + \gamma|\omega|} \frac{p^2 |\tilde{\Sigma}(\omega)|}{\left((v_F p)^2 + \tilde{\Sigma}(\omega)^2\right)^{3/2}}. \tag{C.1}
$$

Introducing the frequency ω_{Max} up to which bosons are slow modes compared to fermions, i.e. up to which $(\gamma\omega)^{1/3} > \tilde{\Sigma}(\omega)/v_F$, one can split the frequency integral into two parts, and define in each of them the reduced momentum $z = p/\text{Min}((\gamma\omega)^{1/3}, \tilde{\Sigma}(\omega)/v_F)$ so that the integral over z only contributes to the numerical prefactor, leading to:

$$\left.\frac{\Delta g}{g}\right|_{q=\Omega=0} \sim \bar{g} \int_0^{\omega_{\text{Max}}} d\omega \frac{\tilde{\Sigma}(\omega)}{\gamma v_F^3 \omega} \sim \frac{\bar{g}}{\gamma v_F^3}\tilde{\Sigma}(\omega_{\text{Max}}) \tag{C.2}$$

One can easily make sure that the frequency ω_{Max} at which $(\gamma\omega)^{1/3} = \tilde{\Sigma}(\omega)/v_F$ exceeds ω_0, such that one should use $\tilde{\Sigma}(\omega) = \omega$ to find ω_{Max}. Substituting, we obtain $\omega_{\text{Max}} \sim (N\bar{g}E_F)^{1/2}$, and

$$\left.\frac{\Delta g}{g}\right|_{q=\Omega=0} \sim \sqrt{\alpha} \tag{C.3}$$

C.2 $q = 0$, Ω finite

Considering the same vertex, now with a finite external frequency, one has:

$$\left.\frac{\Delta g}{g}\right|_{q=0,\Omega} \sim g^2 \int d\omega d^2p \ G(\mathbf{k_F} + \mathbf{p}, \omega + \Omega)G(\mathbf{k_F} + \mathbf{p}, \omega)\chi(\mathbf{p}, \omega)$$

$$\sim \bar{g} \int \frac{d\omega d^2p}{\frac{\gamma|\omega|}{p} + p^2} \frac{1}{i\tilde{\Sigma}(\omega) - v_F p_x - \frac{p_y^2}{2m_B}} \frac{1}{i\tilde{\Sigma}(\omega + \Omega) - v_F p_x - \frac{p_y^2}{2m_B}}, \tag{C.4}$$

where we chose the x axis along $\mathbf{k_F}$.

From the pole structure in p_x of this expression, one expects two contributions to this integral. A first term comes from the branch cut in the bosonic propagator, however this contribution ultimately leads to the same result as the $q = \Omega = 0$ vertex, up to small corrections from the finiteness of Ω. The second contribution arises from taking the poles in the fermionic propagators. At zero external frequency, these two poles were in the same half-plane of p_x, so we could close the integration contour over a different half-plane and only consider the contribution from the branch cut in the bosonic propagator. At a finite Ω, there is a range where ω and $\omega + \Omega$ have different signs, and the two poles are in different half-planes of p_x. The result after integration reads:

$$\left.\frac{\Delta g}{g}\right|_{q=0,\Omega} \sim \frac{\bar{g}}{v_F} \int_0^{\Omega} d\omega \int dp_y \frac{|p_y|}{\gamma|\omega| + |p_y|^3} \frac{1}{\tilde{\Sigma}(\Omega - \omega) + \tilde{\Sigma}(\omega)}, \tag{C.5}$$

where we slightly rearranged the frequency integral.

Performing the integration over p_y, we are left with:

$$
\begin{aligned}
\left.\frac{\Delta g}{g}\right|_{q=0,\Omega} &\sim \frac{\bar{g}}{\gamma^{1/3}v_F}\int_0^\Omega d\omega \frac{\omega^{-1/3}}{\tilde{\Sigma}(\Omega-\omega)+\tilde{\Sigma}(\omega)} \\
&\sim \frac{\bar{g}}{(\omega_0\gamma v_F^3)^{1/3}} \\
&\sim \text{Const.},
\end{aligned}
\tag{C.6}
$$

where we assumed that Ω is small, i.e. $\tilde{\Sigma}(\Omega) = \omega_0^{1/3}\Omega^{2/3}$. This vertex thus reduces to a numerical constant, that does not contain any small parameter.

C.3 q finite, $\Omega = 0$

Conversely, the same vertex taken at finite external momentum q, but zero external frequency writes:

$$
\begin{aligned}
\left.\frac{\Delta g}{g}\right|_{q,\Omega=0} &\sim g^2\int d\omega d^2p\; G(\mathbf{k_F}+\mathbf{p}+\mathbf{q},\omega)G(\mathbf{k_F}+\mathbf{p},\omega)\chi(\mathbf{p},\omega) \\
&\sim \bar{g}\int \frac{d\omega d^2p}{\frac{\gamma|\omega|}{p}+p^2}\frac{1}{i\tilde{\Sigma}(\omega)-v_Fp_x-\frac{p_y^2}{2m_B}} \\
&\qquad\times\frac{1}{i\tilde{\Sigma}(\omega)-v_Fq_x-v_Fp_x-\frac{p_y^2}{2m_B}-\frac{q_yp_y}{m_B}},
\end{aligned}
\tag{C.7}
$$

where p_x is the projection of $\mathbf{p}$ along $\mathbf{k_F}$.

Like its $q=0$ counterpart, this vertex is characterized by poles in p_x from the fermionic propagators lying in the same half-plane. The only nonzero contribution then comes from the branch cut in the bosonic propagator. At the branch cut, $p_x \sim p_y$ which allows us to neglect the quadratic curvature terms in the fermionic Green's functions.

This makes possible a direct integration over p_y. This integral can be separated from the rest of the expression, and reads:

$$
\begin{aligned}
\int dp_y\frac{p}{\gamma|\omega|+p^3} &= \frac{1}{|p_x|}\int_{-\infty}^{+\infty}dz\frac{\sqrt{1+z^2}}{(1+z^2)^{3/2}+\gamma\frac{|\omega|}{|p_x|^3}} \\
&= \frac{2p_x^2}{\gamma|\omega|}\int_0^{+\pi/2}du\frac{1}{\frac{|p_x|^3}{\gamma|\omega|}+(\cos u)^3},
\end{aligned}
\tag{C.8}
$$

where we successively defined $z = p_y/|p_x|$ and $z = \tan u$.

This last integral can be approximated by its asymptotic form, namely:

$$
\int \frac{dp_y \, p}{\gamma|\omega| + p^3} =
\begin{cases}
\frac{\pi}{|p_x|}, \text{ if } |p_x|^3 \gg \gamma\omega \\
\frac{4\pi}{3\sqrt{3}} \frac{1}{(\gamma|\omega|)^{1/3}} - \frac{1}{2} \frac{p_x^2}{\gamma|\omega|} \log \frac{p_x^2}{(\gamma|\omega|)^{2/3}} \\
+ \left(\log 2 - \frac{1}{2}\right) \frac{p_x^2}{\gamma|\omega|}, \text{ if } |p_x|^3 \ll \gamma\omega
\end{cases}
\tag{C.9}
$$

The only non-vanishing contribution once we take the integral over p_x comes from the log term. After expanding in q_x, this contribution reads:

$$
\left.\frac{\Delta g}{g}\right|_{q,\Omega=0} - \left.\frac{\Delta g}{g}\right|_{q=\Omega=0} \sim \frac{\bar{g}v_F}{\gamma}q_x \int \frac{d\omega}{|\omega|} \int dp_x \frac{p_x^2 \log p_x^2}{\left(i\tilde{\Sigma}(\omega) - v_F p_x\right)^3}.
\tag{C.10}
$$

Defining the scaled momentum $z = v_F p_x / \tilde{\Sigma}(\omega)$ and performing the integration over z, one obtains two terms, the dominant one being:

$$
\left.\frac{\Delta g}{g}\right|_{q,\Omega=0} - \left.\frac{\Delta g}{g}\right|_{q=\Omega=0} \sim i\frac{\bar{g}}{\gamma v_F^2}q_x \int_{|v_F q_x|} \frac{d\omega}{\omega} \log[i\tilde{\Sigma}(\omega)],
\tag{C.11}
$$

where the frequency integral runs over $|\tilde{\Sigma}(\omega)| > |v_F q_x|$ since as we expanded in $v_F q_x$, we assumed that it was smaller than $|\tilde{\Sigma}(\omega)|$.

Performing the remaining integral, one finds:

$$
\left.\frac{\Delta g}{g}\right|_{q,\Omega=0} - \left.\frac{\Delta g}{g}\right|_{q=\Omega=0} \sim \frac{q_x}{k_F} \log|q_x|.
\tag{C.12}
$$

C.4 q, Ω finite

Finally, we consider the general vertex where both external bosonic momentum and frequency are non-zero. In analytic form, this writes:

$$
\left.\frac{\Delta g}{g}\right|_{q,\Omega} \sim g^2 \int d\omega d^2p \; G(\mathbf{k_F} + \mathbf{p} + \mathbf{q}, \omega + \Omega) G(\mathbf{k_F} + \mathbf{p}, \omega) \chi(\mathbf{p}, \omega)
$$

$$
\sim \bar{g} \int \frac{d\omega d^2p}{\frac{\gamma|\omega|}{p} + p^2} \frac{1}{i\tilde{\Sigma}(\omega) - v_F p_x - \frac{p_y^2}{2m_B}}
$$

$$
\times \frac{1}{i\tilde{\Sigma}(\omega + \Omega) - v_F q_x - v_F p_x - \frac{p_y^2}{2m_B} - \frac{q_y p_y}{m_B}},
$$

where p_x is defined as $p_x = \mathbf{p} \cdot \mathbf{k_F}$.

Integrating over p_x first, there are two contributions. One comes from the branch cut in the bosonic propagator, and gives similar results to the $(q = 0, \Omega = 0)$ and the $(q$ finite, $\Omega = 0)$ vertices up to small correction from the finiteness of the external

frequency. We neglect it here and focus on the other contribution which comes from the poles in the fermionic propagators:

$$\left.\frac{\Delta g}{g}\right|_{q,\Omega} \sim i\frac{\bar{g}}{v_F}\int_0^\Omega d\omega \int dp_y \frac{|p_y|}{\gamma|\omega| + |p_y|^3}$$
$$\times \frac{1}{i\tilde{\Sigma}(\Omega-\omega) + i\tilde{\Sigma}(\omega) - v_F q_x - \frac{q_y p_y}{m_B}}, \quad (C.13)$$

where the simplification of the frequency integral comes from the poles in p_x.

This vertex correction strongly depends on the interplay between the external q_x, q_y and Ω, and is in particular quite sensitive to the momentum anisotropy. We now analyze the various possibilities.

For the generic case where $q_x \sim q_y$ (we use the notation q to designate them both), one can neglect the quadratic term in the fermionic dispersion, allowing to perform the integration over p_y, leaving us with:

$$\left.\frac{\Delta g}{g}\right|_{q,\Omega} \sim i\frac{\bar{g}}{v_F\gamma^{1/3}}\int_0^\Omega \frac{d\omega\ \omega^{-1/3}}{i\tilde{\Sigma}(\Omega-\omega) + i\tilde{\Sigma}(\omega) - v_F q}. \quad (C.14)$$

Restricting ourselves to the quantum-critical regime (i.e. $\Omega \leq \omega_0$) for which $\tilde{\Sigma}(\omega) = \omega_0^{1/3}\omega^{2/3}$, one has:

$$\left.\frac{\Delta g}{g}\right|_{q,\Omega} = \mathcal{F}\left(\frac{v_F q}{\Sigma(\Omega)}\right), \quad (C.15)$$

where $\mathcal{F}(x) = \int_0^1 \frac{dz}{z^{1/3}}\frac{1}{(1-z)^{2/3}+z^{2/3}+ix}$, has the following asymptotic behavior:

$$\begin{cases} \mathcal{F}(x \ll 1) &= O(1) \\ \mathcal{F}(x \gg 1) &= O\left(\frac{1}{x}\right) \end{cases} \quad (C.16)$$

If the typical q is on the bosonic mass shell, then $q \sim (\gamma\Omega)^{1/3}$, and one has:

$$\left.\frac{\Delta g}{g}\right|_{q,\Omega} \sim \frac{\Sigma(\Omega)}{v_F q} \sim \sqrt{\alpha}\left(\frac{\Omega}{\omega_{\text{Max}}}\right)^{1/3}. \quad (C.17)$$

However, we encountered in previous computations (e.g. self-energies) that a strong anisotropy can be observed between the components of the bosonic momentum, with $q_y \gg q_x$. In this case, the full expression of the vertex correction is a bit complicated and we choose to present here the most relevant case for which the curvature term dominates over $v_F q_x$ in the fermionic propagator. The vertex correction then no longer depends on q_x and writes:

$$\left.\frac{\Delta g}{g}\right|_{q,\Omega} \sim \frac{\bar{g}}{v_F}\int_0^\Omega d\omega \int_0^\infty dp_y \frac{p_y}{\gamma\omega + p_y^3}\frac{\tilde{\Sigma}(\Omega-\omega) + \tilde{\Sigma}(\omega)}{\left(\tilde{\Sigma}(\Omega-\omega) + \tilde{\Sigma}(\omega)\right)^2 + \left(\frac{q_y p_y}{m_B}\right)^2}, \quad (C.18)$$

Defining $u = p_y/(\gamma\omega)^{1/3}$ and $z = \omega/\Omega$, it is possible to rewrite the vertex correction in this regime as:

$$\left.\frac{\Delta g}{g}\right|_{q,\Omega} \sim \mathcal{G}\left(\beta\frac{(\gamma\Omega)^{1/3}}{q_y}\right) \tag{C.19}$$

where $\beta = \frac{m_B}{Nm}$ and $\mathcal{G}(x)$ is the following double integral:

$$\begin{aligned}
\mathcal{G}(x) &= \int_0^\infty \frac{du\ u}{1+u^3} \int_0^1 \frac{dz\ z^{-1/3}\ \left((1-z)^{2/3} + z^{2/3}\right)}{\left((1-z)^{2/3} + z^{2/3}\right)^2 + \frac{u^2 z^{2/3}}{x^2}} \\
&\sim x^2 \log^2 x \qquad \text{if } x \ll 1. \tag{C.20}
\end{aligned}$$

C.5   4-leg vertex

In this paragraph, we compute the renormalized 4-leg vertex $\Gamma_2(q,\Omega)$ presented in Fig 2.3, which reads:

$$\begin{aligned}
\Gamma_2(q,\Omega) \sim \bar{g}^2 \int d\omega \int d^2p\ \chi_s\left(\frac{\Omega+\omega}{2}, \frac{\mathbf{p}+\mathbf{q}}{2}\right) \chi_s\left(\frac{\Omega-\omega}{2}, \frac{\mathbf{q}-\mathbf{p}}{2}\right) \\
\times G\left(\frac{\Omega+\omega}{2}, \mathbf{k_F} + \frac{\mathbf{p}+\mathbf{q}}{2}\right) G\left(\frac{\Omega-\omega}{2}, \mathbf{k_F} + \frac{\mathbf{q}-\mathbf{p}}{2}\right). \tag{C.21}
\end{aligned}$$

Performing the integration over p_x, projection of $\mathbf{p}$ along $\mathbf{k_F}$, we obtain:

$$\begin{aligned}
\Gamma_2(q,\Omega) &\sim \frac{\bar{g}^2}{v_F} \int_0^\Omega \frac{d\omega\ dp_y}{\gamma(\Omega-\omega) + (q^2 + p_y^2 - 2q_yp_y)^{3/2}} \\
&\times \frac{1}{i\tilde{\Sigma}\left(\frac{\Omega+\omega}{2}\right) + i\tilde{\Sigma}\left(\frac{\Omega-\omega}{2}\right) - v_Fq_x - \frac{q_y^2+p_y^2}{4m_B}} \\
&\times \frac{\sqrt{(q^2 + p_y^2)^2 - 4q_y^2p_y^2}}{\gamma(\Omega+\omega) + (q^2 + p_y^2 + 2q_yp_y)^{3/2}}. \tag{C.22}
\end{aligned}$$

It is convenient at this stage to define the reduced variables $z = \omega/\Omega$ and $y = p_y/|q_y|$:

$$\begin{aligned}
\Gamma_2(q,\Omega) &\sim \bar{g}\frac{(\gamma\Omega)^{1/3}}{|q_y|^3} \int_0^1 \frac{dz\ dy}{\frac{\gamma\Omega}{|q_y|^3}(1-z) + |1-y|^3} \frac{|1-y^2|}{\frac{\gamma\Omega}{|q_y|^3}(1+z) + |1+y|^3} \\
&\times \frac{1}{i\left[(1-z)^{2/3} + (1+z)^{2/3}\right] - \frac{v_Fq_x}{\Sigma(\Omega)} - \frac{1+y^2}{\beta}\left(\frac{|q_y|^3}{\gamma\Omega}\right)^{2/3}}. \tag{C.23}
\end{aligned}$$

where we assumed that $\Omega \leq \omega_0$, and we used that in all our computations, the perpendicular component of the bosonic momentum is always either dominant or comparable to the parallel one, so that one has $q_y \sim q$.

Comparing this renormalized vertex with the bare one given by $\Gamma_1(q, \Omega) \sim \frac{\bar{g}q_y^{-2}}{1+\frac{\gamma|\Omega|}{|q_y|^3}}$, one has for the ratio of the two:

$$
\frac{\Gamma_2}{\Gamma_1} \sim \frac{(\gamma\Omega)^{1/3}}{|q_y|} \int_0^1 \frac{dz\ dy}{\frac{\gamma\Omega}{|q_y|^3}(1-z) + |1-y|^3 \frac{\gamma\Omega}{|q_y|^3}(1+z) + |1+y|^3} \frac{|1-y^2|}{}
$$
$$
\times \frac{1}{i\left[(1-z)^{2/3} + (1+z)^{2/3}\right] - \frac{v_F q_x}{\Sigma(\Omega)} - \frac{1+y^2}{\beta}\frac{|q_y|^2}{(\gamma\Omega)^{2/3}}} \tag{C.24}
$$

which only depends on two parameters: the ratios $\frac{v_F q_x}{\Sigma(\Omega)}$ and $\frac{|q_y|^3}{\gamma\Omega}$.

In the generic case of an external bosonic momentum on the mass shell, i.e. $q_x \sim q_y \sim (\gamma\Omega)^{1/3}$ one has:

$$
\frac{\Gamma_2}{\Gamma_1} \sim \frac{\Sigma(\Omega)}{v_F q_x} \sim \sqrt{\alpha}\left(\frac{\Omega}{\omega_{\text{Max}}}\right)^{1/3}. \tag{C.25}
$$

On the contrary, for a typical $q_x \sim \Sigma(\Omega)/v_F$ and $q_y \sim (\gamma\Omega)^{1/3}$:

$$
\frac{\Gamma_2}{\Gamma_1} \sim \beta, \tag{C.26}
$$

up to logarithmic factors.

APPENDIX D

Static spin susceptibility

D.1 Diagrams

In this Appendix we present the details of our calculations of the singular terms in the static spin susceptibility. We discuss in great detail the calculation of the first two diagrams in Fig. 3.2 (vertex and self-energy correction diagrams). These two diagrams can be computed explicitly both away from QCP and at QCP. We labeled the total contribution from these two diagrams as $\Pi_A(q, 0)$. The remaining two diagrams (their total contribution is $\Pi_B(q, 0)$) cannot be computed explicitly at QCP, and we compute them in an approximate scheme.

In explicit form, the first two diagrams in Fig. 3.2 are given by:

$$
\begin{aligned}
\Pi_{1a}(q, 0) = \Gamma_a \frac{\bar{g}^2}{(2\pi)^6} \int d^2K d\omega d^2l d\Omega \; G(\omega, k)^2 \\
\times \; G(\omega + \Omega, k + l)G(\omega, k + q)\chi_s(l, \Omega)
\end{aligned}
\tag{D.1}
$$

$$
\begin{aligned}
\Pi_{1b}(q, 0) = \Gamma_b \frac{\bar{g}^2}{(2\pi)^6} \int d^2K d\omega d^2l d\Omega \; \chi_s(l, \Omega)G(\omega, k)G(\omega, k + q) \\
\times \; G(\omega + \Omega, k + l)G(\omega + \Omega, k + q + l)
\end{aligned}
\tag{D.2}
$$

where $\Gamma_{a,b}$ are numerical prefactors coming from spin summation. Note that for symmetry reasons, one has to count the first diagram twice, so that the total contribution reads:

$$
\Pi_A(q, 0) = 2\Pi_{1a}(q, 0) + \Pi_{1b}(q, 0).
\tag{D.3}
$$

D.1.1 First diagram

To prove our point, we try to expand the products of fermionic Green's functions into a simpler form:

$$
\begin{aligned}
G(\omega, k)^2 G(\omega + \Omega, k + l) G(\omega, k + q) &= \frac{G(\omega, k)^2 G(\omega, k + q)}{\kappa(l, \omega, \Omega)} - \frac{G(\omega, k) G(\omega, k + q)}{\kappa(l, \omega, \Omega)^2} \\
&+ \frac{G(\omega + \Omega, k + l) G(\omega, k + q)}{\kappa(l, \omega, \Omega)^2}, \quad \text{(D.4)}
\end{aligned}
$$

where $\kappa(l, \omega, \Omega) = i(\Sigma(\omega + \Omega) - \Sigma(\omega)) - v_F l_x$

The interest of such a splitting up is that one can reduce this drastically by performing the integration over k. In fact:

$$
\int d\varepsilon_k G(\omega, k) G(\omega, k + q) = 0, \quad \text{(D.5)}
$$

since all the poles in ε_k are in the same half-plane.

For this reason, we are left with:

$$
\Pi_{1a}(q, 0) = 2\Gamma_a \frac{\bar{g}^2}{(2\pi)^6} \int d^2K d\omega d^2l d\Omega \; \chi_s(l, \Omega) \frac{G(\omega + \Omega, k + l) G(\omega, k + q)}{\kappa(l, \omega, \Omega)^2}. \quad \text{(D.6)}
$$

Let's keep this expression as it is for the moment and move on to the second diagram.

D.1.2 Second diagram

Following the same path, we can rewrite the product of fermionic Green's functions as:

$$
\begin{aligned}
G(\omega, k) G(\omega + \Omega, k + l) & G(\omega + \Omega, k + l + q) G(\omega, k + q) = \\
& \frac{G(\omega, k) G(\omega, k + q) - G(\omega, k) G(\omega + \Omega, k + l + q)}{\kappa(l, \omega, \Omega)^2} \\
& + \frac{G(\omega + \Omega, k + l) G(\omega + \Omega, k + l + q)}{\kappa(l, \omega, \Omega)^2} \\
& - \frac{G(\omega + \Omega, k + l) G(\omega, k + q)}{\kappa(l, \omega, \Omega)^2}, \quad \text{(D.7)}
\end{aligned}
$$

with the expression of κ defined above.

Once again, the integration over ε_k may give zero if the poles are in the same half-plane, which reduces our previous expression to:

$$
\begin{aligned}
\Pi_{1b}(q, 0) = -\Gamma_b \frac{\bar{g}^2}{(2\pi)^6} & \int d^2K d\omega d^2l d\Omega \; \chi_s(l, \Omega) \\
& \times \left(\frac{G(\omega + \Omega, k + l) G(\omega, k + q)}{\kappa(l, \omega, \Omega)^2} + \frac{G(\omega, k) G(\omega + \Omega, k + l + q)}{\kappa(l, \omega, \Omega)^2} \right). \quad \text{(D.8)}
\end{aligned}
$$

114

Changing k into $k - q$ in the second part of the integral, we have:

$$\Pi_{1b}(q,0) = -\Gamma_b \frac{\bar{g}^2}{(2\pi)^6} \int d^2K d\omega d^2l d\Omega \; \chi_s(l,\Omega)$$
$$\times \left(\frac{G(\omega+\Omega,k+l)G(\omega,k+q)}{\kappa(l,\omega,\Omega)^2} + \frac{G(\omega,k-q)G(\omega+\Omega,k+l)}{\kappa(l,\omega,\Omega)^2} \right). \quad \text{(D.9)}$$

One can then notice that $\varepsilon_{k-q} = \varepsilon_k - v_F q \cos\theta$ changes to ε_{k+q} if one changes θ into $\theta - \pi$. This finally leads to:

$$\Pi_{1b}(q,0) = -2\Gamma_b \frac{\bar{g}^2}{(2\pi)^6} \int d^2K d\omega d^2l d\Omega \; \chi_s(l,\Omega) \frac{G(\omega+\Omega,k+l)G(\omega,k+q)}{\kappa(l,\omega,\Omega)^2}. \quad \text{(D.10)}$$

From what precedes, we have:

$$\Pi_A(q,0) = 2\left(1 - \frac{\Gamma_b}{\Gamma_a}\right)\Pi_{1a}(q,0). \quad \text{(D.11)}$$

Spin summation prefactors can be easily computed, and are given by:

$$\begin{cases} \Gamma_a = \displaystyle\sum_{\alpha,\beta,\gamma,\delta} \sigma^Z_{\alpha\beta}\boldsymbol{\sigma}_{\beta\gamma}\cdot\boldsymbol{\sigma}_{\gamma\delta}\sigma^Z_{\delta\alpha} = 6 \\[3mm] \Gamma_b = \displaystyle\sum_{\alpha,\beta,\gamma,\delta} \sigma^Z_{\alpha\beta}\boldsymbol{\sigma}_{\beta\gamma}\sigma^Z_{\gamma\delta}\boldsymbol{\sigma}_{\delta\alpha} = -2 \end{cases}$$

This finally leads to:

$$\Pi_A(q,0) = \frac{8}{3}\Pi_{1a}(q,0). \quad \text{(D.12)}$$

D.2 Away from the QCP

In the Fermi-liquid regime we have

$$\Pi_A(q,0) = \frac{16N\bar{g}^2}{(2\pi)^6} \int d^2K d\omega d^2l d\Omega \; \frac{1}{(i(1+\lambda)\omega - \epsilon_k)^2} \frac{1}{\xi^{-2} + l^2 + \gamma\frac{|\Omega|}{l}}$$
$$\times \frac{1}{i(1+\lambda)(\omega+\Omega) - \epsilon_{k+l}} \frac{1}{i(1+\lambda)\omega - \epsilon_{k+q}} \quad \text{(D.13)}$$

where we used for the fermionic self-energy $\Sigma(\omega) = \lambda\omega$, since we are deep in the Fermi liquid phase in this case.

Defining $\cos\theta = \frac{\mathbf{k}\cdot\mathbf{l}}{|\mathbf{k}||\mathbf{l}|}$ and $\cos\theta' = \frac{\mathbf{k}\cdot\mathbf{q}}{|\mathbf{k}||\mathbf{q}|}$, and integrating over k and ω, one has:

$$\Pi_A(q,0) = i\frac{16Nm\bar{g}^2}{(2\pi)^5} \int_0^{2\pi} d\theta \int_0^{2\pi} d\theta' \int_{-\infty}^{+\infty} d\Omega \int_0^{\infty} \frac{dl\, l}{\xi^{-2} + l^2 + \frac{\gamma|\Omega|}{l}}$$
$$\times \frac{\Omega}{(i(1+\lambda)\Omega - v_F l \cos\theta)^2} \frac{1}{i(1+\lambda)\Omega - v_F q \cos\theta' - v_F l \cos\theta}. \quad \text{(D.14)}$$

115

The integral over θ' then gives:

$$
\Pi_A(q,0) = -\frac{4Nm\bar{g}^2}{\pi^4} \int_0^\pi d\theta \int_0^\infty d\Omega \int_0^\infty dl \, \frac{l}{\xi^{-2} + l^2 + \frac{\gamma\Omega}{l}}
$$
$$
\frac{\Omega}{((1+\lambda)\Omega + iv_F l \cos\theta)^2} \frac{1}{\sqrt{(v_F q)^2 + (\Omega(1+\lambda) + iv_F l \cos\theta)^2}}. \quad \text{(D.15)}
$$

It is convenient to rescale the variables at this stage, introducing $\Omega' = \frac{(1+\lambda)\Omega}{v_F q}$ and $l' = \frac{l}{q}$, so that the previous expression reduces to:

$$
\Pi_A(q,0) = -\frac{4Nm\bar{g}^2}{\pi^4 v_F(1+\lambda)^2}|q| \int_0^\pi d\theta \int_0^{+\infty} d\Omega' \int_0^\infty dl' \, \frac{l}{\xi^{-2} + \frac{\gamma v_F}{1+\lambda}\frac{\Omega'}{l'}}
$$
$$
\times \frac{\Omega'}{(\Omega' + il'\cos\theta)^2} \frac{1}{\sqrt{1 + (\Omega' + il'\cos\theta)^2}}, \quad \text{(D.16)}
$$

where we kept only the leading order in q.

Defining z and ϕ as $z\cos\phi = l'$ and $z\sin\phi = \Omega'$, one is left with:

$$
\Pi_A(q,0) = -\frac{4Nm\bar{g}^2}{\pi^4 v_F(1+\lambda)^2}|q| \int_0^\pi d\theta \int_0^\infty dz \int_0^{\pi/2} d\phi \, \frac{\cos\phi}{\xi^{-2} + \frac{\gamma v_F}{1+\lambda}\tan\phi}
$$
$$
\times \frac{z\sin\phi}{(\sin\phi + i\cos\phi\cos\theta)^2} \frac{1}{\sqrt{1 + z^2(\sin\phi + i\cos\phi\cos\theta)^2}}. \quad \text{(D.17)}
$$

Subtracting the constant part $\Pi_A(0,0)$, and integrating over z, this leads to:

$$
\delta\Pi_A(q,0) = \frac{4Nm\bar{g}^2}{\pi^4 v_F(1+\lambda)^2}|q| \int_0^{\pi/2} \frac{d\phi \, \cos\phi\sin\phi}{\xi^{-2} + \frac{\gamma v_F}{1+\lambda}\tan\phi} \int_0^\pi \frac{d\theta}{(\sin\phi + i\cos\phi\cos\theta)^4}. \quad \text{(D.18)}
$$

The angular integration over θ can be done explicitly and gives:

$$
\int_0^\pi \frac{d\theta}{(\sin\phi + i\cos\phi\cos\theta)^4} = \frac{\pi}{2} \sin\phi(5\sin^2\phi - 3). \quad \text{(D.19)}
$$

Substituting this into the expression of $\delta\Pi_A$, we are left with the following final result:

$$
\delta\Pi_A(q,0) = -\frac{2\bar{g}}{\pi^2 v_F(1+\lambda)} |q| \, \mathcal{H}\left(\frac{1+\lambda}{\gamma v_F \xi^2}\right), \quad \text{(D.20)}
$$

where $\mathcal{H}$ is defined as:

$$
\mathcal{H}(x) = \int_0^{\pi/2} d\phi \, \frac{\cos\phi\sin^2\phi(3 - 5\sin^2\phi)}{\tan\phi + x}. \quad \text{(D.21)}
$$

116

In the two limits,

$$\mathcal{H}(0) = \frac{1}{3}, \quad \mathcal{H}(x \gg 1) \simeq \frac{2}{3x^2} \tag{D.22}$$

As one approaches the QCP, ξ gets bigger, and one can take the asymptotic form of $\mathcal{H}(x)$ for small x: $\mathcal{H}(0) = 1/3$. Rearranging the prefactor for this limit, we are left with:

$$\Pi_A(q,0) \underset{\xi \to \infty}{=} -\frac{8}{9\pi}\xi^{-1} |q|. \tag{D.23}$$

D.3 At criticality

At the QCP, we have:

$$
\begin{aligned}
\Pi_A(q,0) &= \frac{16N\bar{g}^2}{(2\pi)^6} \int d^2K d\omega d^2 l d\Omega \; \frac{1}{l^2 + \gamma\frac{|\Omega|}{l}} \; \frac{1}{(i\Sigma(\omega) - \epsilon_k)^2} \\
&\times \frac{1}{i\Sigma(\omega + \Omega) - \epsilon_{k+l}} \; \frac{1}{i\Sigma(\omega) - \epsilon_{k+q}}
\end{aligned}
\tag{D.24}
$$

where we considered that, close to criticality, the self-energy dominates completely the bare ω term in the fermionic propagators.

We expand both energies as $\epsilon_{k+l} = \epsilon_k + v_F l_x + \frac{l_y^2}{2m_B}$ and $\epsilon_{k+q} = \epsilon_k + v_F q \cos\theta$, and perform the integration over ϵ_k, leading to:

$$
\begin{aligned}
\Pi_A(q,0) = i\frac{16Nm\bar{g}^2}{(2\pi)^5} \int_0^{2\pi} d\theta \int_{-\infty}^{+\infty} dl_x \int_{-\infty}^{+\infty} d\Omega \int_0^\Omega d\omega \\
\int_{-\infty}^\infty \frac{dl_y \; l}{\gamma|\Omega| + l^3} \frac{1}{\left(i\Sigma(\Omega - \omega) + i\Sigma(\omega) - v_F l_x - \frac{l_y^2}{2m_B}\right)^2} \\
\times \frac{1}{i\Sigma(\Omega - \omega) + i\Sigma(\omega) + v_F q \cos\theta - v_F l_x - \frac{l_y^2}{2m_B}}.
\end{aligned}
\tag{D.25}
$$

The integration over l_x brings two contributions. One comes from the poles in the fermionic propagator, and can be neglected here since both poles are in the same half-plane. The other contribution comes from the branch cut in the bosonic propagator, and since at the branch cut $q_x \sim q_y$, one can safely drop the quadratic term in the fermionic propagators. This allows us to integrate over l_y. Out of the terms arising from this integral, the only non-vanishing ones come from the non-analyticities of the integrated bosonic propagator defined as:

$$\int dl_y \chi(\mathbf{l}, \Omega) = \int dl_y \frac{1}{l^2 + \frac{\gamma v_F |\Omega|}{\sqrt{(v_F l)^2 + c^2 \Sigma(\Omega)^2}}}, \tag{D.26}$$

We use here the full form of the polarization operator, Eq. (A.8) as we will see that typical $v_F l_x \geq \Sigma(\Omega)$, and typical l_y are only larger in logarithmic sense.

117

This integral was performed in a slightly different form in (C.9), but the method is the same: introducing u such that $\tan u = \frac{v_F l_y}{\sqrt{(v_F l_x)^2 + \Sigma(\Omega)^2}}$, one has:

$$\int dl_y \chi(\mathbf{l}, \Omega) = \frac{(v_F l_x)^2 + c^2 \Sigma(\Omega)^2}{\gamma v_F^2 |\Omega|} \int_0^{\pi/2} \frac{du}{\cos^3 u - \delta \, \cos^2 u + \epsilon}, \tag{D.27}$$

where we introduced $\delta = \frac{c^2 \Sigma(\Omega)^2 ((v_F l_x)^2 + c^2 \Sigma(\Omega)^2)^{1/2}}{\gamma v_F^3 |\Omega|}$ and $\epsilon = \frac{((v_F l_x)^2 + c^2 \Sigma(\Omega)^2)^{3/2}}{\gamma v_F^3 |\Omega|}$.

In the process of integrating over l_x, two non-analytic contributions arise from (D.27).

One comes from $l_x \gtrsim (\gamma \Omega)^{1/3}$ and goes like $\frac{\pi}{(\gamma |\Omega|)^{1/3}}$. Plugging this back into Π_A and subtracting $\Pi_A(0,0)$, we obtain

$$\delta \Pi_A^{(1)}(q,0) N \sim m \bar{g}^2 v_F^2 q^2 \int_{-\infty}^{+\infty} \frac{dl_x}{|l_x|} \int_{-\infty}^{+\infty} d\Omega \int_0^\Omega \frac{d\omega}{(i\Sigma(\Omega - \omega) + i\Sigma(\omega) - v_F l_x)^5}$$

where we subtracted $\Pi_A(0,0)$ (hence the notation $\delta \Pi_A$) and expanded in q.

We further simplify the integrals, noticing that the fermionic propagator is dominated by $v_F l_x$ since $l_x \sim (\gamma \Omega^{1/3})$:

$$
\begin{aligned}
\delta \Pi_A^{(1)}(q,0) \quad &\sim \quad q^2 \frac{N m \bar{g}^2}{v_F^3} \int_0^{\omega_{\text{Max}}} d\Omega \int dl_x \frac{\Omega}{l_x^6} \\
&\sim \quad q^2 \frac{N m \bar{g}^2}{v_F^3 \gamma^{5/3}} \int_0^{\omega_{\text{Max}}} \frac{d\Omega}{\Omega^{2/3}} \\
&\sim \quad \sqrt{\alpha} q^2, \tag{D.28}
\end{aligned}
$$

where we substituted $l_x \sim (\gamma \Omega^{1/3})$ in the last steps.

The other non-analytic contribution from (D.27) comes from typical $v_F l_x \sim \Sigma(\Omega)$. It can be seen from an expansion of (D.27) for small values of both δ and ϵ, and goes like:

$$-\frac{(v_F l_x)^2 + c^2 \Sigma(\Omega)^2}{2 v_F^2 \gamma |\Omega|} \log \left((v_F l_x)^2 + c^2 \Sigma(\Omega)^2 \right) .) \tag{D.29}$$

One can explicitly verify that to get the logarithm, we only need the polarization operator $\Pi(l, \Omega)$ to order $1/l^3$.

Substituting (D.29) into the expression for Π_A and subtracting the constant part, we obtain:

$$
\begin{aligned}
\Pi_A^{(2)}(q,0) = i \frac{8 N m \bar{g}^2}{(2\pi)^5 \gamma v_F} q \int_0^{2\pi} d\theta \int_{-\infty}^{+\infty} dl_x \int_{-\infty}^{+\infty} \frac{d\Omega}{|\Omega|} \\
\int_0^\Omega d\omega \frac{\cos \theta \left[(v_F l_x)^2 + c^2 \Sigma(\Omega)^2 \right]}{(i\Sigma(\Omega - \omega) + i\Sigma(\omega) - v_F l_x)^3} \\
\times \frac{\log \left((v_F l_x)^2 + c^2 \Sigma(\Omega)^2 \right)}{i\Sigma(\Omega - \omega) + i\Sigma(\omega) + v_F q \cos \theta - v_F l_x}. \tag{D.30}
\end{aligned}
$$

Using the $\theta \longleftrightarrow -\theta$ symmetry, and splitting the integral over Ω into two parts, one can rearrange this expression as:

$$
\begin{aligned}
\Pi_A^{(2)}(q,0) &= i\frac{Nm\bar{g}^2}{c\pi^5\gamma v_F^2}q \int_0^\pi d\theta \int_{-\infty}^{+\infty} dz \int_0^{+\infty} \frac{d\Omega}{\Omega} \int_0^\Omega d\omega \frac{1}{\Sigma(\Omega)} \\
&\times \frac{\cos\theta(1+z^2)}{\left(i\frac{\Sigma(\Omega-\omega)+\Sigma(\omega)}{c\Sigma(\Omega)} - z\right)^3} \frac{\log(1+z^2)}{i\frac{\Sigma(\Omega-\omega)+\Sigma(\omega)}{c\Sigma(\Omega)} + \frac{v_F q\cos\theta}{c\Sigma(\Omega)} - z}, \quad \text{(D.31)}
\end{aligned}
$$

where we defined $z = v_F l_x/(c\Sigma(\Omega))$.

Let's now isolate the integral over z, given by:

$$
J = \int_{-\infty}^{+\infty} dz \frac{(1+z^2)\log(1+z^2)}{(ia-z)^3(ia+b-z)}, \quad \text{(D.32)}
$$

where $a = \frac{\Sigma(\Omega-\omega)+\Sigma(\omega)}{c\Sigma(\Omega)}$ and $b = \frac{v_F q\cos\theta}{c\Sigma(\Omega)}$, and $a \geq 0$.

Performing the contour integration in the lower half-plane (where lies the branch-cut), one gets:

$$
\begin{aligned}
J &= -2\pi \int_1^\infty dy \frac{1-y^2}{(y+a)^3(y+a-ib)} \\
&= -2\pi \int_1^\infty dy \frac{(1-y^2)(y+a+ib)}{(y+a)^3\left((y+a)^2+b^2\right)}. \quad \text{(D.33)}
\end{aligned}
$$

Once (D.33) is plugged back into (D.31), only the imaginary term survives due to the symmetry of the integral in θ. We are left with:

$$
\begin{aligned}
\Pi_A^{(2)}(q,0) &= \frac{4Nm\bar{g}^2}{c^2\pi^4\gamma v_F}q^2 \int_0^{\pi/2} d\theta \int_1^{+\infty} dy \int_0^{+\infty} d\Omega \\
&\int_0^1 dw \frac{1}{\Sigma(\Omega)^2} \frac{\cos^2\theta}{\left[c^{-1}\left((1-w)^{2/3}+w^{2/3}\right)+y\right]^3} \\
&\times \frac{1-y^2}{\left[y+c^{-1}\left((1-w)^{2/3}+w^{2/3}\right)\right]^2 + \left(\frac{v_F q\cos\theta}{c\Sigma(\Omega)}\right)^2}, \quad \text{(D.34)}
\end{aligned}
$$

where we changed variables, defining $w = \omega/\Omega$.

Introducing the new variable $t = \left(\frac{c\Sigma(\Omega)}{v_F q\cos\theta}\right)^{3/2}$, this rewrites:

$$
\begin{aligned}
\Pi_A^{(2)}(q,0) &= \frac{4Nm\bar{g}^2}{c^{3/2}\pi^4\gamma v_F^{3/2}\omega_0^{1/2}}q^{3/2} \int_0^{\pi/2} d\theta\,(\cos\theta)^{3/2} \\
&\times \int_1^{+\infty} dy \int_0^1 dw \frac{1}{\left[c^{-1}\left((1-w)^{2/3}+w^{2/3}\right)+y\right]^3} \\
&\times \int_0^{+\infty} dt \frac{1-y^2}{1+t^{4/3}\left[y+c^{-1}\left((1-w)^{2/3}+w^{2/3}\right)\right]^2}. \quad \text{(D.35)}
\end{aligned}
$$

119

A final change in variables leads to:

$$
\Pi_A^{(2)}(q,0) = \frac{4Nm\bar{g}^2}{c^{3/2}\pi^4\gamma v_F^{3/2}\omega_0^{1/2}}q^{3/2}\int_0^{\pi/2}d\theta\,(\cos\theta)^{3/2}\int_0^{+\infty}dv\,\frac{1}{1+v^{4/3}}
$$

$$
\times\int_1^{+\infty}dy\int_0^1 dw\frac{1-y^2}{\left[c^{-1}\left((1-w)^{2/3}+w^{2/3}\right)+y\right]^{9/2}} \tag{D.36}
$$

where $v = t\left[y+c^{-1}\left((1-w)^{2/3}+w^{2/3}\right)\right]^{3/2}$

Performing the integral over y, one is left with three independent integrals contributing to the numerical prefactor:

$$
\Pi_A^{(2)}(q,0) = -\frac{32Nm\bar{g}^2}{105\pi^4\gamma v_F^{3/2}\omega_0^{1/2}}q^{3/2}\int_0^{\pi/2}d\theta\,(\cos\theta)^{3/2}\int_0^{+\infty}dv\,\frac{1}{1+v^{4/3}}
$$

$$
\times\int_0^1 dw\,\frac{5c+2\left((1-w)^{2/3}+w^{2/3}\right)}{\left(c+(1-w)^{2/3}+w^{2/3}\right)^{5/2}} \tag{D.37}
$$

These integrals can be performed separately and read:

$$
\int_0^{\pi/2}d\theta\,(\cos\theta)^{3/2} = \frac{\sqrt{2}\pi^{3/2}}{6\left[\Gamma\left(\frac{3}{4}\right)\right]^2} \simeq 0.8740
$$

$$
\int_0^{+\infty}\frac{dv}{1+v^{4/3}} = \frac{3\pi\sqrt{2}}{4} \simeq 3.3322
$$

$$
\int_0^1 dw\,\frac{5c+2s(w)}{(c+s(w))^{5/2}} \simeq 0.9438 \tag{D.38}
$$

and we used the notation $s(w) = (1-w)^{2/3}+w^{2/3}$.

Collecting all integrals, and rearranging the prefactor, the final result for the contribution of the first two diagrams then writes:

$$
\Pi_A^{(2)}(q,0) = -0.1053\,\sqrt{k_F}\,q^{3/2}. \tag{D.39}
$$

D.4   The other two diagrams

The computation of the other two diagrams in Fig. 3.2 can be carried out following the same path. Far away from criticality, when $\gamma v_F\xi^2/(1+\lambda)$ is small, and one can just expand perturbatively in the interaction, the sum of these two "drag" diagrams, which we label here and in the main text as Π_B, was shown in [41] to be equal to $\Pi_A(q,0)$ to the leading order in $\bar{g}$ (which in our model is $\bar{g}^3$, see (D.20 -D.22)). Near criticality such simple relation no longer holds, but $\Pi_A(q,0)$ and $\Pi_B(q,0)$ remain of the same sign and of comparable magnitude.

At criticality, we obtained for $\Pi_B(q,0)$

$$\Pi_B(q,0) = \frac{\sqrt{2}}{3^{3/4}4\pi^4} \, q^{3/2}\sqrt{k_F}I \tag{D.40}$$

where in rescaled variables (e.g., momentum is in units of q)

$$I = \int d\Omega dx x \int_0^{2\pi} d\theta \frac{S^2(x,\Omega,\theta)}{S_1(x,\Omega)S_1(x+\cos\theta,\Omega)} \tag{D.41}$$

and $S(x,\Omega,\theta)$ and $S_1(x,\Omega)$ are given by

$$\begin{aligned}
S(x,\Omega,\theta) &= \int_0^\Omega d\omega \int_0^{2\pi} \frac{d\theta_1}{i\Sigma^* - x\cos(\theta_1)} \\
&\times \frac{1}{i\Sigma^* - \cos(\theta+\theta_1) - x\cos\theta_1} \tag{D.42} \\
S_1(x,\Omega) &= \int_0^\Omega \frac{d\omega}{x^2 + (\Sigma^*)^2} \tag{D.43}
\end{aligned}$$

where we introduced $\Sigma^* = \Sigma^*(\omega,\Omega) = (\Omega - \omega)^{2/3} + \omega^{2/3}$.

We could not evaluate this integral explicitly, and we compute it under two simplifying assumptions

- we compute $S_1(x,\Omega)$ by expanding to leading order in $(\Sigma^*/x)^2$, evaluating the frequency integral and plugging the result back into the denominator. This way, we approximated $S_1(x,\Omega)$ by

$$S_1(x,\Omega) \approx \frac{\Omega}{x^2 + (c\Omega^{2/3})^2} \tag{D.44}$$

  where $c \approx 1.2$ (see (A.6) This procedure is similar to the one which led to (A.8).

- We replace Σ^* by the same $c\Omega^{2/3}$ in the integrand for $S(x,\Omega,\theta)$

- We assume that internal momenta are larger than the external one, i.e $x \gg 1$ (x is measured in units of q), neglected terms $O(1)$ compared to $O(x)$ and set the lower limit of the integration over x at some number b.

- We choose b by applying the same approximate computation scheme to the first part $\Pi_A(q,0)$ and requesting that the result coincide with the exact expression, Eq. (D.39).

Carrying out this calculation for $\Pi_B(q,0)$ we obtain

$$\Pi_A^{(2)}(q,0) \approx -0.14 \, \sqrt{k_F} \, q^{3/2}. \tag{D.45}$$

This is the result that we cite in the text.

APPENDIX E

Two-loop renormalization of the charge susceptibility

In this Appendix we show that the singular contributions to the static charge susceptibility from individual diagrams cancel out in the full expression of $\chi_c(q)$.
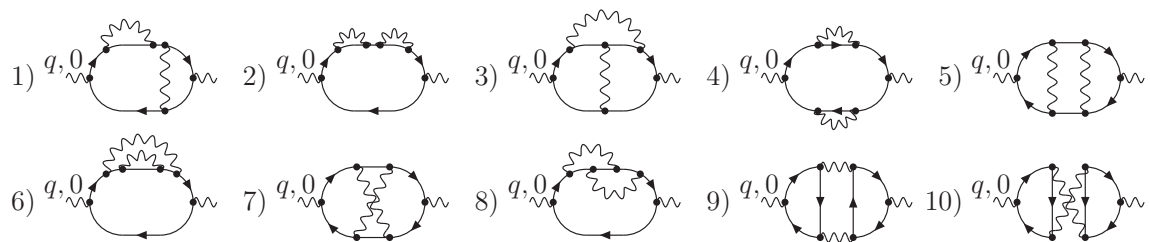
Figure 5.1: The 10 two-loop diagrams for the charge susceptibility.

There are 10 different two-loop diagrams for the charge susceptibility, presented in Fig. 5.1. The last two diagrams are identical to the ones we considered in the main text. We already argued there that these two diagrams cancel out in the case of a QCP in the charge channel.

The other eight diagrams have to be considered together. We demonstrate that the total contribution from these eight diagrams vanishes once one linearizes the dispersion of the intermediate fermions. This still leaves out the contributions from

non-linear terms in the dispersion, but one can show that these contributions are regular.

To begin, consider one of these diagrams, e.g., diagram 7 in Fig. 5.1. In analytic form, the contribution from this diagram is:

$$
\begin{aligned}
\Pi_7(q) &= 2 \int d^2q_1 d\omega_1 d^2q_2 d\omega_2 \, G_k G_{k+q} G_{k+q_1} G_{k+q_2+q} \\
&\times G_{k+q_1+q_2} G_{k+q_1+q_2+q} \chi_{q_1} \chi_{q_2},
\end{aligned}
\tag{E.1}
$$

where we labeled $q_i = (\mathbf{q}_i, \omega_i)$, and the combinatoric factor 2 comes from the summation over spin indices.

Introduce now

$$
G_k G_{k+q_i} = \frac{1}{\alpha_{q_i}} \left(G_k - G_{k+q_i} \right),
\tag{E.2}
$$

where

$$
\alpha_{q_i} = i\omega_i - q_i \cos \theta_i,
\tag{E.3}
$$

and θ_i is the angle between $\mathbf{k} \approx \mathbf{k}_F$ and $\mathbf{q}_i$. Shortening the notations further as $q_1 \equiv 1$ and $q_2 \equiv 2$, using the symbolic notation $\int_{1,2}$ for the 6-dimensional integral over q_1 and q_2, and applying (E.2), we obtain:

$$
\Pi_7(q) = 2 \int_{1,2} \chi_1 \chi_2 \left[\frac{G_{k+q} G_{k+1+2}}{\alpha_1^2 \alpha_2^2} - \frac{G_{k+q} G_{k+1+2}}{\alpha_1 \alpha_2 (\alpha_1 + \alpha_2)^2} - 2 \frac{G_{k+q} G_{k+1}}{\alpha_2^2 (\alpha_1^2 - \alpha_2^2)} \right]
\tag{E.4}
$$

Similarly,

$$
\Pi_8(q) = 2 \int_{1,2} \chi_1 \chi_2 \left[\frac{G_{k+q} G_{k+1+2}}{\alpha_1 \alpha_2 (\alpha_1 + \alpha_2)^2} - 2 \frac{G_{k+q} G_{k+1}}{\alpha_1^2 (\alpha_1^2 - \alpha_2^2)} \right]
\tag{E.5}
$$

and further

$$
\Pi_5(q) = 2 \int_{1,2} \chi_1 \chi_2 \left[\frac{G_{k+q} G_{k+1+2}}{\alpha_1 \alpha_2 (\alpha_1 + \alpha_2)^2} + 2 \frac{G_{k+q} G_{k+1}}{\alpha_1^2 (\alpha_1^2 - \alpha_2^2)} \right]
\tag{E.6}
$$

$$
\Pi_3(q) = 2 \int_{1,2} \chi_1 \chi_2 \left[-\frac{G_{k+q} G_{k+1+2}}{\alpha_1^2 \alpha_2^2} + 2 \frac{G_{k+q} G_{k+1}}{\alpha_1^2 \alpha_2^2} \left(\frac{\alpha_1^2 + \alpha_2^2}{\alpha_1^2 - \alpha_2^2} \right) \right]
\tag{E.7}
$$

$$
\Pi_2(q) = 4 \int_{1,2} \chi_1 \chi_2 \frac{G_{k+q} G_{k+1}}{\alpha_1^2 \alpha_2^2} \left(\frac{\alpha_2^2}{\alpha_1^2 - \alpha_2^2} \right)
\tag{E.8}
$$

$$
\Pi_1(q) = 4 \int_{1,2} \frac{\chi_1 \chi_2}{\alpha_1^2 \alpha_2^2} \left[G_{k+q} G_{k+1+2} \frac{\alpha_2^2}{\alpha_1^2 - \alpha_2^2} - G_{k+q} G_{k+1} \frac{3\alpha_2^2 - \alpha_1^2}{\alpha_1^2 - \alpha_2^2} \right]
\tag{E.9}
$$

$$
\Pi_4(q) = \int_{1,2} \frac{\chi_1 \chi_2}{\alpha_1^2 \alpha_2^2} \left[G_{k+q} G_{k+1+2} - 2 G_{k+q} G_{k+1} \right]
\tag{E.10}
$$

and finally,

$$
\Pi_6(q) = \int_{1,2} \frac{\chi_1 \chi_2}{\alpha_1^2 \alpha_2^2} \left[G_{k+q} G_{k+1+2} \frac{\alpha_1^2 + \alpha_2^2}{(\alpha_1 + \alpha_2)^2} - 2 G_{k+q} G_{k+1} \right]
\tag{E.11}
$$

Collecting the prefactors for $G_{k+q} G_{k+1+2}$ and $G_{k+q} G_{k+1}$ from all of the eight contributions we find that they do cancel out.

124

APPENDIX F

Mass-shell singularity

In this Appendix, we analyze in more detail the form of the self-energy near the fermionic mass shell. The interest to the mass-shell behavior of the self-energy was triggered by recent studies of the self-energy near a mass shell in a 2D Fermi liquid [33] and for 2D Dirac fermions [56]. In both cases, the lowest-order self-energy diverges at the mass-shell, which forces to re-sum the perturbative series.

At first glance, the same situation holds in our analysis at the QCP. Evaluating the self-energy in a two-loop expansion *around free fermions* and using the fermionic dispersion with the curvature, we obtain near the mass shell [57]

$$\Sigma(\mathbf{k}, \omega) \sim \frac{1}{N^2}(i\omega - \epsilon_k) \ \left[N \log \frac{i\omega - \epsilon_k}{\epsilon_k}\right]^2. \tag{F.1}$$

This result implies that the quasiparticle residue $Z \propto d\Sigma/d\epsilon_k$ logarithmically diverges on the mass shell of free fermions. Without the curvature of the dispersion, the divergence would be stronger than logarithm.

The issue we now have to address is whether Z still diverges on the mass shell if we expand around the Eliashberg solution, i.e., around fermions with

$$G_0(\mathbf{k}, \omega) = \frac{1}{i\tilde{\Sigma}(\omega) - \epsilon_k}, \tag{F.2}$$

where, we remind, $\tilde{\Sigma}(\omega) = \omega + \Sigma(\omega)$.

It turns out that this is not the case: the expansion around the Eliashberg solution leads to a finite residue Z.

Mass-shell singularity

At the two-loop order, we obtain, instead of (F.1):

$$\Sigma(\mathbf{k}, \omega) \sim \frac{1}{N^2} \int_0^1 dz \int_{1-z}^1 dz' \, (i\Sigma(\omega)\psi_{z,z'} - \epsilon_k) \left[\log \frac{N(i\Sigma(\omega)\psi_{z,z'} - \epsilon_k)}{\epsilon_k} \right]^2 \quad \text{(F.3)}$$

where

$$\psi_{z,z'} = (1-z)^{2/3} + (1-z')^{2/3} + (z+z'-1)^{2/3}. \quad \text{(F.4)}$$

For simplicity, we restricted ourselves to the quantum critical regime where $\tilde{\Sigma}(\omega) \approx \Sigma(\omega)$. If $\psi_{z,z'}$ were equal to a constant, as it is when the system is in the Fermi liquid regime, and $\Sigma(\omega) = \lambda\omega$, then Z would diverge at $\omega = \epsilon/(1+\lambda)$. However, since $\Sigma(\Omega - \omega) + \Sigma(\omega)$ does not reduce to $\Sigma(\Omega)$, we have two additional integrations over z and z', and the logarithmic singularity is washed out. In particular, at $\epsilon_k = i\Sigma(\omega)$, i.e. at the "Matsubara mass shell", we have

$$Z_{eff} \sim \frac{1}{N^2} \left[\frac{\pi^2}{6} \log^2 N - 4.08 \log N + 2.88 \right], \quad \text{(F.5)}$$

in which case Z_{eff} is just a constant. Combining this with our earlier result that the renormalization of ϵ_k is also finite, Eq. (2.65), we obtain for the full fermionic Green's function at the smallest ω and ϵ_k

$$G(\mathbf{k}, \omega) = \frac{Z_{eff}}{i\tilde{\Sigma}(\omega) - \epsilon_k^*}, \quad \text{(F.6)}$$

where ϵ_k^* differs from ϵ_k by a constant factor.

Part II

Bosonic approach to quantum impurity models

CHAPTER 5

Introduction and motivations

Contents

This first chapter is a general introduction to the Kondo model. After briefly recalling the history and the physics behind the Kondo effect, we review some of the experiments where the Kondo effect plays a major role. This experimental relevance is used to motivate the present work.

5.1 Kondo and Anderson models: a brief review

5.1.1 History of the Kondo effect

The Kondo effect was explained by Jun Kondo in 1964. It solved a 30 year old experimental puzzle, known as the resistance minimum. Kondo's theory however was incomplete, and one had to wait the work of Wilson, ten years later, to fully understand the low-temperature physics of the Kondo effect.

□ **Resistance minimum**

For electrons in a perfect lattice, the conductivity at low temperature diverges as there is no scattering, and consequently no current dissipation. At finite temperature, the essential mechanism for current dissipation lies in the scattering off phonons. At low enough temperature, the contributions from the phonons decay rapidly, and the scattering by defects and impurities in the metal host become the main source of dissipation. The low-temperature resistance saturates in this case at a finite value which depends on the number of defects in the material: adding more of them increases the residual resistance but does not affect the character of the temperature dependence.

However, since the pioneering work of de Hass et al. [58], there have been many observations of a low temperature increase in the resistance of metals, leading to a minimum of resistance (see Fig. 5.1). The later observation that the minimum depended on the concentration of impurities indicated it as being an impurity phenomenon.

In 1964, Kondo considered the interaction between a single magnetic ion, embedded inside a non-magnetic metal, and the conduction electrons of the latter [59]. He was motivated by a recent experimental work by Sarachik and collaborators [60] who observed a correlation between the existence of a Curie-Weiss term in the impurity susceptibility (signaling the existence of local moments) and the occurrence of the resistance minimum. Convinced that the magnetic character of the impurity was responsible for the resistance minimum, rather than crystal field effects or the impurity charge, he considered the following Hamiltonian[1]:

$$H = \sum_{\mathbf{k}} \sum_{\alpha=\pm} \epsilon_{\mathbf{k}} c_{\mathbf{k}\alpha}^{\dagger} c_{\mathbf{k}\alpha} + J_K \sum_{\mathbf{k},\mathbf{k}'} \sum_{\alpha\beta} \mathbf{S} \cdot \left(c_{\mathbf{k}\alpha}^{\dagger} \frac{\boldsymbol{\sigma}_{\alpha\beta}}{2} c_{\mathbf{k}'\beta} \right) \tag{5.1}$$

where $c_{\mathbf{k}\alpha}^{\dagger}$ and $c_{\mathbf{k}\alpha}$ are creation and annihilation operators for the conduction electrons, with momentum $\mathbf{k}$ and spin α. While the first term is a generic kinetic term for the band of electrons, the second term describes the interaction between the impurity spin $\mathbf{S}$ and the local density of spin of the conduction electrons.

---

[1]This Hamiltonian, often called the "Kondo Hamiltonian", was not introduced by Kondo but by Zener [61]. Kondo is however the first one to have found the log term in the resistivity.

Treating the coupling between the localized impurity spin and the sea of conduction electrons up to third order in perturbation theory, he found that the resistivity associated to such magnetic impurities reads:

$$\rho(T) = \rho_{\text{host}}(T) + a\rho_0 J_K^2 + b\rho_0^2 J_K^3 \log\left(\frac{D}{T}\right) \tag{5.2}$$

where $\rho_{\text{host}}(T)$ is the resistivity of the metal in absence of the magnetic impurities, ρ_0 is the density of states at the Fermi level, D is the bandwidth and a, b are constants proportional to the impurity density.

It follows that for an antiferromagnetically coupled impurity spin, Kondo's theory correctly describes the observed minimum of resistivity: it can be attributed to the log term which overshadows the phonon contribution to the resistivity at low enough temperature (see Fig. 5.1).

Physically, the interacting term in (5.1) generates local inter-exchange of spins between the magnetic impurity and the conduction band. This induces strong correlations between the electrons and ultimately leads to an increase in the resistivity. The Kondo effect is a true many-body problem: a first electron scattering off the impurity flips its spin, so that a second electron interacting with the local moment now sees an impurity whose spin changed because of the first electron. The electrons are now correlated due to the impurity.
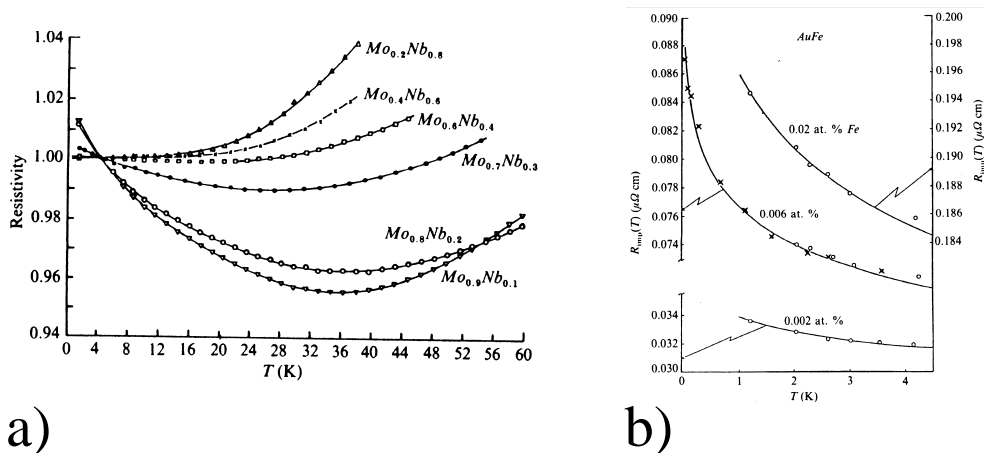

Figure 5.1: a) Data from [60] showing the minimum of resistance for Fe impurities in Mo-Nb alloys; b) Resistivity fits from Kondo's original paper [59] using the expression he derived, Eq. 5.2.

☐ **The Kondo problem**

Although Kondo's theory explains the resistance minimum, it also makes the unphysical prediction that the resistance diverges at even lower temperatures. This

divergence signals the breakdown of Kondo's perturbative treatment. Resumming the logarithmically divergent terms, a natural scale appears, below which any kind of perturbative expansion is bound to fail. This temperature scale is known as the Kondo temperature T_K, and is given by:

$$T_K \sim D e^{-1/(\rho_0 J_K)} \tag{5.3}$$

as one can argue from (5.2), by comparing the last two terms.

Anderson's work on the so-called "poor man's scaling" [62] inferred that a ground-state with an infinite coupling develops, the impurity being bound to a conduction electron in a singlet state. The behavior at low-temperature would then be similar to that of a non-magnetic impurity, the impurity spin being compensated.

Wilson's numerical renormalization group confirmed this hypothesis [63]. He could obtain definitive results for the ground-state and low-temperature behavior of the system. Wilson highlighted the existence of a dynamically generated temperature scale, corresponding to the Kondo temperature T_K, where the systems undergoes a cross-over towards a strong-coupling regime for the case of an antiferromagnetic coupling J_K. The system is then characterized by the formation of a Kondo singlet.

At high temperature, $T \gg T_K$, the impurity spin and the electrons are only weakly coupled: one can compute the properties of the system from a perturbative expansion around the free impurity regime. At low temperature, $T \ll T_K$, one enters the strong coupling regime: the conduction electrons screen out the impurity spin, forming with it a spin singlet state. Note that in this respect, the Kondo effect is a simple example of asymptotic freedom: the theory is trivial at high energy (free local moment), but much more complex at low energy (many-body object).

5.1.2 Anderson model

The Anderson model [64] is a generalization of the simple model used by Kondo, which takes into account charge fluctuations. In this model, the magnetic impurity is a localized electronic orbital, whose charge can now fluctuate. The associated Hamiltonian writes:

$$H = \sum_{\mathbf{k}} \sum_{\sigma=\pm} \epsilon_{\mathbf{k}} c_{\mathbf{k}\sigma}^{\dagger} c_{\mathbf{k}\sigma} + V \sum_{\mathbf{k}\sigma} \left(c_{\mathbf{k}\sigma}^{\dagger} f_{\sigma} + f_{\sigma}^{\dagger} c_{\mathbf{k}\sigma} \right) + \epsilon_f \sum_{\sigma} f_{\sigma}^{\dagger} f_{\sigma} + U n_{f\uparrow} n_{f\downarrow} \tag{5.4}$$

where $n_{f\sigma} = f_{\sigma}^{\dagger} f_{\sigma}$.

This model takes into account the generic kinetic term for the band of conduction electrons, an hybridization V between the localized orbital and the metallic host, the energy ϵ_f of the orbital, and finally a Coulomb repulsion term on the site of the impurity.

To get some insight into this model, let's consider the case $V = 0$, the so-called "atomic limit" (where the localized states are uncoupled from the conduction

electrons). In this situation, there are three energy configurations for the states of the localized f electrons:

- zero occupation, with a total energy $E_0 = 0$

- single occupation by a spin σ, with an energy $E_{1,\sigma} = \epsilon_f$

- double occupation with a spin $\uparrow$ and a spin $\downarrow$, with energy $E_2 = 2\epsilon_f + U$

If the ground-state corresponds to single occupation, then the system has two-fold degeneracy corresponding to spin $\frac{1}{2}$, and displays an associated magnetic moment. The other two configurations are non-degenerate and therefore non-magnetic.

It follows that in the atomic limit, the condition for the formation of a local moment is that the singly-occupied configuration lies lowest in energy. Turning on the hybridization with the conduction band, we expect that for $V \ll U$ the ground-state of the ion is essentially the same as in the atomic limit. Therefore, the Kondo model can be seen as a limiting case of the Anderson one, where the valence fluctuations of the localized orbital can be neglected.

Schrieffer and Wolf [65] used a canonical transformation (which amounts to generalizing the second-order perturbation theory to encompass off-diagonal matrix elements) to prove that if the singly occupied state is the ground-state in the atomic limit, then the effective Hamiltonian for a small hybridization is obtained by taking into account virtual excitations to the zero and double occupied states. This effective Hamiltonian reduces to the one used by Kondo, in the local moment regime defined as $U + \epsilon_f > E_F$ and $\epsilon_f < E_F$.

This can be readily seen from (5.4) by taking the limit of infinitely low energy for the orbital and the Coulomb repulsion: $\epsilon_f = -U/2 \rightarrow \infty$. In this regime, only the singly-occupied states survive, and they couple to the conduction electrons via an antiferromagnetic coupling $J_K \sim 4V^2/U$ which comes from virtual hopping onto the high-energy states of valence 0 and 2.

Note finally that because of the possibility of valence fluctuations, the physics of the Anderson model is richer than that of the Kondo model (which cannot treat, e.g., the mixed valent regime). Quite often, the theoretical formulation of experimental setups makes use of the Anderson model, and later reduces to a Kondo model in the local moment regime.

5.1.3 Experimental and theoretical relevance: the revival

Why would anyone still want to study a physical phenomenon that was explained more than 30 years ago? Although the Kondo effect is a well-known and widely studied phenomenon, it continues to capture the interest of both theorists and experimentalists [66].

Among the examples of the revival of the Kondo effect (some of which we detail in the next sections), one of the most interesting ones comes from the experimental

observation of the Kondo or Abrikosov-Suhl resonance [67, 68]. Due to the formation of the Kondo singlet state, which involves conduction electrons close to the Fermi surface, the Kondo effect results in the presence of an acute perturbation in the renormalized density of states at the Fermi energy: the "Kondo resonance".

Until very recently, physicists could only infer the role of the Kondo effect by measuring bulk properties like the resistance or the magnetic susceptibility. With the development of nanotechnology and one of its central tools – the Scanning Tunneling Microscopy or STM – it is now possible to image a surface with atomic resolution, and measure the Kondo resonance from the current versus voltage characteristics.

a)   b)
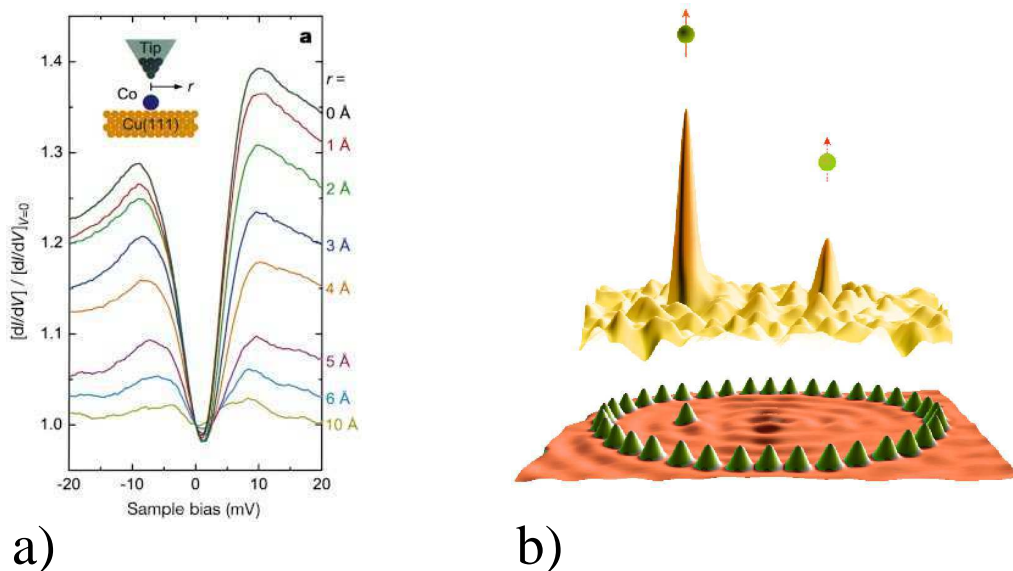
Figure 5.2: a) Differential tunnel conductance of the tip at various distances r from the impurity, taken from [69]. The anti-resonance close to zero bias is a hallmark of the Kondo effect. b) Ellipse of atoms with an impurity at one of the foci. The top part is a plot of the measured density of states on the surface, revealing a sharp peak located at both foci, even where the impurity is not present.

This has been done experimentally by two groups [70, 71] who measured the differential tunnel conductance at the site of the impurity (an atom of Co deposited on gold surface, and Ce on silver). Manoharan and collaborators [69] took it to the next level by building an ellipse of atoms around a cobalt impurity placed at one of the focal points. The STM-measured energy spectrum revealed the existence of a Kondo resonance at the site of the impurity but also at the second focus, despite the absence of any magnetic impurity at that location. Since then, this phenomenon, labeled as "quantum mirage", has led to many other experimental and theoretical studies [72].

The development of nanotechnology has rekindled interest in the Kondo effect. However, the study of these systems is limited by construction as one cannot modify the properties of the magnetic impurity or its coupling to the bulk electrons. This is precisely the next step physicists are aiming at, with the so-called "quantum dots".

5.2 Quantum dots

The ambition of this section is not to give a detailed review of the quantum dot physics[2], but rather to introduce the main concepts, explain the relevance of the Kondo effect in these systems and provide a motivation for our current work.

5.2.1 Charge quantization

Quantum dots are small semiconductor devices, man-made "droplets of charge" ranging from 10 to 1000 nm in size, where the number of trapped electrons can be tuned precisely by varying external parameters, from one to several thousand. They are made of an isolated patch containing an electron gas, coupled via tunnel barriers to one or two leads, and capacitively to a gate electrode, allowing to change the electrostatic potential of the dot (see Fig. 5.3).

These devices are often referred to as "artificial atoms", as the confinement of electrons leads to quantized energy levels as in an atom. The tremendous difference being that quantum dots allow one to scan through the entire periodic table by simply changing a voltage.

The electronic states in the dot can be probed by transport when a small tunnel coupling is allowed between the dot and the surrounding reservoir of electrons: the so-called source and drain leads. The key idea behind the study of quantum dots, is to create devices where quantum effects, such as the quantization of charge, are important. In order to do so, one has to fulfill two conditions:

- work at low temperature: $\dfrac{e^2}{C} \gg k_B T$ (where C is the capacitance of the dot)

  When tunneling occurs between the dot and the leads, the charge on the island suddenly changes by the quantized amount e. The associated change in the Coulomb energy is conveniently expressed in terms of the capacitance C of the island so that the electrostatic potential increases by an amount $E_c = e^2/C$, known as the charging energy[3]. This charging energy plays a significant role only at temperatures much below it, when states of different charge are well separated in energy.

---

[2]See [73] for a complete review of the subject, or [74, 66] for a friendly introduction to this field.

[3]For that, we assumed that the Coulomb interaction between the electrons is independent on the number N of electrons in the island. This is known as the "constant-interaction" model. Despite its simplicity, this model is remarkably accurate and allows to describe the measurements. For a detailed justification of the model, see the review of Aleiner et al. [75].

- restrict to the weak conductance regime: $G \ll \dfrac{e^2}{h}$

  This means that the tunnel barriers must be sufficiently opaque such that the electrons are located either in the dot or in the leads, and not delocalized over the whole circuit.

The first criterion can be met by making the dot small (recall that the capacitance of an object scales with its typical radius), and the second by weakly coupling the dot to the leads.

a)   b)   c)
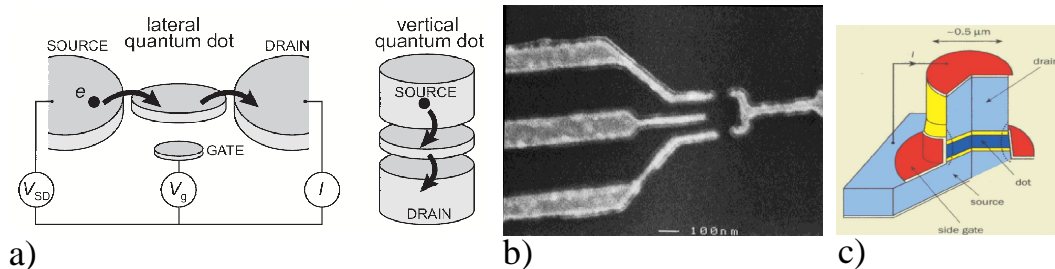
Figure 5.3: a) Schematic diagram of the lateral and vertical quantum dots (from [73]); b) Top surface of the Single Electron Transistor (SET) used in the experiments of Goldhaber-Gordon et al. [76]; c) Vertical dot structure (from [77]).

5.2.2   Coulomb blockade

In the regime of quantized charge tunneling mentioned above, the energy of a dot containing $N + 1$ electrons is greater than one containing N electrons: extra energy is therefore needed to add an electron to the dot and no current will flow until this energy is provided by increasing the voltage. This phenomenon is known as the "Coulomb blockade".

Indeed, a voltage V_g applied to the gate can change continuously the island's electrostatic energy: it lowers the energy of electrons in the droplet relative to the Fermi level in the leads. If we sweep V_g, the build up of electrostatic energy is compensated by tunneling of discrete charges onto the dot. Formally, the potential energy of a dot with N electron and a gate voltage V_g is given, in first approximation, by:

$$E = \frac{Q^2}{2C} + QV_g = \frac{1}{2}E_c N\left(N - 2\frac{CV_g}{e}\right) \tag{5.5}$$

Starting from a dot with N electrons and increasing V_g, one reaches a point where the energy of the two configurations with N and $N + 1$ electrons are degenerate. Because of this charge degeneracy, the allowed fluctuation in the number of electrons on the dot leads to a current flow and results in peaks of the conductance as a function of the gate voltage: the so-called "Coulomb oscillations" (see Fig. 5.4).

a)   b)
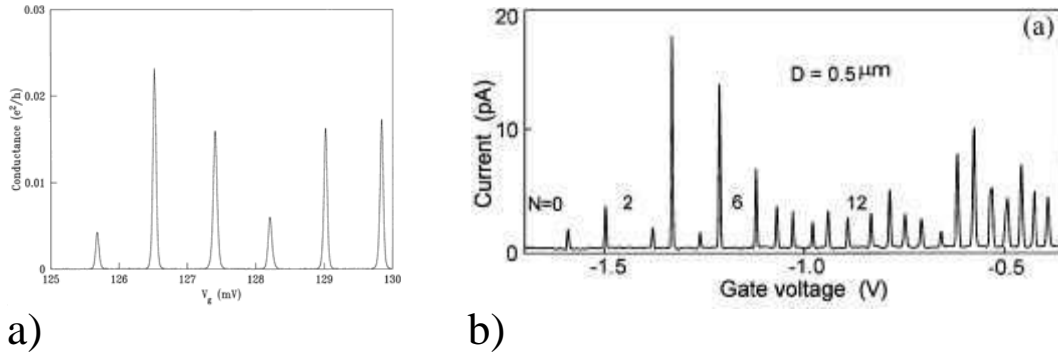
Figure 5.4: Conductance in the Coulomb blockade regime: a) for a lateral quantum dot [78], showing sharp periodically spaced peaks; b) for a vertical quantum dot [79], showing the appearance of multiplets corresponding to shell filling.

This mechanism allows one to control the current through the dot via a small change in the gate voltage V_g. For this reason, this device is also called a "single-electron transistor" (SET).

Refining a bit the model used to derive (5.5), one can take into account the energy spectrum ϵ_p of the states trapped on the dot, and consider the case where the energy spacing cannot be neglected compared to the charging energy. In this case, the energy one has to pay to add an electron to the state p is given by the charging energy. As soon as this state is filled, the energy cost increases in order to account for the energy difference between the states p and $p+1$, in addition to the charging energy. This leads to Coulomb oscillations organized in multiplets separated by an energy $E_c + \epsilon_{p+1} - \epsilon_p$, where the peaks inside a given multiplet are separated by an energy E_c. This shell structure has been observed in vertical quantum dots [79] and clearly justifies the name "artificial atoms" for these devices (see Fig. 5.4).

5.2.3   Kondo physics in quantum dots

□ **Conventional Kondo effect**

We have just seen that a voltage applied to the gate electrode controls the number N of electrons on the dot. If an odd number of electrons is trapped within the island, the total spin of the dot S is necessarily non-zero. This localized spin, embedded between large reservoirs of electrons, is susceptible to undergo a Kondo effect. The relevance of the Kondo physics for these systems was predicted theoretically by Glazman and Raikh [80] and Ng and Lee [81]. The basic punch-line is that the formation of a Kondo singlet between this localized spin and the electrons of the leads, is responsible for the development of a peak in the density of states of the localized spin (the so-called "Kondo resonance") pinned at the Fermi energy of the

leads. Since the transport properties are determined by electrons with energies close to the Fermi level, the Kondo resonance is expected to have a dramatic influence on, e.g., the conductance of the dot.

For small dots, the quantized energy difference between different electronic states (for a given number of electrons N on the island) becomes important. When the temperature becomes lower than this energy spacing, a system with an odd number of electrons on the dot effectively behaves as a spin-1/2, coupled to a gas of free fermions (the two leads), and can be described by an Anderson model with the following Hamiltonian:

$$H = \sum_{\mathbf{k},\sigma} \sum_{a=L,R} \epsilon_{\mathbf{k}} c_{a\mathbf{k}\sigma}^{\dagger} c_{a\mathbf{k}\sigma} + E_c n_{d\uparrow} n_{d\downarrow} + \epsilon_0 \sum_{\sigma} d_{\sigma}^{\dagger} d_{\sigma} + \sum_{\mathbf{k},\sigma} \sum_{a=L,R} V_a \left(c_{a\mathbf{k}\sigma}^{\dagger} d_{\sigma} + d_{\sigma}^{\dagger} c_{a\mathbf{k}\sigma} \right)$$

(5.6)

where we introduced the $c_{a\mathbf{k}\sigma}^{\dagger}$ fermionic fields to describe the electrons of the leads, as well as the fermionic $d_{\sigma}^{\dagger}$ for the localized spin of the dot.

When the temperature is larger than the coupling between the leads and the dot, one recovers the Coulomb oscillations and the conductance shows periodically spaced peaks (not very sharp if the coupling is not small enough). As the temperature is lowered, one eventually goes below the Kondo temperature. In this regime, the development of the Kondo resonance strongly enhances the conductance of the dot provided that the number of electrons on the dot is odd (as we have just argued in the previous paragraph). This leads to an even-odd effect on the dot: if the number of trapped electrons is even, the conductance drops towards zero, whereas if it is odd, it increases dramatically and eventually reaches the unitary value of $2e^2/h$ at low temperature. The Kondo effect not only suppresses the Coulomb blockade, but is also able to make the dot completely transparent (the conductance is maximal in the zero temperature limit).

These consequences of the Kondo effect have been observed experimentally [76, 82].

□ **New directions**

The quantum dots provide new opportunities to control the Kondo effect, and although the results described thus far resemble what happens for an impurity in a metal, these devices allow to study regimes inaccessible with magnetic impurities, bringing the Kondo effect to a whole new level.

To name a few examples of these new directions for the Kondo effect, one has:

- the effect of a magnetic field (singlet-triplet transition and associated two-stage screening) [84];

- the experimental realization of a two-impurity Kondo system using double quantum dots [85, 86];

a)   b)
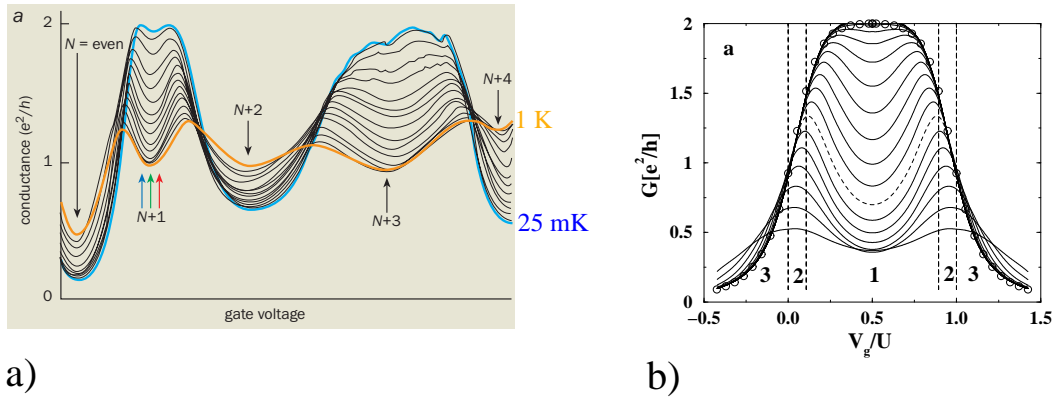
Figure 5.5: a) Experimental observation of the effect of the Kondo resonance on the conductance of a dot [82]; b) These lineshapes could be recovered theoretically using a numerical renormalization group approach [83].

- the physics out-of-equilibrium (high voltage, three-terminal SET,...);

- the coupling of a quantum dot to magnetic leads;

- the proposed experimental setups to explore the two-channel Kondo effect [87]

A lot of these effects require a better theoretical understanding of the Anderson and the Kondo models, in particular out of equilibrium, where very powerful tools like the Bethe ansatz are not so easy to extend [88]. We believe that some of the unanswered questions that these new directions raise can be, if not solved, at least better formulated, thanks to simple approaches capturing the low-temperature behavior of the Kondo effect, generalized to encompass the physics out of equilibrium. This is one of our main motivation for the present work.

5.3   Heavy fermions and the Kondo lattice

Another important application of the Kondo effect comes not from the single impurity physics, but from dense ordered lattices of impurities, and its relevance for a whole family of compounds known as "heavy fermion systems".

5.3.1   Kondo lattice

In a system containing many dilute impurities, the conduction electrons form with the network of localized spins, a set of Kondo singlets roughly independent from each other. When the density of impurity increases, correlations appear between them, due to the Kondo interaction with the conduction band.

□ RKKY interaction

As early as 1940, Frölich and Nabarro [89] discussed the possibility of a ferromagnetic interaction between nuclear spins mediated by the hyperfine coupling with the surrounding cloud of electrons. Later on, Ruderman and Kittel [90] computed from a second-order perturbation expansion the effective coupling between nuclear spins. Kasuya [91] and Yosida [92] proposed an extension of this mechanism to localized inner d-electron spins, coupled via an indirect exchange mediated by the conduction electrons. This long-range spin-spin interaction is now known as the Ruderman-Kittel-Kasuya-Yosida or "RKKY interaction".

When a magnetic moment is introduced into a metal, it polarizes the surrounding carriers by means of the Kondo interaction and induces Friedel oscillations in the spin density around the magnetic ion [93]. If another local moment is introduced, it couples with the first one, giving rise to the following long-range interaction:

$$J_{RKKY}(\mathbf{x} - \mathbf{x}') = -J_K^2 \chi(\mathbf{x} - \mathbf{x}') \quad \text{where} \quad \chi(\mathbf{q}) = 2 \sum_{\mathbf{k}} \frac{f(\epsilon_{\mathbf{k}}) - f(\epsilon_{\mathbf{k+q}})}{\epsilon_{\mathbf{k+q}} - \epsilon_{\mathbf{k}}} \qquad (5.7)$$

At zero temperature, for a parabolic band, one has:

$$J_{RKKY}(r) \sim -J_K^2 \rho_0 \frac{\sin(2k_F r) - 2k_F r \cos(2k_F r)}{2(2k_F r)^4} \qquad (5.8)$$

where ρ_0 is the density of states at the Fermi level, and r is the distance from the impurity (see Fig. 5.6). The oscillating part with a period $2k_F$ is characteristic of Friedel oscillations. As a consequence, the sign of the RKKY interaction depends on the distance between the impurities, and the typical strength of the coupling is $E_{RKKY} \sim J_K^2 \rho_0$.

□ Donicah's picture

Comparing the typical energy scale associated to the Kondo ($T_K \sim D e^{-1/(\rho_0 J_K)}$) and the RKKY ($T_{RKKY} \sim \rho_0 J_K^2$) interactions, one expects for the low temperature regime:

- for large values of the Kondo coupling constant, $T_K \gg T_{RKKY}$, one expects the Kondo effect to be the dominant interaction, leading to the formation of local singlets roughly independent of one another. This suggests the formation of a Fermi liquid ground-state,

- for small values of J_K, $T_{RKKY} \gg T_K$. A magnetically ordered state is favored in this case. This magnetic order prevents spin-flip processes to occur, and the Kondo resonance to develop.

As one varies the Kondo coupling continuously, the system is expected to go from a magnetically ordered to a Fermi liquid ground-state, with a quantum critical point separating the two at zero temperature. These arguments and the associated pictorial phase diagram that emerges from them (see Fig. 5.6), are known as the Doniach picture [94].

However, it is important to keep in mind the crudeness of these arguments: this description is only qualitative. First of all, the exponential form of the Kondo temperature used in this discussion comes from the single-impurity physics, and may very well change substantially once we treat the lattice model. Second, and more importantly, both the expressions for T_K and J_{RKKY} relies on the assumption of a somewhat large electronic bandwidth. It follows that for $J_K \sim D$, these expressions should not be taken too seriously. It turns out that, as they stand, the Kondo coupling for which both scales are of the same order of magnitude corresponds to $J_K \sim D$.
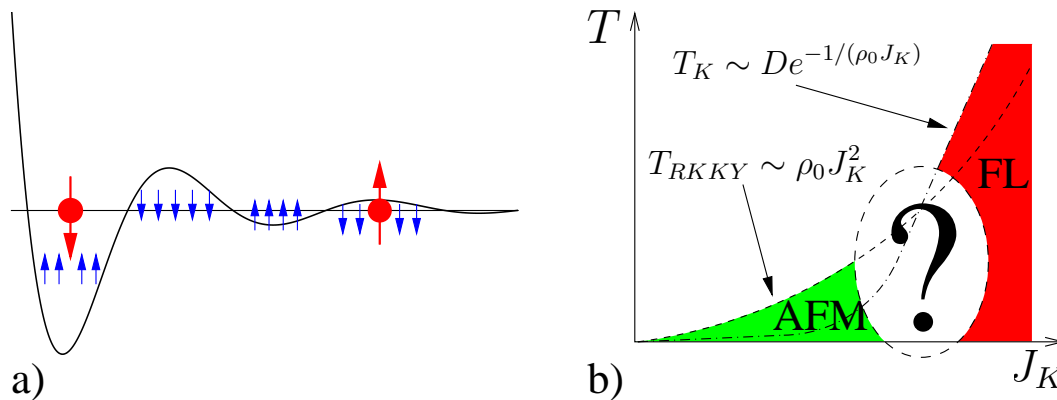
Figure 5.6: a) Illustration of the electron spin polarization (in blue) around a magnetic impurity (in red) giving rise to Friedel oscillations and inducing an RKKY interaction between impurity spins; b) Doniach phase diagram, with an antiferromagnetically ordered phase (AFM) at low J_K and a Fermi liquid phase (FL) at large J_K.

5.3.2 Heavy fermion: a prototypical Kondo lattice

There exists a whole family of compounds that can be thought of as a dense lattice of local moments embedded in a metallic host. They are known as "heavy fermions".

☐ Heavy fermions

In 1975, Andres, Graebner and Ott [95] pointed out that the low-temperature behavior of $CeAl_3$ is that of a metal, with strongly renormalized physical properties. They had just discovered one of the first examples of heavy fermion metal.

Heavy fermion materials are rare-earth or actinide-based compounds, containing f-electron elements (U, Ce, Yb). They are distinguished at low temperatures by an anomalously large specific heat coefficient, with correspondingly large Pauli paramagnetic susceptibility (here "large" means 2 to 4 orders of magnitude larger than, say, Cu). These properties can be described within the framework of Landau's Fermi liquid theory, by considering a large renormalized mass, as big as 10^4 bare electronic mass, hence the name "heavy fermion" associated to these compounds (see Fig. 5.7).

Microscopically, one of the most important properties of the 4-f and 5-f elements is the small spatial extent of their radial probability. One can thus consider that heavy fermion materials are made of localized f orbitals arranged in a periodic lattice, interacting with delocalized conduction electrons.

For this reason, the heavy fermion compounds are thought to be described by the periodic Anderson model, whose Hamiltonian writes:

$$H = \sum_{\mathbf{k}} \sum_{\sigma=\pm} \epsilon_{\mathbf{k}} c_{\mathbf{k}\sigma}^{\dagger} c_{\mathbf{k}\sigma} + V \sum_{i,\sigma} \left(c_{i\sigma}^{\dagger} f_{i\sigma} + f_{i\sigma}^{\dagger} c_{i\sigma} \right) + \epsilon_f \sum_{i,\sigma} f_{i\sigma}^{\dagger} f_{i\sigma} + U n_{fi\uparrow} n_{fi\downarrow} \quad (5.9)$$

where the f electrons hybridize with the conduction electrons c.

In practice, due to the large local repulsion, and the weak hybridization of the $4-f$ and $5-f$ shells, most lanthanides and actinides-based compounds have stable valence states and concomitant local magnetic moments, which allows the reduction of the previous Hamiltonian, Eq. (5.9), to the one of the Kondo lattice model.

□ QCP and Non-Fermi liquid

Heavy fermion materials offer a unique opportunity to study quantum criticality under controlled conditions: by applying pressure, doping, or magnetic field, it is possible to tune the ground-state of the system from a magnetically ordered state to a Fermi liquid, through a quantum critical point.

A wide body of evidence suggests that the effective mass m^* of the fermionic quasiparticles in the paramagnetic Fermi liquid diverges as one approaches the QCP. This divergence leads to a breakdown of Landau's Fermi liquid theory, and the state which forms above the QCP is referred to as a non-Fermi liquid[4].

Among the wide range of physical properties that departs from the Fermi liquid behavior at criticality, one sees many common features[5] (see Fig. 5.7):

- diverging specific heat coefficient at the QCP:

$$\frac{C_v}{T} \sim c \log \left(\frac{T_0}{T} \right) \quad \text{or, more rarely} \quad \sim T^{-1+\lambda} \quad (5.10)$$

---

[4]This designation, already used in the text for MnSi, actually encompasses a broad range of different behaviors. Quoting Altshuler: "The difference between a Fermi liquid and a non-Fermi liquid is like the difference between a banana and a non-banana".

[5]For a review of the experimental data of the non-Fermi liquid behavior of f-electron metals, see e.g. [96].
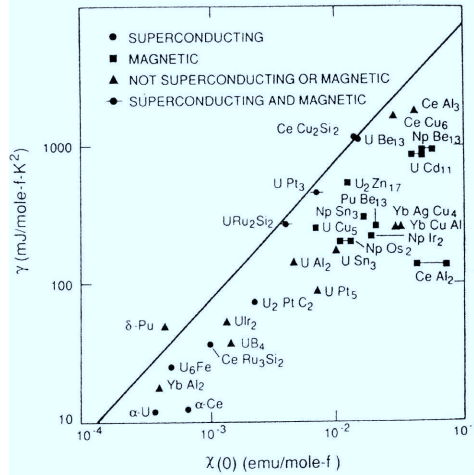
Compound	C_v/T	$\rho(T)$
$YbRh_2Si_2$	$\log T$	T
$CeCoIn_5$		T
$CeCu_{6-x}Au_x$	$\log T$	T
$CeCu_{6-x}Ag_x$	$\log T$	$T^{1.1}$
$CeNi_2Ge_2$	$\log T$	$T^{1.4}$
$CeCu_2Si_2$	$\log T$	$T^{1.5}$
$YbAgGe$	$\log T$	T
$CePd_2Si_2$	$T^{-0.5}$	$T^{1.2}$

a)   b)

Figure 5.7: a) Specific heat coefficient and Pauli susceptibility of a few heavy fermion materials in the Fermi liquid regime; b) Selected list of heavy fermion compounds, and their associated properties in the quantum critical regime.

with $0.5 \leq \lambda \leq 0.9$. This suggests that the effective mass $m^* \to \infty$ at the QCP.

- quasi-linear resistivity:

$$\rho(T) \sim \rho_0 + AT^{1+\epsilon} \tag{5.11}$$

where $0 \leq \epsilon \leq 0.6$ at the QCP. This quasi-linear behavior is seen on a temperature range going from half a decade up to three decades (for Ge-doped $YbRh_2Si_2$ [97]).

- a non-Curie spin susceptibility:

$$\chi^{-1}(T) = \chi_0^{-1} + CT^a \tag{5.12}$$

where $a < 1$.

In addition to this non-Fermi liquid behavior, scaling properties could be measured for a few compounds: in $YbRh_2Si_2$, the differential susceptibility exhibits H/T scaling [98] and in $CeCu_{6-x}Au_x$, neutron scattering measurements showed E/T scaling in the dynamical spin susceptibility [99].

None of the theoretical approaches devised to date, could explain all of these features (though some could recover partial results). The key ingredient that is generally missing is the competition between the Kondo effect and the development of magnetic correlations: most approaches have focused on one or the other unsuccessfully.

143

The bosonic scheme we develop in the next chapters of this manuscript is an attempt at bridging this gap. As we argue in Chapter 6 and 7, such a procedure does recover the Fermi liquid behavior (at least the expected thermodynamics) and allows one to study the effect of magnetic correlations. The extension to the lattice - though not yet achieved - could lead to extremely useful insights in building a mean-field theory susceptible to describe the quantum phase transition between antiferromagnetism and the heavy electron fluid.

CHAPTER 6

Single impurity multichannel Kondo model

Contents

In this chapter, we introduce and analyze the antiferromagnetic multichannel Kondo model for a single impurity. After deriving the saddle-point equations and recalling the results known for the overscreened and the underscreened regime, we study in details the physical properties of the exactly screened scenario.

6.1 Background

6.1.1 Generalized Kondo model

As a starting point, we consider the generalized Kondo model as introduced by Coqblin and Schrieffer [100]. This model is a generalization of the original one studied by Kondo, where the $SU(2)$ symmetry group has been extended to $SU(N)$. The Hamiltonian then writes:

$$H = \sum_{\mathbf{k}} \sum_{\sigma=1}^{N} \epsilon_{\mathbf{k}} c_{\mathbf{k}\sigma}^{\dagger} c_{\mathbf{k}\sigma} + \frac{J_K}{N} \sum_{\mathbf{k},\mathbf{k}'} \sum_{\alpha,\beta} S_{\alpha\beta} c_{\mathbf{k}\beta}^{\dagger} c_{\mathbf{k}'\alpha} \tag{6.1}$$

where the spin flavor now runs from 1 to N, and the antiferromagnetic Kondo coupling has been rescaled to preserve the same scaling in N for the kinetic and the interacting part of the Hamiltonian. The $c_{\mathbf{k}\sigma}^{\dagger}$ and $c_{\mathbf{k}\sigma}$ fields correspond respectively to the creation and annihilation of a conduction electron with momentum $\mathbf{k}$ and spin index σ.

The impurity spin $S_{\alpha\beta}$ now satisfies the commutation rules of the $su(N)$ algebra, namely:

$$[S_{\alpha\beta}, S_{\gamma\delta}] = \delta_{\beta\gamma} S_{\alpha\delta} - \delta_{\alpha\delta} S_{\gamma\beta} \tag{6.2}$$

□ Representation

While any irreducible representation of $SU(N)$ could be used to describe the impurity spin, historically, two representations retained attention:

- Schwinger bosons [101]

  This amounts to introducing N bosonic fields b_α, whose total number is constrained to be related to the size S of the impurity spin via the relation:

$$\sum_{\alpha} b_{\alpha}^{\dagger} b_{\alpha} = P = 2S \tag{6.3}$$

  The $S_{\alpha\beta}$ operator is then defined as:

$$S_{\alpha\beta} = b_{\alpha}^{\dagger} b_{\beta} - \frac{P}{N} \delta_{\alpha\beta} \tag{6.4}$$

146

where one can easily check that the commutation rule is satisfied, and the second term is introduced to make the operator traceless. Such a representation corresponds, in terms of Young tableaux, to a single line of P boxes (see Fig.6.1a). Note that in the case of a line representation, there is no upper boundary for P.

- Abrikosov pseudo-fermions [67]

  This is the fermionic counterpart of the previous one. One introduces here a set of fermionic operators f_α, verifying:

  $$S_{\alpha\beta} = f_\alpha^\dagger f_\beta - \frac{Q}{N}\delta_{\alpha\beta} \tag{6.5}$$

  $$\sum_\alpha f_\alpha^\dagger f_\alpha = Q \tag{6.6}$$

  In terms of Young tableaux, this representation corresponds to a column of Q boxes, where by construction $0 \leq Q \leq N$ (see Fig.6.1b).
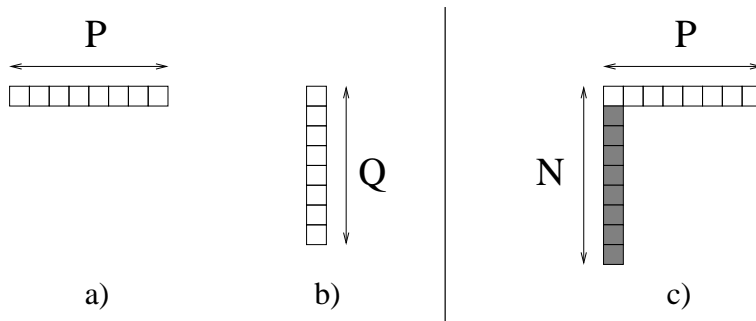
Figure 6.1: a) and b) Two examples of representation of $SU(N)$, c) Strong coupling limit of the single channel model. The white boxes correspond to the bosonic line representation and the gray ones to the conduction electrons.

Earlier treatments of the Kondo and Anderson models made use of a fermionic representation of the impurity spins [102, 103]. However, one of our ultimate goals is to describe the competition between magnetism and the Kondo effect in the lattice version of this model. It turns out that a bosonic representation of the localized spin is well suited to describe local moment magnetism[1], as it provides a simple way of handling long-range magnetic order via Bose condensation [105]. For this reason, we focus in the rest of this text only on the Schwinger boson representation of the impurity spins.

---

[1]One of the first successful applications of a Schwinger boson mean-field theory was carried out by Arovas and Auerbach [104] on quantum Heisenberg models.

□ Channel index

One can use Young tableaux to investigate the strong coupling solution of the generalized Kondo model: one combines the first box of the line representation with a column of boxes representing the conduction electrons to form a spin singlet. One then notices from Fig. 6.1c, that unless $P = 1$, this model describes an underscreened impurity, where only a fraction of the original spin is screened by the conduction electrons, leaving a residual spin of size $S = \frac{P-1}{2}$. In order to overcome this, Parcollet and Georges [106] introduced a multichannel version of the generalized Kondo model. The idea is to multiply the number of electronic flavors by introducing a channel index μ that runs from 1 to K. The Kondo interaction is left unchanged as no channel anisotropy is introduced. The new Hamiltonian, which now has the symmetry $SU(N) \times SU(K)$, is given by:

$$H = \sum_{\mathbf{k}} \sum_{\sigma=1}^{N} \sum_{\mu=1}^{K} \epsilon_{\mathbf{k}} c_{\mathbf{k}\sigma\mu}^{\dagger} c_{\mathbf{k}\sigma\mu} + \frac{J_K}{N} \sum_{\mathbf{k},\mathbf{k}'} \sum_{\alpha,\beta} \sum_{\mu} b_{\alpha}^{\dagger} b_{\beta} c_{\mathbf{k}\beta\mu}^{\dagger} c_{\mathbf{k}'\alpha\mu} \tag{6.7}$$

where we have replaced the impurity spin operator by the Schwinger boson representation, and dropped the constant term proportional to the total number of electrons at the site of the impurity.

This Hamiltonian is the starting point for all the work presented in this chapter.

6.1.2 Strong coupling limit

The multichannel Kondo Hamiltonian allows us to tune separately the parameters P and K, i.e. the size of the impurity spin and the total number of channels. This gives access to three regimes with very different physics. In order to get a first flavor of the physics associated to these regimes, we study the strong coupling behavior of the model using arguments due to Nozières and Blandin [107].

□ Nozières-Blandin analysis

In the strong coupling limit, the kinetic energy of the conduction electrons is negligible, and finding the ground state then amounts to minimizing the Kondo energy. In this limit, the impurity tends to trap as many electrons as possible (i.e. one per channel) with spin opposite to the one sitting at the impurity site. This results in a local effective spin of size $S - \frac{K}{2} = \frac{P-K}{2}$, hence three possibilities:

- $K < P$: Underscreened

  The trapped electrons cannot quench completely the impurity spin, so that the dressed impurity remains magnetic with a spin of reduced size. Virtual hopping to the first layer of neighbors with strength t generates a new Kondo effect between the residual spin and the conduction electrons with a weak

ferromagnetic coupling $J_{\text{eff}} \sim \frac{t^2}{J_K}$ which vanishes in the infinite coupling limit, suggesting that the $J_K \to \infty$ fixed point is stable.

- $K = P$: Exactly screened

  The ground state is non degenerate and the strong coupling fixed point is attractive: the usual Fermi liquid picture applies.

- $K > P$: Overscreened

  Like the underscreened case, this leads to a finite residual spin, weakly coupled to the conduction electrons. However, the sign of this residual spin is opposite to the starting impurity spin S, so that the effective Kondo coupling between this residual spin and the conduction electrons is now antiferromagnetic: the $J_K \to \infty$ fixed point is now unstable.

The strong coupling arrangement of spins for the impurity and the trapped electrons for the various cases is presented in Fig. 6.2.
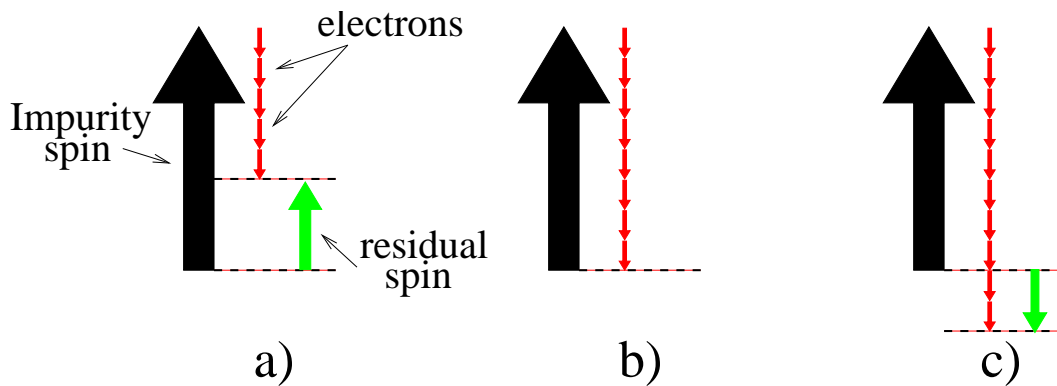
Figure 6.2: Schematic view of the three screening regimes: a) Underscreened case, b) Exactly screened case, c) Overscreened case. The large black arrow corresponds to the impurity spin, the small red ones to the electrons and the green arrow to the residual spin

□ **Using Young tableaux**

As one extends the original symmetry to $SU(N)$, the same kind of arguments hold but the derivation is more involved. However, there is a much easier and more convenient way of describing the physics of the strong coupling limit by using Young tableaux.

The idea is that for any given line representation of the impurity spin, each box can combine with a column of $N - 1$ boxes representing the conduction electrons in order to form a spin singlet (the Pauli principle imposes that the total number

149

of boxes per column cannot be greater than the spin degeneracy N). For a single channel, this is represented by Fig.6.1c. As soon as one increases the number of channels, it becomes possible to form a singlet between the second box of the line representation and a column of conduction electrons taken in another channel.
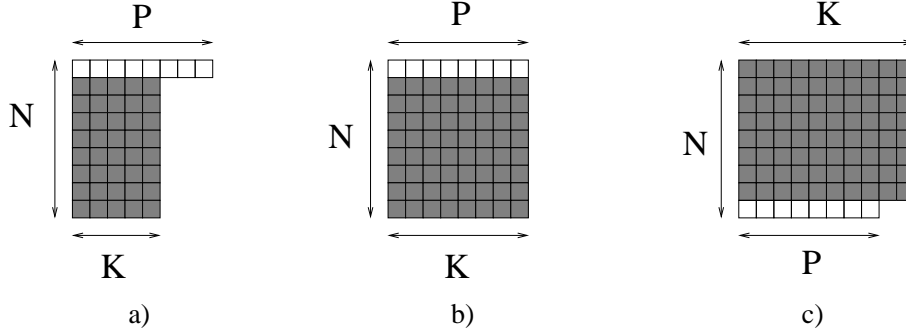
Figure 6.3: a) Underscreened case, b) Exactly screened case, c) Overscreened case. The impurity spin is described by a line of white boxes and the conduction electrons by gray boxes.

For a given size of the impurity spin, i.e. a given length P of the line representation, one can identify three regimes depending on the total number of channels, just like in the $SU(2)$ case. One expects the following strong-coupling limits:

- Underscreened: $P > K$

  The conduction electron screens part of the impurity spin, leaving behind a residual spin of size $S = \frac{P-K}{2}$. The expected low-energy physics is then the one of a local moment, decoupled from the conduction electron band at zero temperature. As one departs slightly from this strong-coupling fixed point, a weak ferromagnetic effective Kondo interaction is restored signaling the stability of this fixed point.

- Exactly screened: $P = K$

  The impurity spin is totally screened in this case and forms an antiferromagnetic singlet. The impurity site is then locked and acts as a scattering center for the conduction electrons. One expects the low-energy physics to be Fermi-liquid like with a finite phase shift on the site of the impurity.

- Overscreened: $P < K$

  The number of screening channels is too important. A residual spin of size $S = \frac{K-P}{2}$ now remains. However, a small departure from this fixed point leads to a residual antiferromagnetic Kondo interaction, so that the strong-coupling fixed point is unstable and the system flows towards a stable infra-red fixed point. One expects from other investigations that this fixed point is non-Fermi-liquid like.

It follows that the generalization of the Kondo model to the $SU(N)$ symmetry gives qualitatively similar results to the $SU(2)$ case, which motivates the study of the generalized multichannel Kondo model in the large-N limit.

These three regimes are represented in Fig.6.3, where the impurity spin is described by white boxes and the conduction electrons by gray ones.

6.1.3 Saddle-point equations

In order to derive the large-N equations, we consider the multichannel Hamiltonian with a bosonic representation of the impurity spin, where we explicitly include the constraint on the total number of Schwinger bosons via a Lagrange multiplier. The action then reads:

$$
\begin{aligned}
S \;=\; & \int_0^\beta d\tau \sum_{\mathbf{k},\sigma,\mu} c_{\mathbf{k}\sigma\mu}^\dagger(\tau)\,(\partial_\tau + \epsilon_{\mathbf{k}})\,c_{\mathbf{k}\sigma\mu}(\tau) + \int_0^\beta d\tau \sum_\alpha b_\alpha^\dagger(\tau)\,(\partial_\tau - \lambda(\tau))\,b_\alpha(\tau) \\
& + \frac{J_K}{N} \sum_{\alpha,\beta,\mu} \int_0^\beta d\tau\; \psi_{\beta\mu}^\dagger(\tau)\psi_{\alpha\mu}(\tau)b_\alpha^\dagger(\tau)b_\beta(\tau) \\
& + p_0 N \int_0^\beta d\tau\;\lambda(\tau) - \frac{p_0 J_K}{N}\int_0^\beta d\tau \sum_{\alpha,\mu}\psi_{\alpha\mu}^\dagger(\tau)\psi_{\alpha\mu}(\tau) \qquad (6.8)
\end{aligned}
$$

where $\psi_{\alpha\mu}^\dagger = \frac{1}{\sqrt{\mathcal{N}}}\sum_{\mathbf{k}} c_{\mathbf{k}\alpha\mu}^\dagger$ creates an electron in the Wannier state at the impurity site.

Taking the limit of infinite N, one has to rescale the parameters P and K with N in order to describe a non-trivial case. We then define the following rescaled parameters:

$$
P = p_0 N \qquad K = \gamma N \qquad (6.9)
$$

It is important to notice that this rescaling in N preserves the distinction between the three regimes: $p_0 > \gamma$ corresponds to the underscreened case, $p_0 = \gamma$ to the exactly screened case and $p_0 < \gamma$ to the overscreened case.

The first step is to integrate out of the partition function all of the conduction electrons, apart from the ones at the impurity site. We then decouple the interacting term by introducing an auxiliary Grassmanian field[2] $\chi_\mu(\tau)$ for every channel index,

---

[2]Note that the fields χ_μ contain no time derivative, so that instantaneously they behave as inert neutral fields.

which leaves us with the following action:

$$
\begin{aligned}
S \;=\; & -\int_0^\beta d\tau d\tau' \sum_{\sigma,\mu} \psi_{\sigma\mu}^\dagger(\tau) G_{c0}^{-1}(\tau-\tau')\,\psi_{\sigma\mu}(\tau') - \frac{1}{J_K}\int_0^\beta d\tau \sum_\mu \chi_\mu^\dagger(\tau)\chi_\mu(\tau) \\[2mm]
& + p_0 N \int_0^\beta d\tau\,\lambda(\tau) + \int_0^\beta d\tau \sum_\alpha b_\alpha^\dagger(\tau)\,(\partial_\tau - \lambda(\tau))\,b_\alpha(\tau) \\[2mm]
& + \frac{1}{\sqrt{N}} \sum_{\alpha,\mu}\int_0^\beta d\tau \,\left(\psi_{\alpha\mu}^\dagger(\tau) b_\alpha(\tau)\chi_\mu(\tau) + \chi_\mu^\dagger(\tau) b_\alpha^\dagger(\tau)\psi_{\alpha\mu}(\tau)\right)
\end{aligned}
\tag{6.10}
$$

where we have dropped the $\frac{p_0 J_K}{N}\psi^\dagger\psi$ term since it only contributes to the local electronic Green's function to the order $1/N$.

The bare local conduction electron Green's function G_{c0} is given by:

$$
G_{c0}(i\omega_n) = \sum_{\mathbf{k}} \frac{1}{i\omega_n - \epsilon_{\mathbf{k}}}
\tag{6.11}
$$

The actual choice of the conduction band does not matter much as long as we are interested in a regime of temperature much smaller than the bandwidth: we only probe the low-energy excitations, and only the density of states at the Fermi level really matters.

There are two different ways of obtaining the saddle-point equations for the Green's functions. First, we choose to derive them following the work of [106]. Then, we derive them from a Luttinger-Ward[108, 109, 110] perspective, as this will turn out to be useful in many aspects in the rest of the text.

$\square$ Derived from the action

The first step is to integrate the remaining conduction electrons out of the partition function to end up with an effective action depending only on the Schwinger bosons and the χ fermions:

$$
\begin{aligned}
S \;=\; & \int_0^\beta d\tau \sum_\alpha b_\alpha^\dagger(\tau)\,(\partial_\tau - \lambda(\tau))\,b_\alpha(\tau) - \frac{1}{J_K}\int_0^\beta d\tau \sum_\mu \chi_\mu^\dagger(\tau)\chi_\mu(\tau) \\[2mm]
& - \frac{1}{N}\int_0^\beta d\tau d\tau' \sum_\mu \chi_\mu(\tau')\chi_\mu^\dagger(\tau)\,G_{c0}(\tau-\tau') \sum_\alpha b_\alpha(\tau')b_\alpha^\dagger(\tau) \\[2mm]
& + p_0 N \int_0^\beta d\tau\,\lambda(\tau)
\end{aligned}
\tag{6.12}
$$

It is useful at this stage to introduce the following precursors to the Green's functions:

$$
N_\chi(\tau,\tau') = \sum_\mu \chi_\mu(\tau')\chi_\mu^\dagger(\tau) \qquad\qquad N_b(\tau,\tau') = \sum_\alpha b_\alpha(\tau')b_\alpha^\dagger(\tau)
\tag{6.13}
$$

One now introduces two new fields labeled $Q(\tau, \tau')$ and $\bar{Q}(\tau, \tau')$, conjugated respectively to $N_\chi(\tau, \tau')$ and $N_b(\tau, \tau')$. The idea is to generalize to a path-integral formulation the following result:

$$\int dX dY \ e^{-AXY + X\phi + Y\psi} = \text{Const.} \times e^{\phi A^{-1}\psi} \tag{6.14}$$

The partition function can be rewritten as $Z = \int \mathcal{D}Q\mathcal{D}\bar{Q}\mathcal{D}\lambda \ e^{-S(Q,\bar{Q},\lambda)}$ with the effective action expressed in terms of these new fields:

$$
\begin{aligned}
S(Q, \bar{Q}, \lambda) &= N \int_0^\beta d\tau d\tau' \ \bar{Q}(\tau, \tau') G_{c0}^{-1}(\tau - \tau') Q(\tau, \tau') + p_0 N \int_0^\beta d\tau \ \lambda \\
&\quad - N \log Z_b(Q, \bar{Q}, \lambda) - K \log Z_\chi(Q, \bar{Q}, \lambda)
\end{aligned} \tag{6.15}
$$

where the partial partition functions are defined as:

$$
\begin{aligned}
Z_b &= \int \mathcal{D}b^\dagger \mathcal{D}b \ e^{-\int_0^\beta d\tau \ b^\dagger(\tau)(\partial_\tau - \lambda(\tau))b(\tau) + \int d\tau d\tau' Q(\tau,\tau')b(\tau')b^\dagger(\tau)} \\
Z_\chi &= \int \mathcal{D}\chi^\dagger \mathcal{D}\chi \ e^{-\int_0^\beta d\tau \ \chi^\dagger(\tau)(\partial_\tau - \lambda(\tau))\chi(\tau) + \int d\tau d\tau' \bar{Q}(\tau,\tau')\chi(\tau')\chi^\dagger(\tau)}
\end{aligned} \tag{6.16}
$$

The important element here is that every term in $S(Q, \bar{Q}, \lambda)$ scales like N, so that in the large-N limit one can apply the method of steepest descent. The saddle-point is such as the derivatives of $S(Q, \bar{Q}, \lambda)$ with respect to its variables all vanish:

$$
\begin{aligned}
\frac{\delta S(Q, \bar{Q}, \lambda)}{\delta Q(\tau, \tau')} &= 0 \implies \bar{Q}(\tau, \tau') = -G_{c0}(\tau - \tau')G_b(\tau' - \tau) \\
\frac{\delta S(Q, \bar{Q}, \lambda)}{\delta \bar{Q}(\tau, \tau')} &= 0 \implies Q(\tau, \tau') = -\gamma G_{c0}(\tau - \tau')G_\chi(\tau' - \tau) \\
\frac{\delta S(Q, \bar{Q}, \lambda)}{\delta \lambda(\tau)} &= 0 \implies p_0 = -G_b(\tau = 0^-)
\end{aligned} \tag{6.17}
$$

where we use the conventional definition of the Green's functions as:

$$
\begin{cases}
G_b(\tau) &= -\langle Tb(\tau)b^\dagger(0)\rangle_Z &= -\langle Tb(\tau)b^\dagger(0)\rangle_{Z_b} \\
G_\chi(\tau) &= -\langle T\chi(\tau)\chi^\dagger(0)\rangle_Z &= -\langle T\chi(\tau)\chi^\dagger(0)\rangle_{Z_\chi}
\end{cases} \tag{6.18}
$$

A careful look at (6.18) and (6.16) suggests that $Q(\tau, \tau')$ (resp. $\bar{Q}(\tau, \tau')$) is trivially related to the self-energy $\Sigma_b(\tau - \tau')$ (resp. $\Sigma_\chi(\tau - \tau')$):

$$\Sigma_b(\tau) = \gamma G_{c0}(\tau)G_\chi(-\tau) \qquad \Sigma_\chi(\tau) = -G_{c0}(\tau)G_b(-\tau) \tag{6.19}$$

where the self-energies are defined as:

$$G_b^{-1}(i\nu_n) = i\nu_n + \lambda - \Sigma_b(i\nu_n) \qquad G_\chi^{-1}(i\omega_n) = J_K - \Sigma_\chi(i\omega_n) \tag{6.20}$$

153

These saddle-point equations are valid for any shape of the conduction band, in particular there is no need to impose particle-hole symmetry. The striking feature of these saddle-point equations is that they are expressed in terms of the one-particle Green's functions only, so that once the solution is achieved, one gets access to a large variety of physical quantities (free energy, entropy, correlation functions, ...).

□ Derived from a Luttinger-Ward picture

It is possible to derive the self-consistent equations for the self-energies starting from the free energy of the model. In the Baym-Kadanoff[111, 112] formalism, the free energy can be recast as a functional of the various Green's functions one has to consider[3]:

$$
\begin{aligned}
F &= NT \sum_n \log(-G_b^{-1}(i\nu_n)) - KT \sum_n \log(-G_\chi^{-1}(i\omega_n)) \\
&\quad -NKT \sum_n \log(-G_c^{-1}(i\omega_n)) + NT \sum_n \Sigma_b(i\nu_n)G_b(i\nu_n) \\
&\quad -KT \sum_n \Sigma_\chi(i\omega_n)G_\chi(i\omega_n) - NKT \sum_n \Sigma_c(i\omega_n)G_c(i\omega_n) \\
&\quad +Np_0\lambda + \Phi_{LW}[G_b, G_\chi, G_c]
\end{aligned}
\tag{6.21}
$$

The Luttinger-Ward functional $\Phi_{LW}[G_b, G_\chi, G_c]$ is given by the sum of all 2-particle irreducible diagrams. Some of these diagrams are presented in Fig. 6.4, where we use straight lines for the conduction electron, wavy lines for the Schwinger boson and dashed lines for the $\chi-$fermion full propagators. This sum ultimately reduces to the first leading order diagram, once we take the large-N limit.

Figure 6.4: Some of the skeleton diagrams contributing to the Luttinger-Ward functional.

Using the stationarity of the free energy functional with respect to the Green's functions G_b, G_χ and G_c, one can see that at the saddle-point, the self-energies associated to these fields can be expressed as a derivative of the Luttinger-Ward

---

[3]The actual derivation of this expression for a single impurity Kondo model is given in Appendix A.

functional, leading to:

$$
\begin{aligned}
\Sigma_b(\tau) &= \frac{-1}{N}\frac{\delta\Phi_{LW}}{\delta G_b(\beta-\tau)} &= \underset{O(K/N)}{} \\[2em]
\Sigma_\chi(\tau) &= \frac{-1}{K}\frac{\delta\Phi_{LW}}{\delta G_\chi(\beta-\tau)} &= \underset{O(1)}{} \\[2em]
\Sigma_c(\tau) &= \frac{-1}{NK}\frac{\delta\Phi_{LW}}{\delta G_c(\beta-\tau)} &= \underset{O(1/N)}{}
\end{aligned}
\tag{6.22}
$$

Each of these terms contains a factor $O(1/N)$ from the vertices, but the first two self-energies contain summations over the internal channel or spin indices, elevating Σ_b and Σ_χ to terms of order $O(1)$. However, in the leading order large N approximation, $\Sigma_c \sim O(1/N)$, so that a consistent large N approximation is produced by leaving the conduction electron lines un-dressed.

This provides an alternative diagrammatic derivation of the Parcollet-Georges approach.

□ Causality

It is interesting, now that we have derived the self-consistent equations for the Green's functions, to check that they satisfy the causality rules, i.e. that the imaginary part of the retarded self-energies and Green's functions have the right sign as a function of frequency.

In order to do so, we start expressing the imaginary part of the retarded self-energy and Green's function for the Schwinger boson:

$$
G_b''(\nu+i\delta) = \frac{\Sigma_b''(\nu)}{|\omega+\lambda-\Sigma_b(\nu+i\delta)|^2}
\tag{6.23}
$$

$$
\Sigma_b''(\nu+i\delta) = \pi\gamma J_K^2 \int d\Omega \rho_c(\Omega+\nu)\rho_\chi(\Omega)\left[f(\Omega+\nu)-f(\Omega)\right]
\tag{6.24}
$$

where $f(\omega)$ is the temperature dependent Fermi function.

From this, it follows that G_b respects the causality rules provided that Σ_b does. It is then obvious that $[f(\Omega+\nu)-f(\Omega)]$ has the sign of ν for any given value of Ω, so that, assuming both fermionic fields respect causality, one has:

$$
\Sigma_b''(\nu+i\delta) \propto -\mathrm{Sgn}(\nu)
\tag{6.25}
$$

which is one would expect if G_b were causal.

The same kind of reasoning extends to the χ−fermion: the causality of G_χ is ensured by the causality of Σ_χ, since it is preserved by the Dyson's equation. Its imaginary part is given by:

$$\Sigma''_\chi(\omega + i\delta) = -\pi J_K^2 \int d\Omega \rho_c(\Omega + \omega)\rho_b(\Omega) \left[f(\Omega + \omega) + f(\Omega)\right] \qquad (6.26)$$

It is easy to rewrite $[f(\Omega + \omega) + f(\Omega)]$ as a positive function of both frequencies divided by $\tanh\left(\frac{\beta\Omega}{2}\right)$ which obviously has the sign of Ω for any given value of ω. If both G_c and G_b respects causality, one has $\Sigma''_\chi(\omega + i\delta) < 0$ over the whole range of frequency, so that G_χ is also causal.

As a conclusion, the causality is built into the self-consistent equations, so that recursively, these rules are respected provided that the starting point at high-temperature is itself causal.

□ **Set of equations**

Here is a reminder of the whole set of equations we will refer to, in the rest of this text:

$$
\begin{array}{llr}
\text{Dyson's equations:} & G_b^{-1}(i\nu_n) = i\nu_n + \lambda - \Sigma_b(i\nu_n) & (6.27\text{a}) \\
& G_\chi^{-1}(i\omega_n) = J_K - \Sigma_\chi(i\omega_n) & (6.27\text{b}) \\
\text{Schwinger boson:} & \Sigma_b(\tau) = -\gamma J_K^2 G_c(\tau)G_\chi(\beta - \tau) & (6.27\text{c}) \\
\chi\text{−fermion:} & \Sigma_\chi(\tau) = -J_K^2 G_c(\tau)G_b(\beta - \tau) & (6.27\text{d}) \\
\text{Conduction electron[4]:} & \rho_c(\omega) = \rho_0\Theta\left(D^2 - \omega^2\right) & (6.27\text{e}) \\
\text{Constraint:} & -G_b(\tau = 0^-) = \int d\omega \rho_b(\omega)n(\omega) = p_0 & (6.27\text{f})
\end{array}
$$

where all the spectral functions are defined as $\rho(\omega) = \frac{-1}{\pi}\text{Im}G(\omega + i\delta)$, and $n(\omega)$ is the Bose function.

To conclude, the Kondo problem reduces to this set of coupled integral equations in the large-N limit. Once these equations are solved, their solution gives access to all physical quantities, from the thermodynamics to the correlation functions.

6.2 Known results

The saddle-point equations (6.27c) and (6.27d) have been studied in great details for both the overscreened and the underscreened cases [106, 113]. It is actually

---

[4]We choose a flat band of conduction electron for simplicity but the saddle-point equations are independent on the actual form of the band. Moreover, as argued before, the actual shape of the density of states does not matter at low temperature.

rather hard to solve them exactly: even though these self-consistent equations are nothing but convolutions, the Dyson's equations make the self-consistency much more difficult to handle analytically than one would expect. It is quite interesting that the same set of integral equations gives very different results as one tunes the impurity spin from $p_0 > \gamma$ to $p_0 < \gamma$. This feature is still not well understood from the analytical point of view.

Nevertheless, one can explore some of the properties of these two regimes thanks to two methods:

1. A partial analytic solution at low-temperature. This allows to explore the low-energy behavior, in particular for the overscreened case where conformal field theory helps in the derivation of the scaling function in temperature, the behavior of the entropy and the specific heat.

2. A full numerical solution. This allows to explore the whole range in temperature and in particular the cross-over between the high and the low temperature regimes.

In the next paragraphs, we recall some of the established results concerning the high-temperature and the low-temperature limit for all three regimes of screening.

6.2.1 High temperature regime

At high temperature, the system behaves as a free spin of size $s = p_0/2$: both self-energies are negligible compared to the free part of the Green's functions. This is independent on the number of channels since the Kondo interaction is too small to affect the impurity spin at high temperature.

It follows that the bosonic spectral function is given by a single $\delta-$peak:

$$\rho_b(\omega) = \delta\left(\omega + \lambda\right) \tag{6.28}$$

where the chemical potential λ is set by the constraint (6.27f). It follows that $n(-\lambda) = p_0$, so that one can rewrite the chemical potential as:

$$\lambda^{\text{High T}} = -T \log\left(\frac{1 + p_0}{p_0}\right) \tag{6.29}$$

Replacing the expression for the bosonic Green's function into the free energy (6.21), and neglecting all self-energies with respect to the bare propagators, one has for the impurity free energy:

$$
\begin{aligned}
F_{\text{imp}}^{\text{High T}} &= F - F_{\text{bulk}} = NT \sum_n \log\left(-i\nu_n - \lambda\right) + Np_0\lambda(T) & (6.30) \\
&= NT\left[p_0 \log p_0 - (p_0 + 1)\log(p_0 + 1)\right] & (6.31)
\end{aligned}
$$

where we have subtracted the contribution from the conduction electron band to the free energy, labeled F_{bulk}.

From this, one can easily deduce that the high-temperature limit of the impurity entropy per spin flavor is:

$$s_{\text{imp}}^{\text{High T}} = -\frac{1}{N}\frac{\partial F_{\text{imp}}}{\partial T} = (p_0 + 1)\log(p_0 + 1) - p_0 \log p_0 \qquad (6.32)$$

Finally, one can compute the local susceptibility: this quantity is defined as the susceptibility of the system when only the impurity is coupled to the external magnetic field (see Appendix B for more details about the difference between local and impurity susceptibility). The local susceptibility then writes:

$$
\begin{aligned}
\chi_{\text{loc}} &= \frac{1}{N^2}\int_0^\beta d\tau \sum_{\alpha\beta}\langle S_{\alpha\beta}(\tau)S_{\beta\alpha}(0)\rangle = \int_0^\beta d\tau\, G_b(\tau)G_b(\beta - \tau) \\
\chi_{\text{loc}}^{\text{High T}} &= \frac{p_0(p_0 + 1)}{T}
\end{aligned}
\qquad (6.33)
$$

which, as expected, gives a Curie law with a Curie constant κ depending on the size of the spin: $\kappa = p_0(p_0 + 1)$.

As the temperature is lowered, all these quantities cross-over to their low-T counterpart which now strongly depends on the screening regime considered.

6.2.2 Overscreened case: $p_0 < \gamma$ (OS)

This section is devoted to the results of the overscreened regime. All the analytical results presented in this section have been derived in [106] and [113]. However, all the numerical data have been recomputed for illustrative purposes and as a test for our new set of programs.

☐ Spectral functions

It is possible to extract the low-energy behavior of the Green's functions in the zero temperature limit. This derivation relies on a numerical observation, namely that as the temperature is reduced towards zero, both Green's functions seem to diverge at zero energy. This can be recast as:

$$\lambda - \Sigma_b(0 + i\delta) \xrightarrow[T\to 0]{} 0 \qquad (6.34)$$

$$J_K - \Sigma_\chi(0 + i\delta) \xrightarrow[T\to 0]{} 0 \qquad (6.35)$$

as one can see from the numerical data presented in Fig. 6.5.

Using this as a hint, and a power-law ansatz for the Green's functions, one can perform a low-energy analysis identical in spirit to the one in [114]. The idea is

to plug the ansatz into the self-energy equations and to identify the results self-consistently with the starting functions. This analysis leads to the following power-laws for the Green's functions:

$$G_b(\omega + i\delta) \sim \frac{A_+\theta(\omega) + A_-\theta(-\omega)}{|\omega|^{\frac{\gamma}{1+\gamma}}} \tag{6.36}$$

$$G_\chi(\omega + i\delta) \sim \frac{B_+\theta(\omega) + B_-\theta(-\omega)}{|\omega|^{\frac{1}{1+\gamma}}} \tag{6.37}$$

where $A_\pm$ and $B_\pm$ are constants.

Both Green's functions are singular at zero frequency, with a power-law divergence whose exponent does not depend on the size of the spin. This exponent is the same on both side of the singularity, but the prefactor is different: there is a spectral asymmetry that can be parametrized through the argument $\theta_\pm$ of $A_\pm$ (the self-consistency ensures that $B_\pm$ can be expressed in terms of $|A_\pm|$ and $\theta_\pm$).

Thanks to a procedure similar in many aspects to the proof of the Luttinger theorem for Fermi liquids [108, 109], one can relate the size of the spin to the low-energy parameters $\theta_\pm$, which ultimately leads to:

$$\begin{cases} \sin\theta_+ & = & \sin\left(\dfrac{\pi(\gamma - p_0)}{1 + \gamma}\right) \\[2mm] \sin\theta_- & = & -\sin\left(\dfrac{\pi p_0}{1 + \gamma}\right) \end{cases} \tag{6.38}$$

Finally, it is important to notice that the singularity at zero frequency is actually regularized at finite temperature. From this observation, Parcollet et al. [113] could infer a finite temperature ansatz for the Green's functions that satisfies the saddle-point equations. In the low-energy, low temperature limit, one can see ω/T scaling in the spectral functions, so that at the leading order in temperature:

$$\rho_b(\omega) \propto T^{-\frac{\gamma}{1+\gamma}}\phi_b\left(\frac{\omega}{T}\right) \qquad\qquad \rho_\chi(\omega) \propto T^{-\frac{1}{1+\gamma}}\phi_\chi\left(\frac{\omega}{T}\right) \tag{6.39}$$

where the $\phi_{b,\chi}$ scaling functions have a complicated expression in terms of Γ functions. This feature can be seen numerically from inspecting the zero-energy inverse Green's function as a function of temperature, which turn out to behave as the expected power-laws (see Fig. 6.5).

□ **Entropy and specific heat**

From the scaling function in temperature, it is possible to compute the free energy at low temperature, at the saddle point, and from there to extract the residual entropy of the impurity. This turns out to be much more difficult than it seems, since because of the ω/T scaling of the spectral function, a small temperature Sommerfeld-like expansion is not possible here.
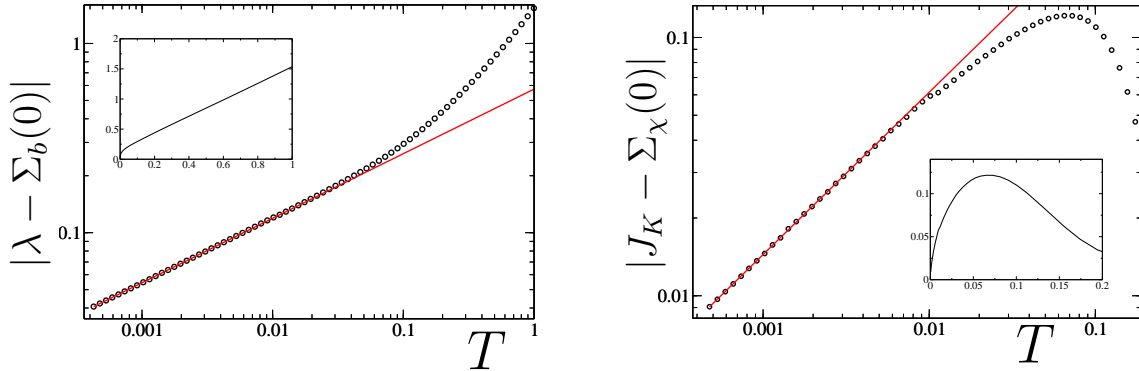
Figure 6.5: OS case: Inverse Green's functions at zero energy as a function of temperature on a double-log plot. The dots correspond to numerical data, and the straight lines to power-law fits, with an exponent of 0.341 and 0.628 for $|\lambda - \Sigma_b(0)|$ and $|J - \Sigma_\chi(0)|$. The corresponding exponents predicted by the analytic treatment are $1/3$ and $2/3$, respectively. The insets show the same data on a linear scale to stress out the vanishing of both quantities at low temperature.

In the overscreened regime, the residual entropy per spin flavor of the impurity is given by:

$$s_{\text{imp}}^{\text{Res}} = \frac{1 + \gamma}{2\pi} \text{Im} \left[\text{Li}_2 \left(e^{2i\frac{\pi p_0}{1+\gamma}} \right) + \text{Li}_2 \left(e^{2i\frac{\pi}{1+\gamma}} \right) - \text{Li}_2 \left(e^{2i\frac{\pi(1+p_0)}{1+\gamma}} \right) \right] \tag{6.40}$$

where $\text{Li}_2(x)$ is the dilogarithm function.
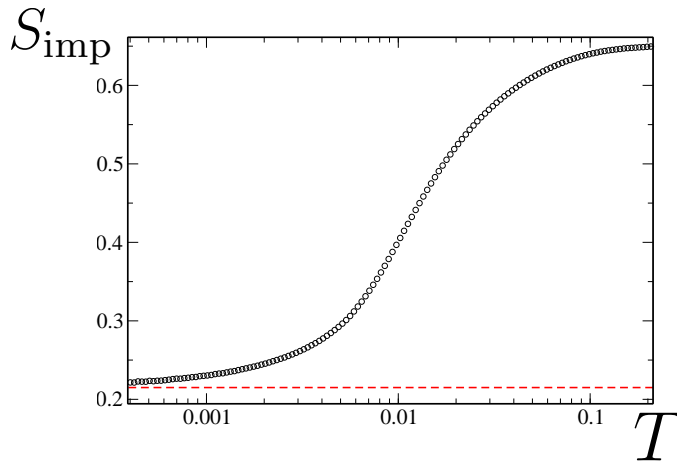
Figure 6.6: OS case: Entropy as a function of temperature in the overscreened case ($p_0 = 0.3, \gamma = 0.4$). The red dotted line corresponds to the residual entropy computed with the expression given in the text, Eq. (6.40).

To access the specific heat coefficient, the expression of the spectral functions to the leading-order in temperature is not sufficient, and one has to push the low-temperature expansion to higher order. This allows to take the second derivative

of the impurity free energy, which leads to the following result for the specific heat coefficient:

$$\gamma > 1 : \quad \frac{C_v}{T} \quad \sim \quad \left(\frac{1}{T}\right)^{\frac{\gamma-1}{\gamma+1}}$$

$$\gamma = 1 : \quad \frac{C_v}{T} \quad \sim \quad \log\left(\frac{1}{T}\right) \tag{6.41}$$

$$\gamma < 1 : \quad \frac{C_v}{T} \quad \sim \quad \text{const.}$$

The asymmetry between the $\gamma < 1$ and the $\gamma > 1$ regimes is an artifact of the Kondo model. In the Anderson model, the symmetry is restored and one finds a diverging specific heat coefficient for $\gamma < 1$, namely $C_v/T \sim (1/T)^{\frac{1-\gamma}{\gamma+1}}$.

□ **Susceptibility**

It is possible from a conformal field theory point of view to derive the temperature dependence of the local spin susceptibility at low temperature. The latter turns out to behave as a function of temperature just like the specific heat coefficient, i.e.:

$$\gamma > 1 : \quad \chi_{\text{loc}} \quad \sim \quad \left(\frac{1}{T}\right)^{\frac{\gamma-1}{\gamma+1}}$$

$$\gamma = 1 : \quad \chi_{\text{loc}} \quad \sim \quad \log\left(\frac{1}{T}\right) \tag{6.42}$$

$$\gamma < 1 : \quad \chi_{\text{loc}} \quad \sim \quad \text{const.}$$

For $\gamma \geq 1$, this can be easily re-derived from the expression of the local susceptibility in terms of the bosonic Green's functions, and the scaling form in temperature of G_b[5]. For $\gamma < 1$, however, the prefactor of the divergent term vanishes so that only a constant term remains in the low temperature limit. Again, this is a peculiarity of the Kondo model and the divergence with the expected power in T is recovered in the Anderson model.

6.2.3 Underscreened case: $p_0 > \gamma$ (US)

This section is devoted to the results of the underscreened regime. Again, all the analytical results presented in this section have been derived in [106] and [115], and the numerical data have been recomputed for illustrative purposes and as a test for our new set of programs.

---

[5]The integral brings a power of T and the two powers of G_b a term in $T^{\frac{2\gamma}{1+\gamma}}$.
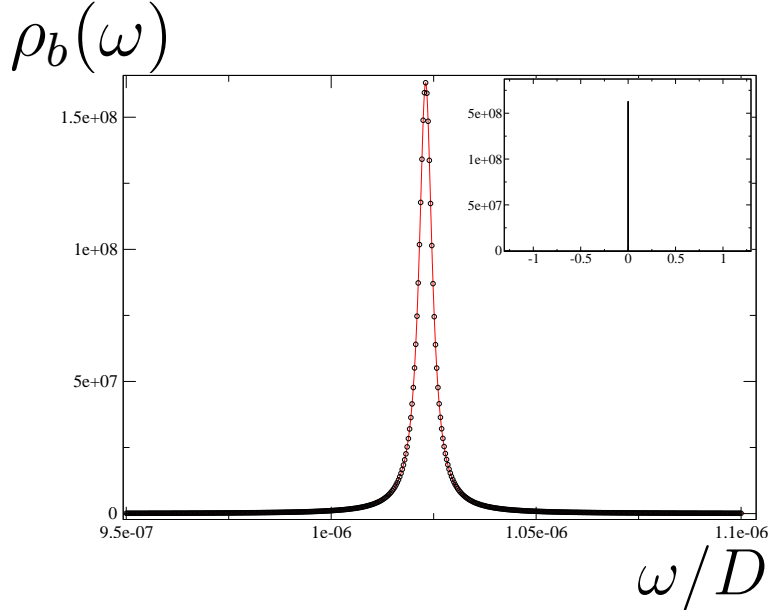
Figure 6.7: US case: Bosonic spectral function at $T \sim 10^{-3}T_K$. The fit is a Lorentzian whose width decreases with temperature, consistent with a δ-peak in the zero temperature limit. In the inset, we show the same spectral function on the scale D.

□ Spectral functions

We know from the strong coupling analysis that the underscreened regime leads to a partially screened impurity spin, so that we expect the physics to look like a residual spin of size $p_0 - \gamma$, weakly ferromagnetically coupled to a bath of conduction electrons.

It follows that the expected bosonic spectral function looks like the one of a local moment, with sub-leading terms:

$$\rho_b(\omega) = \delta(\omega + \mu T) + \Phi_b(\omega) \tag{6.43}$$

where $\mu = -\log\left(\frac{p_0 - \gamma + 1}{p_0 - \gamma}\right)$ as one expects for the chemical potential associated to a spin of size $p_0 - \gamma$.

Of course, in order to maintain the constraint as well as the normalization of this spectral function, one would expect that:

$$\int d\omega \, \Phi_b(\omega) = 0 \qquad \int d\omega \, \Phi_b(\omega) n(\omega) = \gamma \tag{6.44}$$

The self-consistency imposes that upon substituting (6.43) into the self-energy

equation for the $\chi-$fermion, one has:

$$
\begin{aligned}
\Sigma_\chi(\omega) &= \Phi_\chi(\omega) + \rho_0 J_K^2 (p_0 - \gamma) \left[\log \left| \frac{D + \omega - \mu T}{D - \omega + \mu T} \right| - i\pi\Theta(D^2 - (\omega - \mu T)^2) \right] \\
&+ \rho_0 J_K^2 \log \left(\frac{D}{2\pi T} \right) - \rho_0 J_K^2 \left[\Psi \left(\frac{1}{2} - i\frac{\omega - \mu T}{2\pi T} \right) + i\frac{\pi}{2} \right]
\end{aligned}
\tag{6.45}
$$

where $\Phi_\chi(\omega)$ is a sub-leading term arising from $\Phi_b(\omega)$, and $\Psi(x)$ is the di-gamma function.

Noticing that this diverges as $\log T$ as $T \to 0$, and plugging it back into the bosonic self-energy, one has: $\Sigma_b(\omega) - \Sigma_b(0) \sim -\gamma \frac{\omega}{\log T} + \ldots$, so that our ansatz is consistent.

This finally leaves us with the following inverse Green's functions at zero energy:

$$
\begin{aligned}
\lambda - \Sigma_b(0) &\sim \mu T + \ldots \tag{6.46} \\
J_K - \Sigma_\chi(0) &\sim \rho_0 J_K^2 \log T + \ldots \tag{6.47}
\end{aligned}
$$

The divergence of the inverse $\chi-$fermion propagator at zero energy prevents a low-energy analysis like the one carried out for the overscreened case. This logarithmic divergence can be interpreted physically as arising from the effective ferromagnetic coupling between the residual spin and the electronic bath. Since we introduced the χ fermion to decouple the Kondo interaction, the associated Green's function describes the effective Kondo coupling J_K^* between the residual spin and the conducting bath: as $T \to 0$, this coupling becomes negative and vanishes like $1/\log T$, consistent with a marginally irrelevant ferromagnetic coupling.
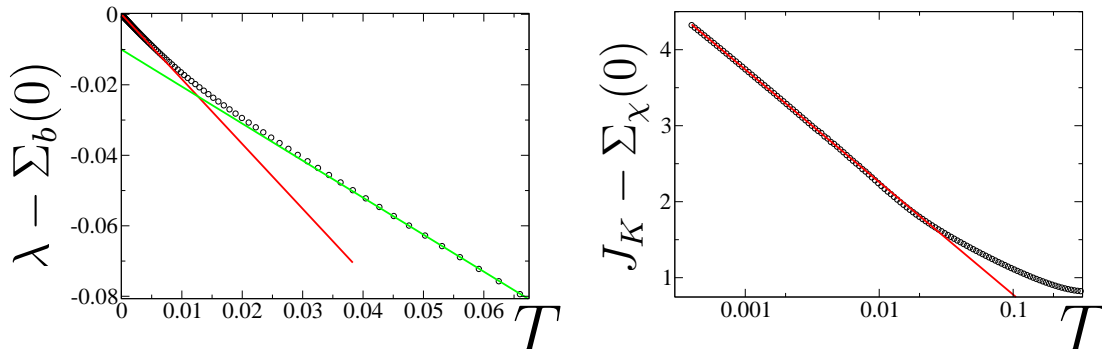
Figure 6.8: US case: Inverse Green's functions at zero energy as a function of temperature. The dots correspond to numerical data, and the straight lines to fits: linear in the case of $\lambda - \Sigma_b(0)$ and logarithmic for $J - \Sigma_\chi(0)$.

The validity of our ansatz is verified from the numerical solution (see Figs. 6.7 and 6.8) where one sees the $\log T$ dependence of J_K^*, as well as the linear behavior of

the renormalized bosonic chemical potential both in the high and low temperature regime with a change of slope related to the change in the size of the effective impurity spin.

☐ Entropy and Susceptibility

The low-temperature physics is dominated by the local moment physics, since the effective coupling between the residual spin and the conduction band vanishes as $T \to 0$. As a consequence, both the entropy and the local susceptibility at zero temperature look like the ones of an isolated spin.

One then expects that the underscreened case at low temperature gives the same behavior as the ones we obtained for the high-temperature regime only for a spin of size $p_0 - \gamma$ instead of p_0. It follows that the residual entropy of the underscreened Kondo model is given by:

$$s_{\mathrm{imp}}^{\mathrm{Low\ T}} = (p_0 - \gamma + 1) \log(p_0 - \gamma + 1) - (p_0 - \gamma) \log(p_0 - \gamma) \qquad (6.48)$$

and the local susceptibility at low-temperature is Curie-like, with a Curie constant $\kappa = (p_0 - \gamma)(p_0 - \gamma + 1)$:

$$\chi_{\mathrm{loc}}^{\mathrm{Low\ T}} \sim \frac{(p_0 - \gamma)(p_0 - \gamma + 1)}{T} \qquad (6.49)$$

which we could verify numerically, as one can see from Fig. 6.9.
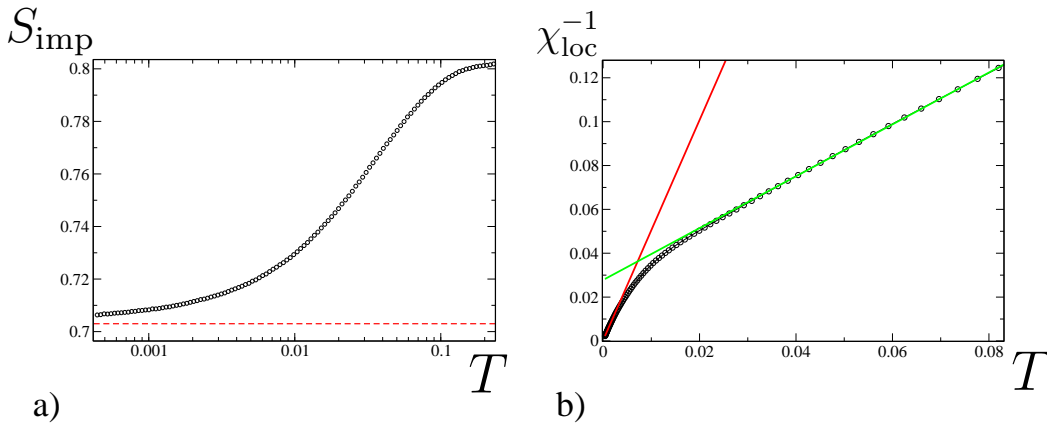
Figure 6.9: US case: a) Entropy as a function of temperature on a logarithmic scale. The residual entropy at the lowest temperature achieved is very close to the theoretical value (red dotted line). b) The inverse local susceptibility is linear in both the high and low-temperature regime, with a net change in slope.

As one takes the $\gamma \to p_0$ limit, one gets closer and closer to the exactly screened case, for which one expects the residual entropy to vanish. It can be readily seen from Eq. 6.48 that $s_{\mathrm{imp}}^{\mathrm{Low\ T}} \to 0$ as $\gamma \to p_0$.

6.3 Exactly screened case: $p_0 = \gamma$ (ES)

In this section we study the perfectly screened case which was thought to be a trivial non-interacting Fermi-liquid as an artifact of the large-N limit. We prove, helped by a numerical solution of the saddle-point equations, that this is not the case: even though the transport properties are indeed trivial in the large-N limit, one can recover the thermodynamics of a truly interacting Fermi liquid. The main results of this section have been published in the Publication 4, the rest is presented here for the first time.

6.3.1 General belief and counter-arguments

Previous works [106] on this large-N limit of the multichannel Kondo model focused on both the overscreened and the underscreened regimes, leaving the perfectly screened case aside. The general belief was that although the Kondo screening occurs at the leading order in N for the impurity, it only happens at a sub-leading order for the conduction electrons, so that the impurity doesn't seem to affect any properties of the Fermi liquid, even at the impurity site and one ends up describing a trivial non-interacting Fermi liquid.

This argument was backed up by the results of the Friedel sum rule [93] which predicts that the conduction electron phase shift on the impurity is given by $\delta_c = \frac{\pi}{N}$ so that both the phase shift and the $T-$matrix vanish in the large-N limit.

Although this argument is correct, the conclusions concerning the trivial Fermi liquid are not. Indeed, a vanishing phase shift only implies that the transport properties of the Fermi liquid cannot be recovered in the large-N limit. What was originally missed is that although the conduction electron self-energy is of order $O(1/N)$, it does participate to the thermodynamics because its effect is multiplied by the N spin components and the K scattering channels producing an $O(N)$ overall contribution.

This statement is not that obvious if one looks at the impurity free energy. The latter is defined as the difference between the total free energy and the bulk one (i.e. the one of the free conduction band). Starting from Eq. 6.21 and removing the bulk free energy $F_{\text{bulk}} = -NKT \sum_n \log\left(G_{c0}^{-1}(i\omega_n)\right)$, one can expand the conduction electron Green's function in $1/N$, so that the remaining terms look like:

$$
\begin{aligned}
F_{\text{imp}} &= NT \sum_n \log(-G_b^{-1}(i\nu_n)) - KT \sum_n \log(-G_\chi^{-1}(i\omega_n)) \\
&\quad + NT \sum_n \Sigma_b(i\nu_n)G_b(i\nu_n) - KT \sum_n \Sigma_\chi(i\omega_n)G_\chi(i\omega_n) \\
&\quad + Np_0\lambda + \Phi_{LW}[G_b, G_\chi, G_c]
\end{aligned}
\tag{6.50}
$$

This does not contain any explicit dependence on the conduction electron self-energy. However, it is possible from this expression to derive a closed form expression for

the impurity entropy. This derivation is presented in Appendix A in the case of a single impurity and we only recall the result here:

$$
\begin{aligned}
\frac{S_{\text{imp}}}{N} &= -\int \frac{d\omega}{\pi} \left[\frac{\partial n(\omega)}{\partial T} \left(\text{Im} \log\left(-G_b^{-1}(\omega)\right) + G_b'(\omega)\Sigma_b''(\omega)\right) \right. \\
&\quad \left. +\gamma \frac{\partial f(\omega)}{\partial T} \left(\text{Im} \log\left(-G_\chi^{-1}(\omega)\right) + G_\chi'(\omega)\Sigma_\chi''(\omega) - G_{c0}''(\omega)\tilde{\Sigma}_c'(\omega)\right) \right] (6.51)
\end{aligned}
$$

where the notation $G'(\omega)$ and $G''(\omega)$ stands for the real and imaginary parts of the retarded Green's function $G(\omega + i\delta)$, and $\tilde{\Sigma}_c(\omega) = N\Sigma_c(\omega) = O(1)$.

It is obvious from (6.51) that the conduction electron self-energy plays a role in the thermodynamics even though it does not enter the self-consistent saddle-point equations. This motivated a careful analysis of the exactly screened regime despite the arguments related to the vanishing phase shift.

6.3.2 Spectral functions

□ **Existence of a gap**

The first interesting feature of the numerical solution of the saddle-point equations is the existence of a gap in both the bosonic and fermionic spectral functions at low temperature (see Fig. 6.10).

Even though we have no way of proving analytically that a gapped solution is favored in the case of a perfectly screened impurity, it is possible to show that a gapped solution is compatible with the saddle-point equations.

The imaginary parts of the self-energies, written in terms of real frequencies and taken at zero temperature, are given by:

$$
\begin{cases}
\Sigma_b''(\omega + i\delta) &= -\pi\gamma J_K^2 \int_0^{-\omega} d\Omega \; \rho_c(\omega + \Omega)\rho_\chi(\Omega) \\[2ex]
\Sigma_\chi''(\omega + i\delta) &= \pi J_K^2 \int_0^{-\omega} d\Omega \; \rho_c(\omega + \Omega)\rho_b(\Omega)
\end{cases}
\tag{6.52}
$$

Assume that the bosonic spectral functions is gapped over the range of frequency $[-g_-, g_+]$, then the χ−fermion self-energy and – upon a substitution in the Dyson's equation – the spectral function are both gapped, over a range of frequency that is now $[-g_+, g_-]$. Conversely, a gap in ρ_χ leads because of the self-consistency to a "mirrored" gap in ρ_b. This analysis is independent on the actual shape of the conduction band. Note finally that we couldn't extract a self-consistent equation for the gap starting from these equations.

The gap in the bosonic spectral function leads to a degenerate choice of the Lagrange parameter λ in the case of the exactly screened spin: when this effective

chemical potential lies within the gap, the ground-state Schwinger boson occupancy[6] locks into the value $n_b = p_0 = \gamma$. Numerically, this manifests itself by a plateau in the bosonic occupancy as a function of λ, at low temperature (see Fig. 6.10). Such a picture suggests that starting from a solution of the saddle point equations, a small change $\delta\lambda$ in the bosonic chemical potential leads to another solution, apparently given by the same set of Green's functions only shifted rigidly in frequency by an amount $\delta\lambda$.

a)   b)
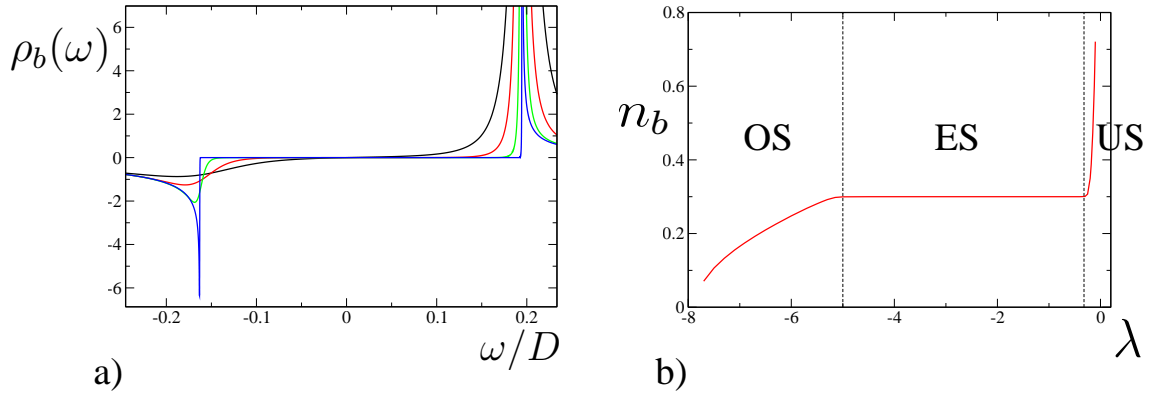
Figure 6.10: ES case: a) Bosonic spectral function as a function of frequency for decreasing temperature. As the gap opens at low energy, both peaks sharpen on the edges of the gapped region. b) Computed bosonic occupancy for $\gamma = 0.3$ when the chemical potential λ is varied (p_0 not being fixed). The plateau corresponds to an exactly screened case (ES).

Just like the stability of the gap, this last feature is also built into the equations. Assume that $\Sigma_\chi(\omega, \lambda + \delta\lambda) = \Sigma_\chi(\omega - \delta\lambda, \lambda)$, then thanks to the Dyson's equation, this property is also verified by G_χ. It follows that, at zero temperature:

$$
\begin{aligned}
\Sigma_b(\omega, \lambda + \delta\lambda) &= \rho_0 \gamma J_K^2 \left(\int_{-D}^{-\omega} d\Omega \, G_\chi'(\Omega - \delta\lambda, \lambda) + i \int_{-\omega}^{0} d\Omega \, G_\chi''(\Omega - \delta\lambda, \lambda) \right) \\
&= \Sigma_b(\omega + \delta\lambda, \lambda) - \rho_0 \gamma J_K^2 \int_{-\delta\lambda}^{0} d\Omega \, G_\chi''(\Omega, \lambda) \\
&= \Sigma_b(\omega + \delta\lambda, \lambda) \quad\quad\quad\quad\quad\quad\quad\quad\quad\quad\quad\quad\quad (6.53)
\end{aligned}
$$

where we used that in the large bandwidth limit $D + \delta\lambda \simeq D$, and the extra term vanishes because of the gap in the $\chi-$fermion spectral function. The rest of the proof is identical: from the rigid shift of Σ_b it is easy to prove that G_b follows the same property, which transmits to Σ_χ via the saddle-point equation in the exact

---

[6]The bosonic occupancy is defined as $n_b = -G_b(\tau = 0^-)$, which is set by the constraint to be equal to p_0.

same way as we have just proved, so that ultimately, one has at zero temperature:

$$
\begin{aligned}
G_b(\omega, \lambda + \delta\lambda) &= G_b(\omega + \delta\lambda, \lambda) \\
G_\chi(\omega, \lambda + \delta\lambda) &= G_\chi(\omega - \delta\lambda, \lambda)
\end{aligned}
\tag{6.54}
$$

It is legitimate to wonder whether the presence of a gap in the spectral functions is an artifact of the large-N limit or if it has a deeper physical meaning in which case it would extend down to $N = 2$. We do not, at this stage, have any evidence to support either scenarios. However, we can argue that if a gap in the bosonic spectral function exists in the $SU(2)$ case, it could be revealed from inspecting the energy spectrum of the bosonic states, e.g. by ways of the Density Matrix Renormalization Group.

□ Renormalized chemical potential

As a consequence of the gapped bosonic spectral function, in the case of the exactly screened impurity, the renormalized chemical potential $\lambda^* = \lambda - \Sigma_b(0)$ does not vanish as a function of temperature unlike the overscreened and underscreened regimes. The bosonic Green's function taken at zero energy is given by $G_b(0) = 1/\lambda^*$ and can be expressed as:

$$
G_b(0) = G_b'(0) = -\fint d\Omega \, \frac{\rho_b(\Omega)}{\Omega}
\tag{6.55}
$$

which is protected by the low-energy gap, and is thus made finite.

Another feature that comes from the numerical investigation is the development of a $\delta-$peak in the bosonic spectral function at the boundary of the gapped region at positive frequency. Unlike the underscreened case, the position of this peak does not evolve as the temperature is lowered, and one can make the following ansatz for the bosonic spectral function:

$$
\rho_b(\omega) = A\delta(\omega - \eta) + \Phi_b(\omega)
\tag{6.56}
$$

where A and η are positive constants, and Φ_b is assumed to be a sub-leading term.

Of course, this ansatz is not enough to capture most of the properties of the perfectly screened impurity but it is sufficient here to self-consistently extract the low-energy behavior of the Green's functions. Substituting this ansatz into the equation for the fermionic self-energy, one has:

$$
\begin{aligned}
\Sigma_\chi(\omega) &= \Phi_\chi(\omega) + A\rho_0 J_K^2 \left[\log\left(\frac{D}{2\pi T}\right) - \Psi\left(\frac{1}{2} + \frac{\omega + \eta}{2i\pi T}\right) - i\frac{\pi}{2}\right] \\
&\underset{T\to 0}{\sim} \Phi_\chi(\omega) - A\rho_0 J_K^2 \log\left(\frac{|\omega + \eta|}{D}\right)
\end{aligned}
\tag{6.57}
$$

This leads to the following contribution once plugged back into the bosonic self-energy:

$$
\Sigma_b(\omega) - \Sigma_b(\eta) \sim B\frac{|\omega - \eta|}{\log|\omega - \eta|}
\tag{6.58}
$$

so that our ansatz is consistent.

As a conclusion, the inverse Green's functions at zero energy read:

$$\lambda - \Sigma_b(0) \quad \xrightarrow[T \to 0]{} \quad \text{Const.} \tag{6.59}$$

$$J_K - \Sigma_\chi(0) \quad \xrightarrow[T \to 0]{} \quad \text{Const.} \tag{6.60}$$

where both these constants are finite, which prevents any kind of low-energy analysis like the one carried out for the overscreened impurity. This is verified numerically (see Fig. 6.11) with a saturation observed on about two decades in temperature.
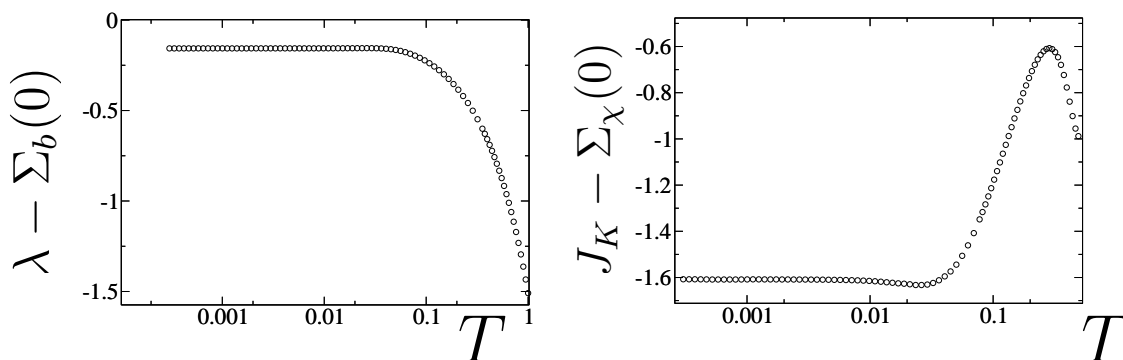
Figure 6.11: ES case: Inverse Green's functions at zero energy as a function of temperature. The dots correspond to numerical data. The logarithmic scale in temperature is used to underline the saturation at low T.

6.3.3 Entropy and specific heat

The gap in both the bosonic and fermionic spectral functions removes the effect of both fields on the low-temperature thermodynamics. Indeed, as the temperature is lowered, one can only probe the low-energy spectrum of each field: the low-temperature physics is then completely dominated by the conduction electrons so that the emergence of the gap ultimately reveals a Fermi liquid.

The consequences of a gapped solution on the low-energy physics can readily be obtained from the impurity entropy defined in (6.51). In the low-temperature regime, it is useful to replace the derivative of the fermionic and bosonic distributions with respect to temperature by their derivative with respect to frequency. Using that $\frac{\partial n(\omega)}{\partial T} = \frac{-\omega}{T} \frac{\partial n(\omega)}{\partial \omega}$ and $\frac{\partial f(\omega)}{\partial T} = \frac{-\omega}{T} \frac{\partial f(\omega)}{\partial \omega}$, one can rewrite the impurity entropy as:

$$
\begin{aligned}
\frac{S_{\text{imp}}^{\text{Low}T}}{N} &= \frac{1}{T} \int d\omega \left[\frac{\partial n}{\partial \omega} s_b(\omega) + \frac{\partial f}{\partial \omega} s_f(\omega) \right] \\
&= \frac{-1}{T} \int d\omega \left[\frac{ds_b}{d\omega} n(\omega) + \frac{ds_f}{d\omega} f(\omega) \right]
\end{aligned} \tag{6.61}
$$

where we define

$$
\begin{cases}
s_b & = & \frac{\omega}{\pi}\left(\operatorname{Im}\log\left(-G_b^{-1}\right) + G_b'\Sigma_b''\right) \\
s_f & = & \frac{\gamma\omega}{\pi}\left(\operatorname{Im}\log\left(-G_\chi^{-1}\right) + G_\chi'\Sigma_\chi'' - G_{c0}''\tilde{\Sigma}_c'\right)
\end{cases}
$$

One can then perform a Sommerfeld expansion at low temperature, which gives:

$$
\frac{S_{\text{imp}}^{\text{Low}T}}{N} = -\frac{\pi^2}{6}T\left(2\left.\frac{d^2 s_b}{d\omega^2}\right|_{\omega=0} + \left.\frac{d^2 s_f}{d\omega^2}\right|_{\omega=0}\right)
\tag{6.62}
$$

It turns out that because of the causality properties of the bosonic Green's functions, one has $G_b''(0) = 0$ and $\Sigma_b''(0) = 0$, which then imposes, after some minor rearrangement, that $\left.\frac{d^2 s_b}{d\omega^2}\right|_{\omega=0} = 0$.

Taking the second derivative of s_f and rearranging the remaining terms, noticing that $\left.\frac{dG_{c0}''}{d\omega}\right|_{\omega=0} = 0$, one has:

$$
\left.\frac{d^2 s_f}{d\omega^2}\right|_{\omega=0} = \frac{2\gamma}{\pi}\left(\left.\frac{dG_\chi'}{d\omega}\right|_{\omega=0}\Sigma_\chi''(0) - G_\chi''(0)\left.\frac{d\Sigma_\chi'}{d\omega}\right|_{\omega=0} + \pi\rho_0\left.\frac{d\tilde{\Sigma}_c'}{d\omega}\right|_{\omega=0}\right)
\tag{6.63}
$$

Recalling that the fermionic spectral function is gapped, this leads to the final expression of the low-temperature impurity entropy:

$$
\frac{S_{\text{imp}}^{\text{Low}T}}{N} = -\frac{\pi^2}{3}\gamma\rho_0 T\left.\frac{d\tilde{\Sigma}_c'}{d\omega}\right|_{\omega=0}
\tag{6.64}
$$

which is linear in T as one would expect from a Fermi liquid.

Note in particular that the specific heat coefficient, defined as $\frac{C_v}{T} = \frac{dS_{\text{imp}}}{dT}$, not only saturates at a constant value at low temperature, but also this constant depends on the renormalized number of channels γ.

The exponential decay of the Fermi and Bose function derivatives imposes that at a given temperature T, only the frequency range $\omega \in [-T, T]$ contributes to the entropy. As a consequence, as one reaches a temperature of the order of the gap in the spectral functions, the contributions to the entropy coming from both the Schwinger bosons and the $\chi-$fermions identically vanish. It follows from this derivation that the typical energy scale over which the Fermi liquid develops (some kind of effective Fermi temperature T^*) is given by the size Δ_g of the gap.

Numerically, one sees a cross-over from the high-temperature regime where the entropy is dominated by the local moment physics and is thus given by a constant, to the low-temperature regime where it becomes Fermi-liquid like and vanishes linearly with temperature (see Fig. 6.12).

6.3.4 Susceptibility and Wilson ratio

Using the numerical solution of the saddle-point equations, we could compute the local magnetic susceptibility, which shows a crossover from a high-temperature Curie law to a saturation at low-temperature characteristic of a screening process (see Fig. 6.12). This saturation defines the scale of the Kondo temperature in this regime since one has:

$$\chi_{\text{loc}} \underset{T \to 0}{\sim} \frac{p_0(p_0 + 1)}{T_K} \tag{6.65}$$

This saturation is consistent with the Fermi liquid picture at low temperature. However, the dynamic susceptibility, defined as $\langle S(t)S(0) \rangle$, vanishes exponentially because of the gap in the bosonic spectral function. We expect the $1/t^2$ variation, characteristic of a Fermi-liquid, to be only present at the order $1/N$.
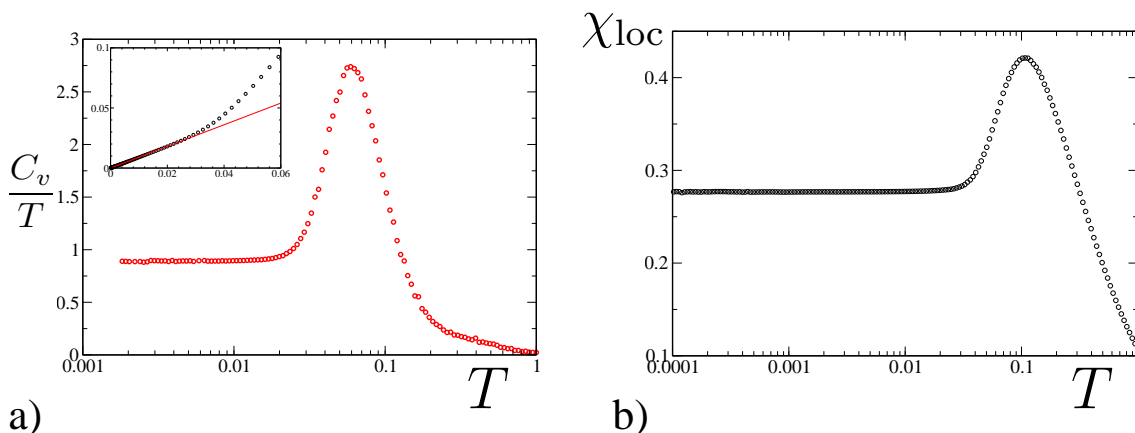
Figure 6.12: ES case: a) Specific heat coefficient for $\gamma = 0.1$ as a function of temperature on a log scale. Inset: the low temperature entropy shows a linear behavior. b) Temperature variation of the local spin susceptibility for $\gamma = 0.1$. The saturation of both quantities is consistent with a Fermi liquid behavior.

From the specific heat and the impurity susceptibility, we could compute the Wilson ratio, defined as:

$$W = \lim_{T \to 0} \frac{\pi^2}{3} \frac{\chi}{C_v/T} \tag{6.66}$$

where the numerical prefactor is chosen so that $W = 1$ for a non-interacting Fermi liquid.

Numerically, the Wilson ratio seems to grow linearly with the number of channels γ, which is confirmed by an analytical computation, similar in spirit to the one of Nozières and Blandin [107]. This amounts to expressing the phase shift of the local Fermi liquid at the impurity site and inspecting its response to variations of the fields coupled to the spin and channel magnetization, which ultimately leads to a relation between the spin, charge, and channel susceptibilities on one hand, and the

specific heat coefficient on the other hand. The complete derivation is presented in Appendix C.

As a result of this analysis, we expect the Wilson ratio to be given by $W = 1 + \gamma$, which is the behavior we recover in our numerical solution (see Fig. 6.13). This form is consistent with the Bethe ansatz results [116], taken in the limit of large values of N.

Such a Wilson ratio suggests, as we already argued from the entropy, that the exactly screened solution of the saddle-point equations describe an interacting local Fermi liquid in the large-N limit.

6.3.5 Scales

We argued, when dealing with the impurity entropy, that the typical energy scale over which the Fermi liquid develops is given by the size of the gap. From various other approaches we expect the crossover scale between the high-temperature local moment physics, and the low-temperature Fermi liquid behavior to be given by the Kondo temperature[7].

From this reasoning, one expects that the gap roughly goes like the Kondo temperature. However, we could not find any analytic derivation that would confirm this result. One has to stress out that the ansatz we have made concerning the bosonic Green's functions is not sufficient here to fully explore the relation between the gap and the Kondo temperature, as one would need an explicit form for the subleading function $\Phi_b(\omega)$.

Numerically, there is quite a striking correspondence between the size of the gap and the Kondo temperature, as can be seen on Fig. 6.13.

6.4 Conclusion

In this chapter, we rederived the saddle-point equations associated to the large-N limit of the multichannel Kondo model using an extension of the Luttinger-Ward formalism. After recalling the main results of the overscreened and underscreened regimes, we studied in details the perfectly screened case. We proved that contrary to the common knowledge, this regime does not correspond to a trivial Fermi liquid. Instead, we showed that despite vanishing transport properties due to an artifact of the large-N limit, one can recover the thermodynamics of an interacting Fermi liquid.

The application of this method to the description of, e.g. quantum dot physics, is made difficult by the vanishing T-matrix in the limit of $N \to \infty$. An attempt to cure this issue is presented in Chapter 8.

---

[7]As one can see, e.g. from the local susceptibility which diverges in $1/T$ until it reaches the Kondo temperature where it just saturates at a constant going like $1/T_K$.
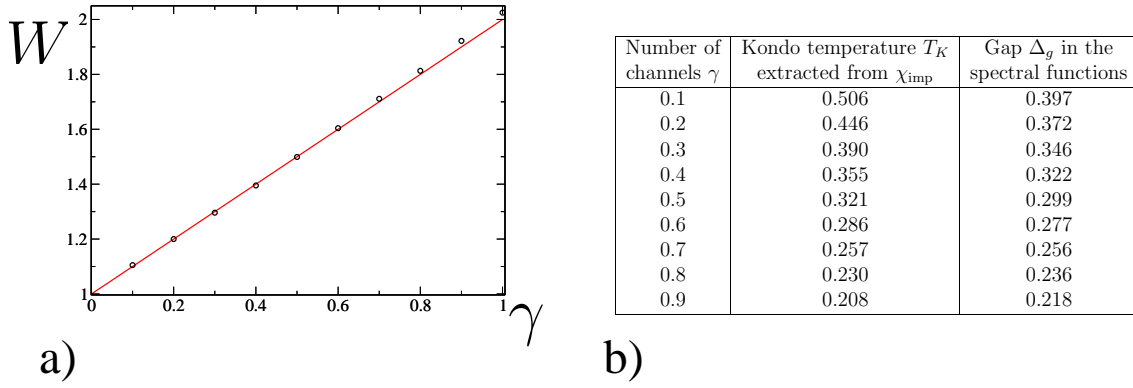
Figure 6.13: ES case: a) Wilson ratio computed for various values of γ (black circles) and compared with the behavior extracted from our Nozières-Blandin analysis (red line), b) Numerical values of the low-T gap and the Kondo temperature for a given Kondo coupling J_K and various γ.

However, an interesting application of this approach lies in the extension to many impurities. The first step towards this route is presented in Chapter 7, with the study of a two-impurity system.

CHAPTER 7

Two-impurity multichannel Kondo model

Contents

Having demonstrated that the large-N bosonic approach captures the thermodynamic properties of the Fermi liquid behavior for the perfectly screened impurity, we show in this chapter that it can also handle magnetic correlations within the two-impurity Kondo model. In this chapter, we explore the phase diagram of the two-impurity Kondo-Heisenberg model and discuss the similarities with the so-called "Jones-Varma" [117] fixed point in $N = 2$. The main results of this chapter have been published in the Publication 4, the rest is presented here for the first time.

7.1 Large-N equations

7.1.1 The model

We now consider two identical impurities coupled to the same sea of conduction electrons, and include for generality a Heisenberg-like interaction between the two localized spins, generated by other exchange processes not involving the conduction electrons. The Kondo interaction is the same as we described in the previous chapter.

Motivated by an extension to the lattice, and its relevance for the heavy fermion problem, we choose to limit ourselves to the case of an antiferromagnetic Heisenberg coupling between the two impurity spins. Moreover, we choose to follow the arguments of Read and Sachdev [118] and describe this Heisenberg interaction in terms of the boson pair operator $B_{12} = \sum_{m,\sigma} \sigma b_{1,m,\sigma} b_{2,m,-\sigma}$, where we recast the N spin indices under the form $\alpha = (m, \sigma)$ (m running from 1 to $\frac{N}{2}$, and $\sigma = \pm$).

Following this choice, the Hamiltonian describing the system is now invariant under spin transformation in the symmetry group $Sp(N)$, subgroup of $SU(N)$ and writes:

$$
\begin{aligned}
H &= H_{\text{band}} + H_K^{(1)} + H_K^{(2)} + H_H \\
H_{\text{band}} &= \sum_{\mathbf{k}} \sum_{m,\sigma} \sum_{\mu=1}^{K} \epsilon_{\mathbf{k}} c^{\dagger}_{\mathbf{k}m\sigma\mu} c_{\mathbf{k}m\sigma\mu} \\
H_K^{(i)} &= \frac{J_K}{N} \sum_{m,m'} \sum_{\sigma,\sigma'} \sum_{\mu} \sum_{i=1,2} b^{\dagger}_{i,m,\sigma} b_{i,m',\sigma'} \psi^{\dagger}_{im'\sigma'\mu} \psi_{im\sigma\mu} \\
H_H &= \frac{J_H}{N} \left(\sum_{m,\sigma} \sigma b^{\dagger}_{1,m,\sigma} b^{\dagger}_{2,m,-\sigma} \right) \left(\sum_{m',\sigma'} \sigma' b_{1,m',\sigma'} b_{2,m',-\sigma'} \right)
\end{aligned}
\tag{7.1}
$$

where $\psi_{im\sigma\mu}$ creates an electron in the Wannier state with spin $\alpha = N + \sigma m + \frac{1-\sigma}{2}$ at the site i.

The number of bosons for each site is enforced by the constraint:

$$
H_{\text{Constraint}} = - \sum_{i=(1,2)} \lambda_i \left(\sum_{m,\sigma} b^{\dagger}_{i,m,\sigma} b_{i,m,\sigma} - p_0 N \right)
\tag{7.2}
$$

and we focus in the rest of this chapter on perfectly screened impurities, so that we restrict ourselves to the case where $p_0 = \gamma$.

Just like the single impurity case treated in the previous chapter, one expects to see different screening regimes in this model. However, we are not interested here in the exploration of these various scenarios, and restrict ourselves to the exactly screened case, fixing the number of channels to match the size of the impurity spins. There is now a new parameter one can tune, namely the Heisenberg coupling, which now competes with the Kondo interaction giving access to two different regimes, pictured in Fig. 7.1:

- For a weak Heisenberg coupling, the two impurity spins prefer to form a singlet with the surrounding conduction electrons. We expect to see two perfectly screened impurities only weakly coupled to each other. The low-energy physics is then expected to be Fermi-liquid like.

- Whereas for a strong Heisenberg coupling, a spin singlet between the two impurity spins is favored. The impurities are locked in a singlet state and act as a scattering center for the conduction electrons, so that the low-energy physics is again Fermi-liquid like, but qualitatively different than the regime of weak Heisenberg coupling.

The most interesting region of the phase diagram turns out to be the crossover region between these two regimes.
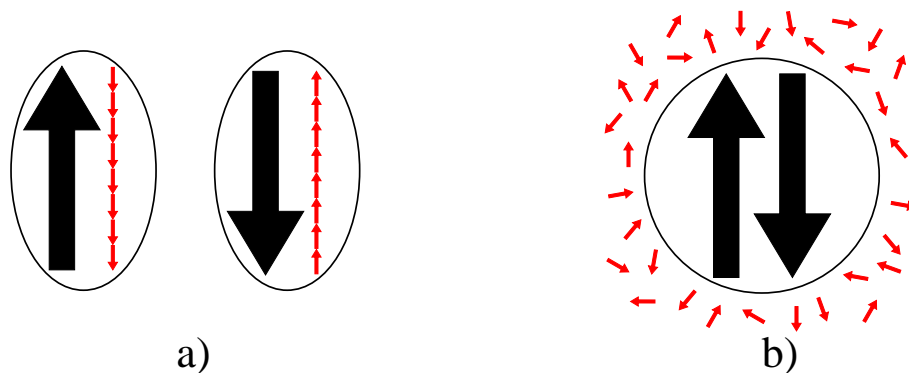
Figure 7.1: Schematic diagram illustrating the two limiting regimes: a) corresponds to the case of a dominant Kondo interaction and b) to a strong Heisenberg coupling. The large black arrows stand for the impurities, the red ones for the electrons.

7.1.2   Saddle-point equations

In order to study the phase diagram of the two-impurity Kondo-Heisenberg model in the large-N limit, we derive a set of saddle-point equations which we then study by

means of numerical as well as analytical investigation when possible. The derivation of the saddle-point equations is quite similar to the one already presented for the single impurity case.

☐ **Derivation**

As a first step, we decouple the Kondo interaction term for both impurities by introducing two sets of Grassmanian fields $\chi_{1,\mu}$ and $\chi_{2,\mu}$, where μ is the channel index, running from 1 to K. After integrating the conduction electrons out of the partition function, the action reads:

$$
\begin{aligned}
S \;=\; & \int_0^\beta d\tau \; \sum_{i,m,\sigma} b_{i,m,\sigma}^\dagger(\tau)\left(\partial_\tau - \lambda_i(\tau)\right) b_{i,m,\sigma}(\tau) - \frac{1}{J_K}\int_0^\beta d\tau \; \sum_{i,\mu} \chi_{i,\mu}^\dagger(\tau)\chi_{i,\mu}(\tau) \\
& -\frac{1}{N}\sum_{i,j}\int_0^\beta d\tau d\tau' \; \sum_\mu \chi_{j,\mu}(\tau')\chi_{i,\mu}^\dagger(\tau)\, G_{c0}(i-j;\tau-\tau')\sum_{m,\sigma} b_{j,m,\sigma}(\tau')b_{i,m,\sigma}^\dagger(\tau) \\
& +\sum_i \int_0^\beta d\tau \;\left(\Delta_{i,\bar{i}}^\dagger(\tau)\sum_{m,\sigma}\sigma b_{i,m,\sigma}(\tau)b_{\bar{i},m,-\sigma}(\tau) + \text{h.c.}\right) \\
& +\frac{N}{J_H}\sum_i\int_0^\beta d\tau \; \Delta_{i,\bar{i}}^\dagger(\tau)\Delta_{i,\bar{i}}(\tau) + p_0 N \sum_i \int_0^\beta d\tau \; \lambda_i(\tau)
\end{aligned}
\tag{7.3}
$$

where we have decoupled the Heisenberg interaction by introducing a "bond" operator $\Delta_{i,\bar{i}}$, and $\bar{i}$ is defined as:

$$
\bar{i} = \begin{cases} 2 & \text{if } \; i=1 \\ 1 & \text{if } \; i=2 \end{cases}
\tag{7.4}
$$

Using the symmetry under the exchange $1 \leftrightarrow 2$, one can argue that the Lagrange multipliers λ_1 and λ_2 are equal: if a solution is obtained with different values of λ_1 and λ_2, then the symmetry leads to another solution where these values are exchanged, suggesting that they are most likely equal. The same kind of reasoning suggests that the bond operators are also trivially related to one another via $\Delta_{12} = -\Delta_{21}$. This allows us to define λ and Δ as:

$$
\begin{cases} \lambda_i & = \; \lambda \\ \Delta_{i,\bar{i}} & = \; \text{Sgn}(\bar{i}-i)\Delta \end{cases}
\tag{7.5}
$$

It is useful at this stage to introduce a spinor notation for the Schwinger bosons

178

$\hat{b}_{i,m}^{\dagger} = (b_{i,m,+}^{\dagger}, b_{i,m,-})$ in order to rewrite the action under the following matrix form:

$$
S = \sum_{i,j} \int_0^\beta d\tau \sum_m \hat{b}_{i,m}^{\dagger}(\tau) \left[\begin{array}{cc} (\partial_\tau - \lambda(\tau))\,\delta_{ij} & 2\mathrm{Sgn}(\bar{i}-i)\Delta(\tau)\delta_{j\bar{i}} \\ -2\mathrm{Sgn}(\bar{i}-i)\Delta^{\dagger}(\tau)\delta_{j\bar{i}} & (-\partial_\tau - \lambda(\tau))\,\delta_{ij} \end{array} \right] \hat{b}_{j,m}(\tau)
$$

$$
- \frac{1}{N} \int_0^\beta d\tau d\tau' \sum_{i,j} N_\chi(i,j,\tau,\tau') G_{c0}(i-j;\tau-\tau') N_b(i,j,\tau,\tau')
$$

$$
- \frac{1}{J_K} \int_0^\beta d\tau \sum_{i,\mu} \chi_{i,\mu}^{\dagger}(\tau)\chi_{i,\mu}(\tau) + 2\frac{N}{J_H} \int_0^\beta d\tau\,\Delta^{\dagger}(\tau)\Delta(\tau)
$$

$$
+ 2p_0 N \int_0^\beta d\tau\,\lambda(\tau) \tag{7.6}
$$

where the matrix is given in the σ-space, and N_b and N_χ are the precursors of the Schwinger boson and $\chi-$fermion Green's function defined as:

$$
N_b(i,j,\tau,\tau') = \sum_{m,\sigma} b_{j,m,\sigma}(\tau') b_{i,m,\sigma}^{\dagger}(\tau) \qquad\qquad N_\chi(i,j,\tau,\tau') = \sum_\mu \chi_{j\mu}(\tau') \chi_{i\mu}^{\dagger}(\tau)
$$

$$
\tag{7.7}
$$

The method is then similar to the one used for the single impurity problem: one introduces the new fields $Q(i,j,\tau,\tau')$ and $\bar{Q}(i,j,\tau,\tau')$ conjugated to $N_\chi(i,j,\tau,\tau')$ and $N_b(i,j,\tau,\tau')$. This leads to an effective action $S(Q,\bar{Q},\lambda,\Delta)$ expressed in terms of these new fields, where every term scales like N so that one can apply the method of steepest descent. The saddle-point equations now write:

$$
\begin{aligned}
\bar{Q}(i,j,\tau,\tau') &= -G_{c0}(i-j;\tau-\tau')\left(G_b^{(++)}(j-i;\tau'-\tau) + G_b^{(--)}(j-i;\tau'-\tau)\right) \\
Q(i,j,\tau,\tau') &= -\gamma G_{c0}(i-j;\tau-\tau')G_\chi(j-i;\tau'-\tau) \\
p_0 &= -\frac{1}{2}\left(G_b^{(++)}(i=j;\tau=0^-) + G_b^{(--)}(i=j;\tau=0^+)\right) \\
\frac{\Delta}{J_H} &= \frac{1}{2}\sum_{i=1,2} G_b^{(-+)}(i-\bar{i};\tau=0^-)
\end{aligned}
$$

$$
\tag{7.8}
$$

where the Green's functions are now defined as:

$$
\begin{aligned}
G_b(i-j;\tau) &= \left[\begin{array}{cc} G_b^{(++)}(i-j;\tau) & G_b^{(+-)}(i-j;\tau) \\ G_b^{(-+)}(i-j;\tau) & G_b^{(--)}(i-j;\tau) \end{array} \right] \\
&= \left[\begin{array}{cc} -\langle Tb_{i,+}(\tau)b_{j,+}^{\dagger}(0)\rangle & -\langle Tb_{i,+}(\tau)b_{j,-}(0)\rangle \\ -\langle Tb_{i,-}^{\dagger}(\tau)b_{j,+}^{\dagger}(0)\rangle & -\langle Tb_{i,-}^{\dagger}(\tau)b_{j,-}(0)\rangle \end{array} \right] \\
G_\chi(i-j;\tau) &= -\langle T\chi_i(\tau)\chi_j^{\dagger}(0)\rangle
\end{aligned}
$$

$$
\tag{7.9}
$$
$$
\tag{7.10}
$$

□ **RKKY interaction**

It is possible to relate the fields Q and $\bar{Q}$ to the self-energies of the Schwinger boson and the $\chi-$fermion. From the saddle-point equations, one can see that the

Two-impurity multichannel Kondo model

Kondo interaction is responsible for local terms arising from $i = j$, but also for a cross-term that couples the two impurities to one another. This cross-term will give rise to a bosonic self-energy in the $SU(N)$ channel, i.e. that renormalizes the $-\langle T b_{i,\pm}(\tau) b_{j,\pm}^{\dagger}(0) \rangle$ term (with $i \neq j$).

This is known as the RKKY interaction [90, 91, 92]. This effective interaction between the impurities is mediated by the conduction band and can be tuned by adjusting the distance between the two impurities. However, we assume here that this distance is always big enough to neglect the RKKY interaction compared to the Heisenberg coupling between the impurities[1].

Qualitatively, the RKKY and the Heisenberg interactions, although arising from a completely different physics, play the same role as they lead to the establishment of short-range antiferromagnetic correlations between the impurities. Moreover, they are both tunable thanks to an external parameter: the distance R between impurities for the RKKY interaction, and the coupling J_H for the Heisenberg one. Our choice of favoring an Heisenberg-like rather than an RKKY interaction is motivated by real materials (where the overlap between orbitals of neighboring atoms is generally taken into account via an Heisenberg coupling), and by the fact that the Heisenberg coupling is conceptually easier to tackle as no retardation effects are present in the large-N limit (whereas one expects the cross-site bosonic self-energy to develop an imaginary part due to the RKKY interaction).

□ Set of equations

From this, it follows that the only non-local terms in our Green's functions are present in the "free" bosonic propagator, and come from the Heisenberg coupling between the impurities.

Since the $\chi-$fermion only sees the Kondo interaction, its propagator – along with both self-energies – is local within our approximation. It then becomes possible to reduce the full set of equations to only local propagators, where the non-locality of the Heisenberg interaction manifests itself through a dependence on Δ of the local bosonic Green's function.

The problem then reduces to the following set of equations:

$$G_b(i\nu_n) = \frac{-i\nu_n + \lambda - \Sigma_b(-i\nu_n)}{(i\nu_n + \lambda - \Sigma_b(i\nu_n))(-i\nu_n + \lambda - \Sigma_b(-i\nu_n)) - 4\Delta^2} \qquad (7.11)$$

$$\Sigma_b(\tau) = -\gamma J_K^2 G_c(\tau) G_\chi(\beta - \tau) \qquad (7.12)$$

$$G_\chi(i\omega_n) = \frac{1}{J_K - \Sigma_\chi(i\omega_n)} \qquad (7.13)$$

$$\Sigma_\chi(\tau) = -J_K^2 G_c(\tau) G_b(\beta - \tau) \qquad (7.14)$$

---

[1]This assumption is motivated by the fact that the RKKY interaction is known to drop very rapidly with the distance between impurities.

with the following constraint on λ and Δ:

$$
\begin{cases}
p_0 & = \displaystyle\int d\omega \; n(\omega)\rho_b(\omega) \\[2mm]
\dfrac{\Delta}{J_H} & = 2\Delta \displaystyle\int \dfrac{d\omega}{\pi} n(\omega)\mathrm{Im}\left(\dfrac{1}{(\omega + \lambda - \Sigma_b(\omega))\left(-\omega + \lambda - \Sigma_b(-\omega)\right)^* - 4\Delta^2}\right)
\end{cases}
\tag{7.15}
$$

where we chose not to simplify the factors of Δ to account for the case where it vanishes.

Note that, just like the single impurity case, these constraints are not invertible and cannot be written as a simple equality directly involving λ or Δ: one needs the knowledge of the bosonic propagator over the whole range of frequency in order to meet these constraints.

7.1.3 General remarks

Before trying to solve eqns (7.11)-(7.14), let us analyze some of their properties.

□ Causality

The equations ruling the evolution of the $\chi-$fermion propagator as a function of frequency are the same as the ones derived in the case of a single impurity, so that the causality of the $\chi-$fermion self-energy and Green's function can be proved following the exact same reasoning.

The same argument holds for the bosonic self-energy. The proof of causality for the bosonic propagator requires some extra work on (7.11), from which one can extract the following imaginary part:

$$
\begin{aligned}
G_b''(\omega) & = \mathrm{Im}\left(\frac{(-\omega + \lambda - \Sigma_b(-\omega))^*}{(\omega + \lambda - \Sigma_b(\omega))\left(-\omega + \lambda - \Sigma_b(-\omega)\right)^* - 4\Delta^2}\right) \\[2mm]
& = \frac{|\omega + \lambda - \Sigma_b(-\omega)|^2\, \Sigma_b''(\omega) - \Delta^2 \Sigma_b''(-\omega)}{\left|(\omega + \lambda - \Sigma_b(\omega))\left(-\omega + \lambda - \Sigma_b(-\omega)\right)^* - 4\Delta^2\right|^2} \\[2mm]
& \propto -A(\omega)\mathrm{Sgn}(\omega) + B(\omega)\mathrm{Sgn}(-\omega)
\end{aligned}
\tag{7.16}
$$

where $A(\omega)$ and $B(\omega)$ are positive for any given frequency, and we assumed that $\Sigma_b(\omega)$ is causal, so that ultimately $G_b''(\omega) \propto -\mathrm{Sgn}(\omega)$, as expected for a causal bosonic propagator.

□ $\Delta \rightarrow 0$ limit

Taking the limit of vanishing Δ in eqns (7.11)-(7.14) leads to the same equations as the one derived in the case of a single impurity.

The constraint on Δ (the second equation in (7.15)), corresponding to the saddle-point in this variable, can also be rewritten as:

$$\Delta = -J_H \langle B_{12} \rangle = -J_H \langle \sum_{m,\sigma} \sigma b_{1,m,\sigma} b_{2,m,-\sigma} \rangle \tag{7.17}$$

In the limit of $\Delta \to 0$, this equation imposes that $\langle B_{12} \rangle = 0$, preventing the formation of pairs of bosons. In this limit, the system behaves as two perfectly screened impurities which are decoupled from each other, on average. Since the impurities are identical, the physical properties averaged over them look like the ones of a single impurity with the same spin.

□ $\Delta \to \infty$ **limit**

In the limit of large Δ, the Heisenberg interaction dominates and as a first approximation, one can neglect the Kondo interaction: this amounts to neglecting the self-energy inside the bosonic propagator. The bosonic spectral function then reads:

$$\rho_b(\omega) = \frac{\lambda + \lambda^*}{2\lambda^*} \delta(\omega + \lambda^*) + \frac{\lambda^* - \lambda}{2\lambda^*} \delta(\omega - \lambda^*) \tag{7.18}$$

where $\lambda^* = -\sqrt{\lambda^2 - \Delta^2}$. This spectral function is made out of two $\delta-$functions, peaked at symmetric positions in frequency, so that one can identify a symmetric gap $\Delta_{\text{gap}} = -2\lambda^*$. By construction, $\lambda^* > \lambda$, but they are both negative so that the bosonic propagator is still causal.

The constraints impose that, in the zero temperature limit:

$$\begin{cases} p_0 & = \int_{-\infty}^{0} d\omega \ \rho_b(\omega) = \dfrac{\lambda - \lambda^*}{2\lambda^*} \\[2mm] \dfrac{1}{J_H} & = 2 \int_{-\infty}^{0} d\omega \ \text{Im} \left(\dfrac{G_b(\omega)}{\lambda - \omega - i\delta} \right) \end{cases} \implies \begin{cases} \lambda & = -J_H(1 + 2p_0) \\[2mm] \Delta^2 & = 4p_0(1 + p_0)J_H^2 \end{cases} \tag{7.19}$$

It follows that in the large Δ limit, which corresponds to the large J_H limit, the gap in the bosonic spectral function increases with J_H. The typical temperature over which a Fermi liquid develops becomes larger (increasing linearly with J_H) but since the Kondo interaction becomes weaker, this Fermi liquid looks more and more like a trivial one, with a vanishing specific heat coefficient as $J_H \to \infty$. This is consistent with the picture of two impurities locked in a spin singlet: they only weakly renormalize the surrounding Fermi liquid which then looks as if it is non-interacting.

7.2 Phase diagram and quantum critical point

In this section, we solve numerically the set of self-consistent equations for various values of the temperature and the Heisenberg coupling. We can isolate three regions

of the $(T_K/J_H, T/J_H)$ phase diagram: a Kondo dominated Fermi liquid, a Heisenberg dominated Fermi liquid and an intermediate region in between. This crossover region between the two Fermi liquids is governed by a quantum critical point, whose existence is underlined by the behavior of the phase shift and the entropy.

7.2.1 Tools for exploring the phase diagram

☐ Free energy and entropy

One can generalize the expression of the free energy functional to encompass the case of a two-impurity Kondo-Heisenberg model. The derivation is quite similar to the one presented in Appendix A, and the reader is referred to the Publication 3 for a detailed calculation in the more general case of a Kondo lattice, so that we only mention here the final result for the model Hamiltonian as defined in (7.1). The averaged impurity free energy is given by:

$$
\begin{aligned}
F_{\text{imp}} &= NT \sum_n \left[\frac{1}{2} \log\left((-i\nu_n + \lambda - \Sigma_b(-i\nu_n)) G_b^{-1}(i\nu_n) \right) + \Sigma_b(i\nu_n) G_b(i\nu_n) \right] \\
&\quad - KT \sum_n \left[\log(-G_\chi^{-1}(i\omega_n)) + \Sigma_\chi(i\omega_n) G_\chi(i\omega_n) \right] + \Phi_{LW}[G_b, G_\chi, G_c] \\
&\quad + N p_0 \lambda
\end{aligned}
\tag{7.20}
$$

Proceeding similarly to Appendix A, one can carry out the temperature derivative of the impurity free energy, which leads to the following expression for the averaged impurity entropy:

$$
\begin{aligned}
\frac{S_{\text{imp}}}{N} &= -\int \frac{d\omega}{\pi} \left[\frac{\partial n(\omega)}{\partial T} \left(\frac{1}{2} \text{Im} \log\left((\tilde{G}_b(-\omega))^* G_b^{-1}(\omega) \right) + G_b'(\omega) \Sigma_b''(\omega) \right) \right. \\
&\quad \left. + \gamma \frac{\partial f(\omega)}{\partial T} \left(\text{Im} \log\left(-G_\chi^{-1}(\omega) \right) + G_\chi'(\omega) \Sigma_\chi''(\omega) - G_{c0}''(\omega) \tilde{\Sigma}_c'(\omega) \right) \right]
\end{aligned}
\tag{7.21}
$$

where $\tilde{G}_b^{-1}(\omega) = \omega + i\delta + \lambda - \Sigma_b(\omega)$ and $\tilde{\Sigma}_c = N\Sigma_c$.

☐ Sum rules and phase shift

It is possible, using our expression of the impurity free energy to derive sum rules associated to the conserved quantities of the system. A detailed proof for a generic Hamiltonian is provided in the Publication 3 and we only sketch here the main aspects of the method and the final result in the case of our two-impurity model.

Each conserved quantity Q which commutes with the Hamiltonian leads to a gauge invariance of the underlying quantum fields, such that the action and all physical properties are invariant under the transformation:

$$
c_{\mathbf{k}\mu\alpha} \to e^{iq_c\theta(\tau)} c_{\mathbf{k}\mu\alpha}, \qquad \chi_\mu \to e^{iq_\chi\theta(\tau)} \chi_\mu, \qquad b_{m,\sigma} \to e^{iq_b\theta(\tau)} b_{m,\sigma}
\tag{7.22}
$$

where q_ζ is the gauge charge associated to each field.

Provided this gauge invariance is unbroken, one can show that this leads to a Ward identity at zero temperature, which then allows to write some kind of generalized Friedel sum rule for the conserved quantity:

$$Q = \frac{1}{\pi}\text{Im}\left[q_b N \log(-G_b^{-1}(0)) - q_\chi K \log(-G_\chi^{-1}(0)) - q_c NK \log(-G_c^{-1}(0))\right] \quad (7.23)$$

where all Green's functions are retarded ones.

Applying (7.23) to the conservation of the total electric charge in the case of our two-impurity model, one can write the change in the total charge related to the impurities as:

$$\Delta Q_e = NK\frac{\delta_c}{\pi} - K\frac{\delta_\chi}{\pi} = 0 \qquad \Longrightarrow \qquad \delta_c = \frac{\delta_\chi}{N} \qquad (7.24)$$

where we used that in the large bandwidth limit this change in the total charge is ruled by the Anderson-Clogston compensation theorem [119] and goes like $O(T_K/D)$, so that it can be neglected. The respective phase shifts[2] are defined as:

$$\begin{cases} \delta_c &= -\text{Im}\log\left(1 - G_{c0}(0)\Sigma_c(0)\right) \underset{N\to\infty}{=} \pi\rho_0\frac{\tilde{\Sigma}'_c(0)}{N} \\ \delta_\chi &= \text{Im}\log\left(J_K - \Sigma_\chi(0)\right) \end{cases} \qquad (7.25)$$

The result of (7.24) ensures that, even though the conduction electron phase shift vanishes in the large-N limit, it is possible to keep track of its evolution at the order $O(1/N)$, thanks to the $\chi-$fermion phase shift, which stays finite in the large-N limit.

□ **Phase diagram**

Solving the set of self-consistent equations, and using the above-defined entropy as a guide, we could map out the $\left(\dfrac{T_K}{J_H}, \dfrac{T}{J_H}\right)$ phase diagram as presented in Fig. 7.2. We now proceed to the detailed study of the three regions we could identify in the phase diagram.

7.2.2 Renormalized Fermi liquid region (I)

We saw that in the limit of vanishing Δ, the physics at low temperature is Fermi-liquid like and the physical properties averaged over the two impurities are the ones of a single impurity with identical spin. In the large-N limit, the expected cross-over between the $\Delta = 0$ and the $\Delta \neq 0$ region (where pair condensation of bosons

---

[2]Note that this definition of the conduction electron phase shift coincides with the argument of the T-matrix $T(\omega) = \frac{G_c(\omega)\Sigma_c(\omega)}{G_{c0}(\omega)}$, up to an additional π.
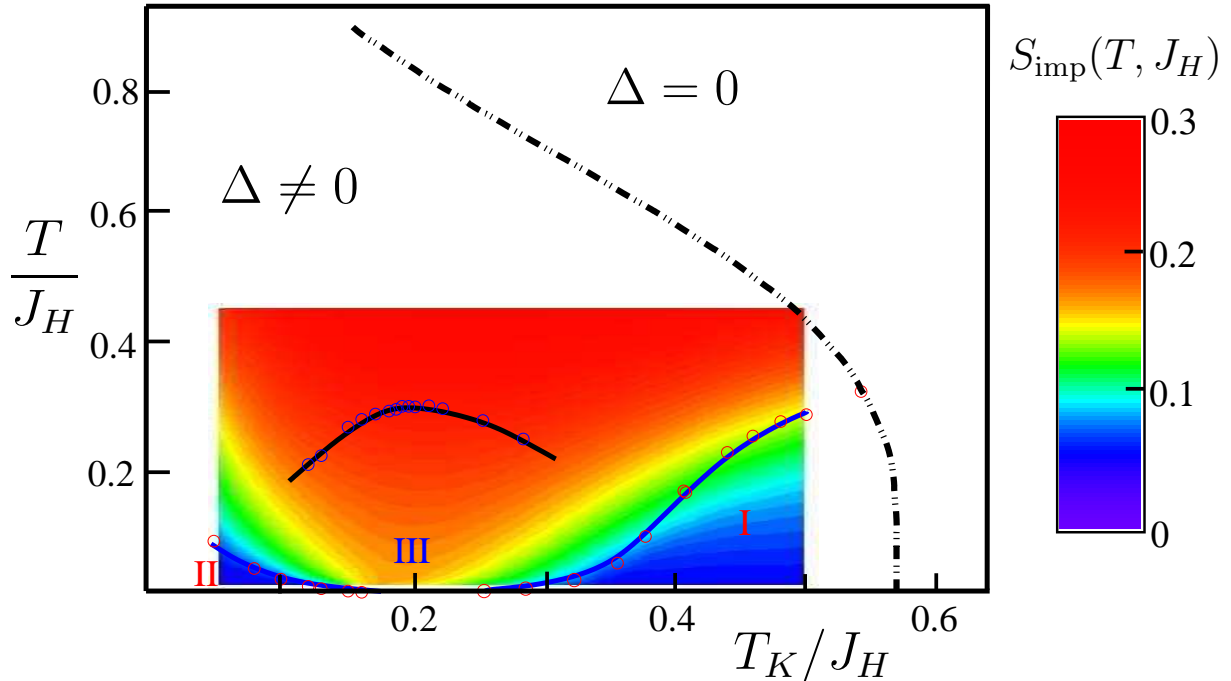
Figure 7.2: Phase diagram of the two-impurity Kondo-Heisenberg model. The circles mark the position of a local maximum in the specific heat. The color coded plot corresponds to the averaged impurity entropy $S_{\text{imp}}(T, J_H)$. Region (I) corresponds to the renormalized Fermi liquid (dominated by the Kondo interaction). Region (II) corresponds to the magnetically correlated region (dominated by the Heisenberg interaction). Region (III) corresponds to the quantum critical regime.

appears) looks like a sharp phase transition and one can identify a line of departure from the unpaired regime (represented as a dotted line in Fig. 7.2). We believe this is a consequence of our mean-field treatment of the Heisenberg interaction, and expect the cross-over to be recovered once fluctuations are included.

We refer to this Fermi liquid region of the phase diagram, as "Kondo dominated", since the value of the Heisenberg coupling is still small enough for the Kondo physics to dominate and the system basically behaves as two impurities screened by the conduction electrons only weakly coupled to each other.

☐ **Entropy**

As bosonic pairs condense, the linear temperature dependence of the entropy is preserved at low temperatures, indicating that the Fermi-liquid behavior survives. As the Heisenberg coupling J_H is increased, one can observe two effects:

- The typical temperature scale below which the Fermi liquid behavior develops drops rapidly as one departs from the $\Delta = 0$ solution. This scale is estimated

from the local maximum of the specific heat linear coefficient (i.e. the inflexion point of the entropy curve).

- The specific heat linear coefficient saturates at a low-temperature value that increases with the Heisenberg coupling.

This suggests that the range in temperature of the Fermi liquid collapses in parallel with an enhancement of the Fermi liquid renormalized parameters.

□ **Spectral functions**

As we argued before, the exactly screened single impurity solution leads to a Fermi liquid with a well-developed gap in the spectral functions confining the Schwinger bosons and the $\chi-$fermions below a temperature of the order of the gap. This picture seems to stay valid in the case of the two-impurity system: the spectral functions look like the ones of a perfectly screened single impurity, with a gap at low-energy, and a saturation of both inverse propagators at zero energy.

However, as the Heisenberg coupling is increased, the confining gap shrinks, which is consistent with the drop of the Fermi liquid scale observed from the entropy data.

In this region, the zero-temperature phase shift of the $\chi-$fermion is equal to π. This result can be understood by relating δ_χ to the sign of the renormalized Kondo coupling constant. Bearing in mind that $\delta_\chi = \text{Im} \log \left(J_K - \Sigma_\chi(0) \right) = -\text{Im} \log J_K^*$, one sees that $\delta_\chi = \pi$ corresponds to a residual ferromagnetic coupling $J_K^* < 0$. This can be understood from a strong coupling point of view, where adding a Schwinger boson to the Fermi liquid ground state increases the impurity spin $S \to S + \frac{1}{2}$ and leads to a tiny residual underscreened spin and thus to an effective ferromagnetic coupling.

7.2.3 Magnetically correlated region (II)

In the opposite limit of a large Heisenberg coupling, one expects the two impurities to screen each other, at which stage the Kondo effect barely plays any role (hence the denomination "Heisenberg dominated" for the corresponding region of the phase diagram). In the phase diagram, Fig. 7.2, this limit corresponds to the lower part of the T/J_H axis. We saw from a brief analysis of the saddle-point equations that for $J_H \to \infty$, a symmetric gap develops in the bosonic spectral function, and the Fermi liquid ground state is given by the original non-interacting conduction band. This behavior is confirmed by our numerical simulation where one sees a symmetric gap, of the order of J_H and a vanishing specific heat coefficient indicating that the impurities do not affect the surrounding conduction bath.

As one slightly departs from this solution (i.e. upon reducing the Heisenberg coupling), a gap survives in the bosonic spectral function and is still symmetric.

Further away, one observes the same kind of features as in the Kondo dominated region, namely a drop in the typical temperature scale T^* below which a Fermi liquid solution develops (associated to a collapse of the confining gap) as well as an increase in the specific heat coefficient (see Fig. 7.3).

The low-temperature phase shift of the $\chi-$fermion extracted from the data seems to vanish, which again can be understood from the point of view of a residual Kondo coupling: $\delta_\chi = 0$ suggests an antiferromagnetic $J_K^* > 0$. In this region, the local moments mutually screen each other so that adding a Schwinger boson at any site leads to a tiny residual spin that can undergo a Kondo effect with the conduction electrons, hence the antiferromagnetic residual coupling.
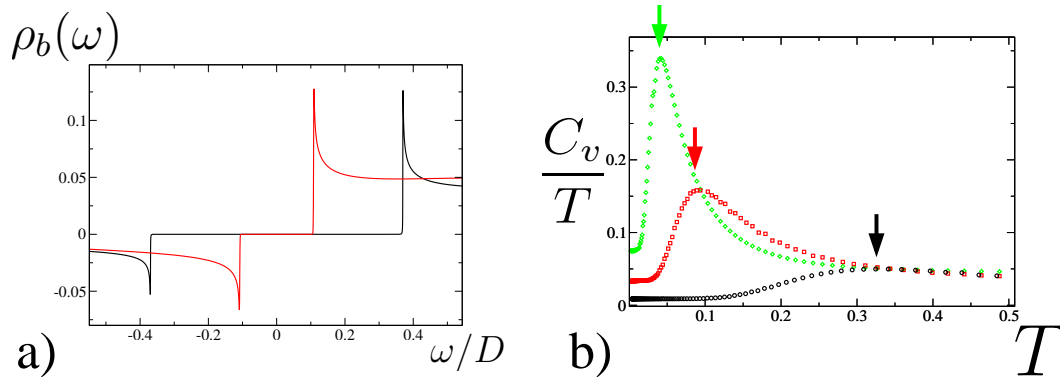
Figure 7.3: Magnetically correlated region (II): a) Symmetric gap in the bosonic spectral function for $J_H = 0.7D$ (red curve) and D (black curve), b) Specific heat coefficient for $J_H = D$ (black circles), $J_H = 0.7D$ (red squares) and $J_H = 0.5D$ (green diamonds). The arrows mark the position of the Fermi temperature T^*.

7.2.4 Quantum critical region (III)

Our numerical results indicate that both Fermi liquid regions (I) and (II) collapse at the same point in the phase diagram, suggesting the presence of a quantum critical point for a value J_H^C of the Heisenberg coupling.

□ **Signatures of a quantum critical point**

The existence of a quantum critical point is confirmed by the following observations:

▷ Closing gap

As one gets closer to J_H^C at low temperature, coming from either region of the phase diagram, the gap in the spectral functions shrinks. It turns out that the collapse of the gap towards zero occurs at the same point as a function of the Heisenberg coupling.

▷ Jump in the phase shift

Upon increasing the Heisenberg coupling, the phase shift of the $\chi-$fermion goes from π in the Kondo dominated region, to 0 in the Heisenberg dominated one. Moreover, because of the confining gap, this phase shift can only be 0 or π. It follows that the phase shift jumps at the point where the gap closes.

▷ Residual entropy

Coming from either side of the quantum critical point, and as approaching J_H^C, the impurity entropy seems to develop a knee at a finite value before dropping suddenly towards zero once the temperature is of the order of the gap. At the point where the gap closes, i.e. right on top of the critical point, the entropy reaches a finite value and saturates, even at the lowest temperatures, suggesting a finite residual entropy.
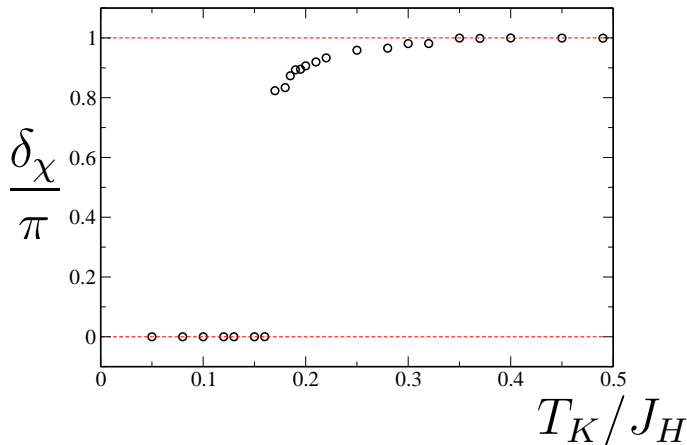
Figure 7.4: χ-fermion phase shift δ_χ/π as a function of the Heisenberg coupling at $T = 0.02T_K$. The intermediate values in the quantum critical regime are attributed to the finiteness of the temperature.

□ **Low-energy analysis**

The numerical solution suggests that, as one approaches the quantum critical point, not only the gap in the spectral functions closes, but also the real part of the inverse Green's functions taken at zero energy vanishes. This allows us to carry out a low-energy analysis at zero temperature, in the spirit of what has been done in the case of the overscreened single impurity.

The technical details of the derivation are provided in Appendix D, and we only mention the results here. Starting from a power-law ansatz for the propagators, one has from the self-consistency conditions:

$$G_b(\omega) \quad \sim \quad \frac{Ae^{i\theta \mathrm{Sign}(\omega)}}{|\omega|^{\frac{2\gamma}{1+2\gamma}}} \tag{7.26}$$

$$G_\chi(\omega) \quad \sim \quad -\frac{1}{A\rho_0 J_K^2(1+2\gamma)} \frac{e^{-i\theta \mathrm{Sign}(\omega)} \mathrm{Sign}(\omega)}{|\omega|^{\frac{1}{1+2\gamma}}} \tag{7.27}$$

where A and θ are parameters fixed by the constraints.

This power-law behavior of the propagators at low-energy is very reminiscent of what has been obtained in the case of the overscreened single impurity. However, the exponents we obtain are the ones that one would expect from a single impurity model with a spin of size $\frac{2S}{N} = \gamma$ and a number of channels $\frac{K}{N} = 2\gamma$.

Close to the critical point, the exactly screened two-impurity model behaves as an overscreened single impurity with an effective doubling of the screening channels. This last result is quite strong since a lot of properties have been derived concerning the overscreened single impurity solution and extends to the critical region of our two-impurity model, like e.g. ω/T-scaling, the existence of a residual entropy, ...

7.3 Discussion

In this section, we highlight the main results of previous studies of two spin-1/2 impurities coupled to a bath of conduction electrons via the Kondo interaction and compare them to our results for the two-impurity multichannel Kondo-Heisenberg model. We do recover similar results for the low-temperature behavior (generalized to a multichannel model) but not for the stability of the critical point.

7.3.1 Jones-Varma critical point

The problem of two spin-1/2 magnetic impurities embedded in a metallic host was first studied by Jones and Varma [117, 120, 121] in the late eighties. They found that for a small antiferromagnetic effective coupling between the impurities, the low-temperature behavior is that of a correlated Kondo effect, i.e. the fixed-point Hamiltonian is that for two independent Kondo impurities but the spin-spin cross correlator $\langle \mathbf{S}_1 \mathbf{S}_2 \rangle$ is non-zero. For a strong coupling between the impurities, no Kondo effect occurs, and the asymptotic phase shift is zero.

In between these two regimes, they found the existence of an unstable non-Fermi liquid fixed point: the so-called "Jones-Varma critical point". This fixed point was then studied in glory details by means of numerical renormalization group [117, 120, 121], conformal field theory [122, 123], and Abelian bosonization [124, 125].

This critical point displays physical properties reminiscent of a two-channel single impurity Kondo problem which we analyze in detail in the next paragraph. However, it turns out that this fixed point is unstable with respect to particle-hole asymmetry. Indeed, it was proved by Affleck et al. [123] that the critical point only exists if the Hamiltonian is invariant under a general particle-hole transformation of the form:

$$
\begin{cases}
\epsilon_{\mathbf{k}'} &= -\epsilon_{\mathbf{k}} \\
(\mathbf{k} + \mathbf{k}') \cdot \mathbf{R} &= 2n\pi, \quad n \in \mathbb{N}
\end{cases}
\tag{7.28}
$$

where $\mathbf{k}'$ is a function of $\mathbf{k}$.

7.3.2   Low-temperature physics close to the QCP

We now review some of the results concerning the Jones-Varma critical point (which we also identify as the $N = 2$ case in what follows) and compare them to the results we obtained for our quantum critical point. Since we studied a slightly different model (generalization to $SU(N)$ and large number of screening channels), and study it in the large-N limit, only a qualitative comparison is relevant here.

□ Two-channel like physics

Our low-energy analysis of the Green's functions at criticality suggests that at the quantum critical point, the system looks like a single impurity coupled to twice as many channels of conduction electron. The antiferromagnetic coupling generates a second set of screening channels

The Jones-Varma critical point was studied using Abelian bosonization, where it could be mapped onto a two-channel single impurity model [124]. The author also argued that the physics responsible for the non-Fermi liquid behavior of this fixed point was the same as the one of an overscreened single impurity coupled to two channels of conduction electrons, so that an effective doubling of the original number of channels is also observed in this model.

□ Entropy

In the case of the Jones-Varma critical point, it was found that the impurity entropy saturates at a finite value of $\log 2/2$ as $T \to 0$ (i.e. half the high temperature value).

In our model, we also find a residual entropy at the QCP at low temperature. According to our low-energy analysis at the QCP, we can argue that this residual entropy is given by the formula derived for the overscreened single impurity, with an effective number of channels $\gamma_{\text{eff}} = 2p_0$:

$$
\lim_{T \to 0} s_{\text{imp}} = \frac{1 + 2p_0}{2\pi} \text{Im} \left[\text{Li}_2 \left(e^{2i\frac{\pi p_0}{1 + 2p_0}} \right) + \text{Li}_2 \left(e^{2i\frac{\pi}{1 + 2p_0}} \right) - \text{Li}_2 \left(e^{2i\frac{\pi(1 + p_0)}{1 + 2p_0}} \right) \right] \tag{7.29}
$$

□ Specific heat coefficient

As one would expect from a two-channel single impurity, the specific heat at the Jones-Varma fixed point diverges as a function of temperature like $\log T$.

Using the results of the overscreened single impurity, combined with our low-energy analysis of the two-impurity quantum critical point, we can deduce that the specific heat diverges at low temperatures for values of the impurity spin such that $p_0 \geq 1/2$. In particular, a logarithmic divergence is recovered for $p_0 = \gamma = 1/2$, which would correspond to the Jones-Varma case, if one were to naively take the $N \to 2$ limit of our result. Moreover, there are two local maxima in the specific heat coefficient as a function of temperature close to the quantum critical point (hence the two sets of dots in the region III of the phase diagram). This double bump feature suggests a two stage quenching process related to the generation of a second set of channels. The same behavior is observed as one approaches the Jones-Varma critical point from the temperature axis (see Fig. 7.5).
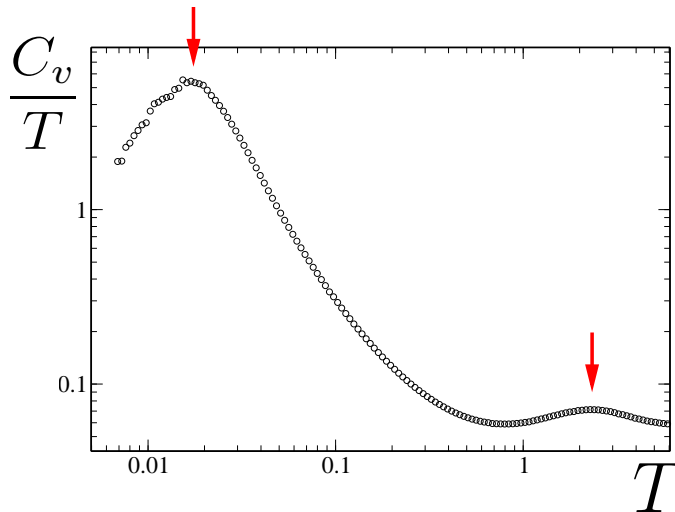
Figure 7.5: Specific heat as a function of temperature, close to the QCP. The double-log scale is used to show the presence of two local maxima in the specific heat.

□ Phase shift

For $N = 2$, it is convenient to rewrite the total phase shift as the sum of an "even" and "odd" component, δ_e and δ_o. This denomination is related to the construction of even and odd parity fields, obtained after an exact reduction of the original Hamiltonian to a one-dimensional one. It can be proved [123] that the particle-hole symmetry defined in (7.28) ensures that both δ_e and δ_o can only take values 0 and $\pi/2$: $\delta_e = \delta_o = \pi/2$ in the Kondo-screening phase, and $\delta_e = \delta_o = 0$ when the

impurities form a singlet. The particle-hole symmetry enforces that the transition between the two regimes can only occur through one or more critical points, hence justifying the existence of the Jones-Varma critical point in this case.

This is precisely the behavior we observed for the $\chi-$fermion phase shift in our model: at zero temperature, it jumps from π in the renormalized Fermi liquid region, to 0 in the magnetically correlated region. The conduction electron phase shift is then given by the extension of the sum rule to our two-impurity Hamiltonian. It follows that the impurity averaged phase shift for the conduction electrons jumps from $\delta_c = \pi/N$ to 0 as one increases the inter-impurity coupling.

□ Uniform susceptibility

We do not notice any remarkable feature in the uniform susceptibility in the low temperature limit: it is non-monotonic as a function of the Heisenberg coupling and grows on both side of the critical region, to finally reach a finite value at the QCP.

This behavior is comparable to the $N = 2$ case where the uniform susceptibility saturates at low temperature for any value of the coupling between impurities.

7.3.3 Stability of the critical point

This is where our results differ most drastically from the ones of the $N = 2$ case.

We saw that for $N = 2$, the particle-hole symmetry as defined in (7.28) plays an important role as if it is not respected, the Jones-Varma fixed point no longer exists. This can be argued from the analysis of the phase shifts. In the particle-hole symmetric case, both δ_e and δ_o can only take values 0 and $\pi/2$, and one goes from a region where $\delta_e = \delta_o = \pi/2$ to a region where $\delta_e = \delta_o = 0$ through the Jones-Varma critical point.

When the particle-hole symmetry is broken (or if it does not respect (7.28)), it becomes possible to cross smoothly from unitary scattering in both even and odd channels ($\delta_e = \pi/2, \delta_o = \pi/2$) to no scattering at all ($\delta_e = 0, \delta_o = 0$).

In the large-N limit, the numerical solution always displays a quantum critical point for a given value of the Heisenberg coupling, independently of the particle-hole symmetry of the conduction band. This survival of the Jones-Varma critical point at large N in the absence of particle-hole symmetry is a consequence of the gap in the spectral functions. In the Kondo screening regime, the two-impurity sum rule imposes that:

$$\delta_e + \delta_o = \frac{2\pi}{N} \tag{7.30}$$

whereas, in the magnetically correlated region of the phase diagram, the total phase shift is 0 since the impurities form a singlet and the surrounding conduction electrons are nearly free.

One could imagine crossing smoothly from one regime to the other but this is prevented by the gap in the spectral functions. If a gap exists, the associated phase

shift for the $\chi-$fermion is forced to be either 0 or π, and one has to go from one to the other through one or more critical points. As we argued when dealing with the perfectly screened single impurity, the gap is expected to arise independently on the shape of the conduction band, and in particular it is not sensitive to particle-hole asymmetry. On the other hand, our analysis of the limiting case $\Delta \to \infty$ suggests the existence of a gap even for a vanishing Kondo effect, i.e. for any conduction band. As a conclusion, we are quite confident that a gapped solution arises in both the Kondo and the Heisenberg dominated regions, leading to a necessary jump in the conduction electron phase shift and to the existence of a critical point separating these two regimes.

7.4 Conclusion

In this chapter, we studied a system of two impurity coupled via an exchange interaction, as well as a Kondo coupling to the bath of conduction electrons. We proved that our method can capture the magnetic correlations appearing in such a system. The comparison of our results to the previous approaches applied to the same system reveals a good qualitative agreement.

A few points deserve some complimentary study.

▷ Spin-spin cross-correlator and staggered susceptibility

In the Jones-Varma study the cross-correlator between impurities and the staggered susceptibility show a remarkable behavior as one approaches the critical point. The staggered susceptibility seems to diverge logarithmically with temperature as one approaches the critical point from above, while the spin-spin cross correlator stays finite over the whole phase diagram (including the Kondo dominated region) and saturates at a constant value at the critical point.

The observation of such features has not been carried out in our model and deserves to be addressed.

▷ Pure Kondo

Another question one might ask concerns the RKKY coupling. We considered here a Kondo-Heisenberg model, but one could argue that a pure Kondo two-impurity model could also be studied.

Indeed, it can be readily seen from scaling arguments that the RKKY coupling has the same scaling as the Heisenberg term, and does not vanish in the large-N limit:

$$ J_{RKKY} \quad \propto \quad \underbrace{\left(\frac{1}{\sqrt{N}}\right)^4}_{4\text{vertices}} \times \underbrace{K}_{\Sigma_\mu} \quad \propto \quad N \qquad (7.31) $$

For an antiferromagnetic coupling, this would require to use adjoint representations for the spins. Our first analysis of this model led to the derivation of saddle-point equations that look the same as the one derived in this chapter under the condition that the conduction electron band respect particle-hole symmetry.

Considering the dramatic importance of particle-hole symmetry in the original Jones-Varma fixed point, it is legitimate to wonder whether it affects the existence of the QCP in this case. Moreover, for the RKKY coupling, it could also appear that the retardation effects slightly change the low-energy analysis carried out for the Kondo-Heisenberg model. We are currently investigating these issues.

CHAPTER 8

Conserving approximation for the single impurity model

Contents

In this chapter, we go back to the case of a perfectly screened single impurity, and investigate a new approach based on a conserving approximation, that cures some of the failures of the original large-N method. We show that this method reproduces the important results of the infinite N limit, and leads to a finite phase shift as well as a finite T-matrix for the Fermi liquid ground-state at low temperature. The main results of this chapter have been published in the Publication 5, the rest is presented here for the first time.

8.1 Model and set of equations

We showed in Chapter 6 that the exactly screened multichannel Kondo model, taken in the large-N limit, leads to a solution that displays the low-temperature thermodynamics of an interacting Fermi-liquid. Nevertheless, the transport properties are the ones of a trivial Fermi liquid, with a vanishing T-matrix and phase shift at the impurity site.

Our main goal in this section is to try to construct a method leading to a Fermi liquid ground-state with both non-trivial thermodynamics and transport properties. Our motivation lies in the extension of such a method to describe the physics of quantum dots out of equilibrium.

8.1.1 Infinite U Anderson model

As pointed out in [115], it is possible to generalize the large-N limit for the Kondo model to the infinite U Anderson model. The latter is a slightly different model, known to display a greater variety of behavior than the Kondo model, as it allows, among others, charge fluctuations on the impurity site.

The model we consider here is a generalized multichannel Anderson model given by the Hamiltonian:

$$
\begin{aligned}
H &= H_K + H_{\text{int}} \\
H_K &= \sum_{\mathbf{k}} \sum_{\sigma=1}^{N} \sum_{\mu=1}^{K} \epsilon_{\mathbf{k}} c_{\mathbf{k}\sigma\mu}^{\dagger} c_{\mathbf{k}\sigma\mu} + \epsilon_0 \sum_{\sigma} b_{\sigma}^{\dagger} b_{\sigma} \\
H_{\text{int}} &= \frac{V}{\sqrt{N}} \sum_{\mathbf{k}} \sum_{\sigma,\mu} \left(c_{\mathbf{k}\sigma\mu}^{\dagger} F_{\mu}^{\dagger} b_{\sigma} + b_{\sigma}^{\dagger} F_{\mu} c_{\mathbf{k}\sigma\mu} \right)
\end{aligned}
\tag{8.1}
$$

where we extended the spin symmetry group to $SU(N)$. Here $c_{\mathbf{k}\sigma\mu}^{\dagger}$ creates a conduction electron with momentum $\mathbf{k}$, channel index μ and spin index σ. The bilinear product $b_{\sigma}^{\dagger} F_{\mu}$ between a Schwinger boson $b_{\sigma}^{\dagger}$ and a slave fermion[1] F_{μ} creates a local-

---

[1]Note that for obscure notational reasons, this fermionic field behaves as the particle-hole symmetric of the χ-fermion used in the context of the Kondo model in previous chapters.

ized electron, which hybridizes with the conduction electron according to H_{int}. The energy ϵ_0 of the singly occupied impurity is taken to be negative.

The constraint preventing the double-occupancy of the impurity site in the $N = 2$ case is replaced here by a constraint on the total number of Schwinger bosons and slave fermions:

$$\sum_\sigma b_\sigma^\dagger b_\sigma + \sum_\mu F_\mu^\dagger F_\mu = p_0 \tag{8.2}$$

and we enforce that $p_0 = \gamma$ since we restrict ourselves to the case of perfect screening.

Following the method of Parcollet and Georges for the Kondo model [106], it is possible to derive a set of saddle-point equations for the infinite U Anderson model in the limit $N \to \infty$, starting from the action and applying the method of steepest descent, after a few transformations (see Section 6.1.3). This set of saddle-point equations reads:

$$
\begin{align}
\Sigma_b(\tau) &= -\gamma V^2 G_c(\tau) G_F(\tau) \tag{8.3a} \\
\Sigma_F(\tau) &= -V^2 G_c(\beta - \tau) G_b(\tau) \tag{8.3b} \\
G_b^{-1}(i\nu_n) &= i\nu_n + \lambda_0 - \epsilon_0 - \Sigma_b(i\nu_n) \tag{8.3c} \\
G_F^{-1}(i\omega_n) &= i\omega_n + \lambda_0 - \Sigma_F(i\nu_n) \tag{8.3d} \\
p_0 &= -G_b(\tau = 0^-) + \gamma G_F(\tau = 0^-) \tag{8.3e}
\end{align}
$$

where we use the conventional definition of the imaginary time Green's function, $G_\phi(\tau) = -\langle T\phi(\tau)\phi^\dagger(0)\rangle$.

A few differences appear compared to the equations governing the Kondo case: the bare propagator of the slave fermion now has a frequency dependence, and the slave fermion F participates in the constraint.

It is possible to recover the Kondo model in the limit:

$$
\begin{cases} V &\to \infty \\ \epsilon_0 &\to -\infty \end{cases} \quad \text{with} \quad J_K = \frac{V^2}{-\epsilon_0} \quad \text{fixed} \tag{8.4}
$$

In this case, the kinetic bosonic term of the Hamiltonian saturates the constraint which becomes independent on the slave fermion F. Defining $G_\chi(\tau) = G_F(\beta - \tau)\frac{\epsilon_0^2}{V^2}$ and the corresponding self-energy, one recovers in the limit stated in Eq. (8.4) the saddle-point equations (6.27) of the multichannel Kondo model, with a chemical potential $\lambda = \lambda_0 - \epsilon_0$.

8.1.2 Conserving approximation

We showed in Chapter 6 that the saddle-point equations can be derived using the Luttinger-Ward functional. The latter is given by the sum of two-particle irreducible diagrams and reduces to a single two-loop diagram in the large-N limit, the other contributions being small in powers of N. Taking the derivative of the

Luttinger-Ward functional $\Phi_{LW}[G_b, G_F, G_c]$ with respect to G_b and G_F, one obtains the equations for the self-energy of the Schwinger boson and the slave fermion. The fermionic self-energy can also be derived from the same procedure: it turns out to be unimportant for the low-energy spectral functions as it scales like $1/N$, but it plays a significant role in the thermodynamics since it enters in the entropy formula as an overall $O(N)$ contribution. Note however that, in this case, the conduction electron self-energy Σ_c is computed at a given temperature using the Green's functions G_b and G_F obtained from solving the saddle-point equations which are themselves independent on Σ_c. In other words, the conduction electron self-energy does not enter the self-consistency loop that only relates G_b and G_F, through the corresponding self-energies.

In this paragraph, we proceed in a slightly different manner, even though the starting point is the same. In the case of the infinite U Anderson model, the Luttinger-Ward functional (Fig. 8.1) looks just the same as in the Kondo model, the only difference coming from a factor $V/\sqrt{N}$ instead of $J_K/\sqrt{N}$ at the vertex.

Figure 8.1: Luttinger-Ward functional grouped in powers of $1/N$. Schwinger bosons are represented by solid lines, slave fermions by dashed lines and conduction electrons by double lines.

Instead of taking the limit of infinite N, we consider the conserving approximation which amounts to neglecting all the diagrams in the Luttinger-Ward functional, but the leading order $O(N)$ term. We emphasize that contrary to the large-N limit where the reduction of the Luttinger-Ward functional was exact, here this is an approximation, as for finite N, we do neglect the higher-order terms.

One may wonder at this stage to what extent this differs from the large-N limit, since we ultimately consider the contribution of the same, unique diagram. The essential difference is that in the case of the conserving approximation stated above, the conduction electron self-energy no longer vanishes, and enters the full self-consistency which now encloses the following set of equations, obtained from taking the derivative of Φ_{LW} with respect to the Green's functions:

$$\Sigma_b(\tau) = -\gamma V^2 G_F(\tau) G_c(\tau) \tag{8.5a}$$

$$\Sigma_F(\tau) = -V^2 G_b(\tau) G_c(\beta - \tau) \tag{8.5b}$$

$$\Sigma_c(\tau) = -\tilde{\gamma} V^2 G_b(\tau) G_F(\beta - \tau) \tag{8.5c}$$

where G_b, G_F and G_c are the fully dressed imaginary-time Green's functions, and we introduced the new parameter $\tilde{\gamma} = \frac{1}{N}$.

The Dyson's equations for all three propagators now read:

$$G_b^{-1}(i\nu_n) = i\nu_n + \lambda_0 - \epsilon_0 - \Sigma_b(i\nu_n) \tag{8.6a}$$

$$G_F^{-1}(i\omega_n) = i\omega_n + \lambda_0 - \Sigma_F(i\nu_n) \tag{8.6b}$$

$$G_c^{-1}(i\omega_n) = G_{c0}^{-1}(i\omega_n) - \Sigma_c(i\omega_n) \tag{8.6c}$$

and we choose the bare conduction electron propagator, so that the associated density of states is a flat band, $\rho_{c0}(\omega) = -\frac{1}{\pi}\mathrm{Im}G_{c0}(\omega + i\delta) = \rho_0\Theta(D^2 - \omega^2)$.

As always, one has to enforce the constraint on the total number of bosons and slave fermions by adjusting the chemical potential λ_0:

$$p_0 = -G_b(\tau = 0^-) + \gamma G_F(\tau = 0^-) \tag{8.7}$$

with $p_0 = \gamma$ in our case, since we focus on the perfectly screened case only.

8.2 Thermodynamics and transport properties

We now solve self-consistently the set of equations (8.5)-(8.6), and study some of the properties of the low-temperature solution. We focus on the thermodynamics, to check whether the new self-consistency preserves the Fermi-liquid like features, and on the transport properties, to see whether this new method leads to interesting non-trivial results.

8.2.1 Existence of a gap

The first important element to stress out is that the full self-consistency does not affect the existence of the gap. The low-temperature Green's functions of both the boson and the slave fermion are gapped at low-energy. Note that the gap also appears in the conduction electron self-energy, but not in the associated full propagator since the bare conduction electron Green's function contains a finite imaginary part:

$$\mathrm{Im}G_c(\omega + i\delta) = \frac{\mathrm{Im}G_{c0}(\omega) + |G_{c0}(\omega)|^2\mathrm{Im}\Sigma_c(\omega)}{|1 - G_{c0}(\omega)\Sigma_c(\omega)|^2} \tag{8.8}$$

This allows to extend the consequences of the gap studied in section 6 to the case of the infinite U Anderson model:

- Rigid shift

  Starting from a given solution of the set of equations (8.5), and applying a small change of the chemical potential, one obtains a new solution of the equations where the Green's functions have been shifted in frequency by the change in λ_0. This can be proved analytically from the self-energy equations

in a similar way to the Kondo model. Note however that only G_b and G_F, and their associated self-energies can be rigidly shifted, Σ_c, although gapped, is not sensitive to a shift in the chemical potential λ_0:

$$
\begin{aligned}
\Sigma_c(\omega, \lambda_0 + \delta\lambda_0) &= -\frac{\tilde{\gamma} V^2}{\pi} \int_{-\infty}^{0} d\Omega \; [G_b''(\Omega, \lambda_0 + \delta\lambda_0) \, G_F(\Omega - \omega, \lambda_0 + \delta\lambda_0)^* \\
&\qquad\qquad\qquad - G_F''(\Omega, \lambda_0 + \delta\lambda_0) G_b(\Omega + \omega, \lambda_0 + \delta\lambda_0)] \\
&= -\frac{\tilde{\gamma} V^2}{\pi} \int_{-\infty}^{0} d\Omega \; [G_b''(\Omega + \delta\lambda_0, \lambda_0) \, G_F(\Omega - \omega + \delta\lambda_0, \lambda_0)^* \\
&\qquad\qquad\qquad - G_F''(\Omega + \delta\lambda_0, \lambda_0) G_b(\Omega + \omega + \delta\lambda_0, \lambda_0)] \\
&= \Sigma_c(\omega, \lambda_0) + \int_{0}^{\delta\lambda_0} d\Omega \; [G_b''(\Omega, \lambda_0) \, G_F(\Omega - \omega, \lambda_0)^* \\
&\qquad\qquad\qquad - G_F''(\Omega, \lambda_0) G_b(\Omega + \omega, \lambda_0)] \quad (8.9)
\end{aligned}
$$

where the last integral vanishes due to the gap in both $G_b''(\omega)$ and $G_F''(\omega)$.

- Low-temperature behavior

  Although the entropy formula changes a little compared to the large-N approach (see next paragraph), one can still argue that the gap in both the bosonic and the fermionic self-energy leads to a low-temperature entropy dominated by the contribution from the conduction electrons. We analyze in the next paragraphs whether this contribution is still Fermi-liquid like.

Finally, the numerical solution of the set of equations suggests that the gap depends in a non-trivial way on the value of N.

8.2.2 Thermodynamics and identities

□ **Entropy**

Following Luttinger and Ward [108, 109, 110], we build the free energy of the system from the various Green's functions and the Luttinger-Ward functional. After subtracting the free energy of the conduction electron gas in the absence of the impurity, we define the impurity free energy as:

$$
\begin{aligned}
F_{\text{imp}} = F - F_{\text{bulk}} &= N \int \frac{d\omega}{\pi} \, n(\omega) \text{Im} \left(\log(-G_b^{-1}(\omega)) + G_b(\omega) \Sigma_b(\omega) \right) \\
&+ K \int \frac{d\omega}{\pi} \, f(\omega) \text{Im} \left(\log(-G_F^{-1}(\omega)) + G_F(\omega) \Sigma_F(\omega) \right) \\
&+ NK \int \frac{d\omega}{\pi} \, f(\omega) \text{Im} \left(\log \left(\frac{G_c^{-1}(\omega)}{G_{c0}^{-1}(\omega)} \right) + G_c(\omega) \Sigma_c(\omega) \right) \\
&+ p_0 N\lambda + \Phi_{LW}[G_b, G_\chi, G_{c0}] \quad (8.10)
\end{aligned}
$$

Applying the same procedure as the one explained in Appendix A for the case of the large-N Kondo model, we can extract from (8.10) a closed-form expression for the impurity entropy which reads:

$$
\begin{aligned}
S_{\text{imp}} \; = \; & -N \int \frac{d\omega}{\pi} \left[\frac{\partial n(\omega)}{\partial T} \left(\text{Im} \log \left(-G_b^{-1}(\omega)\right) + G_b'(\omega)\Sigma_b''(\omega) \right) \right. \\
& + K \frac{\partial f(\omega)}{\partial T} \left(\text{Im} \log \left(-G_\chi^{-1}(\omega)\right) + G_\chi'(\omega)\Sigma_\chi''(\omega) \right) \\
& \left. + NK \frac{\partial f(\omega)}{\partial T} \left(\text{Im} \log \left(\frac{G_c^{-1}(\omega)}{G_{c0}^{-1}(\omega)} \right) + G_c'(\omega)\Sigma_c''(\omega) \right) \right]
\end{aligned}
\tag{8.11}
$$

Numerically, the impurity entropy shows a linear behavior at low temperatures suggesting that a Fermi-liquid state develops below a given temperature T^*, of the order of the gap in the spectral functions. It is possible from the entropy formula (8.11) to extract an analytic expression of the specific heat coefficient at low temperature. Taking the derivative with respect to temperature, this leads after a few rearrangements:

$$
\lim_{T \to 0} \frac{C_v}{T} = -\frac{\pi^2}{3} NK \rho_c(0) \left. \frac{d\Sigma_c'}{d\omega} \right|_{\omega=0}
\tag{8.12}
$$

The conserving approximation applied to the infinite U Anderson model leads to very similar results to the large-N approach: the low-temperature impurity entropy is Fermi-liquid like in both cases and the saturation of the low temperature specific heat coefficient is given by the same expression provided that one replaces the bare conduction electron spectral function by the full one.

□ Friedel sum rule

The expression (8.10) of the impurity free energy allows us to derive sum rules for the conserved quantities. In particular, it is possible to write a sum rule associated with the conservation of the total electric charge. Following the method mentioned in section 7.2.1 and detailed in Publication 3, we can write the change in the total charge Q_e due to the presence of the impurity, as a function of the various Green's functions:

$$
\Delta Q_e = -\frac{1}{\pi} \left[NK \text{Im} \log \left(1 - G_{c0}(0)\Sigma_c(0)\right) - K \text{Im} \log \left(-G_F^{-1}(0)\right) \right]
\tag{8.13}
$$

The change in the total charge can also be written explicitly as $\Delta Q_e = n_c - n_F - n_c^0$, where n_c and n_c^0 corresponds to the number of conduction electron with and without the impurity, and n_F is the number of slave fermions. Note that n_F comes with a minus sign because the slave fermions have an opposite charge compared to the conduction electrons (hence the name "holons" often used to designate them).

In a similar spirit, one can write another sum rule, for the total number Q_{bF} of Schwinger bosons and slave fermions, since this quantity is conserved due to the explicit constraint. Following the same method, we have:

$$
\begin{aligned}
Q_{bF} &= \sum_\alpha \langle b_\alpha^\dagger b_\alpha \rangle + \sum_\mu \langle F_\mu^\dagger F_\mu \rangle \\
&= \frac{1}{\pi} \left[N \mathrm{Im} \log \left(-G_b^{-1}(0) \right) - K \mathrm{Im} \log \left(-G_F^{-1}(0) \right) \right]
\end{aligned}
\tag{8.14}
$$

This can be simplified further using that the renormalized chemical potential $\lambda^* = G_b^{-1}(0)$ is real (because of the gap) and negative so that the first term actually vanishes at low temperature. Since we focus on the exactly screened case, we impose that $Q_{bf} = K$, so that ultimately, the second sum rule, Eq. (8.14), reduces to $\mathrm{Im} \log \left(-G_F^{-1}(0) \right) = -\pi$.

Substituting it into (8.13), and recalling that the conduction electron phase shift is given by $\delta_c = -\mathrm{Im} \log \left(1 - G_{c0}(0) \Sigma_c(0) \right)$, we have the following Friedel sum rule:

$$
\begin{aligned}
\delta_c &= \frac{\pi}{N} \frac{K - n_F}{K} + \frac{\pi \Delta n_c}{NK} \\
&= \frac{\pi}{N} \frac{K - n_F}{K} + O\left(\frac{T_K}{ND} \right)
\end{aligned}
\tag{8.15}
$$

where $\Delta n_c = n_c - n_c^0 = -\frac{NK}{\pi} \int_{-\infty}^0 d\omega \ \mathrm{Im}\left(G_c(\omega) - G_{c0}(\omega) \right)$. According to the Clogston-Anderson compensation theorem [119], the change in the electronic charge due to a Kondo or Anderson impurity vanishes in the large bandwidth limit like the ratio of the Kondo temperature to the bandwidth, allowing us to replace $\Delta n_c = O(N \frac{T_K}{D})$.

We determined the conduction electron phase shift from the numerical solution of the full self-consistent equations, and compared it to the phase shift obtained from plugging the large-N solution into the $O(1/N)$ expression of Σ_c. The results are presented in Fig. 8.2, and show that our conserving approximation preserves the sum rule (8.15) for each value of N.

□ **Yamada-Yosida-Yoshimori identity**

Along with the Friedel sum rule, our conserving approximation preserves some important interrelationships of the Fermi liquid among which the so-called "Yamada-Yosida-Yoshimori" identity, which relates the specific heat coefficient to the spin, charge and channel susceptibilities.

This identity can be derived from Nozières local Fermi liquid theory [126] which relates the quasiparticle spectrum in the Fermi-liquid ground-state to the conduction electron phase shift, and its response to an applied field, or a change in chemical
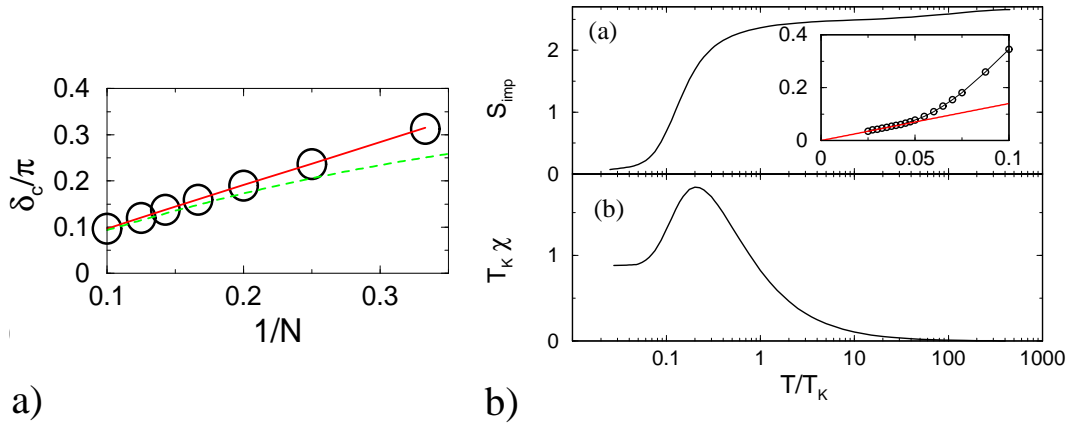
Figure 8.2: a) Phase shifts extracted from the calculated T-matrices, for $K = 1$ and $n_F \simeq 0.04$. The solid line stands for $(K - n_F)/NK$ and the dashed line shows the phase shift obtained without imposing the self-consistency on the conduction electron. b) Entropy and impurity spin susceptibility as a function of temperature, obtained for $K = 1$ and $N = 4$. In the inset: the low-temperature entropy shows a linear behavior.

potential. In the context of our generalized multichannel Kondo or Anderson model, this derivation is presented in Appendix C, and the main result reads:

$$NK(N + K)\frac{\delta C_v}{C_v^{(0)}} = K(N^2 - 1)\frac{\delta\chi_s}{\chi_s^{(0)}} + N(K^2 - 1)\frac{\delta\chi_f}{\chi_f^{(0)}} + (N + K)\frac{\delta\chi_c}{\chi_c^{(0)}} \quad (8.16)$$

where δC_v and $\delta\chi$ are, respectively, the change in the specific heat and the susceptibility due to the impurity, and $\chi_{s,f,c}^{(0)}$ denote the spin, flavor, and charge susceptibility in the absence of the impurity.

Note that in the special case of the Kondo model, the interaction does not affect the charge or the channel index so that both χ_f and χ_c are zero, and the previous result (8.16) reduces to the Wilson ratio:

$$W = \frac{\delta\chi_s/\chi_s^{(0)}}{\delta C_v/C_v^{(0)}} = \frac{N(N + K)}{N^2 - 1} \quad (8.17)$$

where we recover the Bethe ansatz result [116].

□ Susceptibility

Computing numerically the solution to the full set of self-consistent equations in the presence of an external magnetic field coupled to both the conduction electrons and the Schwinger bosons, we extract the impurity susceptibility as a function of temperature. The general shape is similar to the one of the local susceptibility

studied in the large-N limit of the perfectly screened impurity: the $1/T$ behavior at high temperature crosses over after reaching a maximum, and saturates at a finite value as $T \to 0$. This saturation at low temperature is another hint that the conserving approximation does describe some of the physical properties of the Fermi-liquid ground-state.

The major difference compared to the large-N limit is that now, despite the gap in the spectral functions, the frequency-dependent susceptibility is not gapped. This is because the dynamic spin susceptibility no longer writes as a simple convolution of two bosonic propagators like in the large-N limit, and is now made of a whole series of diagrams. This same gap in the spectral functions allows one to extend the derivation carried out by Shiba on the finite U Anderson model [127]: the presence of a finite scale in the excitation spectrum allows one to replace the Matsubara summations by integrals at low temperatures, so that one can generalize Shiba's results to the infinite U Anderson model. In our multichannel version of the Anderson model, the Shiba relationship writes:

$$\left. \frac{\chi_s''(\omega)}{\omega} \right|_{\omega=0} = \frac{\pi N}{2K} \left(\frac{\chi_s}{N} \right)^2 \tag{8.18}$$

where χ_s is the impurity spin susceptibility, and the $''$ notation stands for the imaginary part.

This relationship guarantees that the imaginary part of the frequency-dependent spin susceptibility is linear at low frequencies, ensuring that the spin response function decays as $1/t^2$ in time, as expected from a Fermi liquid.

8.2.3 Transport properties

We now turn to a discussion of the electron scattering off the impurity.

□ T-matrix

The electron scattering is determined by the conduction electron T-matrix, defined as:

$$T(\omega + i\delta) = \frac{G_c(\omega + i\delta)\Sigma_c(\omega + i\delta)}{G_{c0}(\omega + i\delta)} \tag{8.19}$$

As the temperature is lowered, a sharp peak develops in the imaginary part of the T-matrix, close to the Fermi energy. Unlike the peaks appearing in the spectral functions, this feature does not diverge at low temperature, and finally saturates a decade below the Kondo temperature. Note however that the associated structure in the conduction electron self-energy does diverge as $T \to 0$, and the saturation in the T-matrix arises from a compensation between the numerator and the denominator, both dominated by Σ_c at low temperature.

Due to the low-energy gap in the conduction electron self-energy, the T-matrix at the Fermi energy is given by:

$$
\begin{aligned}
T_c''(0) &= \frac{-\pi\rho_0\Sigma_c'(0)^2}{|1 + i\pi\rho_0\Sigma_c'(0)|^2} = \frac{-\frac{\tan^2\delta_c}{\pi\rho_0}}{|1 - i\tan\delta_c|^2} \\
&= -\frac{\sin^2\delta_c}{\pi\rho_0}
\end{aligned}
\tag{8.20}
$$

where we considered the large bandwidth limit, and thus neglected the real part of the bare conduction electron Green's function.

It follows from (8.20) that the fully developed resonance is pinned at the Fermi energy, to the Langreth sum-rule value [128] of $-(\sin^2\delta_c)/(\pi\rho_0)$. This could be verified numerically, as one can see in Fig. 8.3.
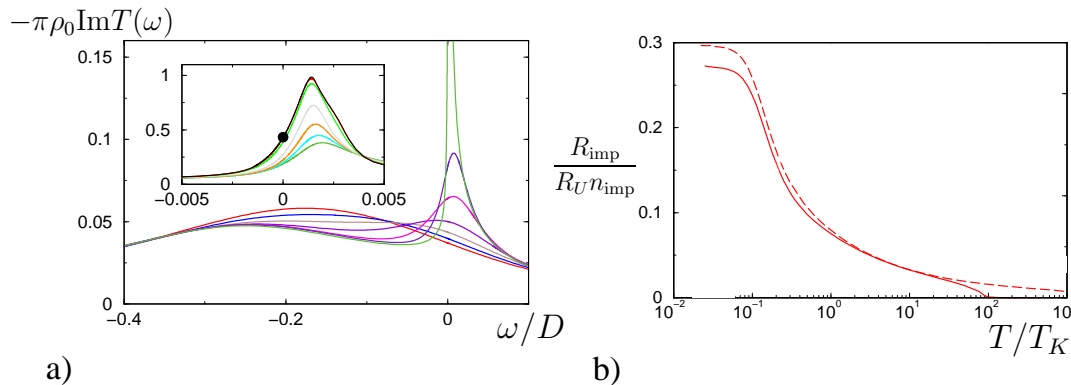
Figure 8.3: a) T-matrix as a function of frequency for decreasing temperature: a resonance develops close to the Fermi energy. Inset: Magnification of the resonance, the dot marks the value $\sin^2\delta_c$. b) Impurity contribution to the resistivity for two different values of the hybridization.

□ Resistivity

Various important physical properties, such as the impurity resistivity in the dilute limit, can be related to the conduction electron T-matrix.

The impurity contribution R_i to the resistivity of the system is connected to the thermal average of the T-matrix:

$$
R_i = n_i R_U \left[\int d\omega \left(-\frac{\partial f}{\partial\omega}\right) \frac{1}{\pi\rho_0|T''(\omega)|}\right]^{-1}
\tag{8.21}
$$

where R_U is the unitary resistivity, and n_i is the density of impurities in the dilute limit.

We plot the resistivity for a given set of parameters in Fig. 8.3. This impurity resistivity increases as one lowers the temperature and saturates at a constant value given by:

$$\lim_{T \to 0} \frac{R_i}{R_U} = n_i \pi \rho_0 |T''(0)| = n_i \sin^2 \delta_c \qquad (8.22)$$

8.3 The $N \to 2$ limit

Our conserving approximation does not only recover the thermodynamic aspects of the Fermi liquid already studied in the large-N limit, but also correctly describes the transport properties of the system via a finite T-matrix.

It is natural to try to extend this scheme down to the physical case of $N \to 2$, and study whether, in the Kondo limit, this recovers the expected properties of the local Fermi liquid, in particular the $\pi/2$ conduction electron phase shift and the quadratic frequency dependence of the conduction electron self-energy.

8.3.1 Spectral functions

□ **Low-energy gap**

The first important feature to notice as one reduces N, is that the gap in the spectral functions shrinks and ultimately seems to close in the limit $N \to 2$.

This leads to two opposite expectations. The closing of the gap looks promising for the recovery of the expected conduction self-energy of the local Fermi liquid, as no gap in Σ_c is known to appear in this case. A collapsing gap is a necessary condition to get the quadratic dependence of the imaginary part Σ_c'', characteristic of a Fermi liquid. On the other side, a vanishing gap suggests that both the Schwinger bosons and the slave fermions contribute to the thermodynamics, which is problematic unless they recombine to generate a Fermi-liquid like behavior.

The absence of a gap also prevents the extension of most of the results concerning the conserving approximation, as they were derived assuming the presence of a scale in the excitation spectrum.

□ **Conduction electron self-energy**

We saw for a given value of N that the low-temperature T-matrix saturates, and that this saturation was associated to a compensation between numerator and denominator of the diverging conduction electron self-energy.

The collapse of the gap does not affect the divergence, and one does not recover the quadratic term in frequency, expected for the local Fermi liquid.

This divergence manifests itself at the boundary of the gap, and leads to a dip in the full conduction electron spectral function which ultimately touches zero at low temperature. As one lowers N towards 2, the gap closes and the dip in the spectral
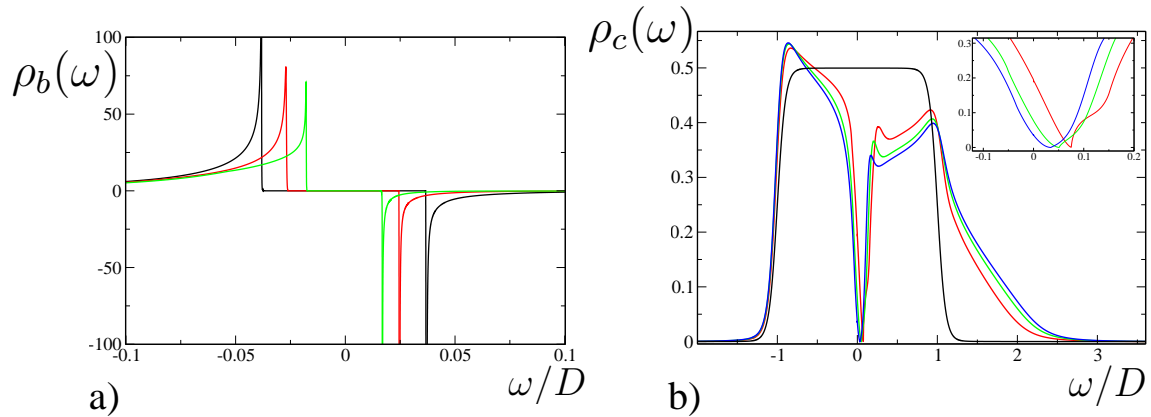
Figure 8.4: a) Closing of the gap in the bosonic spectral function as one reduces N: $1/N = 0.3$ in black, $1/N = 0.4$ in red and $1/N = 0.45$ in green. b) Conduction electron spectral function: for bare fermions (black), for $1/N = 0.3$ (red), 0.4 (green), and 0.45 (blue). The dip gets deeper and closer to the Fermi energy as $N \to 2$. Inset: tip of the dip for the three previous values of N.

function ρ_c gets closer to the Fermi energy. This suggests that at low temperature, the solution of the self-consistent equations in the limit of $N \to 2$ might be better described by a Kondo pseudogap model, where the conduction electron spectral function is depleted close to the Fermi energy.

8.3.2 Low-energy analysis

It is known from other studies on the Kondo pseudogap [129, 130, 131] that the actual behavior of the system at low temperature strongly depends on the power-law decay of the spectral function close to the Fermi energy. In our case, this decay relates to the divergence of the conduction electron self-energy at low temperature, and could be obtained from a low-energy analysis of the set of self-consistent coupled equations (similar to the one carried out for the overscreened single impurity and the quantum critical regime of the two-impurity model) which becomes possible for $N \to 2$ because of the closing gap.

This low-energy analysis is a bit more difficult than the one carried out in the case of the two-impurity system, and now involves all three Green's functions.

Note however that such a low-energy analysis only works well below the Kondo temperature, which itself might vanish in the limit $N \to 2$, as it has been observed in the Kondo pseudogap problem.

We are currently investigating the evolution of the Kondo temperature as a function of N. If this reveals that T_K remains finite as $N \to 2$ (eventually for a given range of the other parameters), such a low-energy analysis would be clearly called on.

207

8.4 What is still missing?

Although the conserving approximation cures some of the drawbacks of the large-N limit, we just argued that it still has some failures. In particular, the low-temperature transport properties are recovered, but not at the level of the conduction electron Green's function. In this section, we briefly explore the possible ways of fixing these remaining issues.

8.4.1 Uncontrolled ways of fixing the method

It seems that the main missing ingredient of both the large-N and the conserving approaches is the absence of vertex corrections. However, a full account of these vertex corrections would not be tractable in any simple way.

A first treatment that might lead to interesting results amounts to neglecting all vertex corrections but the simplest one, for which the external frequencies are taken to be zero (see Fig. 8.5). This would lead to a temperature-dependent renormalization of the Kondo coupling J_K.

Although completely uncontrolled, such an approach could lead to some insight concerning the role of the vertex corrections.

8.4.2 Box representation and matrix models

An idea developed in [132], and earlier in [115], amounts to including on top of the spin index running from 1 to N and the channel index running from 1 to K, a color index running from 1 to Q (where both K and Q scale with N). In terms of Young tableaux, this corresponds to a box representation of the impurity spin, represented in the perfectly screened case by a rectangle of size $K \times Q$ (see Fig. 8.5).

This suggests an analogous treatment to the ones carried out so far. Note however that in this case, the conduction electron no longer plays a special role, since there are $O(N^2)$ flavors of all three fields. As a consequence, all three self-energies are of the same order in N, in particular Σ_c does not vanish in the large-N limit.

Nevertheless, there is a major drawback to this extension. Generalizing the Luttinger-Ward approach derived earlier to this multichannel-multicolor model, one readily sees that the sum of skeleton diagrams does not reduce to a single contribution, even in the large-N limit. There is a profusion of diagrams of order $O(N^2)$, given by the sum of all two-particle irreducible planar diagrams. An attempt to derive the saddle-point equations starting from the action, leads to the introduction of three $K \times K$ matrices: Q, $\bar{Q}$ and λ, analogous to the ones defined in Chapter 6. It follows that in the large-N limit, this model is also very hard to solve from a path-integral perspective.

Unfortunately, there is no simple way of resuming this series of diagrams apart from introducing two-particle irreducible self-energies, in which case the set of

saddle-point equations is hardly tractable in practice.

Cutting the sum to its first two-loop diagram leads precisely to the approach we studied in this chapter, up to a modification of the prefactors to take into account the existence of a new flavor.

a)   b)
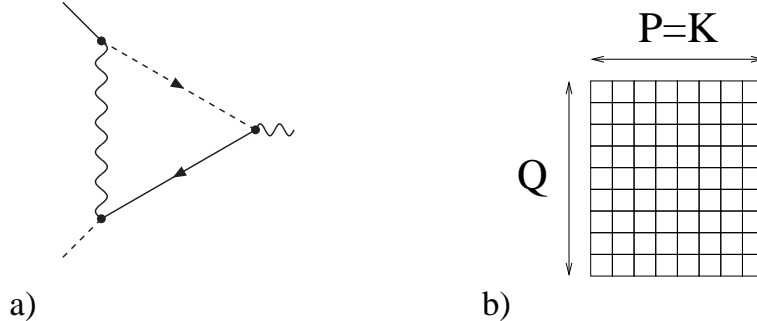
Figure 8.5: a) Simple vertex correction entering the renormalization of the Kondo coupling, b) Young tableaux for the box representation of the impurity spin in the exactly screened case.

8.5 Conclusion

In this chapter, we developed a new conserving approach to the exactly screened infinite U Anderson model. Unlike the large-N limit studied in Chapter 6, this method captures not only the thermodynamic aspects of the local Fermi liquid at low-temperature, but also the transport properties and some important interrelationships typical of the Fermi liquid ground-state.

However, we also proved that although this method cures the main failures of the large-N limit, it does not correctly describe the behavior of the conduction electron self-energy, especially in the limit of $N \to 2$.

One of the possible approaches to solve this issue involves an additional color index, but turns out to be much more difficult to carry out. This raises the question of the description of the Kondo physics with this type of formalism. Maybe the Kondo problem is too complex to be described by a large-N limit and a simple set of saddle-point equations, one can then only access some of the physics of the fully quenched Fermi liquid. This might also be an artifact of the current methods, in which case, a more clever approach, involving a different representation of the impurity spin, or the extension to another symmetry group (e.g. $Sp(N)$), remains to be found.

An interesting development of our conserving approximation lies in the study of non-equilibrium quantum dots. An extension of our approach can be made using a Keldysh generalization [133] of the self-consistency equations[2]. Many features of

---

[2]For a comprehensive review of Keldysh formalism, see e.g. [134]

our method (conserving properties, recovery of the interacting Fermi liquid, incorporation of the spin relaxation effects, . . .) suggest that it will be a robust scheme to examine how spin and conduction electron dephasing effects evolve with voltage in quantum dots.

CHAPTER 9

Kondo lattice models: preliminary results

Contents

In this chapter, we consider a generalization of the Kondo and Kondo-Heisenberg model studied in Chapter 6 and 7 to a lattice. After deriving the large-N equations for these models, we explore some possible treatments leading if not to a full solution, at least to some insight concerning the properties displayed by such a system. Most of this work is very preliminary, and as such, has not been published at the moment.

9.1 Kondo lattice model

The Kondo Hamiltonian studied in Chapter 6 in the case of a single impurity can easily be extended to a large number $\mathcal{N}$ of impurities. In this situation, we consider a regularly spaced lattice of "impurities"[1] in three dimensions, invariant under translation.

9.1.1 Model and saddle-point equations

□ The model

The Hamiltonian of the Kondo lattice is a natural generalization of the single impurity one, which amounts to considering that the Kondo interaction occurs not only at the site of the isolated impurity, but at every site of a regular cubic lattice[2], leading to:

$$
\begin{aligned}
H &= H_{\text{band}} + H_{\text{Kondo}} \quad \text{where} \\
H_{\text{band}} &= \sum_{\mathbf{k}} \sum_{\alpha=1}^{N} \sum_{\mu=1}^{K} \epsilon_{\mathbf{k}} c_{\mathbf{k}\alpha\mu}^{\dagger} c_{\mathbf{k}\alpha\mu} \\
H_{\text{Kondo}} &= \frac{J_K}{N} \sum_{i} \sum_{\alpha,\beta} \sum_{\mu} S_{\alpha\beta}^{i} \psi_{i\beta\mu}^{\dagger} \psi_{i\alpha\mu}
\end{aligned}
\tag{9.1}
$$

where ψ_i is the real-space counterpart of the conduction electron field $c_{\mathbf{k}}$, and we use a bosonic representation of the lattice spins, with the associated constraint:

$$
S_{\alpha\beta}^{i} = b_{i\alpha}^{\dagger} b_{i\beta} - \frac{P}{N} \delta_{\alpha\beta}
\tag{9.2}
$$

$$
\sum_{\alpha} b_{i\alpha}^{\dagger} b_{i\alpha} = P
\tag{9.3}
$$

The electronic dispersion for the cubic lattice is described by a simple constant hopping term between nearest neighbour of the metallic host lattice:

$$
H_{\text{band}} = -t \sum_{\langle i,j \rangle} \sum_{\alpha=1}^{N} \sum_{\mu=1}^{K} c_{i\alpha\mu}^{\dagger} c_{j\alpha\mu} \quad \Longrightarrow \quad \epsilon_{\mathbf{k}} = -2t \left(\cos(k_x a) + \cos(k_y a) + \cos(k_z a) \right)
\tag{9.4}
$$

where a is the impurity lattice spacing.

---

[1]The term "impurities" is a bit misleading here as it suggests some kind of randomness, while we are interested in a regular lattice. We still refer to it though, since this model is a natural extension of the single-impurity one.

[2]The structure of the lattice does not matter much at this stage, we restrict ourselves to the cubic case for simplicity.

Moreover, we focus only on the exactly screened regime, for which the size P of the impurity line representation equals the number K of channels.

We saw that the typical energy scale over which the Kondo singlet develops is not given by the Kondo coupling but rather by the Kondo temperature T_K. We also argued that the Kondo interaction leads, when many impurities are present, to an effective interaction between the localized spins, mediated by the conduction electron: the so-called RKKY interaction [90, 91, 92]. We presented in Chapter 5 Doniach's picture of the Kondo lattice [94], which predicts from comparing the typical energy scale of the Kondo and RKKY interactions that the system can go from a magnetically ordered state (when $T_{RKKY} \gg T_K$) to a Fermi liquid ground-state (when $T_K \gg T_{RKKY}$) upon increasing the Kondo coupling J_K. At zero temperature, this requires the existence of a quantum critical point between the two phases.

□ **Large-N equations**

Proceeding exactly as we did in Chapter 6 (say from a path-integral formalism), it is possible to derive the saddle-point equations for this model in the large-N limit. This requires the introduction of new fields which are now dependent on the position in real space, namely $Q_{ij}(\tau, \tau')$ and $\bar{Q}_{ij}(\tau, \tau')$. These fields are determined from applying the method of steepest descent, and can be related to the bosonic and fermionic self-energies.

In practice, the generalization of the method to a large number of impurities is not more difficult than the original single impurity derivation, and leads to the following set of equations:

$$\text{Dyson's equations:} \quad G_b^{-1}(\mathbf{k}, i\nu_n) = i\nu_n + \lambda - \Sigma_b(\mathbf{k}, i\nu_n) \quad (9.5a)$$

$$G_\chi^{-1}(\mathbf{k}, i\omega_n) = J_K - \Sigma_\chi(\mathbf{k}, i\omega_n) \quad (9.5b)$$

$$\text{Schwinger boson:} \quad \Sigma_b(\mathbf{r}, \tau) = \gamma J_K^2 G_c(\mathbf{r}, \tau) G_\chi(-\mathbf{r}, -\tau) \quad (9.5c)$$

$$\chi-\text{fermion:} \quad \Sigma_\chi(\mathbf{r}, \tau) = -J_K^2 G_c(\mathbf{r}, \tau) G_b(-\mathbf{r}, -\tau) \quad (9.5d)$$

$$\text{Conduction electron:} \quad G_{c0}(\mathbf{k}, i\omega_n) = \sum_{\mathbf{k}} \frac{1}{i\omega_n - \epsilon_{\mathbf{k}}} \quad (9.5e)$$

$$\text{Constraint:} \quad -G_b(\mathbf{r}, \tau = 0^-) = p_0 \delta(\mathbf{r}) \quad (9.5f)$$

Because of the momentum dependence, this set of equations is much more difficult to solve both analytically and numerically: one now has to deal with a convolution over a four-dimensional space. The full-fledge lattice is a hard problem to tackle and one has to think of approximate ways of treating the interesting physics related to this model.

This set of self-consistent equations is only suitable for the description of the Fermi-liquid region of the phase diagram. Indeed, the development of magnetic ordering leads, in this kind of bosonic representation, to a condensation of the

Schwinger bosons and an hybridization of the χ-fermions with the conduction electron fields. In the magnetic state, one has to take into account the bosonic condensation explicitly, and treat the hybridization through the definition of a single fermionic field, whose associated Green's function contains anomalous propagators.

9.1.2 Luttinger sum rule

The Luttinger theorem is among the very few results one can extract from the large-N equations without any further approximation. This can be derived from a Luttinger-Ward perspective in a very similar way to the two-impurity Friedel sum-rule studied in Chapter 7. The full derivation of the Luttinger sum rule for the Kondo lattice model is presented in Publication 3, and we now only highlight the main steps.

The conservation of the total charge leads to a Ward identity, provided that the Schwinger boson is uncondensed, i.e. that we are in the non-magnetic region of the phase diagram. In the paramagnet, this Ward identity allows to write the total electric charge as:

$$Q_e = -\frac{1}{\pi} \sum_{\mathbf{k}} \text{Im} \left[NK \log(-G_c^{-1}(\mathbf{k}, 0 + i\delta)) + K \log(G_\chi^{-1}(\mathbf{k}, 0 + i\delta)) \right] \quad (9.6)$$

which now involves a trace over momentum.

The first term in this expression is the electron Fermi surface volume:

$$-\sum_{\mathbf{k}} \frac{1}{\pi} \text{Im} \log \left[\epsilon_{\mathbf{k}} + \Sigma_c(\mathbf{k}, 0 + i\delta) - \mu - i\delta \right] = \sum_{\mathbf{k}} \Theta(\mu - E_{\mathbf{k}}) = \frac{v_{FS}}{(2\pi)^3}, \quad (9.7)$$

where μ is the chemical potential and the region where $E_{\mathbf{k}} - \mu = \epsilon_{\mathbf{k}} - \mu + \text{Re}\Sigma_c(\mathbf{k}, E_{\mathbf{k}})$ is negative defines the interior of the Fermi surface.

The second term can be interpreted in a similar way - the momentum trace over the logarithm of G_χ^{-1}

$$\sum_{\mathbf{k}} \frac{1}{\pi} \text{Im} \log \left[J_K - \Sigma_\chi(\mathbf{k}, 0 + i\delta) \right] = \sum_{k} \theta[-J_K^*(\mathbf{k})] = \frac{v_\chi}{(2\pi)^3} \quad (9.8)$$

can be seen as the volume of the region in momentum space where the effective interaction $J_K^*(\mathbf{k}) = J_K^2 G_\chi(\mathbf{k}, 0 + i\delta)^{-1}$ is negative, or ferromagnetic.

Following our earlier discussion, the ferromagnetic sign of the residual interaction is a consequence of the fact that additional spins added to the paramagnetic state completely decouple from the Fermi sea. In the simplest scenario, $J_K^*(\mathbf{k}) < 0$ for all $\mathbf{k}$, in which case $\frac{v_\chi}{(2\pi)^3} = 1$, and the sum rule leads to the following result for the Fermi surface volume:

$$N \frac{v_{FS}}{(2\pi)^3} = n_e + 1 \quad (9.9)$$

where n_e is the electron density per unit cell, per conduction electron channel: $n_e = Q_e/K$.

It follows that the total Fermi surface volume expands by one unit per unit cell, due to the Kondo interaction with the lattice of localized spins. To preserve the overall charge density, the electron Fermi surface volume is forced to enlarge to "screen" the finite background density of charged χ-fermions.

In the magnetically ordered state, the boson field condenses, causing the conduction and χ fields to hybridize to produce a single species. In this case, the sum rule becomes:

$$Q_e = -\frac{1}{\pi} \sum_{\mathbf{k}} \operatorname{Im} \log \left[-G_f^{-1}(\mathbf{k}, 0 + i\delta) \right] \tag{9.10}$$

where G_f is the admixed propagator for the combined conduction and χ fields.

The right-hand side cannot be separated into χ and conduction parts, and as such, defines an admixed set of Fermi surfaces, with an average Fermi surface volume which counts the total charge per unit cell:

$$n_e = N \frac{\langle \mathrm{v}_{AFM} \rangle}{(2\pi)^3}. \tag{9.11}$$

If the transition from the paramagnet to the magnetic state occurs via a single quantum critical point, then our results indicate that the transition in the Fermi surface volume at the second order quantum critical point is abrupt: the total Fermi surface volume jumps as one crosses the QCP.

There have been a number of theoretical speculations [135, 136, 137] that in a Kondo or Kondo-Heisenberg lattice model, the conduction electron Fermi surface may jump from "large" to "small" as one tunes through the quantum critical point. Recent experimental work based on Hall measurements [138] provide experimental support for this hypothesis.

9.2 Kondo-Heisenberg lattice model

The other important model we defined in previous chapters is the Kondo-Heisenberg model, where one considers, on top of the Kondo interaction between the localized spins and the bath of conduction electrons, a direct exchange between the impurities, described by an Heisenberg interaction. In this section, we extend the two-impurity model studied in Chapter 7 to the case of a lattice.

9.2.1 Model and saddle-point equations

□ The model

Like the model studied in Chapter 7, we choose to restrict ourselves to the antiferromagnetic Heisenberg coupling, and describe this interaction in terms of the short-range bosonic pair operator.

The Hamiltonian of the Kondo-Heisenberg lattice, with a bosonic representation of the localized spins, is given by:

$$H = H_{\text{band}} + H_{\text{Kondo}} + H_{\text{Heisenberg}} \quad \text{where}$$

$$H_{\text{band}} = \sum_{\mathbf{k}} \sum_{\alpha=1}^{N} \sum_{\mu=1}^{K} \epsilon_{\mathbf{k}} c^{\dagger}_{\mathbf{k}\alpha\mu} c_{\mathbf{k}\alpha\mu}$$

$$H_{\text{Kondo}} = \frac{J_K}{N} \sum_{i} \sum_{\alpha,\beta} \sum_{\mu} b^{\dagger}_{i\alpha} b_{i\beta} \psi^{\dagger}_{i\beta\mu} \psi_{i\alpha\mu}$$

$$H_{\text{Heisenberg}} = \frac{J_H}{N} \sum_{\langle i,j \rangle} \left(\sum_{m\sigma} \sigma b^{\dagger}_{i,m,\sigma} b^{\dagger}_{j,m,-\sigma} \right) \left(\sum_{m'\sigma'} \sigma' b_{i,m',\sigma'} b_{j,m',-\sigma'} \right) \tag{9.12}$$

where $\langle i.j \rangle$ denotes nearest neighbors, and we recast the N spin indices under the form $\left(m = 1 \ldots \frac{N}{2}, \sigma = \pm \right)$.

Like the Kondo lattice model presented in the previous section, this model is expected to display (at least) two ground-states in the exactly screened regime: a magnetic state governed by the Heisenberg interaction and for which the Schwinger bosons condense, and a Fermi liquid state where the Kondo interaction dominates and leads to nearly independent fully quenched impurities.

□ Large-N equations

After decoupling both the Kondo and the Heisenberg interaction terms, introducing in the process two sets of fields ($\chi_{i,\mu}$ and $\Delta_{i,j}$) and integrating the conduction electrons out of the partition function, we end up with an effective action that looks like Eq. (7.3) obtained for the two-impurity system, namely:

$$
\begin{aligned}
S = & \int_0^\beta d\tau \sum_{i,m,\sigma} b^{\dagger}_{i,m,\sigma}(\tau) \left(\partial_\tau - \lambda_i(\tau) \right) b_{i,m,\sigma}(\tau) - \frac{1}{J_K} \int_0^\beta d\tau \sum_{i,\mu} \chi^{\dagger}_{i,\mu}(\tau) \chi_{i,\mu}(\tau) \\
& - \frac{1}{N} \sum_{i,j} \int_0^\beta d\tau d\tau' \sum_{\mu} \chi_{j,\mu}(\tau') \chi^{\dagger}_{i,\mu}(\tau) \, G_{c0}(i-j;\tau-\tau') \sum_{m,\sigma} b_{j,m,\sigma}(\tau') b^{\dagger}_{i,m,\sigma}(\tau) \\
& + \sum_{\langle i,j \rangle} \int_0^\beta d\tau \left(\Delta^{\dagger}_{i,j}(\tau) \sum_{m,\sigma} \sigma b_{i,m,\sigma}(\tau) b_{j,m,-\sigma}(\tau) + \text{h.c.} \right) \\
& + \frac{N}{J_H} \sum_{\langle i,j \rangle} \int_0^\beta d\tau \, \Delta^{\dagger}_{i,j}(\tau) \Delta_{i,j}(\tau) + p_0 N \sum_{i} \int_0^\beta d\tau \, \lambda_i(\tau) \tag{9.13}
\end{aligned}
$$

Since $\Delta_{i,j}$ represents a pair of bosons with opposite "spins" (σ is different for the two bosons involved in the pair), it is symmetric under the exchange $\sigma \to -\sigma$, so that it has to be antisymmetric in space: $\Delta_{i,j} = -\Delta_{j,i}$. We now assume a

static local solution for the chemical potential $\lambda_i = \lambda$ and the bosonic pair field $\Delta_{i,j} = \mathrm{Sgn}(i-j)\Delta$.

We proceed exactly as we did for the two-impurity model studied in Chapter 7: after introducing two new fields $Q(i,j,\tau,\tau')$ and $\bar{Q}(i,j,\tau,\tau')$, we can build an effective action $S(Q, \bar{Q}, \lambda, \Delta)$ where every term scales like N. Relating the bosonic and fermionic self-energies to the fields Q and $\bar{Q}$, the saddle-point equations read:

$$\Sigma_b(\mathbf{r}, \tau) = \begin{bmatrix} \gamma J_K^2 G_\chi(-\mathbf{r}, -\tau)G_{c0}(\mathbf{r}, \tau) & 0 \\ 0 & \gamma J_K^2 G_\chi(\mathbf{r}, \tau)G_{c0}(-\mathbf{r}, -\tau) \end{bmatrix} \quad (9.14a)$$

$$\Sigma_\chi(\mathbf{r}, \tau) = -\frac{J_K^2}{2}G_{c0}(\mathbf{r}, \tau)\left(G_b^{(++)}(-\mathbf{r}, -\tau) + G_b^{(--)}(\mathbf{r}, \tau)\right) \quad (9.14b)$$

$$p_0 = -\frac{1}{2}\sum_{\mathbf{k}}\left[G_b^{(++)}(\mathbf{k}, \tau = 0^-) + G_b^{(--)}(\mathbf{k}, \tau = 0^+)\right] \quad (9.14c)$$

$$\frac{|\Delta|^2}{J_H} = \frac{1}{12}\sum_{\mathbf{k}}G_b^{-+}(\mathbf{k}, \tau = 0^-)\Delta_{\mathbf{k}} \quad (9.14d)$$

where the matrix form is expressed in the space of $\sigma = \pm$ (the χ-fermion propagator being diagonal in this basis), and we considered a cubic structure of spacing a for the lattice of localized spins.

The Dyson's equations have the following expression:

$$G_b^{-1}(\mathbf{k}, i\nu_n) = \begin{bmatrix} i\nu_n + \lambda & -\Delta_{\mathbf{k}} \\ -\Delta_{\mathbf{k}}^* & -i\nu_n + \lambda \end{bmatrix} - \Sigma_b(\mathbf{k}, i\nu_n) \quad (9.15a)$$

$$G_\chi^{-1}(\mathbf{k}, i\omega_n) = J_K - \Sigma_\chi(\mathbf{k}, i\omega_n) \quad (9.15b)$$

where $\Delta_{\mathbf{k}} = -4i\Delta\left[\sin(k_x a) + \sin(k_y a) + \sin(k_z a)\right]$

9.2.2 Uncontrolled local approximation

As the main additional difficulty of this new set of equations lies in the momentum dependence of the propagators, a first simple approximation one can make amounts to neglecting this very momentum dependence in the self-energies. Such an approximation is based on the assumption that the relevant physics leading to the self-energies is local, i.e. that there is very little interplay between the Kondo and Heisenberg mechanisms. This is an *uncontrolled* approximation as no small parameter allows us to neglect the non-local terms. However it might be sufficient to capture the competition between the Kondo screening and the development of magnetism.

Within this local approximation, our set of equations (9.14) and (9.15) dramat-

ically simplifies:

$$\Sigma_b(\tau) = -\gamma J_K^2 G_{c0}(\tau) G_\chi(\beta - \tau) \tag{9.16a}$$

$$\Sigma_\chi(\tau) = -J_K^2 G_{c0}(\tau) G_b(\beta - \tau) \tag{9.16b}$$

$$G_b(i\nu_n) = \sum_{\mathbf{k}} \frac{1}{i\nu_n + \lambda - \Sigma_b(i\nu_n) - \frac{|\Delta_{\mathbf{k}}|^2}{-i\nu_n + \lambda - \Sigma_b(-i\nu_n)}} \tag{9.16c}$$

$$G_\chi(i\omega_n) = \frac{1}{J_K - \Sigma_\chi(i\omega_n)} \tag{9.16d}$$

$$p_0 = -G_b(\tau = 0^-) \tag{9.16e}$$

$$\frac{|\Delta|^2}{J_H} = \frac{1}{12} \sum_{\mathbf{k}} T \sum_n e^{i\nu_n 0^+}$$

$$\times \frac{|\Delta_{\mathbf{k}}|^2}{(i\nu_n + \lambda - \Sigma_b(i\nu_n))(-i\nu_n + \lambda - \Sigma_b(-i\nu_n)) - |\Delta_{\mathbf{k}}|^2} \tag{9.16f}$$

The sum over momentum is evaluated by introducing $\eta_{\mathbf{k}}$ such as $\Delta_{\mathbf{k}} = 4i\Delta\eta_{\mathbf{k}}$. We then define a "density function" for $\eta_{\mathbf{k}}$:

$$\rho(\eta) = \sum_{\mathbf{k}} \delta(\eta - \eta_{\mathbf{k}})$$

$$= \frac{1}{2\pi} \int_{-\infty}^{+\infty} dx \; e^{i\eta x} \left[J_0(x) \right]^3 \tag{9.17}$$

which allows to replace summations over momentum by integrals over η with the function $\rho(\eta)$, which turns out to be the Fourier transform of the Bessel function of the first kind, elevated to the power 3.
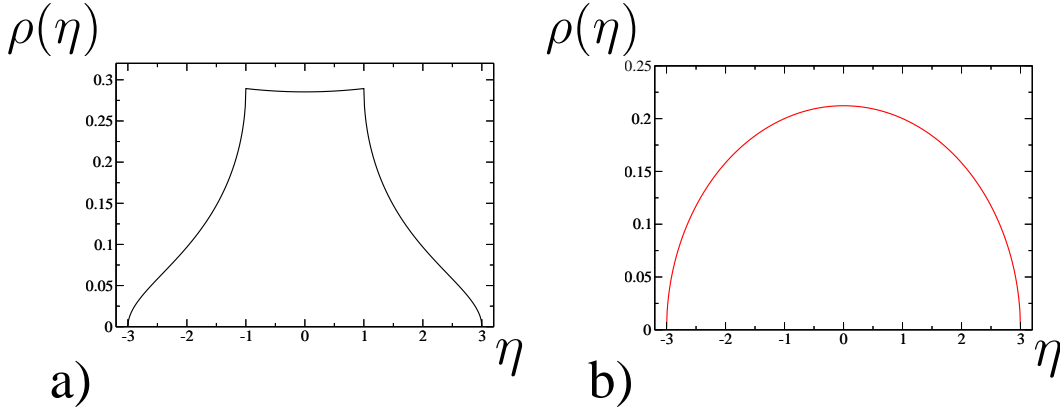

Figure 9.1: a) Plot of the function $\rho(\eta)$ obtained by numerical integration, b) Approximate form of the same function, used to compute analytically the summation over momentum. The edges are the same in both cases and go like $\sqrt{\epsilon}$ for $\eta = \pm(3 - \epsilon)$.

We solved numerically the set of equations (9.16) as a function of temperature, for various values of the Heisenberg coupling. To do so, we replaced the function $\rho(\eta)$ by a slightly modified one (see Fig. 9.1) which allows to perform analytically the momentum summations.

We could map out the phase diagram presented in Fig. 9.2. Along with the line separating the $\Delta = 0$ region, from the region where pairs start condensing, we could also isolate a region of the phase diagram where a magnetic order develops. This transition line is determined by obtaining a solution of the set of self-consistent equations for increasingly larger values of Δ. At fixed temperature, we obtain a critical Δ_c above which the solution for the bosonic spectral function seems to develop some finite weight at zero energy, violating the causality rules. As these rules are built into the equations, this violation signals that the set of equations is no longer valid, which suggests that the Schwinger bosons undergo a condensation.

At low enough fixed temperature, we find a paramagnetic solution in a small region of the phase diagram below the transition line. This result suggests that there exists a region where both a magnetic and a non-magnetic state are present. As a consequence, we expect the transition towards the magnetic state to be of the first order at low temperature.
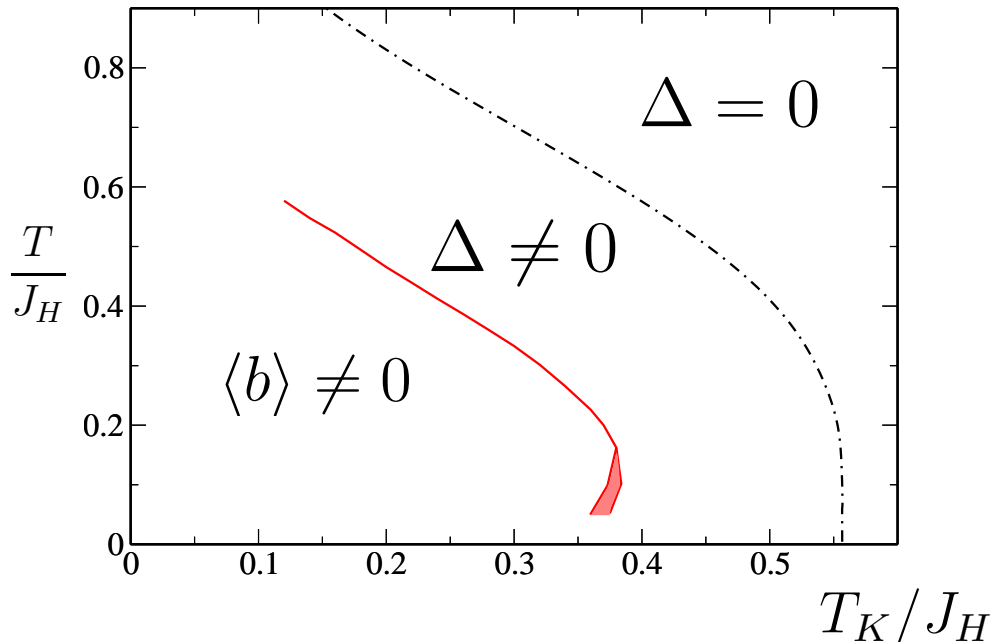
Figure 9.2: Phase diagram of the 3-dimensional lattice with the local approximation. The dashed line separating the region where pair correlations develop is unchanged compared to the two-impurity model studied earlier. The red line corresponds to a transition towards the magnetic region where Schwinger bosons condense. The splitting of this line at low temperature signals the presence of a first order transition into the magnetic state.

9.3 Conclusion

Very few results can be derived concerning these models without making new assumptions. The challenge at this stage is to find clever approximations that would capture the important physics of the problem, while partially allowing a numerical or an analytical treatment of the Kondo lattice model.

9.3.1 Looking for a gap

We saw in our study of the one and two impurity systems that the gap, and more importantly the closing of the gap, plays a significant role in the physics of the system. In the case of the Kondo lattice, we expect the gap to display a momentum dependence. The study of the gap in momentum space could be very insightful as for the relevant physics close to the quantum critical point. However, the study of the gap involves solving the full set of saddle-point equations.

A first step towards this route is to analyze the necessary conditions for a gap to be stabilized by the large-N equations. This might already be sufficient to reduce the relevant region of momentum space.

9.3.2 Kondo hedgehog

Another possible way of getting around the many difficulties related to the lattice is to consider a slightly different model. It can be argued that the competition between the Kondo effect and the magnetic ordering can be successfully mimicked by considering a cruder version of the Kondo lattice model, where we treat the electrons only to the extent that they provide spins which tend to be aligned antiparallel to the localized moments.

This was the reasoning behind Doniach's Kondo necklace model [94]. The large-N treatment developed here could be extended to a two or three dimensional version of Doniach's idea: a Kondo hedgehog model.

9.3.3 Dynamical mean-field theory

As a final example of the possible extensions of our approach to encompass the physics of the lattice, we mention the Dynamical Mean-Field Theory[3] (DMFT).

The use of our approach as an impurity solver or as a two-impurity solver might lead to interesting results when plugged back into a DMFT scheme. Such a treatment of the Kondo lattice model could provide enough of the non-local character of the system and lead to a better understanding of the important elements of the quantum critical regime.

---

[3]A detailed introduction to this technique goes way beyond the scope of this section. For a detailed review on DFMT, the reader is referred to [139]

PUBLICATION 3

Sum rules and Ward identities in the Kondo lattice

Sum rules and Ward identities in the Kondo lattice

P. Coleman,[1,2] I. Paul,[1,3] and J. Rech[1,2,3]

[1]*Kavli Institute for Theoretical Physics, Kohn Hall, UCSB Santa Barbara, Santa Barbara, California 93106, USA*
[2]*Center for Materials Theory, Rutgers University, Piscataway, New Jersey 08855, USA*
[3]*SPhT, L'Orme des Merisiers, CEA-Saclay, 91191 Gif-sur-Yvette France*

We derive a generalized Luttinger-Ward expression for the free energy of a many-body system involving a constrained Hilbert space. In the large-N limit, we are able to explicitly write the entropy as a functional of the Green's functions. Using this method we obtain a Luttinger sum rule for the Kondo lattice. One of the fascinating aspects of the sum rule is that it contains two components: one describing the heavy electron Fermi surface, the other, a sea of oppositely charged, spinless fermions. In the heavy electron state, this sea of spinless fermions is completely filled and the electron Fermi surface expands by one electron per unit cell to compensate the positively charged background, forming a "large" Fermi surface. Arbitrarily weak magnetism causes the spinless Fermi sea to annihilate with part of the Fermi sea of the conduction electrons, leading to a small Fermi surface. Our results thus enable us to show that the Fermi surface volume contracts from a large to a small volume at a quantum critical point. However, the sum rules also permit the possible formation of a new phase, sandwiched between the antiferromagnet and the heavy electron phase, where the charged spinless fermions develop a true Fermi surface.

I. INTRODUCTION

Sum rules play a vital role in condensed matter physics. The most famous sum rule—the Luttinger sum rule,[1–3] defines rigorously the volume of the Fermi surface of a Fermi liquid in terms of the density of electrons:

$$2\frac{v_{FS}}{(2\pi)^D} = n_e, \qquad (1)$$

where v_{FS} is the Fermi surface volume, n_e is the density of electrons per unit cell, and D is the dimension. Historically, sum rules have also played an important role in our understanding of strongly correlated systems. In the context of the Kondo effect for example, the Friedel sum rule,[4–6]

$$\sum_{\lambda} \frac{\delta_{\lambda}}{\pi} = \Delta n_e, \qquad (2)$$

relating the sum of the scattering phase shifts in channels labeled by λ to the number of bound states Δn_e helped to establish a rigorous foundation for the Abrikosov-Suhl resonance[7–9] that develops in Anderson and Kondo impurity models. Later, Martin[10] applied the Luttinger sum rule to the Anderson lattice model, to argue that heavy electron metals must have a "large Fermi surface" that counts both the conduction electrons and also the localized f electrons,

$$2\frac{v_{FS}}{(2\pi)^D} = n_e + 1. \qquad (3)$$

Today, there is a renewed interest in sum rules, in connection with models of strongly correlated electrons. For instance, in the context of high-temperature superconductors, which are Mott insulators when undoped, there has been a longstanding debate over whether the "large" Fermi surface predicted by Luttinger's sum rule might be replaced at low doping, by a "small" Fermi surface determined by the number of doped holes.[11,12] Related issues arise in the context of heavy electron systems, where experimental advances have made it possible to tune through the quantum critical point that separates the heavy electron paramagnet from the local moment antiferromagnet. There have been a number of theoretical speculations that the Fermi surface of the heavy electron material may jump from "large" to "small" at the quantum critical point.[13–15] Recent experimental work, based on de Haas–van Alphen measurements[16] and Hall measurements,[17] provide experimental support for this hypothesis, but the idea has lacked rigorous theoretical support.

The main difficulty in extending sum rules to strongly correlated systems is that the theoretical machinery used and developed by Luttinger and Ward to derive sum rules applies to models with unprojected Hilbert spaces. About eight years ago, Affleck and Oshikawa[18] demonstrated that such sum rules have a more general existence. By using a modification of the Leib–Mattis theorem, Affleck and Oshikawa showed that the "large Fermi surface" that counts both local moments and conduction electrons develops in the one-dimensional $S=1/2$ Kondo model, even though in this case the ground state is not a Fermi liquid. More recently, Oshikawa[19] has extended this derivation to higher-dimensional Kondo lattices. This work suggests that it ought to be possible to extend the Luttinger–Ward approach to Hamiltonian problems with strong constraints.

In this paper, we show how the original methods of Luttinger and Ward can indeed be extended to strongly correlated models. A key element of this work is the construction of a functional relating the free energy of a strongly interacting system to the Green's functions of the projected Hilbert space. Our approach is based on the use of slave particles, such as a Schwinger boson description for the local moments in a Kondo lattice. We begin with a generalization of the Luttinger–Ward free energy functional, appropriate for systems of interacting bosons and fermions,[20,21] which can be compactly written as

Sum rules and Ward identities in the Kondo lattice

$$F = T \underline{\mathrm{Str}}[\ln(-\mathcal{G}^{-1}) + \Sigma\mathcal{G}] + Y[\mathcal{G}], \qquad (4)$$

where $\underline{\mathrm{Str}}[A] = \underline{\mathrm{Tr}}[A_B] - \underline{\mathrm{Tr}}[A_F]$ denotes the supertrace of a matrix containing both bosonic (B) and fermionic (F) components (where the underline notation is used to denote a sum over internal frequencies and a trace over the internal quantum numbers of the matrix). $\mathcal{G} = (\mathcal{G}_0^{-1} - \Sigma)^{-1}$ is the matrix describing the fully dressed Green's function of all elementary particles and fields entering the Lagrangian, including the slave particles, where Σ is the self-energy matrix and $\mathcal{G}_0$ the bare propagator of the fields. The quantity $Y[\mathcal{G}]$ is, diagramatically, the sum of all closed-loop two-particle irreducible skeleton Feynman diagrams. Figure 1 illustrates the sum of diagrams contributing to $Y[\mathcal{G}]$ for a Kondo lattice model. Variations of $Y[\mathcal{G}]$ with respect to the Green's function $\mathcal{G}$ generate the self-energy

$$\delta Y[\mathcal{G}] = -T \underline{\mathrm{Str}}[\Sigma \,\delta \mathcal{G}] \qquad (5)$$

or

$$\Sigma(\omega) = -\beta \frac{\delta Y}{\delta \mathcal{G}(\omega)}, \qquad (6)$$

where the use of the supertrace as the measure for functional derivatives avoids the need to introduce a relative minus sign between Fermi and Bose parts of this expression. Diagrammatically, the functional derivative of Y with respect to $\mathcal{G}$ corresponds to "cutting" one of its internal lines. If we truncate Y to some order in $1/N$, this relationship determines a conserving Kadanoff-Baym approximation.[23] For example, if we take the generating function for a Kondo lattice illustrated in Fig. 1(c), and differentiate the leading order contri-
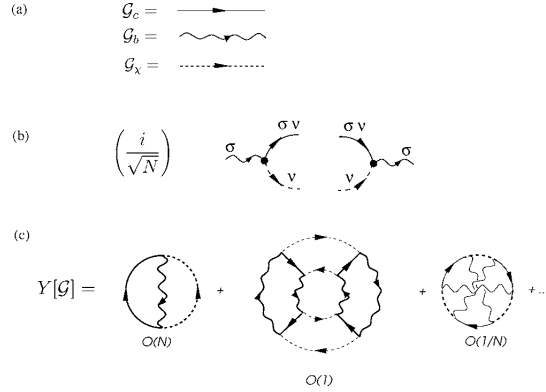
FIG. 1. Illustrating the Luttinger–Ward functional for the Kondo lattice. (a) Fully renormalized propagators for the conduction electrons, χ fermions, and Schwinger bosons, where $\sigma \in [1, N]$ is the spin index and $\nu \in [1, K]$ the channel index, (b) Interaction vertices showing spin (σ) and channel (ν) indices, (c) leading skeleton diagrams for the Luttinger–Ward functional with dependence on $1/N$. The first diagram involves two loops carrying spin and channel quantum numbers, and one pair of vertices and is consequently of order $O(KN/N) = O(N)$. The second diagram has four loops carrying internal quantum numbers and four pairs of vertices, so it is of order $O(N^2 K^2 / N^4) = O(1)$. The final diagram has two quantum number loops and three pairs of vertices, and is hence of order $O(NK/N^3) \sim O(1/N)$.

bution in the large N expansion with respect to $\mathcal{G}$, we obtain the following self-energies:

$$(7)$$

where the cross indicates the line that is eliminated by the functional differential. Each of these terms contains a factor $O(1/N)$ from the vertices, but the first two self-energies contain summations over the internal channel or spin indices,

elevating Σ_b and Σ_χ to terms of order $O(1)$. In the leading-order large N approximation, $\Sigma_c \sim O(1/N)$, so that a consistent large-N approximation is produced by leaving the conduction electron lines undressed. This provides an alternative

224

diagrammatic derivation of the Parcollet–Georges approach to the multichannel Kondo model.[24]

Each conserved quantity Q that commutes with the Hamiltonian leads to a gauge invariance of the underlying quantum fields, such that the action and all physical properties are invariant under the transformation

$$\psi_\zeta(t) \rightarrow e^{i\theta(t)q_\zeta}\psi_\zeta. \tag{8}$$

Here, q_ζ is the gauge charge of the field: it is this quantity that controls the charge of any physical excitations associated with the field. Provided this gauge invariance is unbroken, we show that this leads to a Ward identity at zero temperature,

$$\int_{-i\infty}^{i\infty} \frac{d\omega}{2\pi i} \mathrm{Str}\left[\hat{q}\mathcal{G}\frac{d\Sigma(\omega)}{d\omega}\right] = 0, \tag{9}$$

where the integral runs along the imaginary axis. Luttinger's original work derived the elementary version of this relationship for electrons: here it is seen to hold for interacting species of fields.

Each of these Ward identities leads to a corresponding, generalized Luttinger sum rule given by

$$Q = \frac{1}{\pi}\,\mathrm{Im}\,\mathrm{Tr}\{\hat{q}\ln[-\mathcal{G}_F^{-1}(0 - i\delta)]\}, \tag{10}$$

where $\mathcal{G}_F$ is the complete fermionic Green's function, involving all fermions involved in the description of the constrained Hilbert space, including those introduced as slave particles. In impurity systems, the trace over the logarithms reduces to a sum of phase shifts, and the quantity Q is replaced by ΔQ, the change in Q induced by the impurity. In the limit of infinite bandwidth, $\Delta Q = 0$, which leads to a multiparticle version of the Friedel sum rule,

$$0 = \sum q_\zeta n_\zeta\left(\frac{\delta_\zeta}{\pi}\right), \tag{11}$$

where n_ζ is the spin degeneracy associated with the trace over internal quantum numbers of the field ψ_ζ. In lattice systems, the trace over the log becomes the Fermi surface volume associated with the field ψ_ζ, so that

$$Q = \sum_\zeta\left[q_\zeta n_\zeta \frac{v_{FS}(\zeta)}{(2\pi)^D}\right], \tag{12}$$

where $v_{FS}(\zeta)$ is the Fermi surface volume associated with field ψ_ζ. A closely related Fermi surface sum rule has recently been derived by Powell *et al.* for mixtures of fermions and bosons in atom traps.[25]

In this paper we apply these results to the Kondo lattice model. The key to our approach is the adoption of Schwinger bosons for the description of quantum spins. Schwinger bosons offer a key advantage, because they can describe both the antiferromagnetic and the heavy electron ground states of the Kondo lattice.[26] The Kondo effect induces a development of a retarded interaction in the spin singlet channel between the electrons and the spins. Formally, this interaction manifests itself as the mediating field χ_j in the Hubbard-Stratonovich decomposition of the interaction[24,27,28]

$$J_K\vec{S}_j \cdot c_{j\alpha}^\dagger\vec{\sigma}_{\alpha\beta}c_{j\beta} \rightarrow \frac{1}{\sqrt{N}}(c_{j\alpha}^\dagger b_{j\alpha})\chi_j^\dagger + \frac{1}{\sqrt{N}}(b_{j\alpha}^\dagger c_{j\alpha})\chi_j + \frac{\chi_j^\dagger\chi_j}{J_K}. \tag{13}$$

Here $\vec{S}_j$ is the spin at site j and $c_{j\alpha}^\dagger$ creates an electron at site j. At long times the χ field develops charge dynamics that describe the scaling of the Kondo interaction in both frequency and momentum space. In particular, the $\chi-$ propagator describes the momentum- and frequency-dependent Kondo interaction,

$$-\mathcal{G}_\chi(\mathbf{k},\omega) = \left(\frac{1}{J_K} + \Sigma_\chi(\mathbf{k},\omega)\right)^{-1} = J_K^*(\mathbf{k},\omega). \tag{14}$$

At each point in momentum space, where the Kondo interaction scales to strong coupling, $\mathcal{G}_\chi$ develops a pole. In this way, the physics of the Kondo effect is intimately linked[15] to the possible emergence of a positively charged, spinless Fermi field—a "holon."[29]

Under gauge transformations, the conduction and χ fields have opposite gauge charge,

$$q_c = 1, \quad q_\chi = -1. \tag{15}$$

When we apply the Luttinger–Ward procedure, we find that the physical charge density is given by the total volume of the electron Fermi surface, minus the volume of the holon Fermi surface, as follows:

$$n_e = 2\frac{v_{FS}}{(2\pi)^D} - \frac{v_\chi}{(2\pi)^D}. \tag{16}$$

Here, the volume of the electron Fermi surface is given by the conventional Luttinger formula,

$$v_{FS} = \frac{1}{\pi}\sum_{\mathbf{k}}\,\mathrm{Im}\,\ln[\epsilon_{\mathbf{k}} + \Sigma_c(\mathbf{k},0 - i\delta) - \mu + i\delta]$$
$$= \sum_{\mathbf{k}}\Theta(\mu - E_{\mathbf{k}}), \tag{17}$$

where μ is the chemical potential, $E_{\mathbf{k}} = \epsilon_{\mathbf{k}} + \Sigma_c(\mathbf{k},E_{\mathbf{k}})$ is the renormalized energy of the heavy electrons. Now v_χ is

$$v_\chi = \frac{1}{\pi}\sum_{\mathbf{k}}\,\mathrm{Im}\,\ln\left(\frac{1}{J_K} + \Sigma_\chi(\mathbf{k},0 - i\delta)\right) = \sum_{\mathbf{k}}\Theta[-J_K^*(\mathbf{k})], \tag{18}$$

where $J_K^*(\mathbf{k}) = -\mathcal{G}_\chi(\mathbf{k},0 - i\delta)$.

The meaning of the renormalized coupling constant J_K^* in the paramagnetic phase needs a little discussion. This quantity describes the residual interaction between the electron fluid and any additional spins that are added to the Fermi liquid ground state. If we add an additional Schwinger boson, increasing $S \rightarrow S + \frac{1}{2}$ at a given site, the additional spin unit remains unscreened, because each channel can only screen one spin unit, and all channels are fully screening. If $\omega_b = E(n_b + 1) - E(n_b)$ is the energy to adding one additional spin, then the residual interaction between the additional Schwinger boson and the conduction electrons is $J_K^*(\omega_b)$. Since the additional spin decouples, it follows that $J_K^*(\omega)$ has
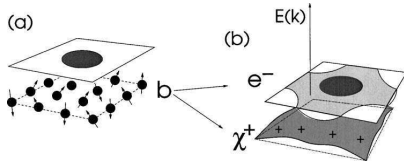
FIG. 2. Schematic diagram illustrating the enlargement of the Fermi surface in the Kondo lattice (a) coupling of local moments to a small Fermi surface; (b) each spin-boson "ionizes" into an electron and a "holon," producing a large electron Fermi surface and a filled holon Fermi sea.

a zero at $\omega = \omega_b$, $J_K^*(\omega_b) = 0$. At higher energies, the residual interaction will become positive, ultimately connecting up to the single-ion scaling behavior $J_K^*(\omega) \sim 1/\ln(T_K/\omega)$. Since J_K^* passes through zero at $\omega = \omega_b$, it follows that at lower energies $\omega < \omega_b$, and in particular, at zero frequency, the residual coupling must be ferromagnetic, i.e $J_K^*(0) < 0$. This, in turn, means that the Fermi sea of holons is entirely full, $v_\chi = (2\pi)^D$, so that

$$n_e = 2\frac{v_{FS}}{(2\pi)^D} - 1. \qquad (19)$$

To preserve the overall charge density, the electron Fermi surface volume is forced to enlarge by one unit per spin to "screen" the finite background density of positively charged holons (Fig. 2).

Let us now consider the antiferromagnet. In this case, the Schwinger boson field condenses, and the χ field becomes hybridized with the conduction electrons. In this case, the holon Fermi surface annihilates with the expanded part of the heavy electron Fermi surface, to reveal a single integrated set of Fermi surface sheets with a "small" volume that encloses the total electron count. If the transition from paramagnet to antiferromagnet occurs via a single quantum critical point, then our results indicate that the transition in the Fermi surface volume at the second-order quantum critical point is abrupt.[30]

Perhaps the most interesting aspect of this picture is that it suggests that the background field of holons can develop dynamics. One intriguing possibility is that the holons are liberated when the Fermi surface volume contracts at the quantum critical point. Another more exotic possibility, allowed by the Ward identities, is the formation of a separate *phase* where the holons develop a Fermi surface, so that $v_\chi = x(2\pi)^D$ is partially filled. This "spin-charge" decoupled phase would be sandwiched between the localized magnetic phase and the fully formed paramagnet. Pépin has recently suggested that the holons might develop a Fermi surface at the quantum critical point.[15] This might provide a mechanism for such a scenario. A good candidate for this phase is the one-dimensional Haldane $S=1$ chain, coupled to two conducting chains to form a one-dimensional, two-channel Kondo lattice. Here, the conjectured intermediate phase would separate a Haldane gap phase and a large Fermi surface phase, leading to Friedel oscillations with wave vector

$q = 2k_F^{(0)} + (\pi/2)x$, intermediate between that of the large ($x = 1$) and small ($x = 0$) Fermi surface.

This paper is divided up into various parts. In the first we develop the Luttinger–Ward free energy expansion for the Kondo lattice. Next, we present a new formula for the entropy of the interacting fluid, expressed exclusively in terms of the Green's functions of the particles. We then go on to derive the Luttinger sum rule in a general form for a constrained system, which we then apply to the Kondo impurity and lattice model. In the final part, we discuss the general implications of our sum rule in the Kondo lattice.

II. LUTTINGER WARD EXPRESSION FOR THE KONDO LATTICE

The Luttinger–Ward approach was originally based on perturbation theory in the strength of the Coulomb interaction. In order to develop these methods for strongly interacting systems, we need to take account of the constraints in the theory, requiring a Luttinger–Ward approach appropriate to gauge theories. In this respect, our efforts to apply the Luttinger Ward approach to the Kondo lattice closely parallel recent efforts to extend the Luttinger-Ward approach to quark-gluon plasmas.[21]

Although the Luttinger-Ward functional may be derived nonperturbatively,[31] the usefulness of any derived sum rules rests on the direct relationship between the Green's functions that enter in the functional and physical excitations. Strongly interacting systems do not generally provide a natural small parameter on which to base a perturbation expansion. Our philosophy is that to develop this control, we need to define a family of large-N models that, in the infinite-N limit, provide a mean-field description of the phases of interest. In the expansion about this limit, $1/N$ then provides a small parameter. The large-N solutions constructed this way will of course satisfy the sum rules we derive, but the sum rules are expected to have a far greater generality.

In the context of our interest in the Kondo lattice, we adopt a family of models given by

$$\mathcal{H} = \sum_{\vec{k},\nu,\alpha} \epsilon_{\vec{k}} c^\dagger_{\vec{k}\nu\alpha} c_{\vec{k}\nu\alpha} + \overbrace{\frac{J_K}{N} \sum_{j\nu\alpha\beta} c^\dagger_{j\nu\alpha} c_{j\nu\beta} b^\dagger_{j\beta} b_{j\alpha}}^{H_I} \qquad (20)$$

Here, we have adopted the Schwinger boson representation, where $b^\dagger_{j\alpha}$ creates a Schwinger boson at site j, with spin component $\alpha \in [1, N]$. The combination $b^\dagger_{j\alpha} b_{j\beta} = S_{\alpha\beta}(j)$ represents the local spin operator and the system is restricted to the physical Hilbert space by requiring that

$$\sum_\alpha b^\dagger_{j\alpha} b_{j\alpha} = 2S, \qquad (21)$$

at each site j. The index $\nu \in [1, K]$ is a channel index that is absent in the physical $SU(2)$ model, but that is included to create a family of large-N models. The "filled shell" case $2S = K$ defines a perfectly screened Kondo lattice, and our discussion will focus on this case. Here $c^\dagger_{\vec{k}\alpha}$ creates a conduction electron of momentum state $\vec{k}$ and spin $\alpha \in (1, N)$. $c^\dagger_{j\alpha}$

$=(1/\sqrt{\mathcal{N}_s})\Sigma c_{\mathbf{k}\alpha}^{\dagger}e^{-i\vec{k}\cdot\vec{x}_j}$ creates an electron at site j, where $\mathcal{N}_s$ is the number of sites in the lattice. The above model is known to have a controlled large-N expansion that contains both magnetic and paramagnetic solutions when N is taken to infinity with $k=K/N$ fixed.

To develop a Luttinger–Ward expansion, we shall factorize the interaction in terms of a Grassman field $\chi_{j\nu}$,

$$H_I \to \sum_{j\nu\alpha}\frac{1}{\sqrt{N}}[(c_{j\nu\alpha}^{\dagger}b_{j\alpha})\chi_{j\nu}^{\dagger}+(b_{j\alpha}^{\dagger}c_{j\nu\alpha})\chi_{j\nu}]+\sum_{j\nu}\frac{\chi_{j\nu}^{\dagger}\chi_{j\nu}}{J_K}, \quad (22)$$

and the Lagrangian becomes

$$\mathcal{L}=\sum_{\vec{k}\alpha\nu}c_{\vec{k}\nu\alpha}^{\dagger}(\partial_{\tau}+\epsilon_{\vec{k}})c_{\vec{k}\nu\alpha}+\sum_{j\alpha}b_{j\alpha}^{\dagger}(\partial_{\tau}+\lambda_j)b_{j\alpha}+\sum_{j\nu}\frac{\chi_{j\nu}^{\dagger}\chi_{j\nu}}{J_K}$$
$$+\sum_{j\nu\alpha}\frac{1}{\sqrt{N}}[(c_{j\nu\alpha}^{\dagger}b_{j\alpha})\chi_{j\nu}^{\dagger}+(b_{j\alpha}^{\dagger}c_{j\nu\alpha})\chi_{j\nu}]-\sum_j 2S\lambda_j. \quad (23)$$

Note that the Grassman fields $\chi_{j\nu}$ contain no time derivative, and so instantaneously they behave as inert, neutral fields. Here λ_j is the static value of the Lagrange multiplier used to enforce the constraint on each lattice site. At finite temperatures the constraint is only enforced on the average, but in the ground state, the value of the conserved quantities n_{bj} will be quantized as a step function of the λ_j. In the range $\lambda_j\in[\lambda_j^-,\lambda_j^+]$ (where $\lambda_j^{\pm}$ are the energy gaps between the physical ground state and the states with $2S\pm1$ Schwinger bosons at site j), the constraint will be precisely satisfied. We shall assume that a translationally invariant choice $\lambda_j=\lambda$ is always available.

For our sum rules, we need to know comparatively little about the nature of the ground state excitations. However, from the the large-N solution of this model, we do know that there are two main classes of solution to the Kondo lattice:

(i) The heavy electron phase, where the Schwinger bosons pair condense in either the Cooper channel ($\langle\sigma b_{i\sigma}^{\dagger}b_{j-\sigma}^{\dagger}\rangle\neq0$ antiferromagnetic interactions) or particle-hole channel ($\langle\sigma b_{i\sigma}^{\dagger}b_{j\sigma}\rangle\neq0$ ferromagnetic interactions). In field-theory language, this is a "Higg's phase" in which the local $U(1)$ symmetry is broken and both the spin and holon excitations can propagate from site to site.

(ii) The magnetic phase, in which the Schwinger bosons individually condense ($\langle b_j\rangle\neq0$) to develop long-range magnetic order. In this phase, the χ_j fields become hybridized with the conduction fields, and $\mathcal{G}_c$ and $\mathcal{G}_{\chi}$ become diagonal members of a single matrix propagator.

In general, we will therefore have to preserve the momentum dependence of the propagators. The bare propagators of the theory are diagonal in momentum, and given by

$$\mathcal{G}_b^{(0)}(\vec{k},i\nu_n)=(i\nu_n\underline{\tau_3}-\lambda\underline{1})^{-1},$$

$$\mathcal{G}_c^{(0)}(\vec{k},i\omega_n)=(i\omega_n-\epsilon_{\vec{k}})^{-1},$$

$$\mathcal{G}_{\chi}^{(0)}(\vec{k},i\omega_n)=-J_K, \quad (24)$$

where we have written the bare boson propagator as a two-dimensional Nambu propagator, to allow for the possible introduction of boson pairing, which develops as antiferromagnetic correlations begin to grow. Formally, we will combine these three propagators into a single propagator, given by

$$\mathcal{G}^{-1}=\begin{bmatrix} i\nu_n\underline{\tau_3}-\lambda\underline{1} & & \\ & i\omega_n-\epsilon_{\vec{k}} & \\ & & -\frac{1}{J_K} \end{bmatrix}-\Sigma, \quad (25)$$

where Σ is a matrix self-energy. Following Luttinger and Ward, we will regard $\mathcal{G}$ as a variational function, and Σ as a derived quantity.

We now consider the effect of tuning up the strength of the Kondo interaction from zero to J_K, by replacing $J_K\to\alpha J_K$ where $\alpha\in[0,1]$, keeping the chemical potential of the conduction electrons and bosons fixed. Now the partition function is given by

$$Z=\mathrm{Tr}[e^{-\beta H}]=\int\mathcal{D}[c,b,\chi]e^{-\int_0^{\beta}\mathcal{L}d\tau}, \quad (26)$$

where $\mathcal{D}[c,b,\chi]$ is the measure of the path integral. If we vary α inside this expression, we obtain

$$\frac{dZ}{d\alpha}=\int\mathcal{D}[c,b,\chi]\sum_{j\nu}\int_0^{\beta}d\tau\left(\frac{1}{\alpha^2 J_K}\chi_{j\nu}^{\dagger}\chi_{j\nu}\right)e^{-\int_0^{\beta}\mathcal{L}\,d\tau}$$
$$=\beta Z\times\frac{1}{\alpha^2 J_K}\sum_{j\nu}\langle\chi_{j\nu}^{\dagger}\chi_{j\nu}\rangle, \quad (27)$$

so that if $F=-T\ln Z$ is the free energy, then

$$\frac{dF}{d\alpha}=-\frac{1}{(\alpha^2 J_K)}\sum_{j\nu}\langle\chi_{j\nu}^{\dagger}\chi_{j\nu}\rangle=-\frac{T}{(\alpha^2 J_K)}\underline{\mathrm{Tr}}[\mathcal{G}_{\chi}], \quad (28)$$

where $\mathcal{G}_{\chi}$ is the Green's function for the χ fermion and $\underline{\mathrm{Tr}}[\mathcal{G}_{\chi}]\equiv K\Sigma_{i\omega_n,\vec{k}}\mathcal{G}_{\chi}(\vec{k},i\omega_n)e^{i\omega_n 0^+}$ denotes a trace over the frequency and momentum of $\mathcal{G}_{\chi}$ (here, $e^{i\omega_n 0^+}$ ensures the normal ordering of the operators). We next consider the expression

$$\widetilde{F}=T\underline{\mathrm{Str}}[\ln(-\mathcal{G}^{-1})+\Sigma\mathcal{G}]+Y[\mathcal{G}]. \quad (29)$$

We will show how this expression generalizes the Luttinger–Ward free energy functional to a mixture of interacting bosons and fermions. Here, we use the notation

$$\underline{\mathrm{Str}}[A]\equiv\underline{\mathrm{Tr}}[A_B]-\underline{\mathrm{Tr}}[A_F]\equiv\sum_{i\nu_n}\mathrm{Tr}[A_B(i\nu_n)]e^{i\nu_n 0^+}$$
$$-\sum_{i\omega_n}\mathrm{Tr}[A_F(i\omega_n)]e^{i\omega_n 0^+} \quad (30)$$

to denote the "supertrace" over the bosonic and fermionic parts of the matrix A. The "underline" notation is used to indicate a sum over both the frequency variable of A and a trace over the internal quantum numbers of A (such as momentum). The supertrace includes a relative minus sign for

the fermionic component of the matrix, and we have explicitly displayed the trace over the discrete Matsubara Bose $[i\nu_n=(2n)\pi T]$ and Fermi $[i\omega_n=(2n+1)\pi T]$ frequencies. In the above expression, the self-energy matrix $\Sigma=\mathcal{G}_0^{-1}-\mathcal{G}^{-1}$. The quantity $Y[\mathcal{G}]$ is the sum of all closed, two-particle irreducible skeleton Feynman graphs for the Free energy.

As mentioned earlier, the Luttinger Ward functional $Y[\mathcal{G}]$ has the property that its variation with respect to $\mathcal{G}$ generates the self-energy matrix,

$$\delta Y[\mathcal{G}] = - T \, \underline{\mathrm{S}}\mathrm{tr}[\Sigma \, \delta\mathcal{G}]. \tag{31}$$

The variation of the first term in $\tilde{F}$ with respect to $\mathcal{G}$ is given by

$$\delta\{T \, \underline{\mathrm{S}}\mathrm{tr}[\ln(-\mathcal{G}^{-1})]\} = T \, \underline{\mathrm{S}}\mathrm{tr}[-\mathcal{G}^{-1} \, \delta\mathcal{G}] \tag{32}$$

By using the relation $\Sigma[\mathcal{G}]=\mathcal{G}_0^{-1}-\mathcal{G}^{-1}$, the variation in the second term in $\tilde{F}$ is given by

$$\delta\{T \, \underline{\mathrm{S}}\mathrm{tr}[([\mathcal{G}_0^{-1}-\mathcal{G}^{-1}]\mathcal{G})]\} = T \, \underline{\mathrm{S}}\mathrm{tr}[\mathcal{G}_0^{-1}\delta\mathcal{G}], \tag{33}$$

so that the total variation of $\tilde{F}$ with respect to $\mathcal{G}$,

$$\delta\tilde{F} = T \, \underline{\mathrm{S}}\mathrm{tr}\left[\left(\overbrace{-\mathcal{G}^{-1}+\mathcal{G}_0^{-1}}^{\Sigma}-\Sigma\right)\delta\mathcal{G}\right] = 0 \tag{34}$$

identically vanishes,

$$\frac{\delta\tilde{F}}{\delta\mathcal{G}} = 0. \tag{35}$$

Now the Hubbard–Stratonovich transformation that we have carried out on the interaction H_I assures that the only place that the coupling constant αJ_K enters, is in $[\mathcal{G}_\chi^0]^{-1}=-1/\alpha J_K$. This means that on the rhs of Eq. (29) α enters explicitly only through $\Sigma_\chi=-(\alpha J_K)^{-1}-[\mathcal{G}_\chi]^{-1}$. Then,

$$\frac{d\tilde{F}}{d\alpha} = \underbrace{\frac{\delta\tilde{F}}{\delta\mathcal{G}}\frac{\partial\mathcal{G}}{\partial\alpha}}_{=0} + \frac{\partial\tilde{F}}{\partial\alpha} = -\frac{T}{(\alpha^2 J_K)}\underline{\mathrm{T}}\mathrm{r}[\mathcal{G}_\chi(\vec{q},i\omega_n)e^{i\omega_n 0^+}]. \tag{36}$$

But by comparison with (28), we see that $d\tilde{F}/d\alpha=dF/d\alpha$ and, since $F(\alpha=0)=\tilde{F}(\alpha=0)$ in the noninteracting case, the two quantities must be equal for all α, i.e.,

$$F = T \, \underline{\mathrm{S}}\mathrm{tr}[\ln(-\mathcal{G}^{-1}) + \Sigma\mathcal{G}] + Y[\mathcal{G}]. \tag{37}$$

There are various points to make about this derivation.

(i) The derivation is very general. Its correctness only depends on the stationarity of $\tilde{F}[\mathcal{G}]$ with respect to variations in $\mathcal{G}$ and the equivalence between $dF/d\alpha$ and $d\tilde{F}/d\alpha$. This means that the above expression will hold for broken symmetry or "Higg's phase" solutions that involve off-diagonal components to $\mathcal{G}$.[20] In the context of the Kondo lattice, this means that $\mathcal{G}$ can be extended to include anomalous boson pairing terms that are driven by short-range antiferromagnetic correlations, or alternatively, off-diagonal terms driven by long-range magnetism, which mix the conduction and χ fermions. This expression can also be used to describe superconducting states, where the conduction electron and χ propagators will contain off-diagonal terms.

(ii) Even though the free energy is a functional of three Green's functions, there is no overcounting.

(iii) The above Free energy functional can be used as a basis for developing conserving approximations that generalize the Kadanoff–Baym approach to a constrained system.[23] In particular, in the large-N limit, the skeleton graph expansion for Y truncates at the leading diagram (Fig. 1), providing the basis for a controlled treatment of both the magnetic and the paramagnetic phases of the Kondo lattice.[24,26]

III. ENTROPY FORMULA

In this section, we derive an approximate formula for the entropy of a Luttinger–Ward system that becomes exact in the large-N limit and in any approximation where the vertex corrections can be neglected. The result, which we shall derive below, is

$$S(T,\mathcal{G}) = \int \frac{d\omega}{\pi} \underline{\mathrm{T}}\mathrm{r}_{B,F}\left[\left(\frac{d\hat{n}(\omega)}{dT}\right)\{\mathrm{Im} \ln[-\mathcal{G}^{-1}(\omega-i\delta)]\right.$$
$$\left. + \mathrm{Im}\,\Sigma(\omega)\mathrm{Re}\,\mathcal{G}(\omega)\}\right], \tag{38}$$

where

$$\hat{n}(\omega) = \begin{bmatrix} n(\omega) & \\ & f(\omega) \end{bmatrix} \tag{39}$$

is the matrix containing the Bose or Fermi-Dirac distribution functions $n(\omega)=[e^{\beta\omega}-1]^{-1}$, $f(\omega)=[e^{\beta\omega}+1]^{-1}$. The trace is carried out over the Bose and Fermi components of both expressions. Here $\mathcal{G}(\omega)$ and $\Sigma(\omega)$ are the self-energies that have been analytically continued onto the real axis. This expression is extremely useful, for it only involves the low-energy part of the Green's functions of the particles, and does not involve the functional $Y[\mathcal{G}]$. A version of this formula was first quoted in the context of lattice gauge theory by Blaizot et al.[21]

Key to our approach is the notion that the Luttinger–Ward functional $F[\mathcal{G}]$ can be rewritten in terms of the *real* frequency Green's functions. This has the advantage that one does not have to deal with the temperature dependence of the Matsubara frequencies. The approach that we adopt is, in fact, reminiscent of the Keldysh approach for nonequilibrium systems.[32,33] To preserve the symmetry between bosons and fermions, it proves useful to introduce a kind of "Keldysh" notation, writing

$$\hat{h}(\omega) = \frac{1}{2} + \hat{\eta}\hat{n}(\omega) = \begin{bmatrix} \frac{1}{2} + n(\omega) & \\ & \frac{1}{2} - f(\omega) \end{bmatrix} \tag{40}$$

Use of this function preserves the "supertrace" symmetry of our approach. Consider the first part of the free energy,

$$F_1 = T \, \mathrm{Str}[\ln(-\mathcal{G}^{-1}) + \Sigma\mathcal{G}]. \tag{41}$$

We replace the summation in this term by an integral over $\hat{n}(\omega)$ around the imaginary axis,

$$T \underline{\mathrm{Str}}[A] \to - \int \frac{d\omega}{\pi} \, \mathrm{Im} \, \mathrm{Str}[\hat{h}(\omega) A(\omega - i\delta)], \qquad (42)$$

where $\mathrm{Str}[A] = \mathrm{Tr}[A_B] - \mathrm{Tr}[A_F]$ is the supertrace over the spatial and internal quantum numbers of A. By distorting the contour around the real axis, we obtain

$$F_1 = - \int \frac{d\omega}{\pi} \, \mathrm{Im} \, \mathrm{Str}[\hat{h}(\omega)\{\ln(-\mathcal{G}^{-1}) + (\mathcal{G}_0^{-1} - \mathcal{G}^{-1})\mathcal{G}\}_{\omega - i\delta}].$$
$$(43)$$

If we vary the Green's function, then we obtain

$$\delta F_1 = - \int \frac{d\omega}{\pi} \, \mathrm{Im} \, \mathrm{Str}[\hat{h}(\omega)\tilde{\Sigma}(\omega)\delta\mathcal{G}]_{\omega - i\delta}, \qquad (44)$$

where we have employed the notation $\tilde{\Sigma} = \mathcal{G}_0^{-1} - \mathcal{G}^{-1}$. In a similar fashion, when we vary $\mathcal{G}$ inside $Y[\mathcal{G}]$, we obtain

$$\delta Y = \int \frac{d\omega}{\pi} \, \mathrm{Im} \, \mathrm{Str}[\hat{h}(\omega)\Sigma(\omega)\delta\mathcal{G}(\omega)]_{\omega - i\delta}. \qquad (45)$$

The condition that the two terms cancel sets $\mathcal{G}_0^{-1} - \mathcal{G}^{-1} = \Sigma$, defining both the real and the imaginary parts of the self-energies in terms of the Green's functions.

We can exploit the stationarity $\delta F / \delta \mathcal{G} = 0$ to simplify the differentiation of the free energy with respect to the temperature. When we differentiate F, we can neglect the temperature dependence of the spectral functions,

$$S(T) = -\frac{dF}{dT} = \left. -\frac{\partial F}{\partial T} \right|_{\mathcal{G}}. \qquad (46)$$

The contribution to the entropy from F_1 is then

$$S_1 = \int \frac{d\omega}{\pi} \, \mathrm{Im} \, \mathrm{Str}\left(\frac{\partial \hat{h}(\omega)}{\partial T} \{ \ln[-\mathcal{G}^{-1}(\omega - i\delta)] \right.$$
$$\left. + \Sigma(\omega - i\delta)\mathcal{G}(\omega - i\delta) \} \right). \qquad (47)$$

The temperature derivative of the second term $Y[\mathcal{G}]$ in (37) requires more careful consideration. The general diagrammatic contribution to Y contains a certain number of frequency summations. When we analytically continue these frequency summations, distorting the contour integrals around the branch cuts of the Green's functions, we pick up "on-shell" contributions from each branch cut of the form

$$h_B(\omega)G_B''(\omega) \qquad (48)$$

and

$$h_F(\omega)G_F''(\omega). \qquad (49)$$

These combinations are nothing more than the "Keldysh" Green's, function well known from nonequilibrium physics.[32,33] In equilibrium, the Keldysh Green's function satisfies the fluctuation dissipation theorem,

$$G_K(\omega) = [G_R(\omega) - G_A(\omega)]2h(\omega) = -4iG''(\omega)h(\omega),$$

where G_R and G_A are the retarded and advanced propagators, respectively. In other words, $hG''(\omega) \equiv (i/4)G_K(\omega)$. The point

is that we can formally imagine evaluating Y in a general steady state, replacing $G_K \to -4ig''(\omega)h(\omega)$ at the end of the calculation. It is, however, equally consistent to compute Y in equilibrium, and substitute $g''(\omega)h(\omega) \to g_K$. The functional Y is closely related to the expectation value of the interaction energy. If we associate an amplitude $\sqrt{\alpha}$ with the strength of each vertex, then the expectation value of the interaction energy has the expansion

$$\langle H_I \rangle = \sum \alpha^n Y_n(\mathcal{G}_K, \mathcal{G}_R, \mathcal{G}_A),$$

where $\mathcal{G}_{K,R,A}$ are the fully renormalized nonequilibrium propagators. The functional Y is the weighted sum

$$Y[\mathcal{G}_K, \mathcal{G}_R, \mathcal{G}_A] = \sum \frac{\alpha^n}{n} Y_n(\mathcal{G}_K, \mathcal{G}_R, \mathcal{G}_A).$$

In this way, we can absorb all thermal functions into the Green's functions, so that all temperature dependence is entirely contained within the Keldysh Green's functions. To differentiate Y with respect to temperature, we need to determine $\delta Y / \delta \mathcal{G}_K$. Unfortunately, Y is not a true generating functional for the Keldysh self-energies, and we must be very careful in taking the next step.

Once we know the variation of Y with respect to the Keldysh Green's function, we can immediately compute the variation with respect to temperature. Now, from (45), we see that we may write

$$\delta Y = \int \frac{d\omega}{\pi} \mathrm{Str}[\Sigma'(\omega)\hat{h}(\omega)\delta\mathcal{G}''(\omega) + \hat{h}(\omega)\Sigma''(\omega)\delta\mathcal{G}'(\omega)].$$
$$(50)$$

If we now identify

$$\hat{h}(\omega)\mathcal{G}'' \equiv \frac{i}{4}\mathcal{G}_K,$$

$$\hat{h}(\omega)\Sigma'' \equiv \frac{i}{4}\Sigma_K, \qquad (51)$$

as the Keldysh components of the propagator and self-energy, respectively, it is very tempting to write

$$\delta Y = \int \frac{d\omega}{\pi} \mathrm{Str}\left[\left(\frac{i}{4}\right)\Sigma'(\omega)\delta\mathcal{G}_K(\omega) + \left(\frac{i}{4}\right)\Sigma_K(\omega)\delta\mathcal{G}'(\omega) \right].$$
$$(52)$$

This form would always be correct if Y were a true generating functional for Keldysh propagators. Unfortunately, in the Keldysh approach, the distinction between the "measurement" and "response" vertices means that, in general, the differential of Y with respect to $\mathcal{G}_K$ does not generate the real part of the self-energy. Fortunately, this difficulty vanishes in the leading large-N approximation, which is sufficient to generate a wide class of noncrossing approximation schemes. Diagrams involving vertex corrections do not satisfy this relationship, and there are corrections to the above diagram. Interestingly enough, however, our large-N expansion does absorb all the "RPA" diagrams of the interaction lines into explicit propagators, enabling the entropy formula

Sum rules and Ward identities in the Kondo lattice

COLEMAN, PAUL, AND RECH

to be derived for interacting collective modes and fermions.

With this proviso, we write

$$\frac{\delta Y}{\delta \mathcal{G}_K(\omega)} = \frac{i}{4}\Sigma'(\omega),$$

where $\Sigma' = \frac{1}{2}[\Sigma(\omega - i\delta) + \Sigma(\omega + i\delta)]$.

It is worth making a short diversion at this point to explicitly demonstrate that this relationship works in the large-N limit. Consider the leading-order form for Y in the large-N expansion,

$$Y_1 = K \times N \times \left(\frac{1}{\sqrt{N}}\right)^2 T^2 \sum_{k,q} G_c(k)G_\chi(q-k)G_b(q), \quad (53)$$

where $k \equiv (i\omega_n, \vec{k})$, $q \equiv (i\nu_n, \vec{q})$ is a shortened space-time notation. When we carry out the Matsubara sums in this expression, we obtain

$$Y = -K \int_{-\infty}^{\infty} \frac{d\omega}{\pi}\frac{d\nu}{\pi} \sum_{\vec{k},\vec{q}} \left\{ G'_c G''_\chi G''_b \left(h_\chi h_b - \frac{1}{4}\right) + G''_c G'_\chi G''_b h_c h_b \right.$$
$$\left. + G''_c G''_\chi G'_b h_c h_\chi \right\}, \quad (54)$$

where we have used the shorthand notation $G_c \equiv G_c(k)$, $h_c \equiv h_c(\omega)$, $G_\chi \equiv G_\chi(q-k)$, etc., which can be rewritten as

$$Y = \frac{K}{4} \int_{-\infty}^{\infty} \frac{d\omega}{2\pi}\frac{d\nu}{2\pi} \sum_{\vec{k},\vec{q}} \text{Re}\{G_{Rc}G_{K\chi}G_{Kb} + G_{Kc}G_{R\chi}G_{Kb}$$
$$+ G_{Kc}G_{K\chi}G_{Rb} + G_{R\chi}G_{Rc}G_{Ab}\}. \quad (55)$$

This last expression can also be derived using the Keldysh formalism to calculate the leading-order expression for $\langle H_I \rangle$.[33] The variation of this expression with respect to G_K gives the leading-order expressions for the boson χ and conduction self-energy; thus, for instance,

$$\frac{\delta Y}{\frac{i}{4}\delta G_{Kb}(q)} = -\frac{i}{4}k \sum_{\vec{k}} \int \frac{d\omega_c}{\pi}[G'_c(k)G_{K\chi}(q-k)$$

$$+ G_{Kc}(k)G'_\chi(q-k)]$$

$$= -k \sum_{\vec{k}} \int \frac{d\omega_c}{\pi}[G'_c(k)G''_\chi(q-k)h(q-k)$$

$$+ G''_c(k)h(k)G'_\chi(q-k)], \quad (56)$$

where the replacement $K \to k = K/N$ occurs because Y contains the contribution of all N spin channels of G_{Kb}, and we are only differentiating with respect to one of them. This result can be independently confirmed using Matsubara techniques.

Let us now return from this digression and continue to calculate the temperature dependence of Y. When we differentiate the general expression with respect to the temperature, we only need to keep track of how each of the thermal functions changes. This leads to the contribution

$$\hat{h}(\omega)\mathcal{G}''(\omega) = \frac{i}{4}\mathcal{G}_K(\omega) \to \hat{h}(\omega)\mathcal{G}''(\omega) + \frac{d\hat{h}(\omega)}{dT}\mathcal{G}''(\omega)\delta T$$

$$= \frac{i}{4}[\mathcal{G}_K(\omega) + \delta\mathcal{G}_K(\omega)], \quad (57)$$

where

$$\frac{i}{4}\delta\mathcal{G}_K(\omega) = \frac{d\hat{h}(\omega)}{dT}\mathcal{G}''(\omega)\delta T. \quad (58)$$

We can now combine these results to obtain

$$\left.\frac{\partial Y}{\partial T}\right|_\mathcal{G} = \int \frac{d\omega}{\pi}\text{Str}\left[\frac{\delta Y}{\frac{i}{4}\delta\mathcal{G}_K(\omega)}\left(\frac{d\hat{h}(\omega)}{dT}\mathcal{G}''(\omega)\right)\right]$$

$$= \int \frac{d\omega}{\pi}\text{Str}\left[\Sigma'(\omega)\left(\frac{d\hat{h}(\omega)}{dT}\mathcal{G}''(\omega)\right)\right], \quad (59)$$

so that

$$S_2 = -\left.\frac{\partial Y}{\partial T}\right|_\mathcal{G} = -\int \frac{d\omega}{\pi}\text{Str}\left[\left(\frac{d\hat{h}(\omega)}{dT}\right)\text{Re}\,\Sigma(\omega)\mathcal{G}''(\omega)\right]. \quad (60)$$

This is a key element in our proof of the entropy equation.

When we add S_1 and S_2 together, S_2 partially cancels the second term in S_1, yielding the final answer

$$S = S_1 + S_2 = \int \frac{d\omega}{\pi}\text{Str}\left[\left(\frac{d\hat{h}(\omega)}{dT}\right)\{\text{Im}\,\ln[-\mathcal{G}^{-1}(z)]\right.$$

$$\left. + \text{Im}\,\Sigma(z)\text{Re}\,\mathcal{G}(z)\}_{z=\omega-i\delta}\right]. \quad (61)$$

We may replace $\hat{h} \to \hat{n}$ and $\text{Str} \to \text{Tr}_{B,F}$ to recover (38). There are a few important points to be made about this result.

(i) Our ability to write the entropy in terms of the Green's functions only works because in the leading-order approximation for Y, there are no hidden collective modes that carry the entropy.

(ii) This approach is general, and can, for example, be applied to the interacting electron gas, and various interacting plasmas, such as the quark gluon plasma.[21] By treating the interaction line as an independent particle (photon), the leading-order approximation generates a generalized RPA-Eliashberg scheme for the self-consistent interaction and electron self-energies. Note that the entropy formula cannot be used in an RPA scheme in which the interaction line is not treated as an independent particle,[22] and it does not work if one includes vertex corrections.

(iii) It may be possible in future work to evaluate a more general expression for $\delta Y/\delta\mathcal{G}_K(\omega)$, permitting one to generalize the entropy formula to higher-order approximations for Y.

IV. CONSERVATION LAWS AND SUM RULES

Sum rules are intimately related to the existence of conserved charges. For example, in the Kondo lattice, there are

three independent types of conserved charges: the electric charge (in each channel), the total spin, and the conserved number of bosons at each site. Each conserved charge corresponds to a gauge invariance of the Lagrangian. For example, the electric charge (for channel ν) is

$$Q_\nu = \sum_{\vec{k},\alpha} c^\dagger_{\vec{k}\nu\alpha} c_{\vec{k}\nu\alpha}, \tag{62}$$

and this quantity is associated with the global gauge transformation,

$$c_{\vec{k}\nu\alpha} \to e^{i\theta_\nu(\tau)} c_{\vec{k}\nu\alpha}, \quad \chi_{j\nu} \to e^{-i\theta_\nu(\tau)} \chi_{j\nu}. \tag{63}$$

The opposite sign in the exponents expresses the opposite charge of the two fields. Similarly, the conserved number of bosons at each site,

$$Q_{bj} = \sum_\alpha b^\dagger_{j\alpha} b_{j\alpha}, \tag{64}$$

generates the local gauge transformation,

$$b_{j\alpha} \to e^{i\theta_b(j,\tau)} b_{j\alpha}, \quad \chi_{j\nu} \to e^{i\theta_b(j,\tau)} \chi_{j\nu}. \tag{65}$$

In phases where these symmetries are unbroken, they give rise to sum rules, which we now derive.

The general form of these gauge transformations is given by

$$\psi_\zeta \to e^{i\theta(\tau)q_\zeta} \psi_\zeta. \tag{66}$$

We can relate this gauge invariance to the conserved charge by examining how the time-derivative terms in the action behave under this transformation. In general, the time derivative part of the action has the form

$$S_0 = \int_0^\beta d\tau\, \psi^\dagger\, \underline{\gamma}\, \partial_\tau \psi, \tag{67}$$

where the elements γ_ζ of the diagonal matrix $\underline{\gamma}$ are unity, $\gamma_\zeta = 1$ for conventional fermions or bosons and zero, $\gamma_\zeta = 0$ for Hubbard–Stratonovich fields without any short-time dynamics, such as the Grassmanian field $\chi_{j\mu}$ introduced in the Kondo lattice. We can relate $\underline{\gamma}$ to the frequency dependence of $\mathcal{G}_0^{-1}$,

$$\underline{\gamma} = \frac{d\mathcal{G}_0^{-1}(\omega)}{d\omega}. \tag{68}$$

Under a time-dependent gauge transformation, the change in the action is given by

$$\Delta S = \left(\int_0^\beta d\tau\, \psi^\dagger e^{-i\theta\hat{q}} \underline{\gamma}\, \partial_\tau e^{i\theta\hat{q}}\, \psi \right) - S_0 = i \int_0^\beta d\tau\, \partial_\tau \theta(\tau) Q(\tau)$$

$$= -i \int_0^\beta d\tau\, \theta(\tau) \partial_\tau Q(\tau), \tag{69}$$

where we have commuted the diagonal matrices $\hat{q}$ and $\underline{\gamma}$ to obtain

$$Q = \psi^\dagger(\hat{q}\underline{\gamma})\psi. \tag{70}$$

Invariance of the action under time-dependent gauge transformations implies that $\partial_\tau Q(\tau) = 0$, i.e., the charge is conserved. In this way, we see that $\hat{q}\underline{\gamma}$ is the single-particle operator associated with the charge Q. Notice that the full charge operator only depends on those fields with a time derivative. When the system is probed at short times, only these fields carry the charge. However, at long times, it is the gauge charge $\hat{q}$ that determines the charge of physical low-energy excitations.

Using (70), we can now write the expectation value of the charge Q in the following compact form:

$$\langle \hat{Q} \rangle = \langle \psi^\dagger_\alpha \hat{q}\underline{\gamma}\psi_\alpha \rangle = -\frac{1}{\beta}\underline{\mathrm{Str}}[\hat{q}\underline{\gamma}\mathcal{G}]. \tag{71}$$

At zero temperature, provided there is a scale to the excitations, then the summations over discrete Matsubara frequencies can be replaced by a continuous integral. In particular,

$$T\,\underline{\mathrm{Str}}[A] \to \int_{-i\infty}^{i\infty} \frac{d\omega}{2\pi i} \mathrm{Str}[A(\omega)] e^{\omega 0^+}, \tag{72}$$

where $\mathrm{Str}[A]$ without an underline indicates a supertrace purely over the spatial variables of A. This enables us to write

$$\langle \hat{Q} \rangle = -\int_{-i\infty}^{i\infty} \frac{d\omega}{2\pi i} \mathrm{Str}[\hat{q}\underline{\gamma}\mathcal{G}(\omega)], \tag{73}$$

where, for clarity, we have temporarily suppressed the convergence factor $e^{\omega 0^+}$. Using (68), $\underline{\gamma} = (d\mathcal{G}_0^{-1})/(d\omega)$, we then obtain at $T=0$,

$$\langle \hat{Q} \rangle = -\int_{-i\infty}^{i\infty} \frac{d\omega}{2\pi i} \mathrm{Str}\left[\hat{q}\frac{d\mathcal{G}_0^{-1}}{d\omega}\mathcal{G} \right]. \tag{74}$$

Now let us consider the effect of the gauge transformation on the Free energy. If we carry out a gauge transformation $\psi_\zeta \to e^{i\theta(\tau)q_\zeta}\psi_\zeta$, with $\theta(\tau) = \Delta\omega\,\tau$, then diagrammatically this has the effect of shifting the frequencies associated with each propagator, $\omega_\zeta \to \omega_\zeta + q_\zeta \Delta\omega$, where q_ζ is the gauge charge of the propagating particle. In the zero temperature limit, this shift in frequency can be made infinitesimally small, $\Delta\omega_\zeta \to \delta\omega_\zeta$.

Diagrammatically, the conservation of charges corresponds to the existence of closed loops (Fig. 3) in the skeleton diagrams of Y through which the conserved charge circulates. The gauge transformation causes the frequency variable in each of these closed loops to shift by an amount $q\,\Delta\omega$. This change does not affect the value of Y, and vanishing of the change in Y then gives rise to new Ward identities.

When the frequency around the closed loops is shifted, each propagator entering into Y changes, with $\delta\mathcal{G}_\zeta(\omega) = (d\mathcal{G}/d\omega)q_\zeta\,\delta\omega$, so that the change in Y at zero temperature is
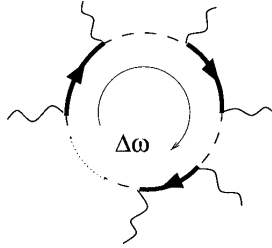
FIG. 3. Illustrating the shift in frequencies around a closed loop in $Y[\mathcal{G}]$ for the Kondo lattice, generated by the gauge transformation associated with charge conservation.

$$\delta Y = -\int_{-i\infty}^{i\infty} \frac{d\omega}{2\pi i} \mathrm{Str}[\Sigma(\omega)\delta\mathcal{G}(\omega)]$$

$$= -\int_{-i\infty}^{i\infty} \frac{d\omega}{2\pi i} \mathrm{Str}\left(\Sigma(\omega)\frac{d\mathcal{G}}{d\omega}\hat{q}\right)\delta\omega = 0, \quad (75)$$

so that

$$0 = \frac{\delta Y[\mathcal{G}]}{\delta\omega} = \int_{-i\infty}^{i\infty} \frac{d\omega}{2\pi i} \mathrm{Str}\left[\Sigma\frac{d\mathcal{G}}{d\omega}\hat{q}\right].$$

Integrating by parts, we obtain the Ward Identity,

$$\int_{-i\infty}^{i\infty} \frac{d\omega}{2\pi i} \mathrm{Str}\left[\frac{d\Sigma}{d\omega}\mathcal{G}\hat{q}\right] = 0. \quad (76)$$

Combining Eqs. (74) and (76), we obtain

$$\langle\hat{Q}\rangle = -\int_{-i\infty}^{i\infty} \frac{d\omega}{2\pi i} \mathrm{Str}\left[\hat{q}\frac{d}{d\omega}\overbrace{(\mathcal{G}_0^{-1}-\Sigma)}^{\mathcal{G}^{-1}(\omega)}\mathcal{G}\right]e^{\omega 0^+}$$

$$= -\int_{-i\infty}^{i\infty} \frac{d\omega}{2\pi i}\frac{d}{d\omega}\{\mathrm{Str}[\hat{q}\ln(-\mathcal{G}^{-1})]\}e^{\omega 0^+}, \quad (77)$$

where we have explicitly reinstated the convergence factor. Folding the integration contour around the negative real axis (as dictated by the convergence factor), we then obtain

$$\langle\hat{Q}\rangle = -\int_{-\infty}^{0} \frac{d\omega}{\pi}\frac{d}{d\omega}\frac{1}{2i}(\mathrm{Str}\{\hat{q}\ln[-\mathcal{G}^{-1}(\omega-i\delta)]\}$$

$$- \mathrm{Str}\{\hat{q}\ln[-\mathcal{G}^{-1}(\omega+i\delta)]\})$$

$$= -\int_{-\infty}^{0} \frac{d\omega}{\pi}\frac{d}{d\omega}\mathrm{Im}\,\mathrm{Str}\{\hat{q}\ln[-\mathcal{G}^{-1}(\omega-i\delta)]\}$$

$$= -\left[\frac{1}{\pi}\mathrm{Im}\,\mathrm{Str}\{\hat{q}\ln[-\mathcal{G}^{-1}(\omega-i\delta)]\}\right]_{-\infty}^{0}. \quad (78)$$

The presence of the minus sign inside the logarithms here is chosen so that the lower bound of the integral vanishes. We are then able to write

$$\langle\hat{Q}\rangle = -\frac{1}{\pi}\mathrm{Im}\,\mathrm{Str}\{\hat{q}\ln[-\mathcal{G}^{-1}(\omega-i\delta)]\}\Big|_{\omega=0}. \quad (79)$$

As it stands, the trace in this expression involves both bosonic and fermionic components. The latter will give rise to Fermi surface volume contributions in the lattice, and to phase shift terms in the case of impurity models. What about the bosons? General arguments lead us to believe that the bosonic component in the trace vanishes. The important point here is that the right-hand side of this sum counts the number of one-particle states that drop to *negative energy*. Whereas fermions can acquire a negative energy through the formation of a resonance or Fermi surface, bosons cannot— they only condense. If the bosons condense, then the symmetry they are associated with is broken, and we can no longer apply the sum rule. If they do not condense, then we expect the associated phase shifts to be zero. The final form of the sum rule is then

$$\langle\hat{Q}\rangle = \frac{1}{\pi}\mathrm{Im}\,\mathrm{Tr}[\hat{q}\ln(-\mathcal{G}_F^{-1})]_{\omega=0-i\delta}, \quad (80)$$

where, for clarity, we have suppressed the frequency argument of the Green's function.

V. KONDO IMPURITY MODEL

As a first illustration of the sum rules, let us apply them to the Kondo impurity model. There are two sum rules to consider here, corresponding to the conservation of Q_c and $n_b = 2S = K$ in the case of the perfectly screened solution. Let us first consider

$$n_b = \sum_\alpha b_\alpha^\dagger b_\alpha. \quad (81)$$

Even though the χ fermions do not enter into this conserved charge, they carry the gauge charge, and we have $(q_c, q_b, q_\chi) = (0, 1, 1)$. Applying the sum rule (79), we deduce

$$\langle n_b\rangle = -\frac{1}{\pi}\mathrm{Im}\,\mathrm{Tr}[\ln(-\mathcal{G}_b^{-1})]_{\omega=i\delta} + \frac{1}{\pi}\mathrm{Im}\,\mathrm{Tr}[\ln(-\mathcal{G}_\chi^{-1})]_{\omega=i\delta}, \quad (82)$$

where, for the moment, we have retained the bosonic trace. When we carry out the trace over the spin components of the boson and the channel components of the χ fermion, we obtain

$$\langle n_b\rangle = -N\frac{\delta_b}{\pi} + K\frac{\delta_\chi}{\pi}, \quad (83)$$

where

$$\delta_b = \mathrm{Im}[\ln(\lambda + \Sigma_b(0-i\delta) + i\delta)],$$

$$\delta_\chi = \mathrm{Im}\left[\ln\left(\frac{1}{J_K} + \Sigma_\chi(0-i\delta)\right)\right], \quad (84)$$

are the "phase shifts" associated with the boson and holon fields. Note in passing that at zero temperature, $\Sigma_b(0-i\delta)$

and $\Sigma_\chi(0-i\delta)$ are purely real. The argument of the logarithm in δ_b is the renormalized chemical potential $\lambda^* = \lambda + \Sigma_b(0)$ of the boson field. In the "filled shell" configuration $2S = K$, the formation of a perfectly screened Kondo singlet generates a gap for the addition of extra Schwinger bosons to the ground state, which forces $\lambda^* > 0$, and $\delta_b = 0$, as argued previously. It follows that

$$\langle n_b \rangle = K \frac{\delta_\chi}{\pi}. \qquad (85)$$

But $n_b = K$ is part of the constraint, so it follows that $\delta_\chi = \pi$. This result can be understood by relating δ_χ to the sign of the renormalized Kondo coupling constant, as follows:

$$\frac{\delta_\chi}{\pi} = \frac{1}{\pi} \operatorname{Im}\left[\ln\left(\frac{1}{J_K} + \Sigma_\chi(0 - i\delta) \right) \right] = \theta(-J_K^*). \qquad (86)$$

In this way, we see that $\delta_\chi = \pi$ corresponds to a residual "ferromagnetic" coupling. This is consistent with our expectations, for when an additional Schwinger boson is added to the Fermi liquid, it increases the impurity spin by one-half unit to form an underscreened Kondo model, where the residual spin coupling is indeed ferromagnetic. By contrast, in an antiferromagnet or spin liquid, the local moments spins pair condense, mutually screening one another. In this situation, an additional Schwinger boson at any one site will now be free to undergo a Kondo effect with the conduction electrons, so the residual spin coupling is antiferromagnetic. These results are also confirmed in the large-N limit.

Let us now turn to the sum rule derived from the conservation of electron charge. Here the conserved quantity is

$$Q_e = \sum_{k,\nu,\sigma} c^\dagger_{\vec{k},\nu,\sigma} c_{\vec{k},\nu,\sigma}, \qquad (87)$$

and the corresponding gauge charges are $(q_c, q_b, q_\chi) = (1, 0, -1)$, so the sum rule becomes

$$Q_e = \frac{1}{\pi} \left(\operatorname{Im} \operatorname{Tr}[\ln(-\mathcal{G}_c^{-1})] - \frac{1}{\pi} \operatorname{Im} \operatorname{Tr}[\ln(-\mathcal{G}_\chi^{-1})] \right) \bigg|_{\omega = 0 - i\delta}. \qquad (88)$$

Now in an impurity model, it is convenient to subtract off the total charge in the absence of the impurity, given by

$$Q_e^{(0)} = \frac{1}{\pi} \operatorname{Im} \operatorname{Tr}[\ln(-\mathcal{G}_{c0}^{-1})]_{\omega = 0 - i\delta}, \qquad (89)$$

where $\mathcal{G}_{c0} \equiv \mathcal{G}_c^{(0)}$ is the noninteracting propagator of the conduction electrons. If we subtract this from (88), we can combine the conduction electron traces and replace $\ln(-\mathcal{G}_c^{-1}) - \ln(-\mathcal{G}_{c0}^{-1}) = \ln(\mathcal{G}_{c0}\mathcal{G}_c^{-1}) = \ln(1 - \mathcal{G}_{c0}\Sigma_c)$. The change in total charge is then given by

$$Q_e - Q_e^{(0)} = \frac{1}{\pi} \operatorname{Im} \operatorname{Tr}[\ln(1 - \mathcal{G}_{c0}\Sigma_c)]_{\omega = -i\delta}$$
$$- \frac{1}{\pi} \operatorname{Im} \operatorname{Tr}[\ln(-\mathcal{G}_\chi^{-1})]_{\omega = -i\delta}. \qquad (90)$$

According to the Anderson-Clogston compensation theorem, the total change in electron charge due to a Kondo or Ander-

son impurity vanishes in the infinite bandwidth limit, and at finite bandwidth the change is of the order of the ratio of the Kondo temperature to the bandwidth $\Delta Q_c = O(T_K/D)$, and can be neglected.[34,35] Setting $\Delta Q_e = Q_e - Q_e^0 = 0$, we obtain

$$\Delta Q_e = 0 = NK \frac{\delta_c}{\pi} - K \frac{\delta_\chi}{\pi}, \qquad (91)$$

where we have identified

$$\delta_c = \operatorname{Im} \operatorname{Tr}_{\vec{k}}[\ln(1 - \mathcal{G}_{c0}\Sigma_c)]_{\omega = -i\delta}, \qquad (92)$$

where the trace is purely over momenta. If we expand the logarithm using a power series, we see that the trace over internal momenta in (92) is accomplished by replacing the momentum-dependent Green's function $\mathcal{G}_c^{(0)}(\vec{k}, \omega)$ by the local electron Green's function $g_0(\omega) = \Sigma_{\vec{k}} \mathcal{G}_c^0(\vec{k}, \omega)$, so that

$$\delta_c = \operatorname{Im} \ln[1 - g_0(\omega)\Sigma(\omega)]|_{\omega = 0 - i\delta}. \qquad (93)$$

In the large bandwidth limit, $g_0(\omega - i\delta) \to i\pi\rho$, where ρ is the density of states per spin per channel, so that

$$\delta_c = \operatorname{Im} \ln[1 - i\pi\rho\Sigma(0)]. \qquad (94)$$

There is thus a direct link between the phase shift of the χ fermion and that of the conduction electrons. Combining this with the earlier result $\delta_\chi = \pi$, we obtain

$$\delta_c = \frac{\delta_\chi}{N} = \frac{\pi}{N}. \qquad (95)$$

Notice the following.

(i) In the large-N limit, the phase shift identity permits us to relate the conduction electron phase shift δ_c, which is $O(1/N)$ to the χ phase shift δ_χ, which is finite in the large N limit. In this way, the sum rules enable us to study the phase shift and Fermi surface volume changes of the Kondo impurity and lattice, in the large-N limit.

(ii) The development of the conduction electron phase shift does not occur because conduction electron states drop beneath the Fermi sea: It is a consequence of the injection of new quasiparticle states into the Fermi sea as a response to the formation of spinless, charged holons.

VI. SUM RULE FOR THE KONDO LATTICE

When we come to consider the Kondo lattice, there are a number of additional subtleties that must be entertained. One of the most important aspects of the discussion here concerns the possibility that the extremal solutions to $F[\mathcal{G}]$ break the $U(1)$ symmetry of the bosons, to produce "Higg's" phase in which the Schwinger bosons either pair condense, or hybridize between sites. In the large-N solutions to the model, these phases appear to develop as a precursor to the formation of the antiferromagnet, where the bosons themselves condense. The main effect on the sum rules is twofold:

(i) We cannot assume that the χ fermion is localized. This implies that we must consider the momentum dependence of the χ fermion.

(ii) Once the Schwinger bosons pair condense, the Ward identities associated with the conservation of n_b no longer

apply, because the Luttinger–Ward functional $Y[\mathcal{G}]$ is no longer invariant under shifts of the boson frequency.

However, we can still take advantage of the Ward identity associated with charge conservation. Provided that the Schwinger boson is uncondensed, i.e., there is no magnetism, then charge conservation guarantees that

$$\int_{-i\infty}^{i\infty} \frac{d\omega}{2\pi i} \text{Tr}_F \left[\frac{d\Sigma}{d\omega} \mathcal{G} \hat{q} \right] = 0 \quad (q_c = 1, q_\chi = -1). \quad (96)$$

Now in the paramagnet, the holon and conduction electron fields are unmixed, so we can replace

$$\text{Tr}_F \rightarrow \text{Tr}_c + \text{Tr}_\chi.$$

This is a special property of the paramagnet. By contrast, in the antiferromagnet, the Schwinger bosons are condensed, so the holon and conduction electron fields admix, and both Σ and $\mathcal{G}$ contain off-diagonal terms so that Tr_F remains a single, integral trace over the two admixed fields.

For the paramagnet, we can write

$$0 = -\int_{-i\infty}^{i\infty} \frac{d\omega}{2\pi i} \text{Str} \left[\frac{d\Sigma}{d\omega} \mathcal{G} \hat{q} \right] \quad (q_c = 1, q_\chi = -1)$$

$$= \int_{-i\infty}^{i\infty} \frac{d\omega}{2\pi i} \text{Tr} \left[\frac{d\Sigma_c}{d\omega} \mathcal{G}_c \right] - \int_{-i\infty}^{i\infty} \frac{d\omega}{2\pi i} \text{Tr} \left[\frac{d\Sigma_\chi}{d\omega} \mathcal{G}_\chi \right]$$

$$= K \int_{-i\infty}^{i\infty} \frac{d\omega}{2\pi i} \int \frac{d^D k}{(2\pi)^D} \left[N \frac{d\Sigma_c(\vec{k}, \omega)}{d\omega} \mathcal{G}_c(\vec{k}, \omega) \right.$$

$$\left. - \frac{d\Sigma_\chi(\vec{k}, \omega)}{d\omega} \mathcal{G}_\chi(\vec{k}, \omega) \right]. \quad (97)$$

It is this identity that permits us to extend the Luttinger sum rule to the case of the paramagnetic Kondo lattice. In the paramagnetic Kondo lattice, the charge sum rule

$$Q_e = \frac{1}{\pi} \{ \text{Im} \, \text{Tr}[\ln(-\mathcal{G}_c^{-1})] - \text{Im} \, \text{Tr}[\ln(-\mathcal{G}_\chi^{-1})] \} |_{\omega=0-i\delta}, \quad (98)$$

now involves a trace over momentum:

$$\frac{Q_e}{K} = N \sum_{\vec{k}} \frac{1}{\pi} \text{Im} \ln[\epsilon_{\vec{k}} + \Sigma_c(\vec{k}, 0 - i\delta) + i\delta]$$

$$- \sum_{\vec{k}} \frac{1}{\pi} \text{Im} \ln \left(\frac{1}{J_K} + \Sigma_\chi(\vec{k}, 0 - i\delta) \right). \quad (99)$$

The first term in this expression is the electron Fermi surface volume,

$$\sum_{\vec{k}} \frac{1}{\pi} \text{Im} \ln[\epsilon_{\vec{k}} + \Sigma_c(\vec{k}, 0 - i\delta) + i\delta] = \sum_{\vec{k}} \theta(-E_{\vec{k}}) = \frac{v_{FS}}{(2\pi)^D}, \quad (100)$$

where the region where $E_{\vec{k}} = \epsilon_{\vec{k}} + \text{Re} \, \Sigma_c(\vec{k}, E_{\vec{k}})$ is negative, defines the interior of the Fermi surface. The second term can be interpreted in a similar way—the momentum trace over the logarithm of $\mathcal{G}_\chi^{-1}$,

$$\sum_{\vec{k}} \frac{1}{\pi} \text{Im} \ln \left(\frac{1}{J_K} + \Sigma_\chi(\vec{k}, 0 - i\delta) \right) = \sum_{\vec{k}} \theta[-J_K^*(\vec{k})] = \frac{v_\chi}{(2\pi)^D}, \quad (101)$$

can be seen as the volume of the region in momentum space where the effective interaction $J_K^*(\vec{k}) = -\mathcal{G}_\chi(\vec{k}, 0)^{-1}$ is negative, or ferromagnetic. Following our earlier discussion, the ferromagnetic sign of the residual interaction is a consequence of the fact that additional spins added to the state completely decouple from the Fermi sea. In the simplest scenario, $J_K^*(\vec{k}) < 0$ for all $\vec{k}$, in which case $v_\chi/(2\pi)^D = 1$, and the sum rule becomes

$$n_e = \frac{Q_e}{K} = N \frac{v_{FS}}{(2\pi)^D} - 1, \quad (102)$$

where n_e is the electron density per unit cell, per conduction electron channel. It follows that the total Fermi surface volume expands by one unit per unit cell,

$$N \frac{v_{FS}}{(2\pi)^D} = n_e + 1. \quad (103)$$

Now if there is some region of momentum space where $J_K^*(\vec{k})$ is not ferromagnetic, it follows that the χ fermions will have a Fermi surface, and the excitation spectrum will now involve charged, spinless fermions. In this phase,

$$n_e = \frac{Q_e}{K} = N \frac{v_{FS}^*}{(2\pi)^D} - \frac{v_\chi}{(2\pi)^D}. \quad (104)$$

Such a "spin-charge decoupled" phase could not develop from a Fermi liquid without a phase transition. As long as the heavy electron fluid does not undergo such a phase transition, the Fermi surface must remain large.

Let us now consider what happens in the antiferromagnet. In the general higher-dimensional case, the boson field condenses, causing the conduction and χ fields to hybridize to produce a single species. In the antiferromagnet, it is more logical to make a particle-hole transformation of the χ field, writing $\psi_{\vec{k}} = \chi_{-\vec{k}}^\dagger$. In this case, $q_\psi = q_c$ have the same charge, and the sum rule becomes simply

$$Q_e = \frac{1}{\pi} \text{Im} \, \text{Tr}_F[\ln(-\mathcal{G}_F^{-1})] \bigg|_{\omega=-i\delta}, \quad (105)$$

where $\mathcal{G}_F$ is the admixed propagator for the combined conduction and ψ fields. The right-hand side cannot be separated into χ and conduction parts, and, as such, defines an admixed set of Fermi surfaces, with an average Fermi surface volume that counts the total charge per unit cell,

$$n_e = N \frac{\langle v_{AFM} \rangle}{(2\pi)^D}. \quad (106)$$

The Fermi surface volume for the antiferromagnet and the paramagnet must then differ by $1/N$th of a unit cell. In the special case of $N=2$, if the spatial unit cell doubles, this formal change in Fermi surface volume is indistinguishable from the new size of the Brillouin zone. However, even in this case, we can imagine more general classes of antiferro-

magnet, such as an incommensurate helimagnet, where the unit cell size is unchanged, but the total Fermi surface volume must jump.

VII. SPIN-CHARGE SEPARATION AND QUANTUM CRITICALITY

Although the sum rules do not provide us with any details of the dynamics, they provide stringent constraints on the way the spectrum of excitations can evolve in the Kondo lattice as we approach the magnetic quantum critical point.

One of the fascinating aspects of our sum rule,

$$n_e = N\frac{v_{FS}}{(2\pi)^D} - \frac{v_\chi}{(2\pi)^D}, \qquad (107)$$

is that it suggests that a Kondo lattice may develop low-lying, spinless charged fermionic excitations near a quantum critical point. This is clearly a controversial idea, the consequences of which we now explore in this discussion. If we take this idea seriously, then two important points seem to emerge.

(i) In the heavy Fermi liquid, spinons have "ionized" into electrons and a background filled sea of holons,

$$b_\sigma \leftrightarrow e_\sigma^- + \chi^+ \qquad (108)$$

It is this ionization process that lies behind the expansion of the Fermi surface and the sum rule.

(ii) There is an intimate link between the Kondo interaction and the formation of holons. The link between the propagator of the holons and the renormalized Kondo interaction,

$$-\mathcal{G}_\chi(\vec{q},\omega) = \frac{1}{\dfrac{1}{J_K} + \Sigma_\chi(\vec{q},\omega)} = J_K^*(\vec{q},\omega), \qquad (109)$$

implies that poles in the holon spectrum correspond to divergences in the Kondo interaction. As magnetism drives the Kondo interaction back to weak coupling, we expect $J^*(\vec{q},\omega)$ to pass through infinity, so the holons should become gapless at some point in this process.

We can, in fact, use the Luttinger–Ward approach to gain insight into the low-energy thermodynamics of the Kondo lattice.[3] Provided the replacement of frequency sums by continuous integrals is valid at low-temperatures, Luttinger argued that the low-energy thermodynamics is determined by the leading logarithm in the free energy functional (4), evaluated with the zero-temperature Green's function. In our case, this leads to the relation

$$F(T) \approx \sum T \, \underline{Str}[\ln(-\mathcal{G}_{(0)}^{-1})] \quad (T \to 0),$$

where $\mathcal{G}_{(0)}$ is the zero temperature Green's function. Carrying out the frequency integrals, this implies that the low-temperature entropy is given by

$$S(T) = \int \frac{d^Dk}{(2\pi)^D} \int \frac{d\omega}{\pi} \overbrace{\left(\frac{dn}{dT} \, \text{Im Tr} \ln - \mathcal{G}_b^{-1}(\vec{k},\omega) + \frac{df}{dT} \, \text{Im Tr} \ln - \mathcal{G}_\chi^{-1}(\vec{k},\omega)\right)}^{\text{spinon and holon entropy}}$$

$$+ \int \frac{d^Dk}{(2\pi)^D} \int \frac{d\omega}{\pi} \left(\overbrace{\frac{df}{dT} \, \text{Im Tr} \ln - \mathcal{G}_c^{-1}(\vec{k},\omega)}^{\text{Fermi liquid}}\right) \qquad (110)$$

where the zero-temperature propagators are to be used. The last term in this expression provides the T-linear entropy of the Fermi liquid; the first two terms are the "spinon" and "holon" contributions. For a Landau Fermi liquid to form, these last terms must clearly be gapped at low temperatures. This feature is observed in the large-N solutions.[26] What it also makes clear, however, is that the holons cannot become gapless without a thermodynamic departure from Fermi liquid behavior, which implies some kind of quantum phase transition.

However, even though the holons are gapped in the Fermi liquid, they can exist as low-lying spinless, charged excitations. It is particularly interesting to speculate that the gap to holon formation closes at a quantum critical point. This is a possibility that can be studied in the large-N limit, but general arguments should hold at finite N, as long as the

Luttinger–Ward approach is valid. One way to go beyond the large-N limit is to carry out a fully self-consistent treatment of the leading Luttinger–Ward free energy functional, updating the conduction electron self-energy and feeding the full conduction electron Green's functions into the calculation of the self-energy for the χ and Schwinger boson field. Such an approximation goes selectively beyond the large-N limit, but it will satisfy the Ward identities. Moreover, assuming that the "filled shell" stability of the fully screened ground state is not an artifact of the large-N limit, we also expect the gap in the Schwinger boson and the χ fermion particle spectrum to be preserved at finite N.

Another way to check the picture emerging from this approach would be to examine low-dimensional systems. Various authors have examined the possibility of a transition from a small to large Fermi surface in the one-dimensional

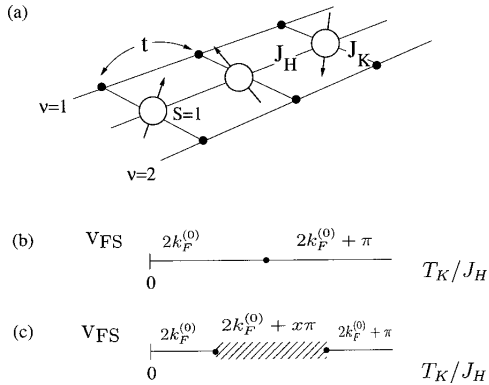# Sum rules and Ward identities in the Kondo lattice

FIG. 4. (a) The two-channel, spin $S=1$ Kondo chain. (b) In the simplest scenario, the transition from a Haldane chain with a small Fermi surface, to the heavy electron phase with a large Fermi surface will occur via a single phase transition. (c) The sum rules allow for an intermediate phase with a Fermi surface that lies between these two extremes.

spin-1/2 Kondo lattice.[36,37] The difficulty with this model is that the gaplessness of the Heisenberg spin-1/2 chain tends to make the Kondo coupling relevant, no matter how small the Kondo temperature. A model that avoids these difficulties is the $S=1$, two-channel Kondo lattice. This model involves

a Haldane spin-1 chain coupled via Kondo interactions to two, one-dimensional, noninteracting Hubbard models, as shown in Fig. 4.

When the Kondo interaction is weak, the Haldane chain is gapped, and the "Fermi surface" of the Kondo lattice is small, giving rise to Friedel oscillations at wave vector $Q = 2k_F^{(0)}$. When the Kondo interaction is strong, a Kondo lattice with a large Fermi surface is expected to form where $Q = 2k_F^{(0)} + \pi$. The way these two phases are linked is particularly interesting. If they are linked by a single quantum critical point, then we expect Q to simply jump at this point [Fig. 4(b)]. However, if the holons form a gapless phase, then over an intermediate range of parameters, we would expect the Friedel oscillations to exhibit an intermediate wave vector [Fig. 4(c)],

$$Q = 2k_F^0 + x\pi. \tag{111}$$

[1] J. M. Luttinger, Phys. Rev. **119**, 1153 (1960).
[2] J. M. Luttinger and J. C. Ward, Phys. Rev. **118**, 1417 (1960).
[3] J. M. Luttinger, Phys. Rev. **121**, 1251 (1961).
[4] J. Friedel, Philos. Mag. **43**, 153 (1952).
[5] J. S. Langer and V. Ambegaokar, Phys. Rev. **121**, 1090 (1961).
[6] D. C. Langreth, Phys. Rev. **150**, 516 (1966).
[7] A. A. Abrikosov, Physics (Long Island City, N.Y.) **2**, 5 (1964).
[8] H. Suhl, Phys. Rev. **138**, A515 (1965).
[9] G. Gruner and A. Zawadowski, in *Progress in Low Temperature Physics*, edited by D. F. Brewer (North-Holland, Amsterdam, 1978), Vol. VIIB, p. 591.
[10] R. M. Martin, Phys. Rev. Lett. **48**, 362 (1982).
[11] B. I. Shraiman and E. D. Siggia, Phys. Rev. Lett. **62**, 1564 (1989).
[12] B. L. Altshuler, A. V. Chubukov, A. Dashevskii A, A. M. Finkel'stein, and D. K. Morr, Europhys. Lett. **41**, 401 (1998).
[13] P. Coleman, C. Pépin, Q. Si, and R. Ramazashvili, J. Phys.: Condens. Matter **13**, R723 (2001).
[14] T. Senthil, M. Vojta, and S. Sachdev, Phys. Rev. B **69**, 035111 (2004).
[15] C. Pépin, Phys. Rev. Lett. **94**, 066402 (2005).
[16] S. Kawarazaki *et al.*, Phys. Rev. B **61**, 4167 (2000).
[17] S. Paschen, T. Lühmann, S. Wirth, P. Gegenwart, O. Trovarelli, Ch. Geibel, F. Steglich, P. Coleman, and Q. Si, Nature (London) **432**, 881 (2004).
[18] M. Oshikawa, M. Yamanaka, and I. Affleck, Phys. Rev. Lett. **78**, 1984 (1997).
[19] M. Oshikawa, Phys. Rev. Lett. **84**, 3370 (2000).
[20] G. M. Eliashberg, Zh. Eksp. Teor. Fiz. **43**, 1005 (1962) [Sov.

Phys. JETP **16**, 780 (1963)].
[21] J.-P. Blaizot, E. Iancu, and A. Rebhan, Phys. Rev. D **63**, 065003 (2001).
[22] G. M. Carneiro and C. J. Pethick, Phys. Rev. B **11**, 1106 (1975).
[23] G. Baym and L. P. Kadanoff, Phys. Rev. **124**, 287 (1961); G. Baym, *ibid.* **127**, 1391 (1962).
[24] O. Parcollet and A. Georges, Phys. Rev. Lett. **79**, 4665 (1997).
[25] S. Powell, S. Sachdev, and H. P. Buchler, cond-mat/0502299 (unpublished).
[26] J. Rech, P. Coleman, O. Parcollet, and G. Zarand, cond-mat/0507001 (unpublished).
[27] P. Coleman and C. Pépin, Phys. Rev. B **68**, 220405 (2003).
[28] P. Coleman and I. Paul, Phys. Rev. B **70**, 035111 (2004).
[29] P. W. Anderson and Z. Zou, Phys. Rev. Lett. **60**, 132 (1988).
[30] To avoid the ambiguities of unit cells, it is important here that the $\vec{Q}$ vector does not have certain values. For a helimagnet, for example, we must avoid the commensurate case where $\vec{Q} = (\pi/N, \pi/N, \pi/N)$, where $N=2$ is the parameter for an SP $(2N)$ generalization.
[31] M. Potthoff, cond-mat/0406671 (unpublished).
[32] J. Rammer and H. Smith, Rev. Mod. Phys. **58**, 323 (1986).
[33] A. Kamenev, cond-mat/0412296 (unpublished).
[34] A. M. Clogston and P. W. Anderson, Bull. Am. Phys. Soc. **6**, 124 (1961).
[35] For a detailed discussion of this point, see Appendix A in P. Coleman and I. Paul, Phys. Rev. B **70**, 035111 (2004).
[36] J. C. Xavier, E. Novais, and E. Miranda, Phys. Rev. B **65**, 214406 (2002).
[37] E. Pivovarov and Q. Si, cond-mat/0304129 (unpublished).

PUBLICATION 4

Schwinger-boson approach to the fully screened Kondo model

PHYSICAL REVIEW LETTERS

Schwinger Boson Approach to the Fully Screened Kondo Model

J. Rech,[1,2,3] P. Coleman,[1,2] G. Zarand,[1,4] and O. Parcollet[3]

[1]*Kavli Institute for Theoretical Physics, Kohn Hall, University of California at Santa Barbara, Santa Barbara, California 93106, USA*
[2]*Center for Materials Theory, Rutgers University, Piscataway, New Jersey 08855, USA*
[3]*Service de Physique Théorique, CEA/DSM/SPhT-CNRS/SPM/URA 2306, CEA/Saclay, F-91191 Gif-sur-Yvette Cedex, France*
[4]*Theoretical Physics Department, Budapest University of Technology and Economics, Budafoki ut 8. H-1521 Hungary*
(Received 6 July 2005; published 9 January 2006)

We apply the Schwinger boson scheme to the fully screened Kondo model and generalize the method to include antiferromagnetic interactions between ions. Our approach captures the Kondo crossover from local moment behavior to a Fermi liquid with a nontrivial Wilson ratio. When applied to the two-impurity model, the mean-field theory describes the ''Varma-Jones'' quantum phase transition between a valence bond state and a heavy Fermi liquid.

PACS numbers: 72.15.Qm, 71.27.+a, 73.43.Nq, 75.20.Hr

Heavy fermion metals have attracted great interest as an arena for the controlled study of magnetic quantum phase transitions [1]. Several recent observations cannot be understood in terms of the established Moriya-Hertz theory of quantum phase transitions [2–4], including the divergence of the heavy electron masses [5], the near linearity of the resistivity [6–9], and E/T scaling in inelastic neutron spectra [10]. The origins of this failure are thought to be linked to the competition between antiferromagnetism and the screening of local moments via the Kondo effect. It remains an unsolved challenge to discover the appropriate mean-field description and the corresponding quantum critical modes which govern these novel quantum phase transitions [1,11–13].

Large-N methods offer a promising route towards this goal. Historically, these methods played a major role in the theory of classical criticality [14], and more recently, in the theory of heavy fermion metals [15,16]. However, progress on quantum phase transitions has been hindered by our inability to capture both the Kondo effect and antiferromagnetism in the leading large N approximation.

In this Letter, we describe new progress towards this goal using Schwinger's boson representation of spins [17]. Unlike traditional fermionic representations of spin [15,16] the Schwinger boson scheme provides a good description of local moment magnetism [17]. However, efforts to generalize this method to the Kondo problem [18,19] have failed to capture the Fermi liquid physics associated with perfect screening of the moment. Here we solve this problem using a method coinvented by one of us (O. P.) [18] which employs a multichannel Kondo model with K screening channels. By tuning the size of the spin S from $S < K/2$ to $S > K/2$, one can describe both the overscreened and underscreened Kondo models. Difficulties were encountered in past work that appeared to exclude treatment of the perfectly screened case, $2S = K$. We show how these difficulties are overcome to reveal the perfectly screened Fermi liquid and we demonstrate how this method captures the competition with antiferromagnetism in its simplest extension to the two-impurity Kondo model.

We begin with the single impurity Kondo model,

$$
\mathcal{H} = \sum_{\vec{k},\nu,\alpha} \epsilon_{\vec{k}} c^\dagger_{\vec{k}\nu\alpha} c_{\vec{k}\nu\alpha} + H_I - \lambda(n_b - 2S),
$$

$$
H_I = \frac{J_K}{N} \sum_{\nu\alpha\beta} \psi^\dagger_{\nu\alpha} \psi_{\nu\beta} b^\dagger_\beta b_\alpha. \tag{1}
$$

In this version of the model, $c^\dagger_{\vec{k}\nu\alpha}$ creates a conduction electron of momentum $\vec{k}$, channel index $\nu \in [1, K]$, spin index $\alpha \in [-j, j]$, where $N = 2j + 1$ is even. $\psi^\dagger_{\nu\alpha} = \frac{1}{\sqrt{\mathcal{N}_s}} \sum_{\vec{k}} c^\dagger_{\vec{k}\nu\alpha}$ creates an electron in the Wannier state at the origin, where $\mathcal{N}_s$ is the number of sites in the lattice. The operator $b^\dagger_\alpha$ creates a Schwinger boson (''spinon'') with spin index $\alpha \in [-j, j]$. The local spin operator is represented by $S_{\alpha\beta} = b^\dagger_\alpha b_\beta - \delta_{\alpha\beta}/N$ and the system is restricted to the physical Hilbert space by requiring $n_b \equiv \sum_\alpha b^\dagger_\alpha b_\alpha \equiv 2S$. The final term in H contains a temperature-dependent chemical potential $\lambda(T)$ that implements the constraint $\langle n_b \rangle = 2S$. We will examine the fully screened case $2S = K$, taking the limit $N \to \infty$ with $k = K/N$ fixed.

The first step is to factorize the interaction in terms of auxiliary spinless fermion fields (''holons''), χ_ν,

$$
H_I \to \sum_{\nu\alpha} \frac{1}{\sqrt{N}} [(\psi^\dagger_{\nu\alpha} b_\alpha)\chi^\dagger_\nu + \text{H.c.}] + \sum_\nu \frac{\chi^\dagger_\nu \chi_\nu}{J_K}. \tag{2}
$$

Following the steps outlined by us in earlier work [20], we now write the free energy as a Luttinger-Ward [21] functional of the one particle Green's functions,

$$
F[\mathcal{G}] = T \text{Str}[\ln(-\mathcal{G}^{-1}) + (\mathcal{G}_0^{-1} - \mathcal{G}^{-1})\mathcal{G}] + Y[\mathcal{G}], \tag{3}
$$

where $\text{Str}[A] = \text{Tr}[A_B] - \text{Tr}[A_F]$ is the graded (super) trace over the Matsubara frequencies, internal quantum numbers of the bosonic (B) and fermionic (F) components of A. $\mathcal{G}_0$ is the bare propagator and $\mathcal{G} = \text{Diag}[\underline{G}_b, \underline{G}_\chi, \underline{G}_c]$, the fully dressed propagator, where

016601-1

$$\underline{G}_b(i\nu_n) = [i\nu_n + \lambda - \Sigma_b(i\nu_n)]^{-1}\delta_{\alpha\alpha'},$$

$$\underline{G}_\chi(i\omega_n) = [-J_K^{-1} - \Sigma_\chi(i\omega_n)]^{-1}\delta_{\nu\nu'}, \qquad (4)$$

$$\underline{G}_c(i\omega_n) = [G_{c0}^{-1}(i\omega_n) - \Sigma_c(i\omega_n)]^{-1}\delta_{\alpha\alpha'}\delta_{\nu\nu'}.$$

$\Sigma(i\omega_n) = \mathcal{G}_0^{-1} - \mathcal{G}^{-1}$ denotes the corresponding self-energies. $G_{c0}(i\omega_n) = \sum_{\vec{k}} 1/(i\omega_n - \epsilon_{\vec{k}})$ is the bare conduction electron Green's function. The quantity $Y[\mathcal{G}]$ is the sum of all closed-loop two-particle irreducible skeleton Feynman diagrams. In the large N limit, we take the leading $O(N)$ contribution to Y (Fig. 1).

The variation of Y with respect to $\mathcal{G}$ generates the self-energy $\delta Y/\delta\mathcal{G} = \Sigma$, which yields $\Sigma_c(\tau) = \frac{1}{N}G_\chi(-\tau) \times G_b(\tau)$. Since Σ_c is of order $O(N^{-1})$ we use the bare conduction propagator G_{c0} in the self-consistent equations,

$$\Sigma_\chi(\tau) = G_b(\tau)G_{c0}(-\tau), \qquad \Sigma_b(\tau) = -kG_\chi(\tau)G_{c0}(\tau). \qquad (5)$$

In practice, we solve these equations using a real time representation of the Green's functions. [See, for example, [19]].

The original work in [18,22] focused primarily on the overscreened Kondo model, where $K > 2S$. The perfectly screened case presented two difficulties. First, the requirement that $K = 2S$ appeared extremely stringent, the slightest deviation from this condition leading to singular departures from Fermi liquid behavior at low temperatures. Second, the conduction electron phase shift δ_c is π/N, suggesting that the effect of the Kondo resonance would completely vanish in the large N limit.

Two new observations shed new light on this problem. First, the perfectly screened case is a stable "filled shell" singlet configuration of the spins, which at strong coupling correspond to "rectangular" Young tableau representations of $SU(N)$. [23,24]. In our gauge theory description of the Kondo model, this stability manifests itself through the formation of a gap in the spinon and holon spectrum. When the chemical potential, λ, lies within this gap, the ground-state Schwinger boson occupancy locks into the value $n_b = K = 2S$ (Fig. 2). Moreover, the gap removes the effect of the spinons and holons at low energies to reveal a Fermi liquid.

Second, although the conduction phase shift δ_c is π/N, its effect on the thermodynamics is multiplied by the N
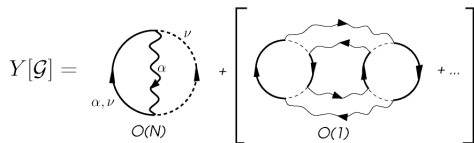
spin components and the K scattering channels, producing an order $O(N \times K/N) \equiv O(N)$ contribution to the free energy. Moreover, a Ward identity $\delta_c = \delta_\chi/N$, where $\delta_\chi = \text{Im} \ln[1 + J_K\Sigma_\chi(0 - i\delta)]$ is the (finite) holon phase shift [19,20] enables us to compute the conduction electron scattering in the large N limit.

In the large N limit the entropy [20] is given by

$$\frac{S(T)}{N} = \int \frac{d\omega}{\pi} \left\{ \frac{dn_B(\omega)}{dT}[\text{Im} \ln(-G_b^{-1}) + G_b'\Sigma_b''] \right.$$
$$\left. + k\frac{dn_F(\omega)}{dT}[\text{Im} \ln(-G_\chi^{-1}) + G_\chi'\Sigma_\chi'' - G_{c0}''\tilde{\Sigma}_c'] \right\}, \qquad (6)$$

where frequency labels ω are suppressed in the integrand, $n_{B/F}$ denote the Bose-Fermi functions, and

$$\tilde{\Sigma}_c(\omega) = N\Sigma_c(\omega) = -\int \frac{d\nu}{\pi} \left\{ \left[\frac{1}{2} - n_F(\nu) \right] G_\chi''(\nu)G_b(\omega + \nu) \right.$$
$$\left. + \left[\frac{1}{2} + n_B(\nu) \right] G_b''(\nu)G_\chi^*(\nu - \omega) \right\} \qquad (7)$$

is the rescaled conduction self-energy. The shortened notation $G(\omega) = G(\omega - i\delta)$ has been used. We can also calculate the local magnetic susceptibility

$$\chi_{\text{loc}}(T) = -2N \int \frac{d\omega}{\pi} \left[\frac{1}{2} + n_B(\omega) \right] G_b'(\omega)G_b''(\omega), \qquad (8)$$

where we have taken the magnetic moment of the local impurity to be $M = \sum_\alpha \text{sgn}(\alpha)b_\alpha^\dagger b_\alpha$. Note in passing that the dynamic counterpart $\langle S(t)S(0)\rangle$ vanishes exponentially due to the gap in the bosonic spectral functions, the $1/t^2$ term characteristic of a Fermi liquid only appearing at the next order in $1/N$.

We have numerically solved the self-consistent equations for the self-energy by iteration, imposing the constraint at each temperature. Figure 3 shows the temperature-dependent specific heat coefficient $\frac{C_V}{T} = \frac{dS}{dT}$ and the *full* magnetic susceptibility $\chi(T)$. There is a smooth crossover from local moment behavior at high temperatures $\chi \sim n_b(1 + n_b)/T$ to Fermi liquid behavior at low temperatures. From a Nozières-Blandin description of the local Fermi liquid [25] (where channel and charge suscep-
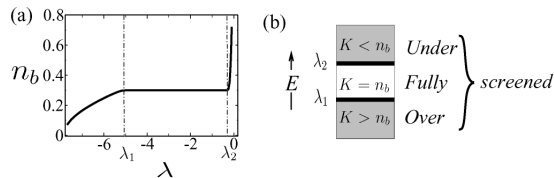

FIG. 1.   Leading contributions to $Y[\mathcal{G}]$ in $1/N$ expansion. Solid, dashed, and wavy lines, respectively, represent G_c, G_χ, and G_b. Each vertex is associated with a factor $i/\sqrt{N}$. Bracketed terms are dropped in the large N limit.

FIG. 2.   (a) Calculated variation of occupancy as a function of boson chemical potential λ in the ground state for $k = 0.3$ and $T/T_K = 0.005$. (b) A spinon gap develops in the fully screened state.
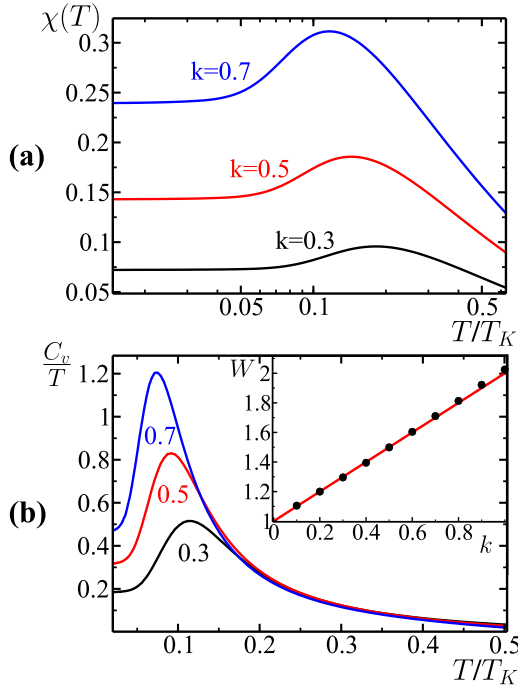
240

FIG. 3 (color online). Showing temperature dependence of (a) impurity magnetic susceptibility and (b) specific heat capacity in the fully screened Kondo model for $k = 0.3, 0.5, 0.7$ (with the Kondo temperature given by $T_K = D e^{-2D/J_K}$, D being the electron bandwidth). Inset calculated Wilson ratio.

tibility vanish), we deduce the Wilson ratio

$$W = \frac{\chi/\gamma}{\chi_0/\gamma_0} = \frac{(1+k)}{1 - 1/N^2}. \qquad (9)$$

This form is consistent with Bethe Ansatz results [23]. We may also derive this result by applying Luttinger-Ward techniques [26] to our model. Our large N approximation reproduces the limiting large N behavior of this expression, $W = 1 + k$; in other words, the local Fermi liquid is interacting in this particular large N limit.

Having demonstrated that our method captures the thermodynamic aspects of the Fermi liquid behavior in the single impurity model, we now show it can handle magnetic correlations within the two-impurity Kondo model,

$$H = \sum_{\vec{k},\nu,\alpha} \epsilon_{\vec{k}} c^\dagger_{\vec{k}\nu\alpha} c_{\vec{k}\nu\alpha} + H_K(1) + H_K(2) - \frac{J_H}{N} B^\dagger_{12} B_{12}, \quad (10)$$

where $H_K(i)$ is the Kondo Hamiltonian for impurity (i) and the antiferromagnetic interaction between the two moments is expressed in terms of the boson pair operator $B_{12} = \sum_\alpha \text{sgn}(\alpha) b_{1\alpha} b_{2-\alpha}$. H is invariant under spin transformations in the symmetry group SP (N) (N-even) [27].

We now factorize the antiferromagnetic interaction [17],

$$-\frac{J_H}{N} B^\dagger_{12} B_{12} \rightarrow \bar{\Delta} B_{12} + B^\dagger_{12} \Delta + \frac{N\bar{\Delta}\Delta}{J_H}. \qquad (11)$$

Boson pairing is associated with the establishment of short-range antiferromagnetic correlations. Once Δ becomes nonzero, the local gauge symmetry is broken, and the Schwinger bosons propagate from site to site. In this state, the holons delocalize, giving rise to a mobile, charged yet spinless excitation that is gapped in the Fermi liquid. Loosely speaking, on a lattice, these excitations are mobile Kondo singlets. However, since the paired Schwinger bosons interconvert from particle to hole as they move, they only induce holon motion within the *same* sublattice. Therefore, in the special case of two-impurity model, so long as the net coupling between the spins is antiferromagnetic, the holons remain localized.

Under these conditions, we can adapt the single impurity equations to the two-impurity model by replacing

$$G_b(\omega) \rightarrow \tilde{G}_b(\omega) = [G_b(\omega)^{-1} - |\Delta|^2 G_b(-\omega)^*]^{-1} \quad (12)$$

in the integral equations. We must also impose self-consistency $\Delta = -J_H \langle B_{12} \rangle$, or

$$\frac{1}{J_H} = -\int \frac{d\omega}{\pi} \text{Im} \left(\frac{1 + 2n_B(\omega)}{G_b^{-1}(\omega) G_b^{-1}(-\omega)^* - |\Delta|^2} \right). \quad (13)$$

We have solved the integral equations with this modified boson propagator. Using the entropy as a guide, we are able to map out the phase diagram (Fig. 4.).

We find that the development of $\Delta \neq 0$ preserves the linear temperature dependence of the entropy at low temperatures, indicating Fermi liquid behavior. However, as the J_H increases, the confining gap for the creation of free spinons and holons collapses towards zero, and the corresponding temperature range of Fermi liquid behavior ultimately vanishes at a critical value of $J_H = J_c$. For $J_H > J_c$, the holon-spinon gap becomes finite again and Fermi liquid behavior reemerges, but the phase shift δ_χ is found to have jumped from π to zero, indicating a collapse of the Kondo resonance. The entropy develops a finite value at the quantum critical point which is numerically identical to half the high temperature entropy of a local moment, $(N/2)[(1 + n_b) \ln(1 + n_b) - n_b \ln n_b]$. Similar behavior occurs at the "Varma-Jones" fixed point [28–30] in the $N = 2$ two-impurity model when the conduction band is particle-hole symmetric. We can in fact identify two maxima in the specific heat, indicating that as in the $N = 2$ Varma-Jones fixed point, the antiferromagnetic coupling generates a second set of screening channels, leading to a two-stage quenching process.

The survival of the Varma-Jones fixed point at large N in the absence of particle-hole symmetry is a consequence of the two-impurity Friedel sum rule,
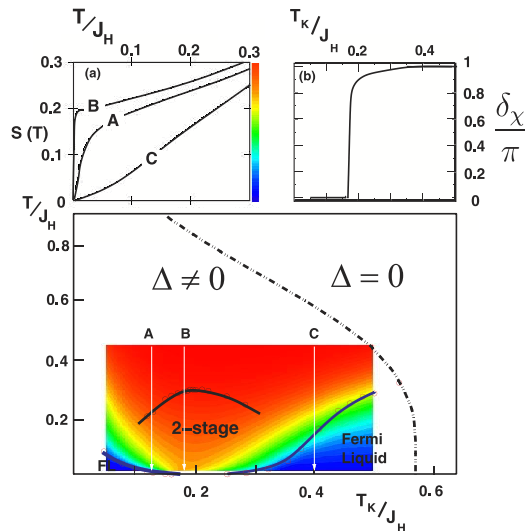
016601-3

FIG. 4 (color online). Phase diagram for the two-impurity Kondo model showing the boundary where boson pairing develops. Color coded contours delineate the entropy around the Varma-Jones fixed point. Black line indicates upper maximum in specific heat, blue line, lower maximum in specific heat where crossover into the Fermi liquid takes place. Inset: (a) entropy for various values of T_K/J_H, (b) showing dependence of δ_χ on T_K/J_H at a temperature $T/T_K = 0.02$.

$$(\delta_+ + \delta_-) = \frac{2\pi}{N}, \qquad (14)$$

where $\delta_\pm$ are the even and odd parity scattering phase shifts. For $N = 2$, it is possible to cross smoothly from unitary scattering off both impurities ($\delta_\pm = \frac{\pi}{2}$), to no scattering off either ($\delta_+ = \pi$, $\delta_- = 0$) while preserving the sum rule, but for $N > 2$, the sum rule cannot be satisfied in the absence of scattering, and the collapse of the Kondo effect must occur via a critical point.

In conclusion, we have shown that a Schwinger boson approach to the fully screened Kondo model can be naturally extended to incorporate magnetic interactions. In the simplest case of a two-impurity Kondo model our approach captures the transition between the state where the two impurities are antiferromagnetically correlated and the Kondo Fermi liquid state. In the large N limit, these two states are separated by a quantum critical point, a possible precursor of an antiferromagnetic quantum critical point. One of the interesting new elements is the appearance of mobile, yet gapped "holon" excitations in the antiferromagnetically correlated Fermi liquid. In the two-impurity model these holons become gapless at the quantum critical point. Future work will examine whether this same scenario also operates at a heavy electron quantum critical point, leading to quantum critical matter with spin-charge decoupling [1,13].

[1] P. Coleman, C. Pépin, Q. Si, and R. Ramazashvili, J. Phys. Condens. Matter **13**, R723 (2001).
[2] T. Moriya and J. Kawabata, J. Phys. Soc. Jpn. **34**, 639 (1973); **35**, 669 (1973).
[3] J. A. Hertz, Phys. Rev. B **14**, 1165 (1976).
[4] A. J. Millis, Phys. Rev. B **48**, 7183 (1993).
[5] J. Custers et al., Nature (London) **424**, 524 (2003).
[6] H. v. Lohneysen et al., Phys. Rev. Lett. **72**, 3262 (1994).
[7] N. Mathur et al., Nature (London) **394**, 39 (1998).
[8] M. Grosche et al., J. Phys. Condens. Matter **12**, L533 (2000).
[9] O. Trovarelli et al., Phys. Rev. Lett. **85**, 626 (2000).
[10] A. Schroeder et al., Nature (London) **407**, 351 (2000).
[11] Q. Si, S. Rabello, K. Ingersent, and J. L. Smith, Nature (London) **413**, 804 (2001).
[12] T. Senthil, S. Sachdev, and M. Vojta, Physica (Amsterdam) **359-361B**, 9 (2005).
[13] C. Pépin, Phys. Rev. Lett. **94**, 066402 (2005).
[14] K. G. Wilson, Phys. Rev. D **7**, 2911 (1973).
[15] N. Read and D. M. Newns, J. Phys. C **16**, 3273 (1983).
[16] A. Auerbach and K. Levin, Phys. Rev. Lett. **57**, 877 (1986).
[17] D. P. Arovas and A. Auerbach, Phys. Rev. B **38**, 316 (1988).
[18] O. Parcollet and A. Georges, Phys. Rev. Lett. **79**, 4665 (1997); O. Parcollet, A. Georges, G. Kotliar, and A. Sengupta, Phys. Rev. B **58**, 3794 (1998).
[19] P. Coleman and I. Paul, Phys. Rev. B **71**, 035111 (2005).
[20] P. Coleman, I. Paul, and J. Rech, Phys. Rev. B **72**, 094430 (2005).
[21] J. M. Luttinger and J. C. Ward, Phys. Rev. **118**, 1417 (1960).
[22] O. Parcollet, Ph.D. thesis, 1998, http://www-spht.cea.fr/pisp/parcollet/ (unpublished).
[23] A. Jerez, N. Andrei, and G. Zarand, Phys. Rev. B **58**, 3814 (1998).
[24] N. Andrei and P. Zinn Justin, Nucl. Phys. **B528**, 648 (1998).
[25] P. Nozières and A. Blandin, J. Phys. (France) **41**, 193 (1980).
[26] A. Yoshimori, Prog. Theor. Phys. **55**, 67 (1976).
[27] N. Read and S. Sachdev, Phys. Rev. Lett. **66**, 1773 (1991).
[28] B. A. Jones and C. M. Varma, Phys. Rev. Lett. **58**, 843 (1987).
[29] B. A. Jones, B. G. Kotliar, and A. J. Millis, Phys. Rev. B **39**, 3415 (1989).
[30] J. Gan, Phys. Rev. Lett. **74**, 2583 (1995).

PUBLICATION 5

Conserving many-body approach to the $U \to \infty$ Anderson model

cond-mat/0601015

Conserving many body approach to the fully screened, infinite U Anderson model.

Eran Lebanon[1], Jerome Rech[1,2], P. Coleman[1] and Olivier Parcollet[2]

[1] *Center for Materials Theory, Serin Physics Laboratory,*
Rutgers University, Piscataway, New Jersey 08854-8019, USA.
[2] *Service de Physique Théorique, CEA/DSM/SPhT - CNRS/SPM/URA*
2306 CEA/Saclay, F-91191 Gif-sur-Yvette Cedex, FRANCE

Using a Luttinger Ward scheme for interacting gauge particles, we present a conserving many body treatment of a family of fully screened infinite U Anderson models that has a smooth crossover into the Fermi liquid state, with a finite scattering phase shift at zero temperature and a Wilson ratio greater than one. We illustrate our method, computing the temperature dependence of the thermodynamics, resistivity and electron dephasing rate and discuss its future application to non-equilibrium quantum dots and quantum critical mixed valent systems.

The infinite U Anderson model is a central element in the theory of heavy electron systems and quantum dots. This model describes a high temperature regime of incoherent valence and spin fluctuations, separated by a crossover from a low temperature Fermi liquid. Over the years since it was first solved by the numerical renormalization group[1] and Bethe Ansatz[2], there have been many attempts to develop alternative diagrammatic approaches with the flexibility to extend to the lattice or to non-equilibrium situations. Examples include the large N slave boson approach [3, 4], the non-crossing approximation (NCA)[5] and various vertex-corrected versions of this same model[6]. However, none of these schemes to date is able to capture the smooth cross-over into a well-developed Fermi liquid. In this paper, we present a new diagramatic solution to this long-standing problem.

The root of these difficulties is traced back to the infinite U constraint which introduces gauge particles, such as the slave boson, which carry fractional charge or spin. The challenge then, is to find a consistent and practical scheme by which these particles disappear in the low-energy Fermi liquid. One approach is to condense the slave boson, but this replaces the cross-over into the Fermi liquid with a fictitious phase transition[3, 4]. In the NCA and its various diagrammatic descendants, the presence of gapless gauge particles prevents the development of a Kondo resonance which properly satisfies the Friedel sum rule[5, 6]. In this paper we extend a recent Schwinger boson description of the Kondo model to encompass the valence fluctuations of the infinite U Anderson model and we show how the past difficulties are removed through the development of a gap in the Schwinger boson and slave fermion spectrum. A new element of the current work, is the use of a Kadanoff Baym scheme that enables us to approximately treat the Anderson model with a finite spin degeneracy $N = 2j + 1$, while preserving a list of exact conserving relations which develop in the the Fermi liquid. Our method is scalable to a lattice, and can also be extended to non-equilibrium settings. To demonstrate the method we compute the

temperature dependent thermodynamics, resistivity and electron dephasing rate in a single impurity model, and discuss how the method can be extended to encompass a non-equilibrium environment.

Our starting point is a Schwinger boson representation for the $SU(N)$ infinite U Anderson model. Schwinger bosons can be used to describe magnetically ordered local moments, and in the limit of large N, this description becomes exact[7]. Recent progress [8, 9] has shown how this scheme can be expanded to encompass the Fermi liquid physics of the Kondo effect. through the study of a family of "multichannel" Kondo models, in which the number of channels K is commensurate with $n_b = 2S$, $(K = 2S)$, where S is the spin of the local moment. By reinstating the valence fluctuations to this model, we obtain the following infinite U Anderson model

$$
\begin{aligned}
\mathcal{H} &= \sum_{\vec{k}\nu\alpha} \epsilon_{\vec{k}} c^\dagger_{\vec{k}\nu\alpha} c_{\vec{k}\nu\alpha} + \frac{V}{\sqrt{N}} \sum_{\vec{k}\nu\alpha} \left[c^\dagger_{\vec{k}\nu\alpha} \chi^\dagger_\nu b_\alpha + \text{H.c} \right] \\
&+ \epsilon_0 \sum_\alpha b^\dagger_\alpha b_\alpha - \lambda(Q - 2S).
\end{aligned}
\tag{1}
$$

Here $c^\dagger_{\vec{k}\nu\alpha}$ creates a conduction electron with momentum $\vec{k}$, channel index $\nu \in [1, K]$, and spin index $\alpha \in [1, N]$. The bilinear product $b^\dagger_\alpha \chi_\nu$ between a Schwinger boson $b^\dagger_\alpha$, and a slave fermion (or holon) operator χ_ν creates a localized electron in the constrained Hilbert space, which hybridizes with the conduction electrons. The $\sqrt{N}$ denominator in the hybridization ensures a well-defined large N limit. The energy of a singly occupied impurity ϵ_0 is taken to be negative. The conserved operator $Q = \sum_\alpha b^\dagger_\alpha b_\alpha + \sum_\nu \chi^\dagger_\nu \chi_\nu$ replaces the no-double occupancy constraint of the infinite U Anderson model, where $Q = 2S = K$ is required for perfect screening.

The characteristic "Kondo scale" of our model is

$$
T_K = D \left(\frac{\Gamma}{\pi D} \right)^{K/N} \exp \left\{ -\frac{\pi|\epsilon_0|}{\Gamma} \right\},
\tag{2}
$$

where D is the conduction electron half bandwidth, $\Gamma = \pi\rho V^2$ is the hybridization width and ρ is the conduction

electron density of states. The Kondo temperature is determined from the high temperature scaling and the prefactor derives from third order terms in the beta function that are finite in the multi-channel large N limit where $K/N = k$ is fixed. Notice however, that the coefficient relating low temperature properties, such as the specific heat coefficient $\gamma = a(1/N, k)/T_K$ to the Kondo temperature, will in general exhibit non-trivial N dependence.

The next step is to construct the LW functional $Y[G]$. The variation of $Y[G]$ with respect to the full Green's functions G_ζ of the conduction, Schwinger boson and slave fermion fields, $\Sigma_\zeta = \delta Y/\delta G_\zeta$, self-consistently determines the self-energies Σ_ζ of these fields[10, 11]. $Y[G]$ is equal to the sum of all two-particle irreducible free energy Feynman diagrams, grouped in powers of $1/N$ [Fig.1(a)]. In our KB approximation we neglect all but the leading order $O(N)$ term in the LW functional, and then impose the full self-consistency generated by this functional. Unlike earlier NCA approaches, the constraint is implemented order by order in $1/N$, by including fluctuations in the chemical constraint λ. By taking the leading order KB approximation we neglect the fluctuations in the gauge field λ, and concentrate on the properties in the grand canonical ensemble where the constraint is imposed on the average. The explicit expressions for the self-energies are then

$$
\begin{aligned}
\Sigma_\chi(\tau) &= V^2 G_b(\tau) G_c(-\tau) \\
\Sigma_b(\tau) &= -(K/N)V^2 G_\chi(\tau) G_c(\tau) \\
\Sigma_c(\tau) &= (1/N)\, V^2 G_b(\tau) G_\chi(-\tau)
\end{aligned}
\tag{3}
$$

where G_b, G_χ and G_c are the fully dressed imaginary time Green's functions of the boson, holon and conduction electrons respectively. Equations (3) are solved self consistently, adjusting the chemical potential λ to satisfy the averaged constraint $\langle Q \rangle = K$.

A key step in the derivation of the Ward identities is the presence of an infrared cutoff in the excitation spectrum, which permits us to replace Matsubara summations by integrals at low temperatures:

$$
T \sum_{i\omega_n} \to \int \frac{d\omega}{2\pi}
$$

This transformation is the key to derivations of the Friedel sum rule, the Yamada-Yosida and Shiba relationships between susceptibilities, specific heat and spin relaxation rates[12–14]. Past attempts to develop conserving approximations to the infinite U Anderson model [15] have run into X-ray singularities in the slave particle spectrum which prevent the above replacement. In the multi-channel approach, the formation of a stable Kondo singlet when $2S = K$ yields a gap in the spinon and holon spectrum [Fig. 1(c)] which stablizes the Fermi liquid at sub-gap energies. This feature permits all of the manipulations previously carried out on the finite U Anderson model to now be extended to infinite U. Each of
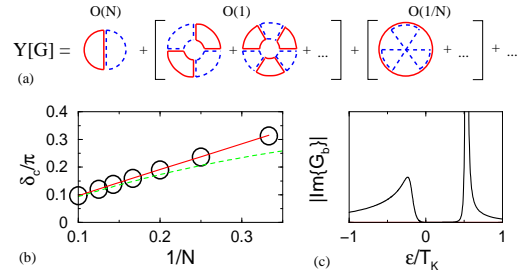

FIG. 1: (a)LW functional expanded in powers of $1/N$. Solid line - Schwinger bosons, dashed lines - holons, double lines - conduction electrons. Loops contribute a factor N, vertices a factor $1/\sqrt{N}$. (b) Phase shift extracted from the t-matrix, for $K = 1$, $n_\chi \approx 0.04$. Solid line: $(K - n_\chi)/(NK)$, dotted line, phase shift obtained without self-consistency on conduction lines, (c) Gapped Schwinger boson spectrum in ground-state.

these relationships are satisfied by the use of the leading LW functional. The Friedel sum rule equates the sum of the electron phase shifts to the charge $K - n_\chi$ on the impurity, where n_χ is the ground-state holon occupancy,

$$
\delta_c = \frac{\pi}{N}\frac{K - n_\chi}{K} + O\left(\frac{T_K}{ND}\right),
\tag{4}
$$

Fig.1(b) shows how the phase shift extracted from the t-matrix in our conserving scheme satisfies this relation.

According to Nozières Fermi liquid theory[16], the quasiparticle spectrum in the Kondo ground-state is related to the conduction electron phase shift. The change in the phase shift in an applied field, or change in chemical potential, is related to the spin, charge and channel susceptibilities, which in turn, leads to a generalized "Yamada-Yosida-Yoshimori" identity[13, 17] describing the distribution of the NK degrees of freedom among the spin, flavor and charge susceptibilities:

$$
NK\frac{\gamma}{\gamma^0} = K\frac{N^2 - 1}{N + K}\frac{\chi_s}{\chi_s^0} + N\frac{K^2 - 1}{K + N}\frac{\chi_f}{\chi_f^0} + \frac{\chi_c}{\chi_c^0}.
\tag{5}
$$

Here γ stands for the specific heat coefficient $\gamma = C/T$, and χ_s, χ_f and χ_c stand for the spin, flavor and charge susceptibilities. $\chi_{s,f,c}^0$ denotes the corresponding susceptibilities in the absence of the impurity. Our identity (5) reduces to the known results for the Wilson ratio in the one channel model[13] and the Kondo limit[18]. By preserving the Friedel sum rule in each channel, our method automatically satisfies this relationship.

Various thermodynamic quantities can be extracted from the numerical solution of the self-consistent equations. Following [11], the entropy $S(T)$ is given by

$$
S = -\text{Tr}_\zeta \int d\epsilon \frac{dn_\zeta}{dT}\left[\text{Im}\ln\left(-G_\zeta^{-1}\right) + G_\zeta'\Sigma_\zeta''\right],
\tag{6}
$$

where the trace denotes a sum over the spin and channel indices of the various fields and n_ζ is the distribution
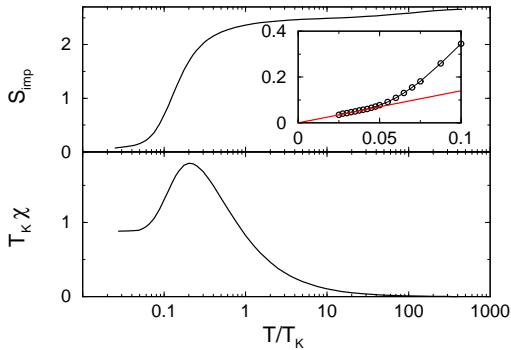
FIG. 2: (a)temperature dependence of impurity entropy S_{imp}. showing linear temperature dependence at low temperature. (b)magnetic susceptibility of impurity vs temperature, calculated for K=1, N=4 (See Fig. 3).
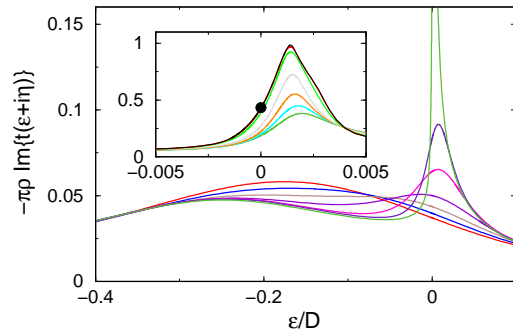

FIG. 3: t-matrix for $\epsilon_0/D = -0.2783$, $\Gamma/D = 0.16$, $N = 4$ and $K = 1$ ($T_K/D = 0.002$). Main frame: T/D=0.1, 0.08, 0.06, 0.04, 0.02, and 0.01. Inset: $T/10^{-4}D$=10, 8, 6, 4, 2, 1, and 0.5. The dot marks $\sin^2\{\pi(K - n_\chi)/NK\}$

function (Fermi for $\zeta = c, \chi$ and Bose for $\zeta = b$). G_ζ and Σ_ζ respectively denote the retarded Green functions and self energies. The single and double primes mark the real and imaginary part respectively. The impurity contribution to the entropy $S_{\text{imp}} = S - S_0$, where S_0 is the entropy of the bare conduction band, is shown in Fig. 2. The linear behavior of the impurity contribution to the entropy at low temperatures marks the saturation of the specific heat coefficient $\gamma_{\text{imp}} = \partial S_{\text{imp}}/\partial T$ and the formation of a local Fermi liquid.

To calculate the spin susceptibility, we couple a small magnetic field to the magnetization, defined as

$$M = \sum_\alpha \text{sgn}(\alpha - \frac{N+1}{2})\left(b_\alpha^\dagger b_\alpha + \sum_{\vec{k},\nu} c_{\vec{k}\nu\alpha}^\dagger c_{\vec{k}\nu\alpha}\right).$$

The impurity magnetization is obtained by subtracting from M the free conduction sea contribution. We compute the magnetization by iterating the solutions to self-consistency in a small magnetic field[19]. Fig. (2) shows the impurity susceptibility $\chi(T)$, which is peaked slightly below T_K and saturates to a constant in the ground-state.

One of the important conservation laws associated with the conservation of spin is the Korringa Shiba relation between the dynamic and static spin susceptibility. On the assumption that the gauge particles are gapped, the LW derivation carried out by Shiba on the finite U Anderson model, can be simply generalized to the infinite U model, to obtain $\chi''(\omega)/\omega|_{\omega=0} = (N\pi/K)(\chi/N)^2$. This relationship guarantees that the power-spectrum of the magnetization is linear at low frequencies, ensuring that the spin response function decays as $1/t^2$ in time. Remarkably, a Fermi liquid, with slow gapless spin excitations is sandwiched beneath the spinon-holon continuum.

We now turn to a discussion of the electron scattering off the impurity, which is determined by the conduction electron t-matrix, $t(z) = \frac{\Sigma_c}{1-G_c^{(0)}\Sigma_c}$, where $G_c^0(z) =$

$\sum_{\vec{k}}(z - \epsilon_{\vec{k}})^{-1}$ is the bare local conduction electron propagator. Various important physical properties, such as the impurity resistivity and the electron dephasing rate in the dilute limit can be related to this quantity. Fig. 3 shows the imaginary part of $t(\epsilon + i\eta)$: as temperature is lowered towards T_K, a resonance peak develops around the Fermi energy. The peak ultimately saturates about a decade below the Kondo temperature and the height of the fully developed resonance at the Fermi energy corresponds to that predicted by the Langreth sum-rule[12] value $-\sin^2\delta_c/\pi\rho$, as shown in Fig.3.

The impurity contribution to the resistivity R_i is related to a thermal average of the $t-$ matrix,

$$\frac{R_i}{R_U} = n_i\left[\int d\epsilon\left(-\frac{\partial f}{\partial \epsilon}\right)|\pi\rho\text{Im}t(\epsilon + i\eta)|^{-1}\right]^{-1}. \quad (7)$$

where R_U is the unitary resistivity of the electron gas and f is the Fermi function. The resistivity (Fig. 4) saturates at low temperatures at the value $n_i R_U \sin^2\delta_c$.

As a final application of the t-matrix, we compute the electron dephasing rate τ_ϕ^{-1} that controls the field dependence of weak electron localization. In the cross-over to the Fermi liquid state, the formation of the Kondo resonance gives rise to a peak in the inelastic scattering[20] and electron dephasing rate [21]. In the dilute limit, the impurity contribution to the dephasing rate is given by $\tau_\phi^{-1} = 2n_i[-\text{Im}t - \pi\rho|t|^2]$ [20, 22, 23]. Fig. 4 shows the computed temperature dependence of the dephasing rate on the Fermi surface.

Our calculation of the dephasing rate captures the cross-over into the coherent Fermi liquid, but the quadratic temperature dependence of the electron dephasing rate expected at low temperatures is absent from the current work. This is because the electron-electron scattering diagrams responsible for the Fermi-liquid contribution to the dephasing rate involve an internal loop of gauge particles which first appears in the subleading
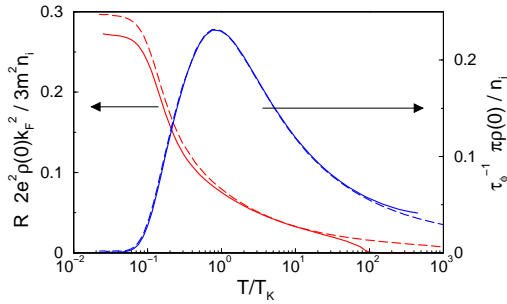
FIG. 4: The impurity contribution to the resistivity R_i and dephasing rate τ_ϕ^{-1} as a function of temperature. Solid lines: the parameters used in Fig. 3, dashed lines: $\Gamma = 0.1D$.

$O(1)$ terms of the LW functional shown in Fig. 1(a). We hope to include the effects of these diagrams in future work by approximating these scattering vertices by their ground-state, on-shell value, which is rigorously related to γ by Ward identities [13].

An interesting direction for future development is the extension to non-equilibrium quantum dots[24]. Calculations of the Kondo physics of voltage biased quantum dots are currently based Keldysh extensions of noncrossing integral equations [25] which do not capture the Fermi liquid physics at low voltage bias. These methods can be readily adapted to the current Schwinger boson scheme[26]. Many features of our approach, its conserving properties, the inclusion of scaling properties up to third order in the beta function and its systematic incorporation of spin relaxation effects on the boson lines, suggest that this will be a robust method to examine how spin and electron dephasing effects evolve with voltage in quantum dots. These methods can also be used to study the voltage dependence [27] of the distribution function and noise in magnetically doped mesoscopic wires[28, 29].

One of the striking features of the Schwinger boson approach to the Kondo and infinite U Anderson models, is the co-existence of a gapless Fermi liquid, sandwiched at low energies between a gapped spinon and holon fluid, arising as a consequence of the development of bound-states within this fluid. The methods presented here can be scaled up to the Anderson and Kondo lattice models, where the Friedel sum rule "upgrades" into the Luttinger sum rule[11]. Here, the local $U(1)$ symmetry is broken down to a global one by the pair-condensed Schwinger bosons[30] and the spinons and holons become propagating excitations of the bulk, whose gap is fundamental to the large Fermi surface. It is this very gap that we expect to collapse at a quantum critical point. The current work, which includes the effects of valence fluctuations, provides a powerful framework for exploring this physics.

[1] K.G. Wilson, Rev. Mod. Phys. **47**, 773 (1975).
[2] For a review see A. Tsvelik and P.B. Wiegmann, Adv. in Phys. **32**, 453 (1983).
[3] A.J. Millis and P.A. Lee, Phys. Rev. B **35**, 3394 (1987).
[4] P. Coleman, Phys. Rev. B **29**, 3035 (1984).
[5] N.E. Bickers, Rev. Mod. Phys. **59**, 845 (1987).
[6] K. Haule et al., Phys. Rev. B **64** 155111 (2001)
[7] D.P. Arovas, and A. Auerbach, Phys. Rev. B **38**, 316 (1988).
[8] O. Parcollet, and A. Georges, Phys. Rev. Lett. **79**, 4665 (1997).
[9] J. Rech, P. Coleman, G. Zaránd, and O. Parcollet,Phys. Rev. Lett. 96, 016601 (2006).
[10] J.-P. Blaizot, E. Iancu and A. Rebhan Phys. Rev. D **63**, 065003 (2001).
[11] P. Coleman, I. Paul, and J. Rech, Phys. Rev. B **72**, 094430 (2005).
[12] D.C. Langreth, Phys. Rev. **150**, 516 (1966).
[13] K. Yamada, Prog. Theor. Phys. **53**, 970 (1975); K. Yoshida and K. Yamada, *ibid.* **53**, 1286 (1975).
[14] H. Shiba, Prog. Theo. Phys 54, 967 (1975).
[15] Y. Kuramoto, Z. Phys. B **53**, 37 (1983); P. Coleman, Phys. Rev. B **28**, 5255 (1983); N.E. Bickers, Rev. Mod. Phys. **59**, 845 (1987); K. Haule et al., Phys. Rev. B 64, 155111 (2001).
[16] P. Nozières and A. Blandin, J. Physique, 41, 193, 1980.
[17] A. Yoshimori, Prog. Theor. Phys **55**, 67 (1976).
[18] A. Jerez, N. Andrei, and G. Zaránd, Phys. Rev. B **58**, 3814, (1998).
[19] E. Lebanon, A. Schiller, and V. Zevin, Phys. Rev. B **64**, 245338 (2001).
[20] G. Zaránd, L. Borda, J.v. Delft and N. Andrei, Phys. Rev. Lett. **93**, 107204 (2004).
[21] C. Van Haesendonck et al., Phys. Rev. Lett. **58**, 1968 (1987); R.P. Peters et al., Phys. Rev. Lett. **58**, 1964 (1987); F.J. Ohkawa, et al., J. Phys. Soc. Jpn. **52**, 1701 (1983).
[22] T. Micklitz, A. Altland, T.A. Costi, and A. Rosch, cond-mat/0509583 (2005).
[23] C. Baüerle et. al. Phys. Rev. Lett. **95**, 266805 (2005).
[24] L. Kouwenhoven and L. Glazman, Physics World, **14** 33 (2001).
[25] N. S. Wingreen and Y. Meir Phys. Rev. **B 49**, 11040 (1994); P. Nordlander et al.,Phys. Rev. Lett. **83**, 808 (1999).
[26] A. Posazhennikova, and P. Coleman, Phys. Rev. Lett. **94**, 036802 (2005).
[27] E. Lebanon, and P. Coleman, Phys. Rev. Lett. **95**, 046803 (2005).
[28] H. Pothier et al., Phys. Rev. Lett. **79**, 3490 (1997); A. Kaminski and L. I. Glazman, Phys. Rev. Lett. **86**, 2400 (2001); G. Göppert and H. Grabert, Phys. Rev. B **64**, 033301 (2001).
[29] J. Kroha and A. Zawadowski, Phys. Rev. Lett. **88**, 176803 (2002).
[30] M. Hermele et al, Phys. Rev. B 70, 214437 (2004).

Appendices

Generalized Luttinger-Ward scheme: free energy and entropy

Contents

In this appendix, we derive the free energy functional and the entropy for a single impurity using a Luttinger-Ward picture. The same kind of derivation extends to the Kondo lattice model and is presented in details in the Publication 3.

A.1   Free energy

The idea of the demonstration is to define a functional of the Green's functions and to prove that this definition matches the one of the free energy.

The full propagators of the theory are given by the following Dyson's equations:

$$
\begin{aligned}
G_b^{-1}(i\nu_n) &= i\nu_n + \lambda - \Sigma_b(i\nu_n) & \text{(A.1)}\\
G_\chi^{-1}(i\omega_n) &= J_K - \Sigma_\chi(i\omega_n) & \text{(A.2)}\\
G_c^{-1}(i\omega_n) &= G_{c0}^{-1}(i\omega_n) - \Sigma_c(i\omega_n) & \text{(A.3)}
\end{aligned}
$$

Following Luttinger and Ward, we will regard $G_{b,c,\chi}$ as a variational function, and $\Sigma_{b,c,\chi}$ as a derived quantity.

Generalized Luttinger-Ward scheme: free energy and entropy

We now consider the effect of tuning up the strength of the Kondo interaction from zero to J_K, by replacing $J_K \to \alpha J_K$ where $\alpha \in [0,1]$, keeping the chemical potential of the conduction electrons and bosons fixed. Now the partition function is given by

$$Z = Tr[e^{-\beta H}] = \int \mathcal{D}[c,b,\chi] e^{-\int_0^\beta \mathcal{L} d\tau} \tag{A.4}$$

where $\mathcal{D}[c,b,\chi]$ is the measure of the path integral. If we vary α inside this expression, we obtain

$$
\begin{aligned}
\frac{dZ}{d\alpha} &= \int \mathcal{D}[c,b,\chi] \sum_\nu \int_0^\beta d\tau \left(J_K \chi_\nu^\dagger \chi_\nu \right) e^{-\int_0^\beta \mathcal{L} d\tau} \\
&= \beta Z \times J_K \sum_\nu \langle \chi_\nu^\dagger \chi_\nu \rangle
\end{aligned}
\tag{A.5}
$$

so that if $F = -T \ln Z$ is the free energy, then

$$\frac{dF}{d\alpha} = -J_K \sum_\nu \langle \chi_\nu^\dagger \chi_{j\nu} \rangle = -K J_K T \sum_n G_\chi(i\omega_n), \tag{A.6}$$

We next consider the expression

$$
\begin{aligned}
\tilde{F} &= NT \sum_n \log(-G_b^{-1}(i\nu_n)) - KT \sum_n \log(-G_\chi^{-1}(i\omega_n)) \\
&\quad - NKT \sum_n \log(-G_c^{-1}(i\omega_n)) + NT \sum_n \Sigma_b(i\nu_n) G_b(i\nu_n) \\
&\quad - KT \sum_n \Sigma_\chi(i\omega_n) G_\chi(i\omega_n) - NKT \sum_n \Sigma_c(i\omega_n) G_c(i\omega_n) \\
&\quad + N p_0 \lambda + \Phi_{LW}[G_b, G_\chi, G_c]
\end{aligned}
\tag{A.7}
$$

where $\Phi_{LW}[G_b, G_\chi, G_c]$ is given by the sum of all closed, two-particle irreducible skeleton Feynman graphs for the Free energy.

As mentioned earlier, the Luttinger Ward functional $\Phi_{LW}[G_b, G_\chi, G_c]$ has the property that its variation with respect to $G_{b,c,\chi}$ generates the self energies,

$$
\begin{aligned}
\delta\Phi_{LW}[G_b, G_\chi, G_c] &= -N \int d\tau \Sigma_b(\tau) \delta G_b(\beta - \tau) - K \int d\tau \Sigma_\chi(\tau) \delta G_\chi(\beta - \tau) \\
&\quad - NK \int d\tau \Sigma_c(\tau) \delta G_c(\beta - \tau)
\end{aligned}
\tag{A.8}
$$

The variation of the log term in $\tilde{F}$ with respect to $G_{b,c,\chi}$ is given by

$$\delta \left(T \sum_n \log(-G^{-1}(i\omega_n)) \right) = -T \sum_n G^{-1}(i\omega_n) \delta G(i\omega_n) \tag{A.9}$$

By using the relation $\Sigma[G] = G_0^{-1} - G^{-1}$, the variation in the remaining terms in $\tilde{F}$ is given by

$$\delta \left(T \sum_n \Sigma(i\omega_n) G(i\omega_n) \right) = T \sum_n G_0^{-1}(i\omega_n) \delta G(i\omega_n) \tag{A.10}$$

Combining these variations with the one of the Luttinger-Ward functional, one sees that the variations of $\tilde{F}$ with respect to the Green's functions identically vanish:

$$\frac{\delta \tilde{F}}{\delta G_b} = \frac{\delta \tilde{F}}{\delta G_c} = \frac{\delta \tilde{F}}{\delta G_\chi} = 0. \tag{A.11}$$

Now the Hubbard Stratonovich transformation that we have carried out on the original Hamiltonian to decouple the Kondo interaction assures that the only place that the coupling constant αJ_K enters, is in $[G_\chi^0]^{-1} = \alpha J_K$. This means that in the r.h.s of Eq. (A.7) α enters explicitly only through $\Sigma_\chi = \alpha J_K - G_\chi^{-1}$. Then,

$$\begin{aligned}
\frac{d\tilde{F}}{d\alpha} &= \underbrace{\frac{\delta \tilde{F}}{\delta G_{b,c,\chi}}}_{=0} \frac{\partial G_{b,c,\chi}}{\partial \alpha} + \frac{\partial \tilde{F}}{\partial \alpha} \\
&= -KJ_K T \sum_n G_\chi(i\omega_n) \tag{A.12}
\end{aligned}$$

But by comparison with (A.6), we see that $\frac{d\tilde{F}}{d\alpha} = \frac{dF}{d\alpha}$ and since, $F(\alpha = 0) = \tilde{F}(\alpha = 0)$ in the non-interacting case, the two quantities must be equal for all α, i.e

$$\begin{aligned}
F &= NT \sum_n \log(-G_b^{-1}(i\nu_n)) - KT \sum_n \log(-G_\chi^{-1}(i\omega_n)) \\
&\quad -NKT \sum_n \log(-G_c^{-1}(i\omega_n)) + NT \sum_n \Sigma_b(i\nu_n) G_b(i\nu_n) \\
&\quad -KT \sum_n \Sigma_\chi(i\omega_n) G_\chi(i\omega_n) - NKT \sum_n \Sigma_c(i\omega_n) G_c(i\omega_n) \\
&\quad +Np_0\lambda + \Phi_{LW}[G_b, G_\chi, G_c] \tag{A.13}
\end{aligned}$$

There are various points to make about this derivation:

- The derivation is very general. Its correctness only depends on the stationarity of $\tilde{F}[G]$ with respect to variations in G and the equivalence between $dF/d\alpha$ and $d\tilde{F}/d\alpha$.

- The above Free energy functional can be used as a basis for developing conserving approximations that generalize the Kadanoff Baym approach to a constrained system[111].

A.2   Entropy

We know from the derivation of the self-energy equations from the Luttinger-Ward functional that $\Sigma_c \sim O\left(\dfrac{1}{N}\right)$. It then becomes possible to expand the electronic Dyson's equation in powers of $1/N$, which in turn leads to the following simplification in the free energy functional:

$$
-NKT\sum_n \log(-G_c^{-1}(i\omega_n)) = -NKT\sum_n \log(-G_{c0}^{-1}(i\omega_n))
$$
$$
+NKT\sum_n \Sigma_c(i\omega_n)G_{c0}(i\omega_n)
$$
$$
-NKT\sum_n \Sigma_c(i\omega_n)G_c(i\omega_n) = -NKT\sum_n \Sigma_c(i\omega_n)G_{c0}(i\omega_n)
$$

Combining these two terms, we are left with a term of order N^2 that corresponds to the free energy of the free electronic gas. Subtracting this bulk free energy from the one we are considering, we are left with the impurity contribution to the free energy, which one can write in terms of retarded Green's functions as:

$$
\begin{aligned}
\frac{F_{\text{imp}}}{N} = & \int \frac{d\omega}{\pi}\, n(\omega)\text{Im}\left(\log(-G_b^{-1}(\omega)) + G_b(\omega)\Sigma_b(\omega)\right) \\
& +\gamma \int \frac{d\omega}{\pi}\, f(\omega)\text{Im}\left(\log(-G_\chi^{-1}(\omega)) + G_\chi(\omega)\Sigma_\chi(\omega)\right) \\
& +p_0\lambda + \frac{1}{N}\Phi_{LW}[G_b, G_\chi, G_{c0}]
\end{aligned} \tag{A.14}
$$

Using the stationarity of the free energy with respect to the Green's functions and the chemical potential, one can directly read from (A.14) the expression for the impurity contribution to the entropy:

$$
\begin{aligned}
\frac{S_{\text{imp}}}{N} = & -\int \frac{d\omega}{\pi}\, \frac{\partial n(\omega)}{\partial T}\text{Im}\left(\log(-G_b^{-1}(\omega)) + G_b(\omega)\Sigma_b(\omega)\right) \\
& -\gamma \int \frac{d\omega}{\pi}\, \frac{\partial f(\omega)}{\partial T}\text{Im}\left(\log(-G_\chi^{-1}(\omega)) + G_\chi(\omega)\Sigma_\chi(\omega)\right) \\
& -\frac{1}{N}\frac{\partial \Phi_{LW}}{\partial T}
\end{aligned} \tag{A.15}
$$

One now has to work a little on the expression of the Luttinger-Ward functional in order to extract a closed form expression for its temperature derivative. First of all, we saw in Chapter 6 that only the leading order diagram of Φ_{LW} survives once we take the large-N limit, so that the Luttinger-Ward functional writes:

$$
\Phi_{LW}[G_b, G_\chi, G_c] = KJ^2 \int d\tau\, G_c(\tau)G_b(\beta - \tau)G_\chi(\beta - \tau) \tag{A.16}
$$

As a starting point, it is useful to convert the imaginary time original expression of the Luttinger-Ward functional into real frequency. In order to do so, we make the following substitution:

$$G_{\text{bosonic}}(\tau) = \int d\omega \; e^{-\omega\tau} n(-\omega)\rho_{\text{bosonic}}(\omega)$$

$$G_{\text{fermionic}}(\tau) = -\int d\omega \; e^{-\omega\tau} f(-\omega)\rho_{\text{fermionic}}(\omega) \tag{A.17}$$

where $0 \leq \tau \leq \beta$.

It follows, after performing the remaining integral over imaginary time:

$$
\begin{aligned}
\frac{\Phi_{LW}[G_b, G_\chi, G_c]}{N} &= -\gamma J^2 \oint d\omega_c d\omega_\chi d\omega_b \; \frac{\rho_b(\omega_b)\rho_c(\omega_c)\rho_\chi(\omega_\chi)}{\omega_\chi + \omega_b - \omega_c} \\
&\quad \times (f(\omega_c)n(-\omega_b)f(-\omega_\chi) + f(-\omega_c)n(\omega_b)f(\omega_\chi)) \\
&= -\gamma J^2 \oint d\omega_c d\omega_\chi d\omega_b \; \frac{\rho_b(\omega_b)\rho_c(\omega_c)\rho_\chi(\omega_\chi)}{\omega_\chi + \omega_b - \omega_c} \\
&\quad \times (f(\omega_\chi)n(\omega_b) - f(\omega_c)n(\omega_b) - f(\omega_c)(1 - f(\omega_\chi)))
\end{aligned}
\tag{A.18}
$$

Taking the derivative with respect to temperature, and using the argument of stationarity of the total free energy with respect to the Green's functions, one can write:

$$
\begin{aligned}
\frac{1}{N}\frac{\partial \Phi_{LW}}{\partial T} &= \gamma J^2 \oint d\omega_c d\omega_\chi d\omega_b \frac{\rho_b(\omega_b)\rho_c(\omega_c)\rho_\chi(\omega_\chi)}{\omega_\chi + \omega_b - \omega_c} \\
&\quad \times \left[\left(f(\omega_\chi)\frac{\partial n(\omega_b)}{\partial T} - f(\omega_c)\frac{\partial n(\omega_b)}{\partial T} \right) \right. \\
&\qquad + \left(n(\omega_b)\frac{\partial f(\omega_\chi)}{\partial T} + f(\omega_c)\frac{\partial f(\omega_\chi)}{\partial T} \right) \\
&\qquad \left. + \left(-n(\omega_b)\frac{\partial f(\omega_c)}{\partial T} - (1 - f(\omega_\chi))\frac{\partial f(\omega_c)}{\partial T} \right) \right]
\end{aligned}
\tag{A.19}
$$

One can recognize in this last expression a combination of Fermi and Bose functions reminiscent of the saddle-point equations for the self-energies. It turns out that using these saddle-point equations, Eq. (A.19) reduces to:

$$
\begin{aligned}
\frac{1}{N}\frac{\partial \Phi_{LW}}{\partial T} &= -\int \frac{d\omega}{\pi}\frac{\partial n(\omega)}{\partial T}G_b''(\omega)\Sigma_b'(\omega) - \gamma \int \frac{d\omega}{\pi}\frac{\partial f(\omega)}{\partial T}G_\chi''(\omega)\Sigma_\chi'(\omega) \\
&\quad - \gamma \int \frac{d\omega}{\pi}\frac{\partial f(\omega)}{\partial T}G_{c0}''(\omega)\tilde{\Sigma}_c'(\omega)
\end{aligned}
\tag{A.20}
$$

where $\tilde{\Sigma}_c = N\Sigma_c \sim O(1)$.

Plugging back the expression for $\frac{\partial \Phi_{LW}}{\partial T}$ into the impurity entropy, one sees that it cancels some of terms from the first part of the expression. The final entropy formula in the large-N limit then reads:

$$
\begin{aligned}
\frac{S_{\mathrm{imp}}}{N} \;=\; & -\int \frac{d\omega}{\pi} \left[\frac{\partial n(\omega)}{\partial T} \left(\mathrm{Im} \log\left(-G_b^{-1}(\omega) \right) + G_b'(\omega)\Sigma_b''(\omega) \right) \right. \\
& \left. + \gamma \frac{\partial f(\omega)}{\partial T} \left(\mathrm{Im} \log\left(-G_\chi^{-1}(\omega) \right) + G_\chi'(\omega)\Sigma_\chi''(\omega) - G_{c0}''(\omega)\tilde{\Sigma}_c'(\omega) \right) \right] \quad \text{(A.21)}
\end{aligned}
$$

As it turns out, a somewhat similar version of this entropy formula has been derived in the context of lattice gauge theory applied to Quantum Chromo-Dynamics, by Blaizot and collaborators [140]. The first attempts at deriving such a closed-form expression for the entropy trace back to the work of Carneiro and Pethick [141]. Note that, as we argue in Publication 3, this expression cannot be generalized to any model and applies here because we retain only the lowest order diagram in the Luttinger-Ward functional.

APPENDIX B

Local vs. impurity susceptibility

Contents

In this appendix, we compare the local to the impurity susceptibility. It is often much easier to compute the local susceptibility rather than the impurity susceptibility. However, most of the known analytical results (in particular for the exactly screened impurity) relates to the impurity susceptibility. We prove in this appendix that they are indeed related and can be considered roughly equal at zero-temperature, in the large bandwidth limit.

B.1 Local susceptibility

By definition, the local susceptibility is the response of the system to an applied external magnetic field that couples to the impurity spin *only*, hence the name

"local". In the case of a Schwinger boson representation of the impurity spin, this local susceptibility can be expressed as:

$$
\begin{aligned}
\chi_{\text{loc}} &= \frac{1}{N^2} \int_0^\beta d\tau \sum_{\alpha\beta} \langle S_{\alpha\beta}(\tau) S_{\beta\alpha}(0) \rangle \\
&= \int_0^\beta d\tau\, G_b(\tau) G_b(\beta - \tau) \\
&= \int \frac{d\omega}{\pi}\, n(\omega) \text{Im}\left[G_b(\omega + i\delta)^2 \right]
\end{aligned}
\tag{B.1}
$$

In terms of Feynman diagrams, one can represent the local susceptibility as a particle-hole bubble of bosonic lines, as is illustrated on Fig. B.1.
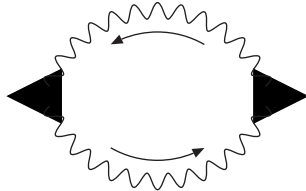

Figure B.1: Local spin susceptibility

B.2 Impurity susceptibility

The impurity susceptibility is defined as the response of the whole system to an external magnetic field, after one subtracts the contribution of the bulk conduction electrons. In this case, the magnetic field is coupled to both the impurity spin and the spin of the conduction electrons:

$$
\chi_{\text{imp}} = \chi_{\text{Total}} - \chi_{\text{bulk}}
\tag{B.2}
$$

In general, this impurity susceptibility is given by an infinite sum of Feynman diagrams. However, in the large-N limit, this sum becomes finite, and one only has to take into account a few diagrams on top of the local susceptibility, as represented in Fig. B.2. It is important to notice that all four[1] diagrams contributing to the impurity susceptibility have the same scaling in N, because every time a pair of vertices is included (factor of $(1/\sqrt{N})^2 = 1/N$) there is also an internal sum over the channel index (bringing a factor of γN).

---

[1]One shouldn't forget that χ_{loc} is the first diagram contributing to the impurity susceptibility

B.2.1 χ_2

The contribution from this diagram writes[2]:

$$
\begin{aligned}
\chi_2 &= -2\gamma J_K^2 T^2 \sum_{n,m} \left(\sum_{\mathbf{k}} \frac{1}{(i\omega_n - \epsilon_{\mathbf{k}})^2} \right) G_\chi(i\omega_n - i\nu_m) G_b(i\nu_m)^2 \\
&= 2T \sum_m V_b(i\nu_m) G_b(i\nu_m)^2 \\
&= 2 \int \frac{d\omega}{\pi} \, n(\omega) \text{Im} \left[V_b(\omega + i\delta) G_b(\omega + i\delta)^2 \right]
\end{aligned}
\tag{B.3}
$$

where we defined the "renormalized vertex" V_b as:

$$
\begin{aligned}
V_b(i\nu_m) &= -\gamma J_K^2 T \sum_n G_{c2}(i\omega_n) G_\chi(i\omega_n - i\nu_m) \\
&= -\gamma J_K^2 \int d\omega_1 d\omega_2 \rho_{c2}(\omega_1) \rho_\chi(\omega_2) \frac{f(\omega_1) - f(\omega_2)}{\omega_1 - \omega_2 - i\nu_m}
\end{aligned}
\tag{B.4}
$$

and $G_{c2}(i\omega_n) = \sum_{\mathbf{k}} \frac{1}{(i\omega_n - \epsilon_{\mathbf{k}})^2} = -\frac{\partial G_c}{\partial \omega}$.

Note that V_b has no dimension.

B.2.2 χ_3

Now that we have defined V_b, the contribution from χ_3 can trivially be rewritten as:

$$
\begin{aligned}
\chi_3 &= T \sum_m V_b(i\nu_m)^2 G_b(i\nu_m)^2 \\
&= \int \frac{d\omega}{\pi} \, n(\omega) \text{Im} \left[V_b(\omega + i\delta)^2 G_b(\omega + i\delta)^2 \right]
\end{aligned}
\tag{B.5}
$$

---

[2]We have dropped here the overall factor of N^2, since we want the impurity susceptibility to be of order $O(1)$.

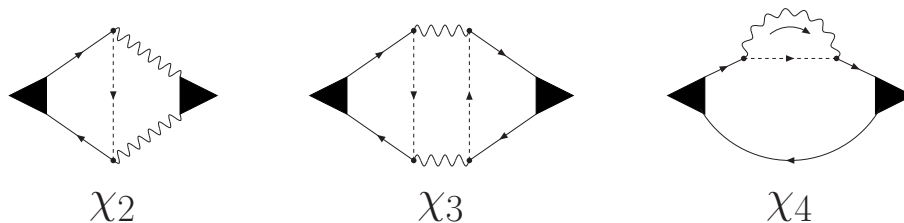$$\chi_2 \qquad\qquad \chi_3 \qquad\qquad \chi_4$$

Figure B.2: Extra diagrams to add to the local susceptibility to compute the impurity susceptibility. The straight lines correspond to the bare conduction electron propagator, the dotted lines to the full fermionic propagator, and the wavy lines to the full bosonic one.

B.2.3 χ_4

From the diagrammatic representation of χ_4, one recognizes the fermionic self-energy Σ_c defined in Chapter 6. χ_4 then writes:

$$
\begin{aligned}
\chi_4 &= -2\gamma N T \sum_n G_{c3}(i\omega_n)\Sigma_c(i\omega_n) \\
&= -2\gamma N \int \frac{d\omega}{\pi}\, f(\omega)\mathrm{Im}\left[G_{c3}(\omega+i\delta)\Sigma_c(\omega+i\delta)\right]
\end{aligned} \tag{B.6}
$$

where $G_{c3}(i\omega_n) = \sum_{\mathbf{k}} \frac{1}{(i\omega_n - \epsilon_{\mathbf{k}})^3} = \frac{1}{2}\frac{\partial^2 G_c}{\partial\omega^2}$.

Keep in mind that the conduction electron self-energy is of order $O(1/N)$ so that the overall external factor of N makes this contribution to the impurity susceptibility of order $O(1)$.

B.2.4 χ_{imp}

Putting everything together, one notices that the first three diagrams can be grouped into a simple form, leading to the final result:

$$
\begin{aligned}
\chi_{\mathrm{imp}} &= \int \frac{d\omega}{\pi} n(\omega) \left[G_b(\omega+i\delta)^2 \left(1 + V_b(\omega+i\delta)\right)^2\right] \\
&\quad + 2\gamma N \int \frac{d\omega}{\pi}\, f(\omega)\mathrm{Im}\left[G_{c3}(\omega+i\delta)\Sigma_c(\omega+i\delta)\right]
\end{aligned} \tag{B.7}
$$

B.3 Zero-temperature limit

In the case of a flat band of conduction electron, one can readily compute G_{c2} and G_{c3}:

$$
\begin{aligned}
G_{c0} &= -i\pi\rho_0\Theta(D^2 - \omega^2) \\
G_{c2} &= i\pi\rho_0\left(\delta(\omega+D) - \delta(\omega-D)\right) \\
G_{c3} &= \frac{-i\pi}{2}\rho_0\left(\delta'(\omega+D) - \delta'(\omega-D)\right)
\end{aligned} \tag{B.8}
$$

where we considered the large bandwidth limit, for which one can dropped the real part of G_{c0} since it is $O(\omega/D)$ smaller than the imaginary part.

From these expressions, one can compute the "renormalized vertex" V_b in the zero-temperature limit:

$$
V_b(\omega+i\delta) = \gamma\rho_0 J_K^2 \left[G'_\chi(-D) - G'_\chi(D)\right] \tag{B.9}
$$

In the large bandwidth limit, the zero-temperature self-energy of the $\chi-$fermion reads:

$$
\begin{aligned}
\Sigma_\chi(D) &= -i\pi\rho_0 J_K^2 p_0 \\
\Sigma_\chi(-D) &= -i\pi\rho_0 J_K^2 (1 + p_0)
\end{aligned}
\tag{B.10}
$$

Combining all these results, we can rewrite the zero-temperature impurity susceptibility as:

$$
\chi_{\text{imp}} = \left(1 + \frac{\pi^2\gamma(1 + 2p_0)(\rho_o J)^3}{[1 + (\pi\rho_0 Jp_0)^2]\,[1 + (\pi\rho_0 J(1 + p_0))^2]} \right)^2 \chi_{\text{loc}} + \gamma N\rho_0 \left.\frac{d\Sigma_c'}{d\omega}\right|_{\omega=-D}
\tag{B.11}
$$

As a conclusion, one can see from this last expression that at zero temperature, in the large bandwidth limit, it is possible to identify the local and the impurity susceptibility:

$$
D \gg T_K \implies \chi_{\text{loc}} \underset{T\to 0}{\sim} \chi_{\text{imp}}
\tag{B.12}
$$

APPENDIX C

Fermi liquid identities

Contents

In this appendix, we derive some of the important interrelationships between physical variables of the Fermi liquid, namely the Yamada-Yosida-Yoshimori relationship between spin, charge, flavor susceptibilities and specific heat [142, 143, 144].

Historically, this relationship was obtained from the analysis of a full perturbation theory. We present here a derivation similar in spirit to the one of Nozières and Blandin [107].

C.1 Scattering phase shift

The two basic electron-electron vertices have the following structure:

$$\Gamma_1 = c^{\dagger}_{\alpha\mu}c^{\dagger}_{\beta\mu'}c_{\beta\mu'}c_{\alpha\mu} \tag{C.1}$$

$$\Gamma_2 = c^{\dagger}_{\beta\mu}c^{\dagger}_{\delta\mu'}c_{\gamma\mu'}c_{\alpha\mu}\boldsymbol{\sigma}_{\alpha\beta}\cdot\boldsymbol{\sigma}_{\gamma\delta} \tag{C.2}$$

where Γ_1 and Γ_2 are recast in terms of Feynman diagrams in Fig. C.1, and $\sigma_{\alpha\beta}$ is a generator of $SU(N)$ verifying:

$$\boldsymbol{\sigma}_{\alpha\beta} \cdot \boldsymbol{\sigma}_{\gamma\delta} = 2\delta_{\alpha\delta}\delta_{\beta\gamma} - \frac{2}{N}\delta_{\alpha\beta}\delta_{\gamma\delta} \tag{C.3}$$

The most general combination invariant under both spin and channel rotation is then:

$$\sum_{\alpha\beta\mu\mu'} \left[A\, c^\dagger_{\alpha\mu} c^\dagger_{\beta\mu'} c_{\beta\mu'} c_{\alpha\mu} + B\, c^\dagger_{\beta\mu} c^\dagger_{\alpha\mu'} c_{\beta\mu'} c_{\alpha\mu} \right] \tag{C.4}$$

where we kept only the dominant terms in the large-N limit.

Considering a small departure from the Fermi liquid fixed point, these interaction terms are expected to be small, and can be treated within first order perturbation theory leading to the following effective Hamiltonian:

$$H_{\text{eff}} = 2 \sum_{\alpha\beta\mu\mu'} \left[A\left(1 - \delta_{\alpha\beta}\delta_{\mu\mu'}\right) + B\left(\delta_{\alpha\beta} - \delta_{\mu\mu'}\right) \right] \langle n_{\beta\mu'} \rangle n_{\alpha\mu} \tag{C.5}$$

where $n_{\alpha\mu} = c^\dagger_{\alpha\mu} c_{\alpha\mu}$ is the number operator, and $\langle n_{\alpha\mu} \rangle$ its expectation value.

One can then determine the scattering phase shift of an incoming conduction electron with quantum numbers α and μ as a function of the energy ϵ and the electron distribution $\delta\langle n_{\alpha\mu} \rangle$ measured from the ground-state. Using the above effective Hamiltonian, it is possible to reduce the general expression of the phase shift as:

$$
\begin{aligned}
\delta_{\alpha\mu} &= \delta_0 + \epsilon\delta' + \sum_{\beta\mu'} \phi_{\alpha\beta}\psi_{\mu\mu'}\delta\langle n_{\alpha\mu} \rangle \\
&= \delta_0 + \epsilon\delta' + \phi_1 \sum_{\beta\mu'} \left(\delta_{\mu\mu'} - \delta_{\alpha\beta}\right) \delta\langle n_{\beta\mu'} \rangle + \phi_2 \sum_{\beta\mu'} \left(1 - \delta_{\alpha\beta}\delta_{\mu\mu'}\right) \delta\langle n_{\beta\mu'} \rangle
\end{aligned} \tag{C.6}
$$

Following [126], the response of this phase shift to various field variations can be related to the specific heat and the susceptibilities.

C.2 Specific heat

Upon increasing the temperature, the electron energy changes like:

$$\tilde{\epsilon}_{\alpha\mu} = \epsilon - \frac{\delta_{\alpha\mu}(\tilde{\epsilon})}{\pi\rho_0} \tag{C.7}$$

where the phase shift is only given by the first two terms, the change of population $\delta\langle n \rangle$ due to an increase in temperature being zero.

This leads to the following change in the electronic density of states:

$$\delta\rho = \rho_0 \left[\frac{d\epsilon}{d\tilde{\epsilon}} - 1 \right] = \frac{\delta'}{\pi} \tag{C.8}$$
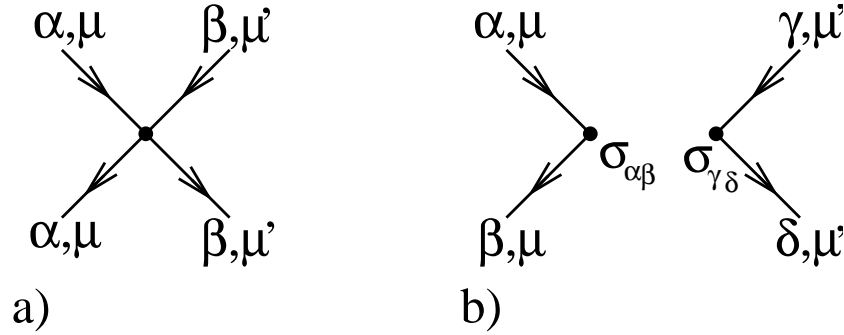
Figure C.1: Diagrammatic representation of the two basic electron-electron vertices: a) is the vertex already existing in the absence of the impurity (denoted as Γ_1), and b) is the vertex related to the scattering off the impurity (defined as Γ_2).

and hence a correction to the specific heat:

$$\frac{\delta C_v}{C_v} = \frac{\delta\rho}{\rho_0} = \frac{\delta'}{\pi\rho_0} \tag{C.9}$$

C.3 Susceptibilities

C.3.1 Charge susceptibility

Upon a small change in the chemical potential of the conduction electron Λ, one probes the change of the charge susceptibility, which can be expressed in terms of the scattering phase shift as:

$$\frac{\delta\chi_c}{\chi_c} = \frac{1}{\pi\rho_0}\frac{\Delta\delta_{\alpha\mu}}{\Delta\Lambda} \tag{C.10}$$

$$= \frac{1}{\pi\rho_0}\left[\delta' + \rho_0\phi_1(N-K) + \rho_0\phi_2(NK-1)\right] \tag{C.11}$$

where we have used that $\epsilon \sim \Delta\Lambda$ and $\delta\langle n\rangle \sim \rho_0\Delta\Lambda$.

C.3.2 Spin susceptibility

In order to extract the spin susceptibility, one has to apply an external magnetic field that couples to the system: the change in the spin susceptibility is then related to the response of the phase shift to this magnetic field in the same fashion as (C.10).

A variation of this magnetic field leads to a change in the electron population $\langle n_{\alpha\mu}\rangle \sim \rho_0\,\mathrm{Sgn}(\alpha - (N+1)/2)$, leading to the following result:

$$\frac{\delta\chi_s}{\chi_s} = \frac{1}{\pi\rho_0}\left[\delta' - \rho_0\phi_1 K - \rho_0\phi_2\right] \tag{C.12}$$

C.3.3 Channel susceptibility

Consider now an equivalent of the magnetic field that couples to the channel flavor. The same analysis as before leads to the channel susceptibility:

$$\frac{\delta\chi_f}{\chi_f} = \frac{1}{\pi\rho_0}\left[\delta' + \rho_0\phi_1 N - \rho_0\phi_2\right] \tag{C.13}$$

where we used that the change of electron population due to a variation of the channel field is $\langle n_{\alpha\mu}\rangle \sim \rho_0\,\mathrm{Sgn}(\mu - (K+1)/2)$.

C.4 Results

Combining (C.9), (C.11), (C.12) and (C.13), one can get rid of the variables δ', ϕ_1 and ϕ_2 and obtain an expression relating the specific heat and the various susceptibilities:

$$NK(N+K)\frac{\delta C_v}{C_v} = K(N^2-1)\frac{\delta\chi_s}{\chi_s} + N(K^2-1)\frac{\delta\chi_f}{\chi_f} + (N+K)\frac{\delta\chi_c}{\chi_c} \tag{C.14}$$

This relationship extends the Yamada-Yosida-Yoshimori relationship to the generalized $SU(N)\times SU(K)$ Kondo model, in the exactly screened case (in the other scaling regimes, one does not have a Fermi liquid at low temperature and the analysis à la Nozières is no longer valid).

In the case of a Kondo impurity, since the interaction conserves the number of conduction electron and does not affect the channel index, one expects that $\delta\chi_c = 0$ and $\delta\chi_f = 0$, so that (C.14) directly gives the Wilson ratio:

$$W = \frac{\delta\chi_s/\chi_s}{\delta C_v/C_v} = \frac{N(N+K)}{N^2-1} \tag{C.15}$$

which recovers the result obtained from Bethe ansatz [116].

Finally, in the large-N limit, this expression of the Wilson ratio reduces to:

$$W = 1 + \gamma \tag{C.16}$$

QCP in the two-impurity model: low-energy analysis

Contents

In this appendix, we derive the low-energy behavior of the Schwinger boson and $\chi-$fermion propagators, at the quantum critical point, in the case of a two-impurity Kondo-Heisenberg model.

D.1 Ansatz

As one approaches the quantum critical point from either side, the numerical solution suggests that both inverse propagators vanish at zero energy. Such a behavior

suggests that the Green's functions diverge like power-laws at zero frequency. Our starting point is then given by the following ansatz for the propagators:

$$G_b(\omega) \sim \frac{A_+\Theta(\omega) + A_-\Theta(-\omega)}{|\omega|^\alpha} \tag{D.1}$$

$$G_\chi(\omega) \sim \frac{B_+\Theta(\omega) + B_-\Theta(-\omega)}{|\omega|^\beta} \tag{D.2}$$

where $\Theta(\omega)$ is the Heaviside function, $A_\pm$ and $B_\pm$ are complex numbers and we separate the positive from the negative energy sectors in case of a spectral asymmetry.

Since we are interested in what happens at the quantum critical point, we consider the zero-temperature limit of the saddle-point equations defining the self-energies:

$$\begin{cases} \Sigma_b(\omega) = -\gamma J^2 \rho_0 \left(\int_{-\omega}^{-D} d\Omega \, G'_\chi(\Omega) + i \int_0^{-\omega} d\Omega \, G''_\chi(\Omega) \right) \\ \Sigma_\chi(\omega) = J^2 \rho_0 \left(\int_{-\omega}^{-D} d\Omega \, G'_b(\Omega) + i \int_0^{-\omega} d\Omega \, G''_b(\Omega) \right) \end{cases} \tag{D.3}$$

where $\rho_0 = \frac{1}{2D}$.

Inserting the ansatz into this set of equations and using Dyson's equations, we are able to extract a new set of self-consistent equations for the parameters of our ansatz, which can then be solved analytically.

D.2 Derivation

D.2.1 Bosonic parameters

Plugging (D.2) into (D.3a), one has:

$$\begin{cases} \Sigma_b(\omega > 0) = \dfrac{\gamma J^2 \rho_0 D^{1-\beta}}{1-\beta}\mathrm{Re}B_- - \dfrac{\gamma J^2 \rho_0 B_-^*}{1-\beta}\omega^{1-\beta} \\ \Sigma_b(\omega < 0) = \dfrac{\gamma J^2 \rho_0 D^{1-\beta}}{1-\beta}\mathrm{Re}B_- + \dfrac{\gamma J^2 \rho_0 B_+^*}{1-\beta}|\omega|^{1-\beta} \end{cases} \tag{D.4}$$

In the two-impurity model, the Dyson's equation for the bosonic propagator reads:

$$G_b^{-1} = \omega + \lambda - \Sigma_b(\omega) - \frac{|\Delta|^2}{-\omega + \lambda - \Sigma_b(-\omega)^*} \tag{D.5}$$

Replacing Σ_b in this last expression by Eq. (D.4), and expanding in the denom-

inator for small frequency, one is left with:

$$
\begin{aligned}
G_b^{-1} \;=\;& \frac{\left(\lambda - \frac{\gamma J^2 \rho_0 D^{1-\beta}\mathrm{Re}B_-}{1-\beta}\right)^2 - |\Delta|^2}{\lambda - \frac{\gamma J^2 \rho_0 D^{1-\beta}\mathrm{Re}B_-}{1-\beta}} - \frac{\gamma J^2 \rho_0 |\omega|^{1-\beta}}{1-\beta}\left(B_+^*\Theta(-\omega) - B_-^*\Theta(\omega)\right) \\
& -\frac{|\Delta|^2}{\left(\lambda - \frac{\gamma J^2 \rho_0 D^{1-\beta}\mathrm{Re}B_-}{1-\beta}\right)^2}\frac{\gamma J^2 \rho_0 |\omega|^{1-\beta}}{1-\beta}\left(B_+\Theta(\omega) - B_-\Theta(-\omega)\right) \qquad \text{(D.6)}
\end{aligned}
$$

Imposing self-consistency with our original ansatz, one can identify:

$$
\begin{cases}
\left(\lambda - \dfrac{\gamma J^2 \rho_0 D^{1-\beta}\mathrm{Re}B_-}{1-\beta}\right)^2 = |\Delta|^2 \\[2ex]
\dfrac{1}{A_+} = \gamma J^2 \rho_0 \dfrac{B_-^* - B_+}{1-\beta} \\[2ex]
\dfrac{1}{A_-} = \gamma J^2 \rho_0 \dfrac{B_- - B_+^*}{1-\beta} \\[2ex]
\alpha = 1 - \beta
\end{cases}
\qquad \text{(D.7)}
$$

D.2.2 Fermionic parameters

One can now do the same procedure for the χ fermions, first inserting (D.1) into (D.3b):

$$
\begin{cases}
\Sigma_\chi(\omega > 0) \;=\; -\dfrac{J^2 \rho_0 D^{1-\alpha}}{1-\alpha}\mathrm{Re}A_- + \dfrac{J^2 \rho_0 A_-^*}{1-\alpha}\omega^{1-\alpha} \\[2ex]
\Sigma_\chi(\omega < 0) \;=\; -\dfrac{J^2 \rho_0 D^{1-\alpha}}{1-\alpha}\mathrm{Re}A_- - \dfrac{J^2 \rho_0 A_+^*}{1-\alpha}|\omega|^{1-\alpha}
\end{cases}
\qquad \text{(D.8)}
$$

Replacing this last expression of Σ_χ into $G_\chi^{-1} = J - \Sigma_\chi$, one has:

$$
G_\chi^{-1}(\omega) = J + \frac{\rho_0 J^2 D^{1-\alpha}\mathrm{Re}A_-}{1-\alpha} - \frac{\rho_0 J^2 |\omega|^{1-\alpha}}{1-\alpha}\left(A_-^*\Theta(\omega) - A_+^*\Theta(-\omega)\right) \qquad \text{(D.9)}
$$

Again, the self-consistency with the original ansatz imposes:

$$
\begin{cases}
J + \dfrac{\rho_0 J^2 D^{1-\alpha}\mathrm{Re}A_-}{1-\alpha} = 0 \\[2ex]
\dfrac{1}{B_+} = -\dfrac{J^2 \rho_0 A_-^*}{1-\alpha} \\[2ex]
\dfrac{1}{B_-} = \dfrac{J^2 \rho_0 A_+^*}{1-\alpha} \\[2ex]
\beta = 1 - \alpha
\end{cases}
\qquad \text{(D.10)}
$$

D.2.3   Analysis of the self-consistent equations

From a first look at the set of equations (D.7) and (D.10), one can already see that $A_+ = A_-^*$ and $B_+ = -B_-^*$, so that we only focus on A_+ and B_+ in what follows. Our set of equations then reduces to:

$$
\begin{cases}
J + \dfrac{\rho_0 J^2 D^{1-\alpha} \mathrm{Re} A_+}{1 - \alpha} = 0 \\[2ex]
\left(\lambda + \dfrac{\gamma J^2 \rho_0 D^{1-\beta} \mathrm{Re} B_+}{1 - \beta} \right)^2 = |\Delta|^2 \\[2ex]
\dfrac{1}{A_+} = -\dfrac{2\gamma J^2 \rho_0 B_+}{1 - \beta} \\[2ex]
\dfrac{1}{B_+} = -\dfrac{J^2 \rho_0 A_+}{1 - \alpha} \\[1ex]
\alpha + \beta = 1
\end{cases}
\tag{D.11}
$$

From the last three equations, one can extract that:

$$
\alpha = \frac{2\gamma}{1 + 2\gamma} \tag{D.12}
$$

$$
\beta = \frac{1}{1 + 2\gamma} \tag{D.13}
$$

It is useful at this stage to rewrite $A_+ = A e^{i\theta}$ and $B_+ = B e^{i\phi}$. Since the product $A_+ B_+$ is a real negative number, one has $\theta + \phi = \pi \ (2\pi)$ and $AB\rho_0 J^2(1 + 2\gamma) = 1$. Everything can then be re-expressed as a function of A and θ as:

$$
G_b(\omega) \sim \frac{A e^{i\theta \mathrm{Sign}(\omega)}}{|\omega|^{\frac{2\gamma}{1+2\gamma}}} \tag{D.14}
$$

$$
G_\chi(\omega) \sim -\frac{1}{A\rho_0 J^2(1 + 2\gamma)} \frac{e^{-i\theta \mathrm{Sign}(\omega)} \mathrm{Sign}(\omega)}{|\omega|^{\frac{1}{1+2\gamma}}} \tag{D.15}
$$

D.3   General remarks

D.3.1   Causality

As a first check, one has to make sure that the final expressions we just obtained satisfy the causality of the retarded Green's functions. Looking at the imaginary part of the bosonic propagator, one can immediately see that $\mathrm{Im} G_b(\omega) \sim \mathrm{Sign}(\omega) \sin\theta$, which has the right properties provided that $\sin\theta$ is negative.

The same inspection on G_χ leads to $\mathrm{Im} G_\chi(\omega) \sim \sin\theta$, so that again the causality rules are respected provided that $\sin\theta$ is negative.

D.3.2   Spectral asymmetry

It is interesting to notice that in this case there is no spectral asymmetry like the one observed for the overscreened single impurity. Indeed, in the case of the two-impurity critical region, the prefactor is either equal or opposite depending whether one is considering the real or the imaginary part of the Green's functions. This feature seems to be a consequence of the particular Dyson's equation for the bosonic field which mixes in this case the positive and negative frequency regions (both $\Sigma_b(\omega)$ and $\Sigma_b(-\omega)$ enter the Dyson's equation giving $G_b(\omega)$).

Conclusion

The work presented here focused on magnetic quantum critical points, as encountered in systems of strongly interacting fermions. Motivated by the growing number of experimental systems whose properties cannot be accounted for by the canonical Hertz-Millis-Moriya theory [3, 13, 14], we tried to provide new theoretical elements to go beyond this description.

In the first part of this work, we studied the ferromagnetic quantum critical point of itinerant metals. Starting from a model describing the interaction between low-energy fermions and spin fluctuations, we constructed a controllable expansion around a non-Fermi liquid solution in the quantum critical regime. From there, we could prove that the Landau damping of the collective critical modes (related to particle-hole excitations) leads to an effective long-range dynamic interaction between fermionic quasiparticles. This interaction is responsible for the emergence of a negative non-analytic correction to the static spin susceptibility, whose consequences are two-fold:

- a Landau-Ginzburg-Wilson field-theoretical description is no longer applicable,

- the ferromagnetic QCP is unstable below a given energy scale.

Considering the latest experimental evidence on itinerant ferromagnets [21, 22], one could argue, based on our results, that the system would favor a first-order phase transition towards a ferromagnetic state at low temperature. However, recent attempts to discriminate between a first and a second order phase transition suggest that the result actually depends on a microscopic scale which itself depends on the material.

In the second part of the present work, we studied an extension of the Kondo model [59], in the limit of large spin degeneracy N and number of channels K [107]. Following the work of Parcollet and Georges [106], we focused on a bosonic representation of the impurity spin. We first studied the case of a single impurity in the large-N limit, restricting ourselves to the regime of exact screening, where very little was known. We could prove that the thermodynamical properties of the system are the ones of a non-trivial Fermi liquid. Our method unexpectedly discovered that a gap develops in the bosonic and fermionic spectral functions, and that this very gap is intimately related to the emergence of Fermi liquid behavior at low temperature.

We then extended this approach and treated the case of two coupled impurities. We could uncover a point in the phase diagram where the low-temperature solution is gapless, suggesting the existence of a quantum critical point. This QCP shares many similar qualitative features with the so-called "Jones-Varma" critical point [117] studied in the physical $N = 2$ case.

In order to cure some of the failures of the original large-N treatment (in particular the vanishing transport properties it predicts), we developed a conserving approximation based on a truncation, at finite N, of the Luttinger-Ward functional. Keeping only the leading order diagram in N, we could derive a slightly modified set of self-consistent equations, whose solution leads to a low-temperature Fermi liquid behavior in both the thermodynamics and the scattering properties. However, the $N \to 2$ limit does not lead to the expected behavior for the resistivity, signaling that the truncation is not accurate enough in this limit: vertex corrections become too important and can no longer be neglected.

Finally, we derived the equations and some very preliminary results concerning an extension of the large-N approach to a Kondo lattice model.

One key element of our large-N bosonic approach is the existence of a gap in the spectral functions. Indeed, many of our results are somewhat connected to this gap. In the one-impurity case, the gap leads to a confinement of the spinon (b) and holon (χ) excitations, revealing a Fermi liquid ground state. In the two-impurity model, the collapse of the gap as one increases the inter-impurity coupling gives rise to a quantum critical point. In the conserving approximation used on the single-impurity model, the gap allows us to extend some important relationships of the Fermi liquid. Quite obviously, an important direction for future work on this topic is to elucidate whether such a gap exists in the physical $N = 2$ case.

It is quite tempting to speculate about the robustness of this gap in the $N = 2$ case (which would then be a real feature of the model rather than an artefact of our approach), and its consequences for the lattice version of the Kondo model. We have observed in the case of two coupled impurities, that the collapse of the confining gap leads to a quantum critical point, along with a whole region of the phase diagram where non-Fermi liquid behavior is observed.

Extending this kind of reasoning to the Kondo lattice, this would lead us to think that in addition to the "magnetic" quantum critical point whose experimental realizations can be explained within the Hertz-Millis-Moriya framework, there exists another family of quantum critical points, not driven by the quantum fluctuations of a magnetic critical mode, but rather by the deconfinement of the spinon and holon excitations (which itself might be related to magnetism).

Further work is required to determine how the heavy Fermi liquid could be destroyed by such a "spin-charge decoupled" quantum critical point. This obviously includes making predictions concerning the physical properties of the system, predictions that could be compared to current experimental results, or suggest new experiments to come.

Bibliography

[1] **T. Andrews** *Phil. trans. Roy. Soc.*, vol. **159**, p. 575, 1869.

[2] **L.D. Landau and E.M. Lifshitz**, *Statistical Physics Part 1*. Pergamon, 3rd Ed., 1994.

[3] **J.A. Hertz** *Phys. Rev. B*, vol. **14**, p. 1165, 1976.

[4] **P. Coleman and A.J. Schofield** *Nature*, vol. **433**, p. 226, 2005.

[5] **H. v. Löhneysen, T. Pietrus, G. Portisch, H. G. Schlager, A. Schröder, M. Sieck and T. Trappmann** *Phys. Rev. Lett.*, vol. **72**, p. 3262, 1994.

[6] **J. Custers, P. Gegenwart, H. Wilhelm, K. Neumaier, Y. Tokiwa, O. Trovarelli, C. Geibel, F. Steglich, C. Pépin and P. Coleman** *Nature*, vol. **424**, p. 524, 2003.

[7] **J. Hubbard** *Proc. Roy. Soc. A*, vol. **276**, p. 238, 1963.

[8] **E.C. Stoner** *Rep. Prog. Phys.*, vol. **11**, p. 43, 1946.

[9] **M.T. Béal-Monod** *Sol. St. Comm.*, vol. **14**, p. 677, 1974.

[10] **J.A. Hertz and M.A. Klenin** *Phys. Rev. B*, vol. **10**, p. 1084, 1974.

[11] **L.D. Landau** *JETP*, vol. **16**, p. 203, 1946.

[12] **T. Moriya and A. Kawabata** *J. Phys. Soc. Jpn*, vol. **34**, p. 639, 1973.

[13] **T. Moriya**, *Spin fluctuations in itinerant electron magnetism*. eds. Springer-Verlag, 1985.

[14] **A.J. Millis** *Phys. Rev. B*, vol. **48**, p. 7183, 1993.

[15] **A.P. Murani, A. Tari and B.R. Coles** *J. Phys. F*, vol. **4**, p. 1769, 1974.

[16] **M. Nicklas, M. Brando, G. Knebel, F. Mayr, W. Trinkl and A. Loidl** *Phys. Rev. Lett.*, vol. **82**, p. 4268, 1999.

[17] **D.A. Sokolov, M.C. Aronson, W. Gannon and Z. Fisk** *Phys. Rev. Lett.*, vol. **96**, p. 116404, 2006.

[18] **C. Pfleiderer, M. Uhlarz, S.M. Hayden, R. Vollmer, H. von Löhneysen, N.R. Bernhoeft and G.G. Lonzarich** *Nature*, vol. **412**, p. 58, 2001.

[19] **S. S. Saxena, P. Agarwal, K. Ahilan, F.M. Grosche, R.K.W. Haselwimmer, M.J. Steiner, E. Pugh, I.R. Walker, S.R. Julian, P. Monthoux, G.G. Lonzarich, A. Huxley, I. Sheikin, D. Braithwaite and J. Flouquet** *Nature*, vol. **406**, p. 587, 2000.

[20] **D. Aoki, A.D. Huxley, E. Ressouche, D. Braithwaite, J. Flouquet, J.-P. Brison, E. Lhotel and C. Paulsen** *Nature*, vol. **413**, p. 613, 2001.

[21] **M. Uhlarz, C. Pfleiderer and S.M. Hayden** *Phys. Rev. Lett.*, vol. **93**, p. 256404, 2004.

[22] **C. Pfleiderer and A.D. Huxley** *Phys. Rev. Lett.*, vol. **89**, p. 147005, 2002.

[23] **C. Pfleiderer, G.J. McMullan, S.R. Julian and G.G. Lonzarich** *Phys. Rev. B*, vol. **55**, p. 55, 1997.

[24] **N. Doiron-Leyraud, I. R. Walker, L. Taillefer, M. J. Steiner, S. R. Julian and G. G. Lonzarich** *Nature*, vol. **425**, p. 595, 2003.

[25] **C. Pfleiderer, D. Reznik, L. Pintschovius, H. von Löhneysen, M. Garst and A. Rosch** *Nature*, vol. **427**, p. 227, 2004.

[26] **D. Belitz, T.R. Kirkpatrick and T. Vojta** *Phys. Rev. B*, vol. **55**, p. 9452, 1997.

[27] **C.J. Pethick and G.M. Carneiro** *Phys. Rev. A*, vol. **7**, p. 304, 1973.

[28] **A.V. Chubukov and D.L. Maslov** *Phys. Rev. B*, vol. **69**, p. 121102(R), 2004.

[29] **A.V. Chubukov and D.L. Maslov** *Phys. Rev. B*, vol. **68**, p. 155113, 2003.

[30] **B.L. Altshuler, L.B. Ioffe and A.J. Millis** *Phys. Rev. B*, vol. **50**, p. 14048, 1994.

[31] **J. Gan and E. Wong** *Phys. Rev. Lett.*, vol. **71**, p. 4226, 1993.

[32] **Ar. Abanov, A. V. Chubukov and J. Schmalian**, *The physics of Superconductors.* K.H. Bennemann and J.B. Ketterson eds, Springer, 2003, 2003.

[33] **A.V. Chubukov, D.L. Maslov, S. Gangadharaiah, L.I. Glazman** *Phys. Rev. B*, vol. **71**, p. 205112, 2005.

[34] **L. B. Ioffe and A. I. Larkin** *Phys. Rev. B*, vol. **39**, p. 8988, 1989.

[35] **P. A. Lee** *Phys. Rev. Lett.*, vol. **63**, p. 680, 1989.

[36] **M.J. Lawler, D.G. Barci, V. Fernández, E. Fradkin and L. Oxman** *Phys. Rev. B*, vol. **73**, p. 085101, 2006.

[37] **A.V. Chubukov and D.V. Khveshchenko** cond-mat/0604376.

[38] **G.M. Eliashberg** *Sov. Phys. JETP*, vol. **16**, p. 780, 1963.

[39] **Ar. Abanov and A. V. Chubukov** *Phys. Rev. Lett.*, vol. **93**, p. 255702, 2004.

[40] **A. Chubukov, A. Finkelstein, R. Haslinger and D. Morr** *Phys. Rev. Lett.*, vol. **90**, p. 077002, 2003.

[41] **D. L. Maslov and A. V. Chubukov** unpublished.

[42] **G. Y. Chitov and A. J. Millis** *Phys. Rev. Lett.*, vol. **86**, p. 5337, 2001.

[43] **G. Y. Chitov and A. J. Millis** *Phys. Rev. B*, vol. **64**, p. 0544414, 2001.

[44] **A.V. Chubukov, D.L. Maslov and A. J. Millis** *Phys. Rev. B*, vol. **73**, p. 045128, 2006.

[45] **V. M. Galitski, A. V. Chubukov and S. Das Sarma** *Phys. Rev. B*, vol. **71**, p. 201302, 2005.

[46] **J. Betouras, D. Efremov and A. Chubukov** *Phys. Rev. B*, vol. **72**, p. 115112, 2005.

[47] **V. Oganesyan, S. A. Kivelson and E. Fradkin** *Phys. Rev. B*, vol. **64**, p. 195109, 2001.

[48] **W. Metzner, D. Rohe and S. Andergassen** *Phys. Rev. Lett.*, vol. **91**, p. 066402, 2003.

[49] **L. Dell'Anna and W. Metzner** *Phys. Rev. B*, vol. **73**, p. 045127, 2006.

[50] **H. Y. Kee and Y. B. Kim** *J. Phys. Cond. Matt.*, vol. **16**, p. 3139, 2004.

[51] **A. J. Millis, A. J. Schofield, G. G. Lonzarich and S. A. Grigera** *Phys. Rev. Lett.*, vol. **88**, p. 217204, 2002.

BIBLIOGRAPHY

[52] **D. Belitz, T. R. Kirkpatrick and T. Vojta** *Rev. Mod. Phys.*, vol. **77**, p. 579, 2005.

[53] **S.A. Brazovskii** *Sov. Phys. JETP*, vol. **41**, p. 85, 1975.

[54] **D. Belitz, T. R Kirkpatrick and A. Rosch** *Phys. rev. B*, vol. **73**, p. 054431, 2006.

[55] **D. Belitz, T. R Kirkpatrick and A. Rosch** cond-mat/0604427.

[56] **A.V. Chubukov and A.M. Tsvelik** cond-mat/0511708.

[57] **D. Maslov** private communication.

[58] **W.J. de Haas, J.H. de Boer and G.J.van den Berg** *Physica*, vol. **1**, p. 1115, 1934.

[59] **J. Kondo** *Prog. Theor. Phys.*, vol. **32**, p. 37, 1964.

[60] **M. Sarachik, E. Corenzwit and L.D. Longinotti** *Phys. Rev. A*, vol. **135**, p. 1041, 1964.

[61] **C. Zener** *Phys. Rev.*, vol. **81**, p. 440, 1951.

[62] **P.W. Anderson** *J. Phys. C*, vol. **3**, p. 2439, 1970.

[63] **K.G. Wilson** *Rev. Mod. Phys.*, vol. **47**, p. 773, 1975.

[64] **P.W. Anderson** *Phys. rev.*, vol. **124**, p. 41, 1961.

[65] **J.R. Schrieffer and P.A. Wolf** *Phys. Rev.*, vol. **149**, p. 491, 1966.

[66] **L.I. Glazman and L.P. Kouwenhoven** *Physics World*, vol. **14**, p. 33, 2001.

[67] **A.A. Abrikosov** *Physics*, vol. **2**, p. 5, 1965.

[68] **H. Suhl** *Phys. Rev.*, vol. **138**, p. A515, 1965.

[69] **H.C. Manoharan, C.P. Lutz and D.M. Eigler** *Nature*, vol. **403**, p. 512, 2000.

[70] **V. Madhavan, W. Chen, T. Jamneala, M.F. Crommie and N.S. Wingreen** *Science*, vol. **280**, p. 567, 1998.

[71] **J. Li and W.-D. Schneider** *Phys. Rev. Lett.*, vol. **80**, p. 2893, 1998.

[72] **G.A. Fiete and E.J. Heller** *Rev. Mod. Phys.*, vol. **75**, p. 933, 2003.

[73] **L.P. Kouwenhoven, C.M. Marcus, P.L. McEuen, S. Tarucha, R.M. Westervelt and N.S. Wingreen**, *Mesoscopic electron transport.* eds L.L. Sohn, L.P. Kouwenhoven and G.Schön (Kluwer), 1997.

[74] **L.P. Kouwenhoven and C.M. Marcus** *Physics World*, vol. **11**, p. 35, 1998.

[75] **I.L. Aleiner, P.W. Brouwer and L.I. Glazman** *Phys. Rep.*, vol. **358**, p. 309, 2002.

[76] **D. Goldhaber-Gordon, H. Shtrikman, D. Mahalu, D. Abusch-Magder, U. Meirav and M.A. Kastner** *Nature*, vol. **391**, p. 156, 1998.

[77] **S. Tarucha, D.G. Austing, S. Sasaki, Y. Tokura, W. van der Wiel and L.P. Kouwenhoven** *Appl. Phys. A*, vol. **71**, p. 367, 2000.

[78] **M.A. Kastner** *Ann. Phys. (Leipzig)*, vol. **9**, p. 885, 2000.

[79] **S. Tarucha, D.G. Austing, T. Honda, R.J. van der Hage and L. P. Kouwenhoven** *Phys. Rev. Lett.*, vol. **77**, p. 3613, 1996.

[80] **L.I. Glazman and M.E. Raikh** *JETP Lett.*, vol. **47**, p. 452, 1990.

[81] **T.K. Ng and P. Lee** *Phys. Rev. Lett.*, vol. **61**, p. 1768, 1988.

[82] **W.G. van der Wiel, S. De Franceschi, T. Fujisawa, J.M. Elzerman, S. Tarucha and L.P. Kouwenhoven** *Science*, vol. **289**, p. 2105, 2000.

[83] **T.A. Costi**, *Concepts in Electron Correlations.* eds A.C.Hewson and V.Zlatic (Kluwer), 2003.

[84] **M. Pustilnik, L.I. Glazman, D.H. Cobden and L.P. Kouwenhoven** *Lecture Notes in Physics*, vol. **579**, p. 3, 2001.

[85] **H. Jeong, A.M. Chang and M.R. Melloch** *Science*, vol. **293**, p. 2221, 2001.

[86] **N. J. Craig, J. M. Taylor, E. A. Lester, C. M. Marcus, M. P. Hanson and A. C. Gossard** *Science*, vol. **304**, p. 565, 2004.

[87] **Y. Oreg and D. Goldhaber-Gordon** *Phys. Rev. Lett.*, vol. **90**, p. 136602, 2003.

[88] **P. Mehta and N. Andrei** cond-mat/0508026.

[89] **H. Frölich and F.R.N. Nabarro** *Proc. Roy. Soc. A*, vol. **175**, p. 382, 1940.

[90] **M.A. Ruderman and C. Kittel** *Phys. Rev.*, vol. **96**, p. 99, 1954.

[91] **T. Kasuya** *Prog. Theor. Phys.*, vol. **16**, p. 45, 1956.

[92] **K. Yosida** *Phys. Rev.*, vol. **106**, p. 893, 1957.

[93] **J. Friedel** *Phil. Mag.*, vol. **43**, p. 153, 1952.

[94] **S. Doniach** *Physica B*, vol. **91**, p. 231, 1977.

[95] **K. Andres, J. Graebner and H. Ott** *Phys. Rev. Lett.*, vol. **35**, p. 1779, 1975.

[96] **G.R. Stewart** *Rev. Mod. Phys.*, vol. **73**, p. 797, 2001.

[97] **J. Custers**, *Quantum-critical behavior in the heavy-fermion compounds $YbRh_2Si_2$ and $CeIn_{3-x}Sn_x$.* PhD thesis, Technische Universität Dresden, 2004.

[98] **P. Gegenwart, Y. Tokiwa, K. Neumaier, C. Geibel and F. Steglich** cond-mat/0406260.

[99] **A. Schroeder, G. Aeppli, R. Coldea, M. Adams, O. Stockert, H. von Löhneysen, E. Bucher, R. Ramazashvili and P. Coleman** *Nature*, vol. **407**, p. 351, 2000.

[100] **B. Coqblin and J.R. Schrieffer** *Phys. Rev.*, vol. **185**, p. 847, 1969.

[101] **J. Schwinger**, *Quantum theory of angular momentum.* Academic, New York, 1965.

[102] **N. Read and R.M. Newns** *J. Phys. C*, vol. **16**, p. 3273, 1983.

[103] **A. Auerbach and K. Levin** *Phys. Rev. Lett.*, vol. **57**, p. 877, 1986.

[104] **D.P. Arovas and A. Auerbach** *Phys. Rev. B*, vol. **38**, p. 316, 1988.

[105] **J.E. Hirsch and S. Tang** *Phys. Rev. B*, vol. **39**, p. 2850, 1989.

[106] **O. Parcollet and A. Georges** *Phys. Rev. Lett.*, vol. **79**, p. 4665, 1997.

[107] **P. Nozières and A. Blandin** *Journal de Physique*, vol. **41**, p. 193, 1980.

[108] **J.M. Luttinger** *Phys. Rev.*, vol. **119**, p. 1153, 1960.

[109] **J.M. Luttinger and J.C. Ward** *Phys. Rev.*, vol. **118**, p. 1417, 1960.

[110] **J.M. Luttinger** *Phys. Rev.*, vol. **121**, p. 1251, 1961.

[111] **G. Baym** *Phys. Rev.*, vol. **127**, p. 1391, 1962.

[112] **G. Baym and L.P. Kadanoff** *Phys. Rev.*, vol. **124**, p. 287, 1961.

[113] **O. Parcollet, A. Georges, G. Kotliar and A. Sengupta** *Phys. Rev. B*, vol. **58**, p. 3794, 1998.

[114] **E. Müller-Hartmann** *Z. Phys. B*, vol. **57**, p. 281, 1984.

[115] **O. Parcollet**, *Effet Kondo et modèles quantiques désordonnés: limites de grand-N*. PhD thesis, Université Paris VI, 1998.

[116] **A. Jerez, N. Andrei and G. Zaránd** *Phys. Rev. B*, vol. **58**, p. 3814, 1998.

[117] **B.A. Jones and C.M. Varma** *Phys. Rev. Lett.*, vol. **58**, p. 843, 1987.

[118] **N. Read and S. Sachdev** *Phys. Rev. Lett.*, vol. **66**, p. 1773, 1991.

[119] **A.M. Clogston and P.W. Anderson** *Bull. Am. Phys. Soc.*, vol. **6**, p. 124, 1961.

[120] **B.A. Jones, C.M. Varma and J.W. Wilkins** *Phys. Rev. Lett.*, vol. **61**, p. 125, 1988.

[121] **B.A. Jones and C.M. Varma** *Phys. Rev. B*, vol. **40**, p. 324, 1989.

[122] **I. Affleck and A.W.W. Ludwig** *Phys. Rev. Lett.*, vol. **68**, p. 1046, 1992.

[123] **I. Affleck, A.W.W. Ludwig and B.A. Jones** *Phys. Rev. B*, vol. **52**, p. 9528, 1995.

[124] **J. Gan** *Phys. Rev. Lett.*, vol. **74**, p. 2583, 1995.

[125] **J. Gan** *Phys. Rev. B*, vol. **51**, p. 8287, 1995.

[126] **P. Nozières** *J. Low Temp. Phys.*, vol. **17**, p. 31, 1974.

[127] **H. Shiba** *Prog. Theor. Phys.*, vol. **54**, p. 967, 1975.

[128] **D.C. Langreth** *Phys. Rev.*, vol. **150**, p. 516, 1966.

[129] **D. Withoff and E. Fradkin** *Phys. Rev. Lett.*, vol. **64**, p. 1835, 1990.

[130] **K. Ingersent and Q. Si** *Phys. Rev. Lett.*, vol. **89**, p. 076403, 2002.

[131] **M. Vojta** *Phys. Rev. Lett.*, vol. **87**, p. 097202, 2001.

[132] **P. Coleman and I. Paul** *Phys. Rev. B*, vol. **70**, p. 1, 2004.

[133] **L.V. Keldysh** *JETP*, vol. **20**, p. 1018, 1965.

[134] **J. Rammer and H. Smith** *Rev. Mod. Phys.*, vol. **58**, p. 323, 1986.

[135] **P. Coleman, C. Pépin, Q. Si and R. Ramazashvili** *J. Cond Matt*, vol. **13**, p. R723, 2001.

[136] **T. Senthil, S. Sachdev and M. Vojta** *Physica B*, vol. **9**, p. 359, 2005.

[137] **C. Pépin** *Phys. Rev. Lett.*, vol. **94**, p. 066402, 2005.

[138] **S. Paschen, T. Lühmann, S. Wirth, P. Gegenwart, O. Trovarelli, Ch. Geibel, F. Steglich, P. Coleman and Q. Si** *Nature*, vol. **432**, p. 881, 2004.

[139] **A. Georges, G. Kotliar, W. Krauth and M.J. Rozenberg** *Rev. Mod. Phys.*, vol. **68**, p. 13, 1996.

[140] **J.-P. Blaizot, E. Iancu and A. Rebhan** *Phys. Rev. D*, vol. **63**, p. 065003, 2001.

[141] **G. M. Carneiro and C. J. Pethick** *Phys. Rev. B*, vol. **11**, p. 1106, 1975.

[142] **K. Yamada** *Prog. Theor. Phys.*, vol. **53**, p. 970, 1975.

[143] **K. Yosida and K. Yamada** *Prog. Theor. Phys.*, vol. **53**, p. 1286, 1975.

[144] **A. Yoshimori** *Prog. Theor. Phys.*, vol. **55**, p. 67, 1976.

Abstract

It took several years after the idea of a zero-temperature phase transition emerged to realize the impact of such a quantum critical point over a large region of the phase diagram. Observed in many experimental examples, this quantum critical regime is not yet understood in details theoretically, and one needs to develop new approaches. In the first part, we focused on the ferromagnetic quantum critical point. After constructing a controlled approach allowing us to describe the quantum critical regime, we show through the computation of the static spin susceptibility that the ferromagnetic quantum critical point is unstable, destroyed internally by an effective dynamic long-range interaction generated by the Landau damping. In the second part, we revisit the exactly screened single impurity Kondo model, using a bosonic representation of the local spin and treating it in the limit of large spin degeneracy N. We show that, in this regime, the ground-state is a non-trivial Fermi liquid, unlike what was advocated by previous similar studies. We then extend our method to encompass the physics of two coupled impurities, for which our results are qualitatively comparable to the ones obtained from various approaches carried out in the past. We also develop a Luttinger-Ward formalism, enabling us to cure some of the drawbacks of the original method used to describe the single impurity physics. Finally, we present the main ideas and the first results for an extension of the method towards the description of a Kondo lattice, relevant for the understanding of the quantum critical regime of heavy fermion materials.

Keywords: Quantum critical point, Itinerant ferromagnetism, Eliashberg theory, Kondo effect, Schwinger bosons, Large-N approach, Luttinger-Ward formalism.

Résumé

Il aura fallu plusieurs années après que l'idée d'une transition de phase à température nulle émerge pour que l'on comprenne l'impact d'un tel point critique quantique sur une vaste région du diagramme de phase. Observé dans de nombreux exemples expérimentaux, ce régime critique quantique n'est toutefois pas encore bien compris sur le plan théorique et nécessite de nouvelles approches. Dans une première partie, nous nous intéressons au point critique quantique ferromagnétique. Après avoir construit une approche contrôlée permettant de décrire le régime critique quantique, nous montrons au travers de la susceptibilité statique de spin que le point critique quantique ferromagnétique est instable, détruit par une interaction effective dynamique à longue portée générée par l'amortissement de Landau des fluctuations de spin. Dans une seconde partie, nous revisitons le cas d'une impureté Kondo exactement écrantée avec une représentation bosonique du spin local et dans une limite de grande dégénérescence de spin N. Nous montrons que dans ce régime, l'état fondamental est un liquide de Fermi non-trivial contrairement à ce qui était communément admis. Nous étendons alors notre méthode au cas de deux impuretés couplées où nos résultats coïncident qualitativement avec les approches déjà existantes. Ensuite, nous développons un formalisme de Luttinger-Ward capable de pallier certains défauts de l'approche originale pour la description d'une impureté isolée. Enfin, nous détaillons les bases ainsi que les premiers résultats de l'extension à un réseau Kondo de moments locaux, pertinent pour la compréhension du régime critique quantique des matériaux de type fermions lourds.

Mots clés : Point critique quantique, Ferromagnétisme itinérant, Théorie d'Eliashberg, Effet Kondo, Bosons de Schwinger, Méthode de grand-N, Formalisme de Luttinger-Ward.